Technical University Delft
Traffic induced vibrations in floating thoroughfares
Ekke Kaspers

Graduation project
Traffic induced vibrations in floating thoroughfares

Technical university Delft
Faculty of Civil Engineering and Geosciences
Specialization: Hydraulic Engineering
Section: Structural Mechanics

Thesis committee:

Prof. Drs. Ir. J.K. Vrijling, Hydraulic Engineering
Prof. Dr. A.V. Metrikine, Structural Mechanics
Dr. Ir. W.G.M. Groenevelt, Applied Mathematics, EWI faculty
Ir. W.F. Molenaar, Hydraulic Engineering

Student:

Ing. E.J. Kaspers

April 2010

"For everything there is an appointed time, and an appropriate time for every activity on earth."

Ecclesiastes 3:1

Table of contents

TUDelft

Appendices

TUDelft

Preface

This thesis documents the graduation project which I took upon me in order to complete my master study in Civil Engineering at Delft University of Technology. I have been working on this project for more than two years now. After studying multibody dynamics, I focussed on mathematical expressions for the wave diffraction phenomenon. To this background, I investigated traffic induced vibrations in floating thoroughfares.

What I learned about myself is that it was quite difficult for me to manage my own project, without knowing where to start and to end and what to do. Although it cost me a lot of time and many sleepless nights, I am quite pleased because of the result.

This study would not have been successfully completed without the help of my committee members and therefore I wish to thank them.
I would like to thank Prof. Drs. Ir. J.K. Vrijling for his great expertise on hydraulic structures which he made available to me so that I could make better decisions in this study. And Prof. Dr. A.V. Metrikine for his expertise on dynamic structures and his critical view on this report. I am also indebted to Ir. W.F. Molenaar, who spend much time in consultancy. And Dr. Ir. W.G.M. Groenevelt from the EWI faculty for his assistance on mathematics, so that I could solve the more difficult problems.
A special thanks to Dr. F.W. Lameris from TNO Bouw en Ondergrond, for making available the recorded data on the pilot project.

Finally, I wish to express my gratitude to my wife, Deborah, my family and friends for their unceasing support and encouragement.

Ekke Kaspers
April 2010

TUDelft

Summary

In this masters project, a technical feasibility study will be performed on a floating thoroughfare that is able to operate in several locations and facilitate traffic under all circumstances. A pilot-based road section that is coming right out of a groundwater-rich part of the (primary) Dutch traffic network was the basis for the computational model. The floating thoroughfare was modelled as a multibody system and simulations were made with the help of a computer program. Traffic, schematized as a series of moving, concentrated loads, was determined and implemented in the computational model. Following that, wave diffraction, as simplification of the fluid dynamics, was assessed and implemented. Different simulations were made in the time domain, thereby simulating the vertical acceleration and angle of the deck due to a single vehicle motion and the resonant behaviour, exhibiting by a series of vehicles. This resulted in a properly working system, although some joint properties and the length of all body sections needed to be adjusted to meet the requirements for 120km/h. Also, the sensitivity of the system was analysed with a parameter study. This allows third parties to design the physical joints in the preliminary stage, for example. A frequency domain response analysis was performed in order to give insight in the accelerations at different frequencies.

TUDelft

List of symbols

xy	Cartesian coordinate system for multibody system	
$X_1 X_2$	coordinate system in vector analysis; axes of inertial frame	
$X_1^i X_2^i$	coordinate system in vector analysis; axes of the global frame of reference	

$\mathbf{A}^i$	rotation matrix for body i	[-]
$\boldsymbol{A}$	factorized matrix	[-]
A	horizontal body surface	[m^2]
A_n	boundary condition associated entry n	[m]
$\mathbf{a}^i$	acceleration of arbitrary point p^i	[m/s^2]
a_c	vertical acceleration of a vehicle	[m/s^2]
$a_{\max,c}$	vertical acceleration level of a vehicle corresponding to velocity	[m/s^2]
a_2^i	scalar that defines the vertical acceleration of the mass of body i	[m/s^2]
B	body width	[m]
$\mathbf{C}$	damping matrix	[kg(m^2)/s]
$\mathbf{C}^i$	damping matrix lumped in body i	[kg(m^2)/s]
C_1	amplitude in frequency domain	[-]
$\mathbf{c}^{jT}$	damping vector representing the stiffness of joint j	[Ns/m]
$\bar{\mathbf{c}}^{jT}$	damping vector in the body coordinate system	[Ns/m]
c	velocity of traffic induced force	[m/s]
$c_{cl/int}$	joint damping parameter associated with location of joint	[Ns/m]
$c_{d,w}$	distributed damping associated with w-direction	[Ns/m/m^1]
$c_{d,\theta}$	distributed damping associated with the body deflection	[Nms/rad/m^1]
$c_{d,w,cr}$	critical distributed damping parameter	[Ns/m/m^1]
c_{wave}	wave celerity	[m/s]
$c_{2,3}$	integer in damping matrix in the second row on third column	[kg(m^2)/s]
d	dimensionless draft	[-]
dt	time step	[s]
$\mathbf{E}$	eigenmatrix containing the eigenvectors	[-]
EI	flexural rigidity	[Nm^2]
$\mathbf{F}$	force vector	[N(m)]
$\hat{\mathbf{F}}$	force amplitude	[N]
$\mathbf{F}_{e/c}^i$	vector containing the sum of the external or constrained forces	[N]
$\mathbf{F}_{k/c}^j$	force inside joint j	[N]
$\boldsymbol{F}_{1/2P}$	excitation force vector associated with load from wheels	[N]
$\boldsymbol{F}_t$	superposition of excitation vectors	[N]
F	buoyancy force	[N]
$\bar{G}^i$	matrix containing directional (unit) vectors	[-]
g	gravitational acceleration	[m/s^2]
$\mathbf{H}_{yF}$	dynamic flexibility coefficient or transfer function	[s^2/kg(m^2)]
H, H_0	fluid depth	[m]
h, h_0	body height	[m]
$\mathbf{I}$	identity matrix	[-]
$\mathbf{I}_{00}^i$	inertia tensor	[kg/m^2]
$\mathbf{i}_3^i$	unity vector	[-]

i	body number	[-]
J^i	mass moment of inertia corresponding to body i	[kgm^2]
j	joint number	[-]
K	stiffness matrix	[kg(m^2)/s^2]
K^i	stiffness matrix lumped in body i	[kg(m^2)/s^2]
K*	modal stiffness matrix	[kg(m^2)/s^2]
K	transform of dispersion relation	[-]
$\mathcal{K}$	hydrodynamic ratio	[-]
k^{jT}	stiffness vector representing stiffness of joint j	[N/m]
$\bar{\mathbf{k}}^{jT}$	stiffness vector in the body coordinate system	[N/m]
k	wave number	[-]
$k_{cl/int}$	joint stiffness parameter associated with location of joint	[Ns/m]
$k_{d,w}$	distributed stiffness associated with the w-direction	[N/m/m^1]
$k_{d,\theta}$	distributed stiffness associated with the θ-direction	[Nm/rad/m^1]
$k_{2,3}$	integer in stiffness matrix in the second row on third column	[kg(m^2)/s^2]
L, L_0	body length	[m]
L^i	length of body i	[m]
l	characteristic length	[m]
M	constant, explicit mass matrix	[kg(m^2)]
M*	modal mass matrix	[kg(m^2)]
M	internal moment due to buoyancy forces	[Nm]
M^i	time related moment due to traffic induced force	[Nm]
$M_{0,c/i}$	external moment exerted by vibrating load	[Nm]
$\mathbf{m}_{00}^i$	mass tensor	[kg]
m	body mass	[kg]
m_b	mass of body per square meter	[kg/m^2]
m_f	added (fluid) mass per square meter	[kg/m^2]
$m_{f,w}$	added (fluid) mass associated with the w-direction	[kg/m^2]
$m_{f,\theta}$	added (fluid) mass per square meter associated with the θ-dir.	[kg/m^2]
m_t	total mass per square meter	[kg/m^2]
m_v	mass of (design) vehicle	[kg]
N	number of bodies	[-]
N_m	number of modes (or waves)	[-]
n	entry number	[-]
nv	number of vehicles	[-]
O^i	origin of body i	[-]
$\dot{\mathbf{P}}^i$	rate of change in momentum of body i	[N]
P	concentrated load from passenger car	[N]
p	hydrodynamic pressure	[N/m^2]
p^i	arbitrary point on body i	[-]
$\bar{\mathbf{Q}}^T$	vector of generalized forces of the total multibody system	[N(m)]
$\bar{\mathbf{Q}}_{R/\theta}^{iT}$	vector of generalized forces associated with coordinate R or θ	[N(m)]
$\mathbf{q}_r^i$	vector of generalized coordinates	[m]
q	equally distributed buoyancy force	[N/m^2]
q	time-periodic pressure	[N/m^2]
q_0	external force or magnitude of distributed load	[N/m^2]

TUDelft

$\mathbf{R}^i$	position vector of the origin of the body reference	[m]
R	complex amplitude of reflected wave	[-]
R_{norm}	normalized reflection wave coefficient	[-]
$\mathbf{r}^i$	global position of arbitrary point on body i	[m]
r	matrix rank	[-]
$\mathbf{S}_{yF}$	dynamic stiffness coefficient	[kgm^2/s^2]
$\mathbf{S}$	diagonal matrix with non-negative numbers on the diagonal	[-]
$\tilde{\mathbf{S}}$	diagonal matrix with rank r	[-]
$\mathbf{S}_t$	truncated diagonal matrix	[-]
T	complex amplitude of transmitted wave	[-]
T_{norm}	normalized transmitted wave coefficient	[-]
T_p	external period	[s]
T^i	kinetic energy	[kgm^2/s^2]
t	time	[s]
t^i	time associated with the position of the traffic induced force	[s]
t_{end}	simulation time	[s]
t_{md}	time interval corresponding to the mutual distance of succeeding vehicles	[s]
t_g	time interval corresponding to the spatial gap between succeeding vehicles	[s]
t_{wb}	time interval corresponding to the wheelbase of a vehicle	[s]
t_{ω_e}	time of revolution corresponding to the structure's natural freq.	[s]
$\mathbf{U}$	unitary matrix in factorization	[-]
$\mathbf{U}_t$	truncated unitary matrix	[-]
$\mathbf{u}^i$	position vector of arbitrary point in the body coordinate system	[-]
$\tilde{\tilde{u}}^i$	skew matrix in which the integers denote the position of an arbitrary point in the body coordinate system	[-]
$\mathbf{V}^*$	unitary matrix in factorization	[-]
$\mathbf{V}_t$	truncated unitary matrix	[-]
$\mathbf{v}^i$	velocity vector of arbitrary point p^i	[m/s]
w	body deflection or upper surface of the fluid	[m]
wb	wheel base	[m]
$\bar{w}$	time-independent averaged value of body deflection	[m]
$\hat{w}_{max}$	maximal kinematical deflection	[m]
w_{sw}	displacement under short wave conditions	[m]
x	horizontal coordinate in the multibody system and diffraction syst.	[m]
$x^i_{r.c.}$	horizontal distance between origin and rotational centre of body i	[m]
$\mathbf{y}$	displacement vector	[m,rad]
y_n	(vertical) displacement in n	[m]
α	spectral frequency	[-]
α_{am}	ratio between vibration velocity and potential at interface fluid / body	[-]
α_0	residue	[-]
α^i	angular acceleration vector of body i	[m/s^2]
γ	residue	[-]

TUDelft

Δw^j	internal displacement inside joint j	[m]
Δw^j_{max}	level of internal displacements	[m]
δW^i	scalar for virtual work of body i	[Nm]
ς	scattering frequency in frequency domain	[-]
η	complex amplitude of surface wave travelling from the left edge of the plate $\{x = 0\}$ to the left	[-]
θ	body rotation or angle describing orientation of body	[rad]
$\bar{\theta}$	averaged body rotation	[rad]
θ_{max}	maximum level of rotation	[rad]
λ_p	wave length	[m]
ξ	complex amplitude of surface wave travelling from the right edge of the plate $\{x = L\}$ to the right	[-]
Π^+	half plane where $\text{Im}(\alpha) > -|\gamma_1|$ with cuts around $-\alpha_0$ and $-\gamma$	[-]
Π^-	half plane where $\text{Im}(\alpha) < |\gamma_1|$ with cuts around α_0 and γ	[-]
ρ	fluid density	[kg/m^3]
ρ_0	body density	[kg/m^3]
Φ	transformed velocity potential	[-]
$\Phi_{1,2}$	transformed velocity potential at interface body / fluid. (subscript refers to x -domain, 1: free surface , 2: interface body / fluid)	[-]
$\Phi_{\pm}$	transform of dispersion relation on interval $\{x \mid L < x < \infty\}$. (subscript refers to domain, a plus for $\{x \mid L < x < \infty\}$, a minus for $\{x \mid -\infty < x < 0\}$	[-]
φ	fluid velocity potential	[m^2/s]
ϕ	dimensionless fluid velocity potential under steady state condition	[-]
Ω	(complex conjugate) eigenvalue matrix	[rad/s]
ω	radian frequency	[rad/s]
$\omega_{0,n}$	natural frequency corresponding to entry n	[rad/s]
ω_n	eigenvalue corresponding with entry n	[rad/s]
$\mathbf{0}$	null matrix	[-]

TUDelft

1   Introduction

Developing floating thoroughfares for all kind of purposes has become more interesting in the past decades. The focus of this report will be on the Dutch infrastructural traffic network. This sound quite unfamiliar but making (a part of) this network (able to) float, is interesting from a political, economical and practical point of view. Floatation will accomplish:

- a rate of accessibility of surface water to dry infrastructure what fits the governmental future policy to 'reclaim land for water'.
- a sustainable solution where (ground)water and infrastructure (read: traffic net) meet each other; water does not 'harm' these structures.
- the highest rate of flexibility when maintenance or network expansion is required.

From previous research, it appeared that the smaller a floating structure becomes, the stronger its performance depend on the environment. To guarantee for accessibility, even when weather conditions become bad, it is necessary for them being placed in an excavation or behind a breakwater, where it is more or less unexposed to troubled water.

Although many studies were performed on floating structures in general, just a single study was performed on floating thoroughfares in the Netherlands, what does not meet the necessary requirements. The floating thoroughfare that was tested – and never applied – was designed for traffic velocities until 80 km/h and must be able to withstand currents and wave attack at a specific location. A floating thoroughfare which becomes part of the traffic network, however, must have nothing to fear from currents and waves but the more from traffic.

Even without waves and currents, a floating thoroughfare has a complex dynamic behaviour. Many structural and hydraulic factors influences the hydrodynamic behaviour, that have not been studied so far. Neither by real time testing nor by a proper simulation model. The development of a computational, analytic, simulation model as well as the assessment of the influence of structural and hydraulic factors on the model's dynamic behaviour (sensibility analysis) is the main objective of this study.

With this knowledge, the model can be used as a design tool to determine the magnitude of factors yet in an early stage of the design process. The model can then answer the questions whether or not floating thoroughfares can be suitable for a wide application. So, apart from the engineering problem to develop a model and to assess the importance of the structural factors, it has to be determined whether a floating thoroughfare can be a feasible solution from a theoretical point of view.

It is therefore important to schematize the problem to be a base for later, when real objectives present themselves and more detailed assessment and model testing is required.

TUDelft

The structure of this report is as follows:

Section 2:   A brief review will be given on historic development of floating bridges. Next, we attempt to categorize the newest type of floating thoroughfare

Section 3:   Section 3 will provide information about the pilot as pioneer for this project. This section end up with future possibilities for application of a floating thoroughfare.

Section 4:   The problem definition and main objective will be discussed here. An input / output diagram for computation will pass the review as well

Section 5:   The schematization of the floating thoroughfare as a multibody system will be elaborated in section 5

Section 6:   In section 6 the model will be programmed in Matlab and eigen motions will be validated and checked

Section 7:   Traffic in its state of appearance will be discussed here

Section 8:   Wave diffraction will be studied and programmed for implementing in the multibody system

Section 9:   Traffic and wave diffraction will be implemented in the multibody system, parameters of 'tuning tools' will be calculated and validated with data from the prototype and the joint's configuration will be examined in this section

Section 10:   A frequency domain response analysis will be performed

Section 11:   Finally, in section 11, conclusions will be drawn and recommendations on further research will be given

TUDelft

2 Definition(s) and alternatives

What is a floating thoroughfare?

From a historical point of view, it is impossible to define an ambiguous answer to this question. Throughout the ages, (socio-) economical, political and industrial developments contributed to the multifaceted development of these type of constructions. Although configurations differ considerably, floating thoroughfares always arouse from the primary demand to satisfy the need for travelling from A to B across water.

The increased pressure on the traffic network and the policy to 'reclaim land for water' are examples of real-time socio-economical and political development in the Netherlands. In the Dutch modern society, however, demands become more comprehensive as well; nowadays, not the need for transport across water but an integral and sustainable approach to the transport problem is normative. To this background, the following definition has been encountered to answer the question here:

A floating thoroughfare is a road that is supported by floating bodies, instead of sand bodies or irremovable supports, and therefore it is able to move with the groundwater level and water level of a river or canal.

The primary function of a modern floating thoroughfare is obviously equal to the function of a traditional road or ordinary bridge: 'serving for a safe and comfort passage for traffic under different kinds of (climatologically) circumstances'. For appropriating a permanent (read: lasting) position in the Dutch infrastructure, however, it is not enough for a floating thoroughfare to meet the functional requirements. A floating thoroughfare must be more attractive or feasible than a road or bridge as well. Being attractive or feasible depend on how a floating thoroughfare is able to anticipate on recent and future demands and development.

In the definition, a new solution ('supported…supports'), dimension ('move…level') and application ('in a river or canal') is introduced for a future road. These ingredients serve as a basis for an attractive and feasible solution.

In this section, a short review will be given on decisive development that gave the floating thoroughfare its multiple faces. After this, we will briefly discuss the road constructing methods and instantly try to categorize the latest idea of the floating thoroughfare.

2.1 Highlights in historic development

Since ancient times, people are used to travel across water differently than by boats. From records, it is known that the first floating bridge, as predecessor of the floating thoroughfare, was already invented in China in the 11th century BC. What the Chinese did, in fact, was making bridge sections out of two or more boats and a (wooden) deck, manoeuvred them into position and anchored them. From an anchored point, the bridge was repeatedly extended in this manner until the upper side was reached.

TUDelft

Due to this design principle, these bridges could also easily be deconstructed and, if section parts are not too heavy, carried, what made them very popular in wartime. Since it was often more feasible to construct a floating in stead of a suspension bridge, the primitive design of a floating bridge even lasts until early modern periods.

As late as the second half of the 19th century, the design of floating bridges eventually developed rapidly. Due to the industrial revolution, modern materials were applied and the boats were replaced by barge-or-boat-like pontoons, changing the name into 'pontoon bridge'. Later, in the beginning of the 20th century, pontoon bridges were constructed that could also carry light automotive vehicles.

During the World Wars, pontoons were extensively used by both the army and the civilians, particularly by the Red Army, which developed fast assault pontoon bridging techniques to facilitate their offensive operations. Due to fast installation requirements, these designs were adapted to be self supporting, and therefore supporting barges or boats were omitted. To an almost comparable extend was the development of permanent pontoon bridges, looming up in sheltered areas, where it was not considered economically feasible to suspend a bridge between anchored piers. Unfortunately, in those days, research could not prevent that many of these structures had to be broken down in their early days or even collapsed.

After the Second World War, research professionalized because of many negative experiences from both the military and the civilian field. Most of the time, dislodgement and inundation of bridges could be contended with a load limit. However, more often it happened that other unrecognizable phenomena dominate the behaviour of the bridge. When a bridge is induced to sway or oscillate due to the regular stride of a group of soldiers or by other types of repeated loads, it can cause hazardous situations and damage to the bridge as well. A lot of research was performed on these topics.

In modern times, due to extensive research, pontoon bridges emerge when they are economically and technically more feasible than a suspension bridge even when the crossings are more than a mile. In the military field, these structures have repeatedly been optimized being now the most modern variant of the pontoon bridge, the Assault Float Ribbon Bridge.

2.2   Categorization of modern floating thoroughfares

From the pontoon bridge development and the nomenclature in the definition, it can be concluded that competition between floating thoroughfares and (fixed) bridges, analogous to floating bridges and fixed bridges, can be expected. However, nothing is farther from the truth. As a matter of fact, it is economically and practically no longer feasible to construct a floating thoroughfare between two opposite sides of a river or canal instead of a bridge, with exclusion of a few exceptions. For example, when a bridge is closed for maintenance and a duplicate road is necessary to fulfil the bridge's task. It is for this reason that the words: 'river' and 'canal' in the definition must be read in its broadest perspective; i.e. as 'spatial elements to construct on' instead of 'obstacles for traffic'. From

TUDelft

this perspective, the latest idea of the floating thoroughfare comes closer to a road than a (floating) bridge.

Assigned as road, floating thoroughfares are not everywhere feasible: in the Holocene regions of the Netherlands, where soft soils dominate the infrastructural domain, roads that are going to be (re)constructed are susceptible for a floating alternative.

Traffic –in particular- in these regions is served by the savings of construction time and low maintenance. Unfortunately, this involves (very) high construction costs. At the same time, it holds that, without taking special measures, the shorter the construction time must be, the larger the settlement becomes and therefore the higher the maintenance costs will rise, generally speaking. Due to special measures, for example, maintenance and settlements can be reduced while construction time can be saved as well. We distinguish four types of special measures (methods) by their capacity to oppose settlement (figure 2.1):
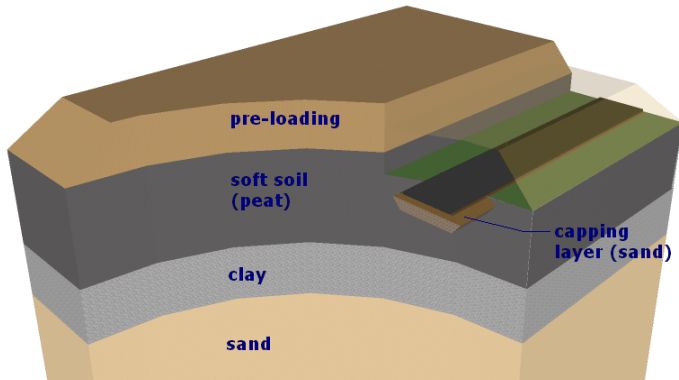
- <u>Traditional method on sand (sand bodies) including preloading</u>. The road bed (capping layer) is filled with sand. Preloading is required to minimize the primary settlement.
- <u>Settlement-reducing method (without preloading)</u>. The road bed is filled with EPS (Extruded Poly Styrene) or porous concrete. Light weight materials are used to reduce the settlement.
- <u>Settlement-forcing method</u>. The road bed is filled with sand and inside the soft subsoil, the air pressure will be decreased (BeauDrain) and the groundwater level lowered (IFCO) to perform the soil to consolidate quicker than normal to reduce the settlement.
- <u>Settlement-free method</u>. These constructions are diverse: self-supporting constructions are able to transfer loads via concrete slabs and piles to the solid ground. A variant is the armed soil construction for which concrete slabs are replaced by a road bed with geo-grids or geo-textiles as armour layer.

In the 'floating method', preliminary roadwork will mainly include excavating and damming of the soft soil while the water table will be maintained. The 'floating method' has technically the most agreement with a settlement-free method, since road structures are 'decoupled' from the subsidence-sensible subsoil. The fundamental difference between both methods is that (fluctuating) (ground) water is considered as threat for the settlement-free method and as construction element in the 'floating method'.

From a technical, (socio-) economical and political point of view, the 'floating method' is needed to overcome (fluctuating) (ground) water problems which will assume increasing seriousness. This new type of road construction method outshines all other methods in the field of sustainability, but - if it involves small floating elements- in the field of flexibility as well. Small elements can be installed rapidly, are transportable and (re)usable at other locations.

Once a complete floating thoroughfare is installed, as part of a (primary) traffic network, it must meet the serviceability and safety demands associated with this traffic network. Unlike floating bridges, floating thoroughfares are expected to be accessible for high speed
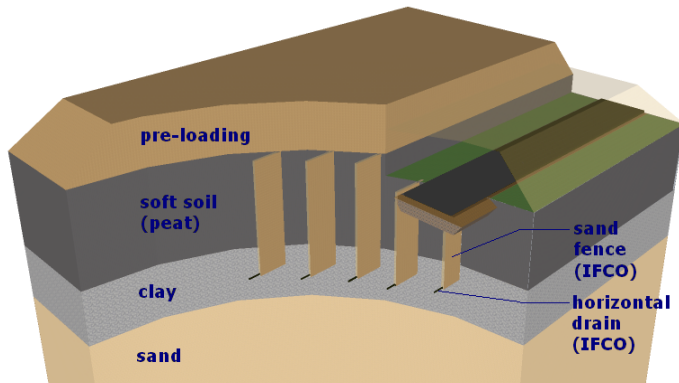
TUDelft

traffic, even when weather conditions become bad. The technical feasibility will be investigated in this report.
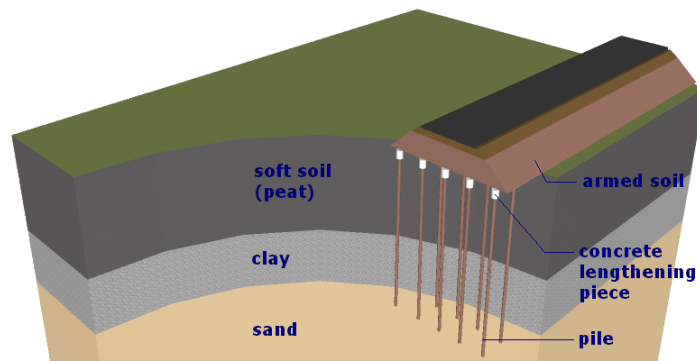
Traditional method on sand including pre-loading
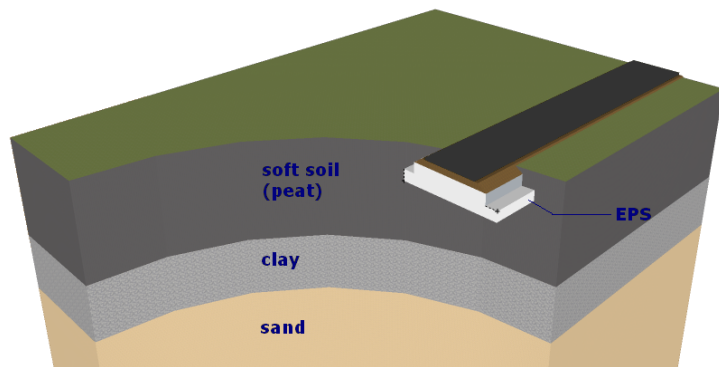
Settlement-reducing method (without preloading)

Settlement-forcing method (IFCO)

Settlement-free method (Kyoto-road)

Figure 2.1   conventional road construction methods

3 Argumentation and most recent research

Since the Second World War, many studies and tests were performed to develop floating bridges and thoroughfares. These studies were necessarily addressed to unrecognizable phenomena (sway, resonance, etc.) which caused a lot of trouble.

Recently, in the Netherlands, research was appointed to a new phenomenon on this topic: induced vibrations by *modern traffic*. The objective of this study was to develop a new type of floating thoroughfare that can be applied to accomplish: 'the transfer of vehicles from the traffic to the fairway network'. Unfortunately, this research was suspended because of too much subjectivity around the concept idea.

In this section, a short review will be given on the unsuccessful prototype study and the possibilities for future floating thoroughfares.

3.1 Why floating thoroughfares?

The main reason to construct a floating thoroughfare is that, due to a (fluctuating) (ground) water level, other construction methods become insufficient or inapplicable. Floating thoroughfares are literally gaining ground because the (ground)water level is forecast to rise during decades to come and water containment is expected to present serious challenges. Consequently, in the vicinity of rivers, (wet) land is yet assigned as flooding basin and more of these political measures will follow.

In the meantime, whether an unconventional construction method is feasible, depend - like conventional construction methods- strongly on local conditions as water table, soil structure, overhead clearance, etc.

For conventional construction methods, calculation models are developed for comparing the pro's and cons in a transparent and objective way. In these models, settings are calculated in proportion to construction time and construction and maintenance costs. On the basis of an 'arbitrary soil configuration' for West Netherlands, Deltares[1] has studied outcomes of 4 available models to six conventional methods, which are illustrated in figure 2.1. Outcomes of this study are evaluated in the table of figure 3.1 and compared with the traditional method on soft soils.

Through the outcomes of this study, critical pro's and cons of the floating construction method can be appointed and assessed without making use of the models themselves.

In the utmost right column of figure 3.1, outcomes associated with the floating construction method are printed in bold type. Regarding the table, we may assume that there is agreement with self supporting construction methods and with EPS construction methods to a less extent. The criterion of 'construction costs' has profound implications and although 'unknown' in this stage, it is expected being not in favour of the floating construction method. This is a consequence of its innovative character as well as extensive demands on the performance, expressed in material and labour costs. Anyhow, costs

[1] refers to publication in journal Land+Water 3/2008

TUDelft

efficiency is indispensable, since self supporting construction methods are offered cost efficiently too. Recently, engineers have developed the Kyoto-road, in which the traditional road bed with concrete piles is replaced by dredged silt, a waste product, with much cheaper wooden piles.

From a technical and practical point of view, spatial occupation and construction time are positive indicators in favour of the floating construction method; for example, a floating double-lane road is approximately 20 meters wide, while a traditional double-lane road, 1 meter above the ground, is measuring less than 45 meters. Construction time is saved due to a superstructure that can easily be constructed out of prefabricated elements. Moreover, prefabrication gives a surplus value to maintenance costs and time as well.

It is important to realize that outcomes are related to the traditional method and based on a standard configuration. This means that for site-specific situations, outcomes may vary and models must determine if a floating thoroughfare is feasible or not in that situation.

Criterion	Indicator	Construction method						
		Trad.	IFCO	BeauDrain	Light weight	EPS	Self support	**floating**
Technical specification	Plainness, rel. setting	0	+	+	+	++	++	**++**
	Spatial occupation	0	+	+	+	+	+	**++**
	Damage to cables, conduit and buildings	0	+	+	+	++	++	**++**
	Damage to road due to increase of capacity	0	-	-	+	++	++	**NA**
Costs	Construction costs	0	-	-	-	--	--	**--**
	Costs for limiting effect on water balance	0	0/-	0/-	0	0/-	0	**0[1]**
	Maintenance costs	0	+	+	+	++	++	**++**
Time	Construction time	0	+	+	+	++	++	**++**
	Time for maintenance	0	+	+	+	++	++	**++**
Remaining	Experience	0	0	0	0	0	-	**--**
	Sensible for right performance	0	-	-	-	--	-	**--**
	Restriction due to underground infrastr.	0	0	0	-	--	-	**-**
	Sensibility for interference (rise water level, loading)	0	0	0	-	--	--	**+/++**
	Construction phases, logistics	0		Location dependent				

+ = favourable, 0 = neutral, - = unfavourable

Figure 3.1   table with score of diverse construction methods relative to traditional method

[1] water balance should not be limited, but maintained. What this maintaining will be is unknown in this stage.

TUDelft

3.2   Unsuccessful prototype study

Expectations ran high in advance of the first study on floating thoroughfares in the Netherlands. Research should determine whether long-term infrastructural bottle-necks can be addressed through these structures. To increase the chance of success, it was the idea to create support as broad as possible. Therefore, this study was performed in cooperation of trade and industry, social organisations and knowledge institutes, under the auspices of the Dutch Directorate General for Public Works and Water management (RWS).

The main infrastructural bottle-neck is the inflexibility of the nearly overcrowded traffic (and railway) network, that is actually getting worse. Because the third network, the fairway network, is just partially crowded by ships and vessels, the idea arose to pursue for uniformity amongst all three networks. The 'transfer' of vehicles from the traffic net to the fairway net was considered as the key to the inflexibility problem, in a short and long term.

A new pilot was launched as part of the innovation programme 'Wegen naar de Toekomst' (roads to the future) in order to examine the feasibility of the vehicle transfer (figure 3.2).

Theoretical research concentrated on testing and monitoring of a prototype. A single-lane prototype was located in a river and subjected to a vehicle that crossed the structure with 30, 50 and 80 km/h. A short description and some important characteristics of this prototype can be found in Appendix I. The prototype passed the tests, but despite this success, developers did not manage to find a suitable location, designation or application. The following has been given as reason for this:

- Tests were addressed to small. Technically, the potential for testing is limited by the small size of the structure. Speeds were limited to 80 km/h and extensive tests with several vehicles on the road were not included. Moreover, site-specific testing was chosen over in situ testing so the link with reality essentially did not exist.
- The design was too exuberant. Based on ideas of trade and industry, a consortium[1] developed a aluminium prototype with intelligent links between the pontoons. Principles as standardisation, little maintenance, recyclable, transportability and prefabrication were held in the design, what made the prototype less suitable as permanent solution. Due to transportability, the pontoons can be carried by lorries, however, their limited size excludes the lorries of making use of this passage. Furthermore, in this temporary performance, it is way too expensive for application. (€5.6 million for 70 meters of thoroughfare!)

Both arguments have their origin in one and the same argument: the idea would have remained subjective. This is because to much freedom was included in the pilot while basically no real objectives were formulated. There was also the case that, because of the broad support, the pilot would be 'adversely' affected. "People would feel nothing for an innovation in this form". This was later (in 2004) confirmed in a development project ('Doorwerking Drijvende Weg') and for this reason the research was temporally suspended.

---

[1] Bayard Aluminium Constructies, DHV Milieu en Infrastructuur, TNO – Bouw and XX-architecten formed the consortium, named: 'De Bouwsteen Combinatie'
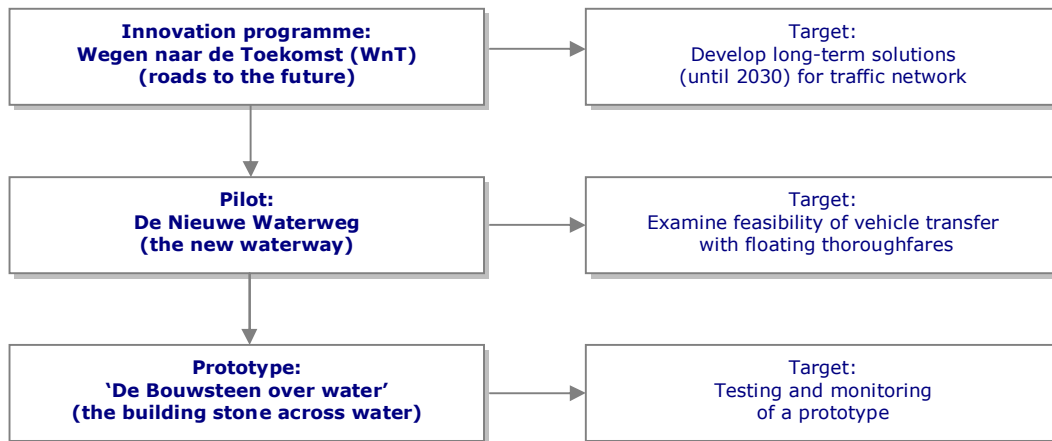
TUDelft

```
┌─────────────────────────────────┐        ┌─────────────────────────────────┐
│   Innovation programme:         │        │   Target:                       │
│ Wegen naar de Toekomst (WnT)    │───────▶│ Develop long-term solutions     │
│   (roads to the future)         │        │ (until 2030) for traffic network│
└─────────────────────────────────┘        └─────────────────────────────────┘
                │
                ▼
┌─────────────────────────────────┐        ┌─────────────────────────────────┐
│   Pilot:                        │        │   Target:                       │
│ De Nieuwe Waterweg              │───────▶│ Examine feasibility of vehicle  │
│   (the new waterway)            │        │ transfer with floating          │
│                                 │        │ thoroughfares                   │
└─────────────────────────────────┘        └─────────────────────────────────┘
                │
                ▼
┌─────────────────────────────────┐        ┌─────────────────────────────────┐
│   Prototype:                    │        │   Target:                       │
│ 'De Bouwsteen over water'       │───────▶│ Testing and monitoring          │
│ (the building stone across water)│       │ of a prototype                  │
└─────────────────────────────────┘        └─────────────────────────────────┘
```

Figure 3.2   targets in the study for a floating thoroughfare

3.3   Possible applications in the near future

As a result of increasing urbanization and industry, in the coming years, there will be more traffic in the Netherlands. A growth of 20%[1], compared to the level of 2000, is forecast for the next decade to come, what is comparable to the growth in past decade. Direct consequences of this growth will be that travel times are 'uncertain' and delays will increase enormously. In 2020, 13% of all vehicular movements over 50 kilometres is maximum 20% longer or shorter than expected and at shorter distances 10 minutes longer or shorter than expected. In 2000 this was just 8%. On the primary traffic network, delays in 2020 will be almost twice as long as in 2000 and for the Randstad[2], where most of the trips are smaller than 30 kilometres, it can rise even harder.

Traffic jams have direct financial consequences for businesses. The social costs of congestion amount to € 1.7 billion in 2020. This concerns the costs of direct travel time loss, valued to travel motives. These costs are further rising by the unreliability of travel time and fallback behaviour to avoid congestion.

The negative scenarios here underlie the Dutch national traffic and transport policy, which is currently in force[3]. The traffic and transport policy, documented in the traffic and transportation plan 'Nota Mobiliteit 2004' (Note Mobility 2004), is aiming for 'reliable' and 'acceptable' travel times all over the (primary) traffic network. As a consequence of this, the economic losses reduces but even more important: the economic centres in the infrastructure are made internationally competitive what is necessary to consolidate the economic position of the Netherlands. The ambition of the policy makers (government represented by the ministry for transport) is that 'reliability' increases to 95% ('uncertainty' reduces to 5%) and that qualities about 'acceptability' (in terms of delay) are fulfilled. The latter demand is for (ring)roads in urban less stringent as for highways.

---

[1] all values are likely to be adjusted in relation to the economic crisis of 2008-2009.
[2] the rim-shaped agglomeration of cities in the western part of the Netherlands
[3] the Note goes through the process of a planning key-decision (pkb) in accordance to the Law on Spatial Planning (WRO) and has a duration of 15 years.

TUDelft

The quality drawn up in the Note is:

- An average travel time during rush hours is maximum 1.5 times longer than an average travel time during other daily hours on a highway.
- An average travel time during rush hours is maximum 2 times longer than an average travel time during other daily hours on a (ring)road in an urban environment.

The question is how to live up to the ambition? The Note proposes packages of measures that can be distinguished by 'mobility-enhancing' measures and 'mobility abatement strategies', which often prove to be innovative.

The main asset in the hands of the government concerning 'mobility abatement strategies' is undoubtedly price policy. Or in other words: a charge per kilometre. The Dutch central planning office (CPB) bases calculations on two different forms of price policy: a uniform charge per kilometre[1] and a place and time dependent charge[2]. These charges have distinct effects on 'reliability', 'vehicle-loss-hours' (as a measure of delay) and other scenarios as road safety and emissions but are –except for safety- much more effective with respect to the present-day fixed taxes policy anyway. Calculations show that 95% more 'vehicle-loss-hours' can be expected in 2020 when policy remain unchanged. The change-over to a uniform charge per kilometre yield a 30% reduction while the change-over to a place and time dependent charge yield an 80% reduction. Due to heavier charges during rush hours, the place and time dependent charge is very effective in controlling 'vehicle-loss-hours' since people are discouraged from driving in places where most 'vehicle-loss-hours' are obtained. Price policy has a similar effect on 'reliability'; positive, and a place and time dependent charge turns out to be more effective than a uniform charge, 90% compared to 88%. However, the fact that calculated levels are still below the quality levels, confirms that price policy alone is not enough to fulfil the ambition here.

According to the Note, it may even be assumed that all 'mobility abatement strategies' together, i.e. the most efficient transport streams within the infrastructure with the possibilities of today, are insufficient to fulfil the ambition here.

The focus in the Note lies on 'mobility-enhancement', i.e. enhancement and further expansion of the (primary) traffic network. With 'enhancement' is primarily intended: (further) 'use'. Examples are ramp metering, ramp and/or exit closure, improvement of connections in the secondary traffic network or separation of traffic streaming. Utilization measures are preferred because of their relative ease and inexpensiveness. With the advantage on road safety and emissions, traffic management measures, such as a dynamic overtaking ban for lorries and speed adjustments, are favourable as well. Unfortunately, utilization and traffic management measures have restrictions and in many cases the quality level is not achieved or sometimes the quality is even getting worse. When the traffic net capacity is already at its limits, the chance on losing quality is the greatest. Applying an integral approach to bottle-necks must prevent that a problem shift

---

[1] use is made of turning €2.5 billion in fixed car tax to a used-based charge.
[2] use is made of a charge to place and time with a concomitant reduction of fixed car tax by approximately € 700 million per year.

TUDelft

occurs, what is quite common in these situations. With bottle-necks is meant: locations where quality levels are not achieved. Figure 3.3 shows the bottle-necks to be solved in order to satisfy the drawn up quantities. Due to the currently inflexible and overcrowded state of the primary (and secondary) traffic network, it often becomes too complicated to solve bottle-necks through utilization alone, what leaves no other alternative than
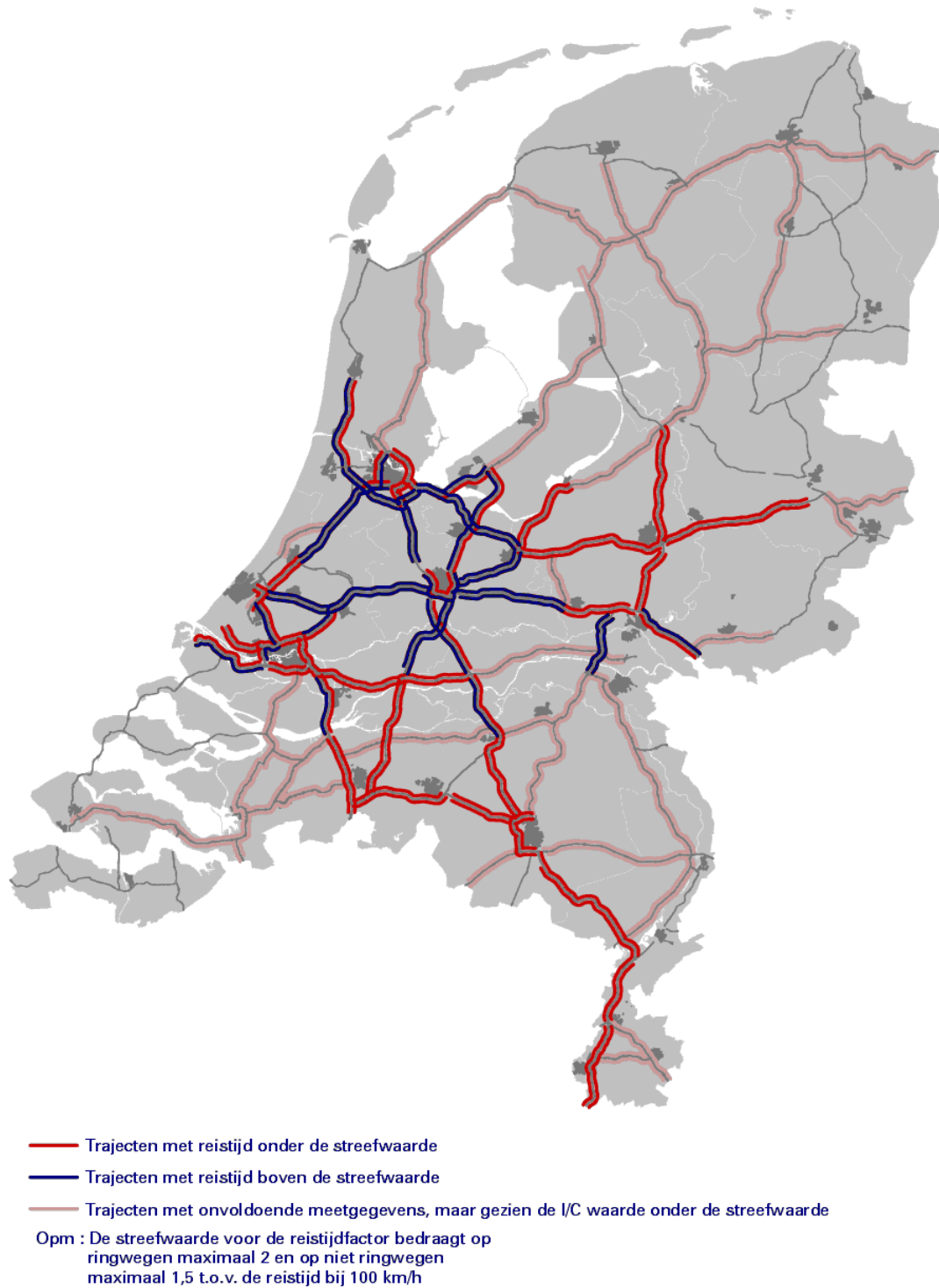

   ━━━━ Trajecten met reistijd onder de streefwaarde

   ━━━━ Trajecten met reistijd boven de streefwaarde

   ━━━━ Trajecten met onvoldoende meetgegevens, maar gezien de I/C waarde onder de streefwaarde

   Opm : De streefwaarde voor de reistijdfactor bedraagt op
        ringwegen maximaal 2 en op niet ringwegen
        maximaal 1,5 t.o.v. de reistijd bij 100 km/h

Figure 3.3   bottle-neck locations (black) in the Netherlands

TUDelft

expansion or construction. The Note recommends road widening stronger than constructing new roads. Only parallel to the most intensively used roads, new roads are planned. These will make the traffic network less sensible for interference so that travel times less 'uncertain' than before. In a few cases, however, will be invested in alternatives to road widening, for example on (ring)roads in an urban area where physical space can be scarce.

One disadvantage of more asphalt is more maintenance. In the period 2011-2020, an amount of approximately €900 million per year will be spend on maintenance only. Since the government intends to clear off outstanding maintenance as well, the total costs can rise over a billion euros per year. Extra maintenance result in extra costs but is also detrimental to road or network accessibility. Nowadays, 5% of all vehicle delays is caused by maintenance activity. Expressed in 'vehicle-delay-hours' this becomes: 3.3 million[1]! Therefore, the aim is to diminish traffic hindrance on the one side and keeping the total maintenance costs over the reference period (lifecycle costs) as low as possible on the other side.

Implementing these measures will cost the Dutch government big money; € 21.5 billion, which is far beyond the governmental budget. To reduce the expenses, construction will be attached to a price policy, so that € 7 billion flows back via charges. Priority is also given to main routes which are most interesting from an economical point of view. Since the routes include three highways, the A2, A4 and A12, they are known as the 'triple-A'-routes. Figure 3.4 shows the 'triple-A'-routes, which are largely located in the Randstad.
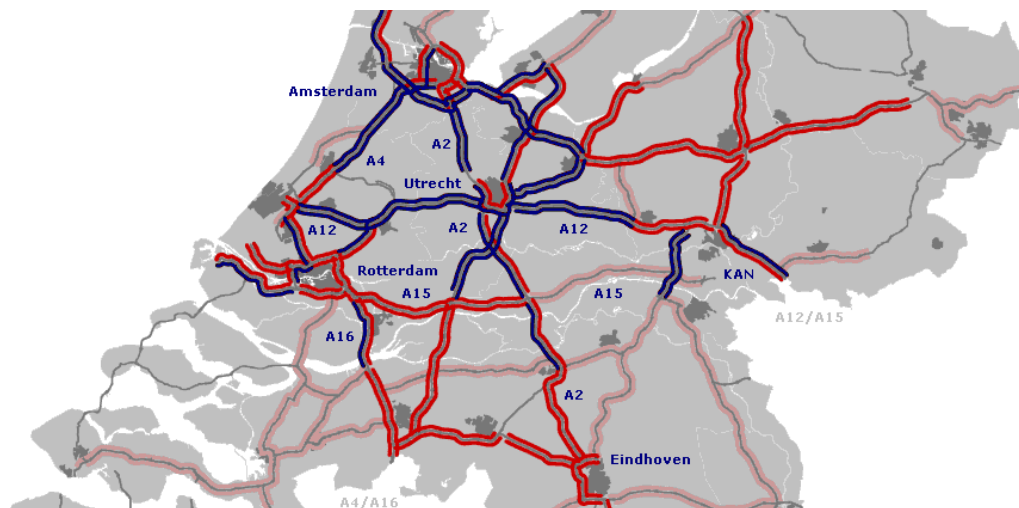

Route	Characteristic feature
A2	Highest rate of employment congestion from international business services (Amsterdam) and 'high-tech' industry (Eindhoven)
A4	The international route (together with A16) relevant to connect Schiphol Airport (with trading industry around Amsterdam) with the main ports in the Rhine-Schelde delta (Rotterdam and Antwerp)
A12	Forms a stable connection (together with A15) between Randstad and Utrecht, Utrecht and the KAN-region and the KAN-region with the Rühr-region in Germany.

Figure 3.4   'triple-A' routes

[1] updated data from RWS, until June 2009. Vehicle-loss-hours on primary network = 65.9 million hours

TUDelft

Reducing expenses whilst satisfying ambitions is achievable by the package: construction-utilization-pricing. The CPB accordingly calculates a reduction in delays of 15% (construction-utilization-uniform charge) over and 35% (construction-utilization-time and space dependent charge) below the reference level! Whether or not qualities about average travel times are met, must still be examined locally. For critical bottle-neck locations, on ring roads around Utrecht, Rotterdam and Eindhoven, calculations are optimistic: 9, 18 and 14 minutes, respectively, where 9,18 and 24 minutes (2 times longer) is the limit. The 'reliability' of travel times is guaranteed by 96% in case of construction-utilization-time and space dependent charge. (94% in case of construction-utilization-uniform charge).

In figure 3.5, the reservation of new routes is designated by dashed lines. Most of them are inside the 'triple-A' zone, due to the priority status. For most routes, the planning studies already commenced, just a few are still on hold.
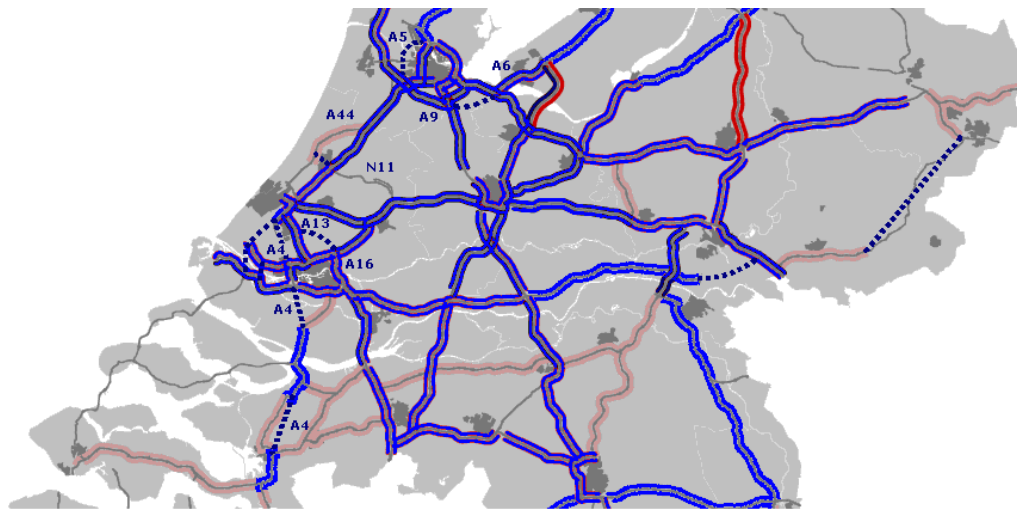
Route	Feature	Status of study in 2010
A4 Hoogvliet - Klaaswaal	Completion of A4	Not started
A4 Delft - Schiedam	Parallel connection for A13	Started
A4 Dinteloord – Bergen op Zoom	Completion of A4	Started
A5 2nd Coentunnel – westrandweg	(Ring)road A10 discharge	Started
A6 – A9	Road extension	Started
A13 – A16	Road extension	Started
N11 – A44	Road extension	Not Started

Figure 3.5   new routes and potential places for road widening inside the 'triple-A' zone

Planning studies are designed for searching an optimal solution, through collecting and assessing (with models of section 3.1) of several solutions, when situations are complex. A decisive factor in the assessment of new road sections in the Western part of the Netherlands is the permanent existence of high water tables. Experience shows that (large-scale) groundwater reduction can have disastrous consequences for agriculture since salinity can occur. Because salinity is common in coastal areas, precaution is needed when building (sections of) the A4, A5, the N11-extension and the A13-A16 connection to avoid damaging the environment.

Often, the problem is solved with return drainage, in which drained water will be pumped into the ground again, but at a respectable distance from the source. However, when the water balance continues to pass salt, the question must be asked again whether drainage is still desirable.

In figure 3.5, roads that are suitable for widening – in and around the 'triple-A'- are highlighted in blue. Usually, roads are suitable for widening from an economical and technical point of view, but sometimes, they are not, what gives rise to the start of a planning study. An example is the planning study for a highway on stilts on the route A27 Utrecht-Breda as an alternative to an extra wide highway. Assessment factors were the lack of overhead space and poor soil conditions on site. Within the triple-A zone, there are several routes for which space and soil factors play a decisive role; (ring) roads around the city of Rotterdam and sections of the A4, A12 and A13 highways, for example.
A so-called 'high option' is actually a little attractive option because it is very expensive and it ruins the landscape. It is therefore important to first explore all 'possibilities' aimed at maximum utilization of overhead space.

Which type of construction (method) will be applied is generally determined by construction and maintenance costs. However, due to a growing impact of roadwork on traffic, in the nearby future, a lower construction time or maintenance period becomes even more important than costs! A result is a shift in the way of tender. The contractor - instead of the government - is managing the road or road section and time overrun or profits will be punished or rewarded by the government. Consequently, in road construction, the emphasis is placed on the lifecycle rather than on which material, method or type of construction will be applied.

3.4   Conclusions

Theoretical research on developing a new kind of floating thoroughfare for the Netherlands was recently suspended because practical research on application of this structure became disappointing. During the research program, an insuperable gap between theory and practice was inadvertently created. This resulted in a thoroughfare that proved to be suitable for the river location in stead of feasible for contending long-term bottle-necks on the Dutch (primary) traffic network.

From subsection 3.3, it can be concluded that, on the short term, a reopening of the practical research seems to be out of the question. There is no urgency since all bottle-necks have theoretically proven to be solvable through a combination of constructing-utilization-pricing, thus without technical innovation on road construction. However, we deliberately write 'seems' because the responsibility for development of technical innovations is passed more and more on to business and industry. Business and industry is eager for (sustainable) innovation especially when short-term gains can be achieved. The sector takes the lead in developing innovations when it becomes convinced about, for example, the fall of the annual €1.7 bilion of social costs by congestion and the creation of new jobs. As soon as business and industry acknowledges the benefits of a floating

TUDelft

thoroughfare, the application of these structures will probably not wait very long and research can be reopend.

TUDelft

4 Problem definition and objectives

A floating thoroughfare is a technically feasible structure.

This is a true but narrow statement. Basically, this is true for one specific location where the structure was subjected to the motion of a single test vehicle. So, if this structure is also feasible outside the location, when vehicle tests are intensified and extended to more realistic situations, is still unknown.

Model tests must prove that floating thoroughfares can be feasible for a wider application from a technical point of view. An 'arbitrarily' chosen road section in the Dutch (primary) traffic network, were poor soil and groundwater dominate the area, represents the decisive situation for the case. The problems that have to be solved and the objectives in this investigation are discussed in this section. The steps to be taken in the calculation process will be illustrated by a flow diagram at the end of this section.

If a floating thoroughfare is feasible within a broader context, i.e. when it is subjected to extensive vehicle movements outside the location, cannot be established on the basis of the test results.

4.1 Problem definition

In the pilot, the prototype was designed for traffic velocities until 80 km/h and it must be able to withstand currents and wave attack at that specific location. Unlike the prototype, a floating thoroughfare which becomes part of the Dutch (primairy) traffic network will not be exposed to currents and waves. However, it will have just more to fear of traffic.

The main problem of this thesis is how to realize (model) a floating thoroughfare that is able to facilitate as a safe and comfortable passage for traffic.

4.2 Objectives

A floating thoroughfare has to be developed that is capable of carrying traffic (single and multiple vehicle(s) with max. velocity: 120 km/h) to such a level that it can become a feasible alternative for a conventional road. Floating thoroughfares have a quite complex dynamic behaviour, even if currents and waves are not involved. Many structural and hydraulic factors influence the (hydro)dynamic behaviour, however, no study had been performed on these factors within the scope of floating thoroughfares. Neither by testing nor by a proper simulation model. With this knowledge, a model can be created to determine the magnitude of these factors at various traffic conditions. The model can be used as design tool to construct a preliminary, theoretical design yet in an early stage of the design process. The main objective of this thesis is therefore twofold:
- to develop a computational, analytic, model of a floating thoroughfare as well as to assess the influence of structural and hydraulic factors on the dynamic behaviour (sensitivity analysis).

TUDelft

- to use the model to prove that a floating thoroughfare is feasible in many applications from a technical point of view.

It is crucial to realize the importance of a pilot as a pioneer when creating a model. Under specified circumstances, it can be applied as verification tool, but most important, it can be used as prediction tool as well. For example, some realistic, decisive traffic conditions can be predefined from the pilot what reduces the number of (computational) tests for the model significantly.

4.3   Input - / output model

For the following sections, an input- / output model is used for the objectives for the previous subsection to prove to come up to expectations.

The floating thoroughfare will be simulated numerically in Matlab and modelled as a rigid multibody system. For the calculations, the ODE23s solver, as presented in section 6, will be applied. ODE means: Ordinary Differential Equation.

The output of the model consists of rotations and displacements of all pontoon sections (bodies) that are involved. Since boundary conditions are denoted as accelerations, displacements will be differentiated twice in time.

The input of the model is divided into structural and hydrodynamic parameters. Structural parameters are discussed in section 5 and, initially, the parameters hold in the pilot will be reference parameters for the sensitivity analysis. Hydrodynamic parameters are calculated from an external, wave diffraction model, to optimize the hydrodynamic behaviour in the model.

After inserting the rigid multibody system in the ODE23s solver, the eigenmotion will be validated and correctness of all input will be checked by decoupling of the system. Then traffic in its proposed state of appearance will be implemented as well as the hydrodynamic parameters. The forced vibrations will be calculated
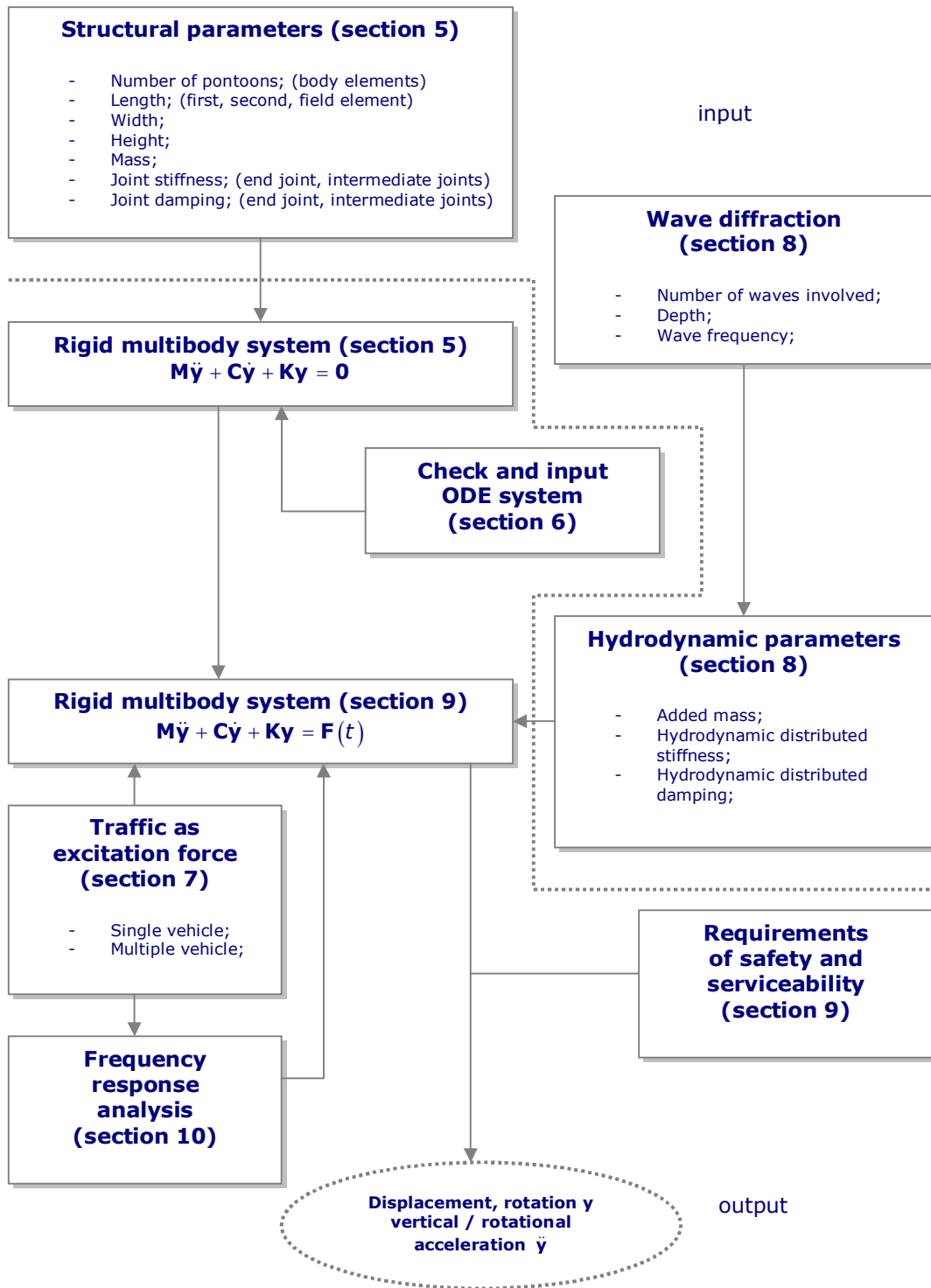
TUDelft

Structural parameters (section 5)

- Number of pontoons; (body elements)
- Length; (first, second, field element)
- Width;
- Height;
- Mass;
- Joint stiffness; (end joint, intermediate joints)
- Joint damping; (end joint, intermediate joints)

input

Wave diffraction (section 8)

- Number of waves involved;
- Depth;
- Wave frequency;

Rigid multibody system (section 5)
$$M\ddot{y} + C\dot{y} + Ky = 0$$

Check and input ODE system (section 6)

Hydrodynamic parameters (section 8)

- Added mass;
- Hydrodynamic distributed stiffness;
- Hydrodynamic distributed damping;

Rigid multibody system (section 9)
$$M\ddot{y} + C\dot{y} + Ky = F(t)$$

Traffic as excitation force (section 7)

- Single vehicle;
- Multiple vehicle;

Requirements of safety and serviceability (section 9)

Frequency response analysis (section 10)

Displacement, rotation y vertical / rotational acceleration $\ddot{y}$

output

Figure 4.1   schematization input- / output

TUDelft

5 Schematization of the floating thoroughfare

For modelling, a proper translation of the floating thoroughfare's mechanism is essential. The mechanism can be schematized with masses, springs and dampers, which is obviously an idealization.

In this section, the mass, stiffness and damping matrices are determined after clearing up the proposed idealization.

5.1 Idealization
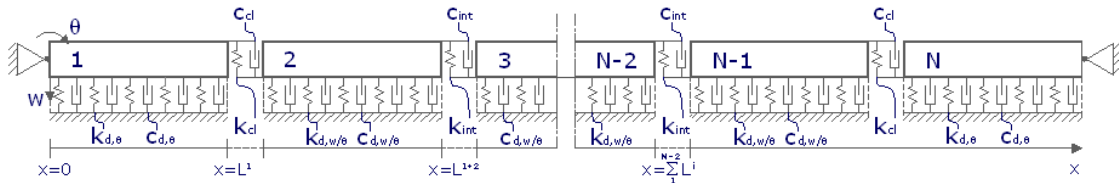
Figure 5.1   schematization of multibody system

Each pontoon is rectangular and box-shaped and does not bend. Bending of a pontoon is negligible with respect to internal displacements in the joints.

The floating thoroughfare will be modelled as a rigid multibody system with *N* bodies. The interconnected bodies facilitate a two degrees of freedom motion (vertical and rotational) per body, except for the end or closing bodies which will perform only the rotational motion. Figure 5.1 shows the schematization of the system.

No horizontal motion is assumed to occur in the multibody system. The hinges govern only vertical support to the floating highway what is in good agreement with the real situation.

5.2 Mass moment of inertia and mass of body

The bodies are rectangular shaped. Body height and width are constant in time and in space and the mass centre coincide the geometric centre. The applied simplifications are only justified for modelling purposes.

The mass of an single body can be calculated from:

$$m = \rho_0 hBL \tag{5.1}$$

Where:

ρ_0 :   body density; $\rho_0 = 102.5 kg/m^3$

L :   body Length; $L = 3.5m$ [1]

h :   height of body; $h = 1.6m$

B :   width of body; $B = 5.4m$

---

[1] For the present being equal for all bodies, but becomes adaptable for $L^{1,N}$ if necessary in section 6 and 7.

This leads to a mass of 3100 *kg*. Since the axes of rotation of closing and intermediate bodies have different positions their mass moments of inertia about these axes will be unequal. Taking the origins of the body reference to the mass centre of the body, the inertial moments becomes:

$$J^{1,N} = \frac{1}{12}\rho_0 hBL^{1,N}\left(4\left(L^{1,N}\right)^2 + h^2\right) = 13317.0 kgm^2$$

$$J^{i} = \frac{1}{12}\rho_0 hBL^{i}\left(\left(L^{i}\right)^2 + h^2\right) = 3825.4 kgm^2 \quad for\left\{i\middle|2 \leq i \leq N-1\right\}$$

(5.2)

In which:

N :   total number of bodies; $N = 20$ [1]

i :   body number

The applied formulas are elaborated in Appendix III.

5.3   Mass Matrix

The mass matrix of the total system is diagonal. This is the result of decoupling mass and inertia by shifting the origins of the body references to the mass centre of each body. The mass matrix **M** has the form:

$$\mathbf{M} = \begin{bmatrix} J^1 & 0 & & & & & & & & \\ 0 & m^2 & 0 & & & zeros & & & & \\ & 0 & J^2 & 0 & & & & & & \\ & \vdots & & \ddots & \vdots & & & & & \\ & & & 0 & m^i & 0 & & & & \\ & & & & 0 & J^i & 0 & & & \\ & & & & & \vdots & \ddots & \vdots & & \\ & zeros & & & & 0 & m^{N-1} & 0 & & \\ & & & & & & 0 & J^{N-1} & 0 & \\ & & & & & & & 0 & J^N \end{bmatrix}$$

(5.3)

Since the vertical degree of freedom is omitted, the mass of the closing bodies is zero in the matrix, so analogous to equation 5.2 we write:

$$m^{1,N} = 0$$

$$m^{i} = \rho_0 hBL^{i} = 3100 kg \quad for\left\{i\middle|2 \leq i \leq N-1\right\}$$

(5.4)

5.4   Body stiffness matrix: first, second and field body

In principle, two physical elements contribute to the stiffness properties of the system:
- Joint elements
- Fluid foundation

---

[1] $N = 20$ is the prototype number, in section 6 and 10, the value can differ from 20.

TUDelft

How the design of joints for the new type of floating thoroughfare will look like, is unknown in this stage of the investigation. Basically, the calculated joint stiffness is the basis for the preliminary design. Assuming that joints will react 'stiff' in the vertical direction and that an infinitesimally small internal displacement is allowed, the joint elements can be modelled in its mechanically simplest form, i.e. as vertical linear spring elements (figure 5.1). We assume further that, as a matter of refinement, manipulation of two joints - between the closing and intermediate bodies- can be done independently from all others. The reason for this is twofold: firstly, we expect them to behave differently with respect to the neighbouring ones while a more equivalent behaviour is desirable and secondly, one of the two topics of interest in this thesis concerns entering the system by vehicles so this measure creates also a more effective and easier way to manipulate the dynamic behaviour of the floating structure.

Concerning the fluid foundation, initially, Archimedes Law, as a rough approximation will provide stiffness parameters for buoyancy. In case of vertical equilibrium we will find with a fluid density of $\rho = 1000\,kg/m^3$ and a gravitational acceleration of $g = 9.81\,m/s^2$:

$$k_{d,w} = k_d = \rho g B = 52974\,N/m/m^1 \tag{5.5}$$

Where a couple of equally distributed springs experiences the buoyancy phenomenon. Subscript $_d$ and $_w$ indicate that stiffness is distributed and initiated in the w-direction. 'Averaged' expressions can be found for the angular motion as shown in figure 5.2. Similar substitution leads to:

$$k_{d,\theta}^{1,N} = \frac{1}{3}\rho g B \left(L^{1,N}\right)^2 = \frac{1}{3}k_d\left(L^{1,N}\right)^2 = 216311\,Nm/rad/m^1$$

$$k_{d,\theta}^{i} = \frac{1}{12}\rho g B\left(L^i\right)^2 = \frac{1}{12}k_d\left(L^i\right)^2 = 54078\,Nm/rad/m^1 \quad for\,\{i\,|\,2 \le i \le N-1\} \tag{5.6}$$

In section 8, another interpretation will be introduced, making also use of the damping capacity of the fluid; the wave diffraction approximation. Therefore, we explicitly denote buoyancy approximation or wave diffraction approximation if an indistinct situation will be announced.
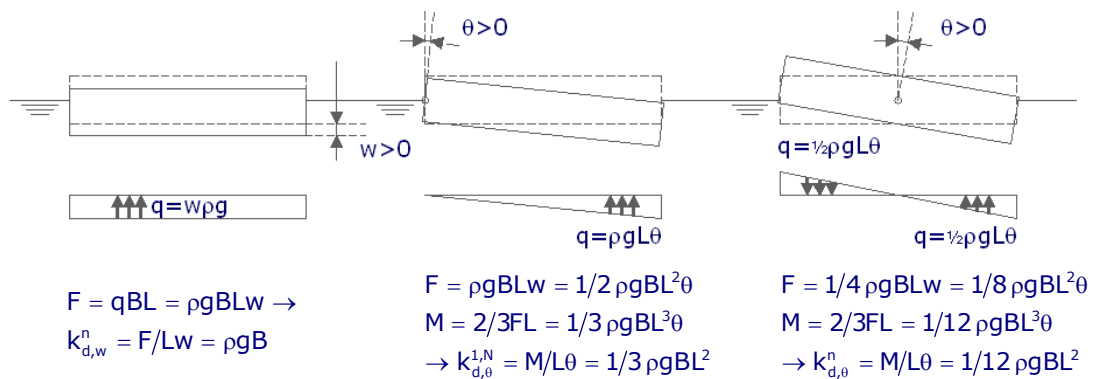
Figure 5.2   **stiffness parameters for buoyancy**

5.4.1 Derivation of body stiffness matrices

The derivation of the body stiffness matrices can be found in Appendix II. The matrices are subtracted from the force vector $\mathbf{F}^i$ and the displacement vector $\mathbf{y}$:

$$\mathbf{F^i} = \mathbf{K^i y} \rightarrow \begin{bmatrix} F_w \\ F_\theta \end{bmatrix}^i = \begin{bmatrix} k_{1,1} & k_{1,2} & k_{1,3} & k_{1,4} & k_{1,5} & k_{1,6} \\ k_{2,1} & k_{2,2} & k_{2,3} & k_{2,4} & k_{2,5} & k_{2,6} \end{bmatrix}^i \begin{bmatrix} w^{i-1} \\ \theta^{i-1} \\ w^i \\ \theta^i \\ w^{i+1} \\ \theta^{i+1} \end{bmatrix} \tag{5.7}$$

The following non-zero integers are determined for the first body, $\{i = 1\}$:

$$k_{2,4} = -k_{cl}\left(L^i\right)^2 - \frac{1}{3}k_d\left(L^i\right)^3 ,$$
$$k_{2,5} = k_{cl}L^i , k_{2,6} = -k_{cl} L^i L^{i+1}/2 \tag{5.8}$$

$k_{2,4}$ has the same expression as in equation 5.8 , $k_{2,5}$ as well as $k_{2,6}$ are zero now but $k_{2,1}$ and $k_{2,2}$ are non zero for the last body $\{i = N\}$. They read:

$$k_{2,1} = -k_{cl}L^i , k_{2,2} = -k_{cl} L^{i-1}/2 L^i \tag{5.9}$$

The second body with $\{i = 2\}$ gives:

$$k_{1,1} = k_{cl} , k_{1,2} = k_{cl}L^{i-1} , k_{1,3} = -k_{cl} - k_{int} - k_dL^i$$
$$k_{1,4} = -\left(k_{int} - k_{cl}\right)L^i/2 , k_{1,5} = k_{int} , k_{1,6} = -k_{int} L^{i+1}/2$$
$$k_{2,1} = -k_{cl} L^i/2 , k_{2,2} = -k_{cl}L^{i-1} L^i/2 , k_{2,3} = -\left(k_{int} - k_{cl}\right)L^i/2$$
$$k_{2,4} = -\left(k_{cl} + k_{int}\right)\left(L^i/2\right)^2 - \frac{1}{12}k_d\left(L^i\right)^3 , k_{2,5} = k_{int} L^i/2$$
$$k_{2,6} = -k_{int} L^i/2 L^{i+1}/2 \tag{5.10}$$

Where for the last but one body differs from the second by:

$$k_{1,1} = k_{int} , k_{1,2} = k_{int} L^{i-1}/2$$
$$k_{1,5} = k_{cl} , k_{1,6} = -k_{cl}L^{i+1}$$
$$k_{2,1} = -k_{int} L^i/2 , k_{2,2} = -k_{int} L^{i-1}/2 L^i/2$$
$$k_{2,5} = k_{cl} L^i/2 , k_{2,6} = -k_{cl} L^i/2 L^{i+1} \tag{5.11}$$

At last, the field bodies $\{i | 3 \le i \le N - 2\}$ denote:

TUDelft

$$k_{1,1} = k_{int} \, , k_{1,2} = k_{int} \, L^{i-1}/2 \, , k_{1,3} = -2k_{int} - k_d L^i$$

$$k_{1,5} = k_{int} \, , k_{1,6} = -k_{int} \, L^{i+1}/2$$

$$k_{2,1} = -k_{int} \, L^i/2 \, , k_{2,2} = -k_{int} \, L^{i-1}/2 \, L^i/2 \tag{5.12}$$

$$k_{2,4} = -2k_{int} \left(L^i/2 \right)^2 - \frac{1}{12} k_d \left(L^i \right)^3$$

$$k_{2,5} = k_{int} \, L^i/2 \, , k_{2,6} = -k_{int} \, L^i/2 \, L^{i+1}/2$$

In the functions 5.8-12, k_{cl} and k_{int} are joint stiffness parameters associated with the location of that specific joint. The stiffness matrix of the total system can be assembled with the body stiffness matrices as we subsequently superpose the decoupled motions to one vector. With the use of Matlab, it is an easy task to assemble a large system, see Appendix V.2.

5.5 Body damping matrix: first, second and field body

It is not clear now if energy by traffic induced motion need to be absorbed in order to satisfy safety and serviceability demands. Nevertheless, we expect the joint elements be able to dissipate energy if necessary so the element is equipped with a (vertical) dashpot, see figure 5.1. Concerning the fluid foundation, the wave diffraction approximation will simulate the effect of pushing aside fluid (water) beneath the structure during a downward motion. Equally distributed dashpots will exhibit the estimated physical behaviour.

5.5.1 Derivation of body damping matrices

The derivation of the body damping- and stiffness matrices has been done simultaneously in Appendix II. Because proportional damping (to only **K**) will be obtained equation 5.8 transforms into:

$$\mathbf{F^i} = \mathbf{C^i \dot{y}} \rightarrow \begin{bmatrix} F_w \\ F_\theta \end{bmatrix}^i = \begin{bmatrix} c_{1,1} & c_{1,2} & c_{1,3} & c_{1,4} & c_{1,5} & c_{1,6} \\ c_{2,1} & c_{2,2} & c_{2,3} & c_{2,4} & c_{2,5} & c_{2,6} \end{bmatrix}^i \begin{bmatrix} \dot{w}^{i-1} \\ \dot{\theta}^{i-1} \\ \dot{w}^i \\ \dot{\theta}^i \\ \dot{w}^{i+1} \\ \dot{\theta}^{i+1} \end{bmatrix} \tag{5.13}$$

In which $\mathbf{C^i}$ is related to the time derivative of the displacement vector **y** (viscous damping). In practice, $\mathbf{C^i}$ can be constructed out of $\mathbf{K^i}$ by simply replacing all k's by c's (in equation 5.8-12).

TUDelft

6   Numerical simulation with Matlab

In continuation of the previous section, the rigid multibody system will be analysed by a numerical integration method for solving the initial value problems. Numerical integration will be preferred instead of analytical solutions with eigenvalue problems, because the number of degrees of freedom can be large. Once the programming ended, the system's eigenvalues need to be validated and checked on input errors, for example.

6.1   Numerical solver

The equation of motion can be written as:

$$\mathbf{M\ddot{y}} + \mathbf{C\dot{y}} + \mathbf{Ky} = \mathbf{F}(t) \tag{6.1}$$

Where $\mathbf{M}$, $\mathbf{C}$ and $\mathbf{K}$ are $2N-2$ -by- $2N-2$ matrices and $\mathbf{y}$ and $\mathbf{F}$ are 1 –by- $2N-2$ vectors. Like many other computing devices, Matlab's ODE solvers deal with a discretisation methods for first order ordinary differential equations (ODE's) and cannot (directly) cope with higher order ODE's. A variable transformation will tackle that problem: With a state space formulation as result, equality $\mathbf{y}_2 = \dot{\mathbf{y}}_1$ is substituted into equation 6.1:

$$\begin{aligned}\mathbf{Y}_2 &= \dot{\mathbf{Y}}_1 \\ \mathbf{M\dot{y}}_2 + \mathbf{Cy}_2 + \mathbf{Ky}_1 &= \mathbf{F}(t)\end{aligned} \tag{6.2}$$

Or in matrix notation:

$$\begin{bmatrix} \mathbf{I_{2N-2}} & \mathbf{0_{2N-2}} \\ \mathbf{0_{2N-2}} & \mathbf{M} \end{bmatrix}\begin{bmatrix} \dot{\mathbf{y}}_1 \\ \dot{\mathbf{y}}_2 \end{bmatrix} = \begin{bmatrix} \mathbf{0_{2N-2}} & \mathbf{I_{2N-2}} \\ \mathbf{-K} & \mathbf{-C} \end{bmatrix}\begin{bmatrix} \mathbf{y}_1 \\ \mathbf{y}_2 \end{bmatrix} + \begin{bmatrix} \mathbf{0} \\ \mathbf{F}(t) \end{bmatrix} \tag{6.3}$$

Where:
$\mathbf{0_{2N-2}}$: $2N-2$ -by- $2N-2$ null matrices
$\mathbf{I_{2N-2}}$: $2N-2$ -by- $2N-2$ identity matrix

Since the mass matrix is a constant matrix, we are forced to use the ODE 23s solver for this problem. In general, the ODE 23s solver solves all ODE's in the form:

$$\mathbf{M}\dot{y} = f(t, y) \tag{6.4}$$

Where:
$\mathbf{M}$:   explicit, constant mass matrix.
$\dot{y}$:   general velocity coordinate or vector.
$f(y,t)$:   right hand side of the ODE, dependent of y and t (not necessary).

with the initial value:

$$y(t_0) = y_0 \tag{6.5}$$

TUDelft

The ODE 23s solver is based on a modified Rosenbrock formula[1] of order 2 and is a so called one step solver. This implies that for every time step the state will be recalculated. Besides this, the solver allows us to insert tolerance criteria (or relative tolerance of 10^{-3} and absolute tolerance of 10^{-6} by default) in order to prevent unstable and divergent computation. If the first calculation step does not satisfy the tolerance criteria, a next will follow with a smaller step size. The solver provides on the one hand output in the form of a mixed velocity/displacement vector of size $2N-2$ while on the other hand the argument

$$[\texttt{t},\texttt{y}] = \texttt{ode23s}\,(\texttt{odefun},\texttt{tspan},\texttt{y0},\texttt{options})\,; \tag{6.6}$$

Where:

`[t,y]` :	solution matrix `y` where each row corresponds to a time returned in the column vector `t` .
`odefun` :	function that evaluates the right side of the ODE.
`tspan` :	vector specifying the interval of integration
`y0` :	vector of initial conditions.
`options` :	optional integration argument using the odeset-function

need to be specified as input. Examples can be looked up in Appendix V.3.

6.2   Validation of dynamic behaviour; spreading of frequencies

In this subsection, the dynamic behaviour will be examined by imposing an initial displacement of say 0.1 m to the system after it was decoupled by its different (visco-) elastic elements; a model with exclusive spring-dashpot elements between the bodies and a model in which hinges perform the connection between the bodies as they are subjected to an elastic foundation. Both models will provide insight in the nature (magnitude and spreading) of the principal or natural frequencies of the multibody system which we want to investigate. We expect the system with elastic foundation to vibrate in the lower modes, whereas the other system vibrates in the higher ones. Decoupling, however, is permitted as long as the system is linear. The superposition principle holds so that back around, enumeration lead to natural frequencies of the total, uncoupled system, as schematized in figure 6.1. In general, validation is justified as long as the displacements are small.
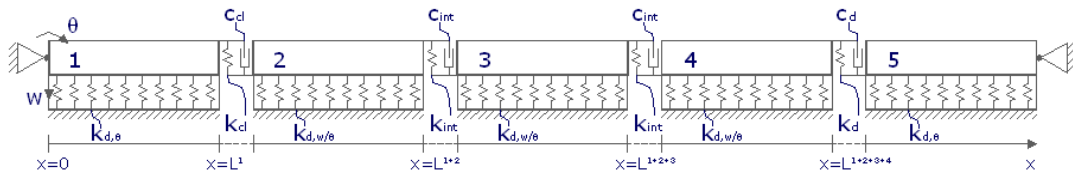
Figure 6.1   schematization of superimposed system

---

[1] we implicitly allow the state –space system to reduce to a Rosenbrock system for discretization. This is a method to deal with singular matrices.

TUDelft

6.2.1 Decoupled system

The schematization of both systems is shown in figure 6.2 and the homogeneous equations can be denoted as:

$$\mathbf{M\ddot{y}} + \mathbf{C\dot{y}} + \mathbf{Ky} = \mathbf{0} \tag{6.7}$$
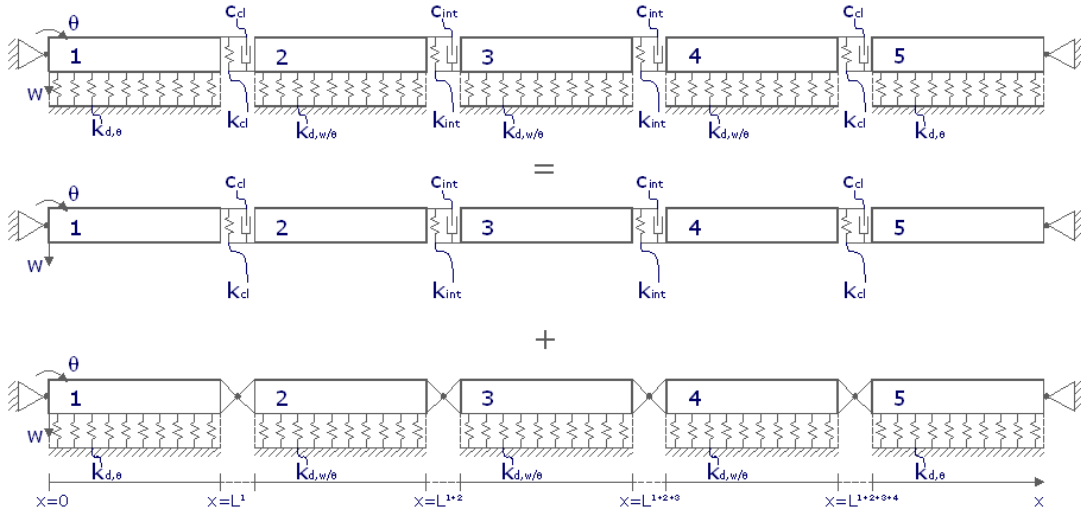
Figure 6.2 schematization of decoupled system

Because the damping is arbitrary (not proportional) the well known method for the Modal analysis [2] does not provide an uncoupled system. A more general procedure must be used. Equation 6.7 can be reformulated in a space state formulation, therefore a new variable must be introduced:

$$\tilde{\mathbf{y}} = \begin{bmatrix} \dot{\mathbf{y}} \\ \mathbf{y} \end{bmatrix} \tag{6.8}$$

Substitution of equation 6.8 into equation 6.7 gives:

$$\begin{bmatrix} \mathbf{0_{2N-2}} & \mathbf{M} \\ \mathbf{M} & \mathbf{C} \end{bmatrix} \dot{\tilde{\mathbf{y}}} + \begin{bmatrix} \mathbf{-M} & \mathbf{0_{2N-2}} \\ \mathbf{0_{2N-2}} & \mathbf{K} \end{bmatrix} \tilde{\mathbf{y}} = \begin{bmatrix} \mathbf{0} \\ \mathbf{0} \end{bmatrix} \tag{6.9}$$

This can be summarized as:

$$\tilde{\mathbf{M}}\dot{\tilde{\mathbf{y}}} + \tilde{\mathbf{K}}\tilde{\mathbf{y}} = \mathbf{0} \tag{6.10}$$

Where $\tilde{\mathbf{M}} = \begin{bmatrix} \mathbf{0_{2N-2}} & \mathbf{M} \\ \mathbf{M} & \mathbf{C} \end{bmatrix}$ and $\tilde{\mathbf{K}} = \begin{bmatrix} \mathbf{-M} & \mathbf{0_{2N-2}} \\ \mathbf{0_{2N-2}} & \mathbf{K} \end{bmatrix}$. With Ω as the complex-conjugate eigenvalue matrix of $\tilde{\mathbf{M}}^{-1}\tilde{\mathbf{K}}$ and $\mathbf{E}$ is the corresponding eigenvector equation 6.10 can be transformed by its orthogonality property into:

$$\mathbf{E}^{\mathsf{T}}\tilde{\mathbf{M}}\dot{\tilde{\mathbf{y}}} + \mathbf{E}^{\mathsf{T}}\tilde{\mathbf{K}}\tilde{\mathbf{y}} = \mathbf{E}^{\mathsf{T}}\tilde{\mathbf{M}}\mathbf{E}\dot{\tilde{\mathbf{y}}}' + \mathbf{E}^{\mathsf{T}}\tilde{\mathbf{K}}\mathbf{E}\tilde{\mathbf{y}}' = \tilde{\mathbf{M}}^{*}\dot{\tilde{\mathbf{y}}}' + \tilde{\mathbf{K}}^{*}\tilde{\mathbf{y}}' = \mathbf{0} \tag{6.11}$$

TUDelft

This is a fully decoupled differential equation. By multiplying the left hand side of this equation with $\left(\tilde{\mathbf{M}}^{*}\right)^{-1}$ and with the help of relation $\left(\tilde{\mathbf{M}}^{*}\right)^{-1}\tilde{\mathbf{K}}^{*}=\Omega$ we find:

$$\dot{\tilde{\mathbf{y}}}'+\Omega\tilde{\mathbf{y}}'=\mathbf{0} \qquad (6.12)$$

Where Ω is a diagonal matrix with ω_n $for\{n|1\leq n\leq 4N-4\}$ on the main diagonal. Substitution of equation 6.8 (with $\tilde{\mathbf{y}}=\mathbf{E}\tilde{\mathbf{y}}'$ from equation 6.11) into 6.12 leads to:

$$\dot{y}_n+\omega_n y_n=0 \quad for\{n|1\leq n\leq 4N-4\} \qquad (6.13)$$

since $y_n\neq 0$. Because we are only interested in displacements, the general coordinates must be replaced by a displacement variable. Because $y_n=\begin{bmatrix}w_n & \varphi_n\end{bmatrix}^T$ (see equation II.2) equation 6.13 changes into:

$$\dot{w}_n+\omega_n w_n=0 \quad for\{n|1\leq n\leq 2N-4\} \qquad (6.14)$$

in which n is halved minus two, since $y_n=\begin{bmatrix}0 & \theta_n\end{bmatrix}^T$ $for\{n|1,N\}$

With $\left(\mathbf{M}^{*}\right)^{-1}\mathbf{K}^{*}=\Omega$ Matlab can determine $\omega_{0,n}$ as has been done in Appendix V.2. As an example we set the boundary condition at $A_n=0.1/nm$ and the number of bodies $N=5$ in order to govern clear graphs for both cases. The (real part of the) homogeneous solution becomes:

$$w_n(t)=A_n e^{\left(-\text{Re}[\omega_{0,n}]t\right)}\cos\left(\text{Im}[\omega_{0,n}]t\right) \quad for\{n|1\leq n\leq 2N-4\} \qquad (6.15)$$

Where:
$A_n=0.1/nm$
$N=5$

Let us focus on the model with hinged bodies on the elastic foundation first. The following natural frequencies are calculated by Matlab:

$$\omega_{0,1}=\omega_{0,3}=\omega_{0,5}=0+7.734i$$

The even numbered frequencies, $\omega_{0,2},\omega_{0,4}$ and $\omega_{0,6}$ are the complex conjugates of respectively $\omega_{0,1},\omega_{0,3}$ and $\omega_{0,5}$. As can be seen in equation 6.15, the real and imaginary values of the natural frequencies govern respectively the damping and oscillating motion in the system. The system will vibrate in 3 vertical modes that do not damp out. The modes should oscillate in the same frequency, the so called cut-off frequency. The formula for the cut-off frequency reads [2]:

$$\omega_0=\sqrt{\frac{k_d}{\rho_0 A}} \qquad (6.16)$$

With $\rho_0=102.5\,kg/m^3$, $A=8.64m^2$ and $k_d=52974\,N/m/m^1$, the natural frequency equals:

TUDelft

$$\omega_0 = 7.734 rad / s \hspace{4cm} (6.17)$$

what validates the hinged multibody system with an elastic foundation. Figure 6.3 shows the response of the system in time.
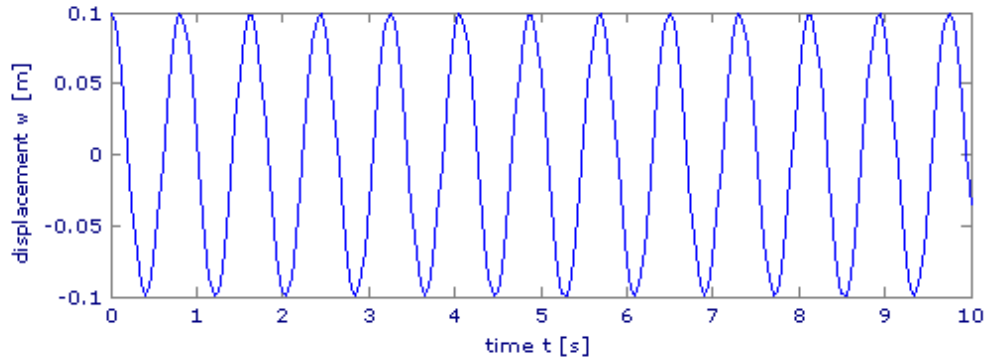
Figure 6.3 **response of hinged bodies on an elastic foundation to an initial displacement of 0.1m**

The second model with exclusive spring-dashpot elements between the bodies moves with the following natural frequencies:

$$\omega_{0,1} = 0.721 + 11.986i$$
$$\omega_{0,3} = 0.423 + 9.183i$$
$$\omega_{0,5} \approx 0 + 0i$$

where we keep the joint stiffness values proportional to the buoyancy stiffness value, $k_{cl/int} = 6*10^4 N/m$, and the joint damping at 1% of this value. As previously denoted, $\omega_{0,2}, \omega_{0,4}$ and $\omega_{0,6}$ are the complex conjugates of respectively $\omega_{0,1}, \omega_{0,3}$ and $\omega_{0,5}$. As previously assumed, the (non-zero) natural frequencies found here are slightly higher than the fundamental natural frequencies due to the elastic foundation, see equation 6.15. Subsequently, if we also focus on the real values of the natural frequencies, we see (in a broader spectrum than shown here) that the damping capacity increases as the system oscillates quicker. As a matter of fact, the configuration of the joints in particular will be quite important for controlling the forced vibrations exerted by (high speed) traffic load. The single natural frequency, $\omega_{0,5}$, with close-to-zero values causes a motion that is around a non-zero mean, just like a chain that experiences no support in the middle. This in contrast to the hinged multibody system with elastic foundation that is perfectly balanced at this point. Figure 6.4 shows the response of the system in time.

TUDelft
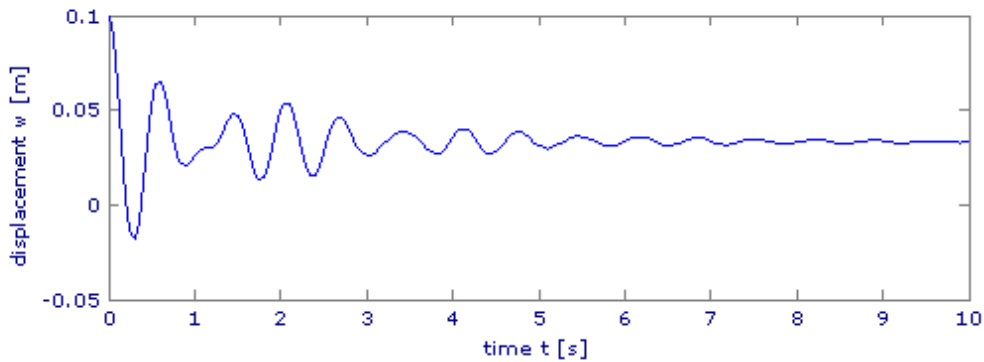
Figure 6.4   **response of interconnected bodies with spring-dashpot elements to initial**

                displacement of 0.1m

6.2.2 Superimposed system

With superposition of the decoupled systems the superimposed system as depicted in figure 6.5 will obviously return.
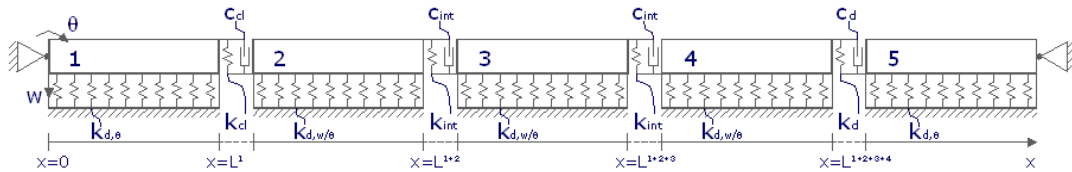
Figure 6.5   **schematization of superimposed system**

The following natural frequencies are associated with the superimposed system:

$$\omega_{0,1} = 0.720 + 14.004i$$
$$\omega_{0,3} = 0.422 + 11.969i$$
$$\omega_{0,5} = 6.802 * 10^{-4} + 7.430i$$

The (squared) frequencies must be equal to the (quadratic) sum of the frequencies of both decoupled systems, according to the superposition principle. This is approximately true; the superimposed system vibrates in three vertical modes from which the undamped third mode is quite similar to the modes from the hinged model with elastic foundation. The first and second modes, however, resemble the damped modes from the model with spring-dashpot elements better, but the oscillation is larger due to the foundation. In the response of the superimposed system, in figure 6.6, these findings can be observed as well; in the first five seconds, there is an apparent contribution of spring-dashpot elements to the response. After five seconds the contribution of the spring-daspot elements has vanished leaving behind the oscillatory response of the foundation, but with a reduced amplitude.
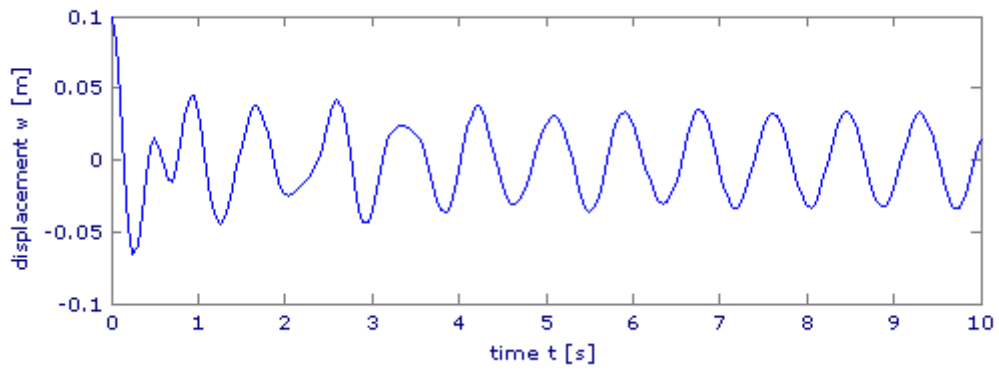
Figure 6.6   **response of infinite beam to initial displacement of 0.1m**

7 Idealization of traffic

For modelling, a proper translation of the traffic induced forces is crucial. In proportion of the topic of interest, traffic will be modelled as single vehicle and multiple vehicles. A single vehicle need to be constructed for the study of impact-like vibrations near the entrance of the structure and multiple vehicles when resonant vibrations are generated.

7.1 Design vehicle and design velocity

The design vehicle and the design velocity are the main design criteria for the floating highway structure. According to the standard[1] the design vehicle is defined to be an imaginary –non-existing- vehicle which represents all vehicles in a country or all vehicles that will cross the structure. This implies that all its features are determined statistically, what means that data is lumped in its 5th or 95th percentile. Since the design of the structure is already known (= pilot project design), the design vehicle is also known; a passenger car. Some specifications are depicted in figure 7.1:
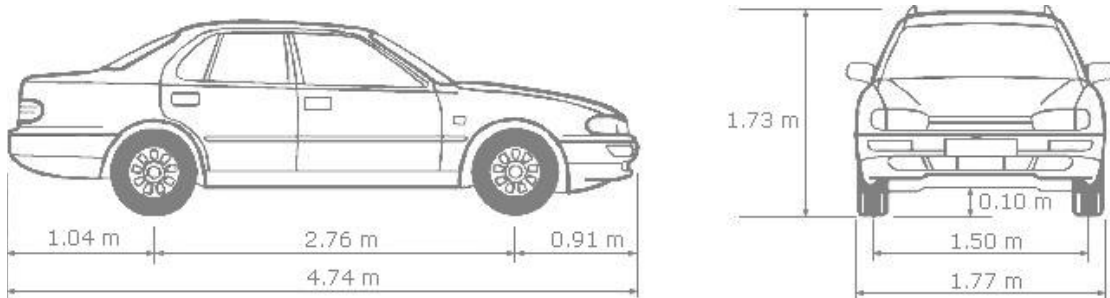
Feature	Magnitude	percentile
Length	4.74 m	95
Width	1.77 m	95
Height	1.73 m	100
Bottom space	0.10 m	0
Turning circle	11.50 m	95
Trace width	1.50 m	95
Wheel base	2.76 m	95
Maximum speed	42 m/s (150 km/h)	5
Minimum deceleration	5.2 m/s^2	95
Mass	1990 kg	95

Figure 7.1   table with specifications of design vehicle: passenger car (A.S.V.V. 2004)

For the sake of simplicity and to create an upper bound for calculation, the traffic load induced by passenger car(s) will be implemented in the one dimensional model as two concentrated vertical loads, near the front and rear wheels. See figure 7.2. The mass distribution will be assumed 50/50[2] Such schematization ensures that all energy of the vehicle is transmitted to the structure so that maximum vibrations will be experienced in any situation. In reality, however, shock absorbers (viscous dampers) and springs in the

---

[1] NOA 2007, 'Nieuwe Ontwerprichtlijnen Autosnelwegen' (new directive for designing highways) and A.S.V.V. 2004, 'Aanbevelingen verkeersvoorzieningen voor bebouwde kom (recommendations traffic facilities in urban areas)
[2] Depends on many factors such as speed, suspension, tire pressure, dynamic vehicle movement, etc,therefore not in standards. 50/50 is considered a broad estimate.

TUDelft

car's suspension dissipate energy and consequently reduce the vibration amplitudes near the wheels. The schematization of both systems is exhibited in figure 7.3. A second simplification encounters the velocity of the passenger car. The velocity will be kept constant in time because propagation speed of the vertical waves in the structure is also constant in time. Resonant vibrations are most likely to occur now. Design velocities are 30, 50, 80, 100 and 120 km/h.
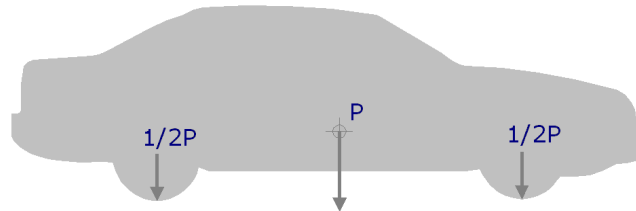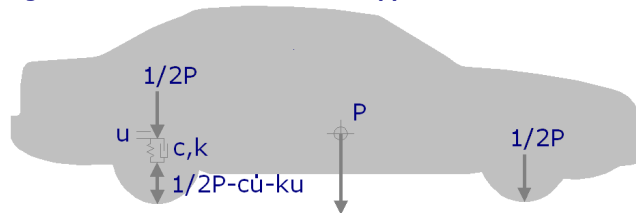

Figure 7.2   **schematization of applied forces**

Figure 7.3   **schematization two different types of energy transfer**

7.2   Traffic load by single vehicle

The traffic load as a single force in vector form has been derived in Appendix III. The vector dependent not only in time but must also be discretized in time intervals, depending on which body the force is located at a certain time. This excitation force vector $\mathbf{F}(t)$ can be written as sequence of vectors (matrix):

$$\mathbf{F}(t) = \begin{bmatrix} M^1(t) \\ F^2 \\ M^2(t) \\ \vdots \\ F^i \\ M^i(t) \\ \vdots \\ F^{N-1} \\ M^{N-1}(t) \\ M^N(t) \end{bmatrix} \xrightarrow[\substack{\text{in} \\ \text{time}}]{\text{discr.}} \begin{bmatrix} M^1(t) & 0 & & & & & \\ 0 & F^2 & & & & & \\ 0 & M^2(t) & & & zeros & & \\ & & \ddots & & & & \\ & & & F^i & & & \\ & & & M^i(t) & & & \\ & & & & \ddots & & \\ & zeros & & & F^{N-1} & 0 & \\ & & & & M^{N-1}(t) & 0 & \\ & & & & & 0 & M^N(t) \end{bmatrix} \tag{7.1}$$

With:

$$F^i = P$$
$$M^i(t) = P\left(ct^i - x^i_{r.c.}\right) \tag{7.2}$$

     Where:

     F^i :   traffic induced force at body i , $P = m_v g$

     m_v :   mass of design vehicle

$M^i(t)$:   time related moment due to traffic induced force

c :   integer for the constant velocity of the traffic induced force

t^i :   time associated with the position of the traffic induced force.

$x_{r.c.}^i$:   horizontal distance between origin and rotational centre of
                  body i
                  ($x_{r.c.}^1 = 0$, because rotational centre coincides origin).

The size of the matrix is determined by the number of degrees of freedom in and the number of time intervals: $2N - 2$ by N . Time intervals are equally distributed since c is a constant integer and denotes for $\{i | 1 \leq i \leq N\}$:

$$\left\{ t^i \Big| \sum_1^i L^{i-1} \Big/ c < t \leq \sum_1^i L^i \Big/ c \right\} \tag{7.3}$$

Where $L^0 = 0$. In Matlab the composed vector in expression 7.1 can easily be programmed by executing `if` and `else` statements for integers, as showed in Appendix V.3. To complete the model for a single vehicle, the single vector must be split up in two equally sized vectors, which differ from each other only by a time variable. With $\boldsymbol{F_{1/2P}}(t)$ located at the front wheels, the rear wheels appear to have a time delay of wb/c with respect to the front, so for the rear wheels we denote:

$$\boldsymbol{F}(t) \rightarrow \boldsymbol{F_{1/2P}}(t - wb/c) = \boldsymbol{F_{1/2P}}(t - t_{wb}) \tag{7.4}$$

Where wb stands for wheel base. The total excitation for the vehicle becomes now:

$$\boldsymbol{F_t}(t) = \boldsymbol{F_{1/2P}}(t) + \boldsymbol{F_{1/2P}}(t - t_{wb}) \tag{7.5}$$

In next sections, we deliberately omit the notation $_{1/2P}$ when we denote $\boldsymbol{F_{1/2P}}(t)$.

7.3   Traffic load by multiple vehicle

For multiple vehicle simulation just a(n) (infinite) series of the vectors in expression 7.5 has to be superposed to the excitation. The total excitation force in case of constantly distanced multiple vehicle yields:

$$\boldsymbol{F_t}(t) = \begin{matrix} \boldsymbol{F}(t) + \\ \boldsymbol{F}(t - t_{wb}) + \\ \boldsymbol{F}(t - t_{wb} - t_g) + \\ \boldsymbol{F}(t - 2t_{wb} - t_g) + \\ \boldsymbol{F}(t - 2t_{wb} - 2t_g) + \\ \ldots \end{matrix} = \begin{matrix} \boldsymbol{F}(t) + \\ \boldsymbol{F}(t - t_{wb}) + \\ \boldsymbol{F}(t - t_{md}) + \\ \boldsymbol{F}(t - t_{wb} - t_{md}) + \\ \boldsymbol{F}(t - 2t_{md}) + \\ \ldots \end{matrix} = \sum_{w=0}^{1} \sum_{v=0}^{\infty} \boldsymbol{F}(t - wt_{wb} - vt_{md}) \tag{7.6}$$

Where:

t_g :   time interval corresponding to the spatial gap between succeeding vehicles

t_{md} :   time interval corresponding to the mutual distance of succeeding vehicles
                 ($t_{md} = t_g + t_{wb}$). In section 6, a critical situation will be investigated when t_{md}
                 equals t_{ω_e} , i.e. time of revolution corresponding to the structure's natural
                 frequency

TUDelft

Input of these series of vectors requires a sudden stop. Basically, when simulation ends. During simulation, an unknown number of vehicles cross the left end of the structure. This number, noted as nv, is approximated by t_{end}/t_{md}. The last term of expression 7.6 will be implemented as follows:

$$\boldsymbol{F_t}(t) = \sum_{w=0}^{1} \sum_{v=0}^{nv} \boldsymbol{F}\left(t - wt_{wb} - vt_{md}\right) \tag{7.7}$$

In which v has been cut off by the number of vehicles (nv). After using the conditional statements to construct a single force vector, the multiple force vector will be constructed by looping all forces with different time variables and sticking them together afterward. Appendix V.3 shows an appropriate Matlab code.

TUDelft

8 Wave diffraction

Wave diffraction will be studied [4,5] and used to optimise the multibody system as proposed in section 5. This implies first that we investigate numerically the effect of the frequency of different acting loads both on the vibration amplitudes of the fluid and on the amount of fluid that will be displaced in the neighbourhood of a single floating body element. Next, distributed parameters for stiffness and damping and added mass can be assessed as a result of this study.

8.1 Steady state vibrations for the vertical motion

The static situation is shown in figure 8.1.
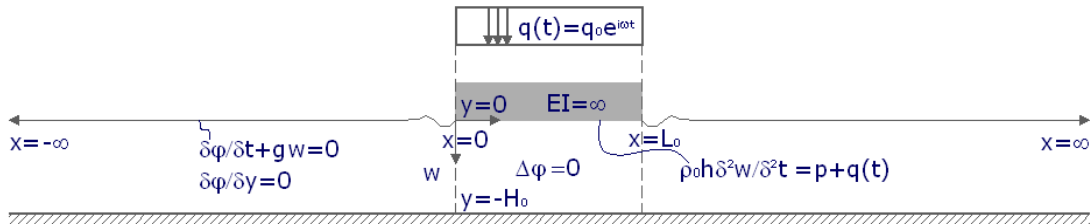
Figure 8.1 **flow diagram with applied boundaries in case of the steady state vibrations for vertical motion**

By making use of plausible (read: linear) assumptions for fluid, body and load (see figure 8.1) the boundary value problem can be solved analytically in the frequency domain, as has been done in Appendix VI. After some algebra we find the body deflection in case of a periodic equally distributed load[1]:

$$w(x) = \sum_{j=1}^{\infty} \frac{\tanh(\alpha_j H)}{K'_2(\alpha_j)} \left[\alpha_j^3 K_+(\alpha_j) \left(e^{-i\alpha_j(x-L)} \xi_j + e^{i\alpha_j x} \eta_j \right) \right] \tag{8.1}$$

With the system:

$$\begin{bmatrix} 1 & -c_{jm} \\ -c_{jm} & 1 \end{bmatrix} \begin{bmatrix} \xi_j \\ \eta_j \end{bmatrix} = \begin{bmatrix} f_j^1 \\ f_j^2 \end{bmatrix}$$

$$c_{jm} = \frac{\alpha_m^2 e^{i\alpha_m L} K_+(\alpha_m)}{\alpha_j^2 K'_-(\alpha_m)(\alpha_m + \alpha_j)} \tag{8.2}$$

$$f_j^1 = \frac{1}{\alpha_j^3 K_+(0)} = f_j^2 = \frac{1}{\alpha_j^3 K_-(0)}$$

Where:

j, m :   number of residue

α :   scattering frequency of frequency domain (Fourier Transform [3])

H :   dimensionless fluid depth

K'_2 :   Fourier Transform of dispersion relation (derivative) of surfaces waves on interface body / fluid. (subscript refers to x -domain, 1: free surface , 2:

---

[1] body deflection expressed in residual coordinates [3].

interface body / fluid)

$K_\pm$: Fourier Transform of dispersion relation on interval $\{x \mid L < x < \infty\}$.

(subscript refers to domain, a plus for $\{x \mid L < x < \infty\}$, a minus for

$\{x \mid -\infty < x < 0\}$, per definition: $K_+K_- = K_2/K_1$)

x : dimensionless coordinate

L : dimensionless body length

ξ : (complex) amplitude of surface wave travelling from the right edge

of the plate $\{x = L\}$ to the right

η : (complex) amplitude of surface wave travelling from the left edge

of the plate $\{x = 0\}$ to the left

The analysis starts with carrying out a series of calculations for the following values of the physical quantities:

- fluid depth $H_0 = 1.1m$
- external force $q_0 = 1000\,N/m^2$
- body length $L_0 = 3.5m$
- body density $\rho_0 = 102.5\,kg/m^3$
- fluid density $\rho = 1000\,kg/m^3$
- body height $h_0 = 1.6m$
- external period $T_p = 0.85s; 1s; 1.5s; 2s; 4s$.

The values are stored in the text-file hydrodynamic parameters.txt and linked to different M-files. Hydrodynamic parameters.txt can be viewed in Appendix V.1.

For the fluid depth we hold the lower bound and all other dimensions are conform the dimensions in the pilot. Fluid density and body density will be defined for the initial draft and the period of the acting load will be kept variable to fulfil the aim of this investigation.

For the construction of calculations of complex amplitudes and body deflections, we refer to the Matlab codes (M-files) in Appendix V.4. In the M-files, residual coordinates (zeros/poles) need to be defined before getting looped into other functions. Appendix IV tells us that an *infinite* number of residual coordinates are involved: one real coordinate and an infinite number of imaginary coordinates for each analyticity domain (Appendix VI, figure IV.2).

Now an important question is: is it possible to approach the infinite number by a finite number (N_m)? If yes, how large must N_m be?

According to Cauchy's Residue Theorem [3], the residual coordinates in the complex frequency plane correspond to the scattering frequencies of the propagating waves in the frequency domain. Furthermore, real and imaginary coordinates are subjected to oscillating and exponentially decaying waves, respectively, so we may conclude that an induced superimposed one-directional (surface)wave is built out of one oscillating wave and an infinite number of exponentially decaying waves. Arranging the number of coordinates (in figure IV.2) from zero, near the origin, to infinity, along the imaginary axis, the higher number correspond automatically to the faster decaying waves (or *m*odes). Approaching infinity by N_m will discard the fastest decaying modes only. In figure 8.2 we have plotted the body deflection versus the relative body length for various external

TUDelft

periods. It can be seen here that curves converge to the horizontal axis when N_m is increasing. Since relative displacements (= vertical displacement / total length) are in the order of 1%, a rounding off error on the vertical displacement is acceptable when smaller than 1% of 1% ($\approx 2*10^{-4}m$). This implies that infinity may be replaced by $N_m = 80$ when applying the algorithm denoted in Appendix VI. Expression 8.1 can consequently be rewritten into:

$$w(x) \cong \sum_{j=1}^{N_m} \frac{\tanh(\alpha_j H)}{K'_2(\alpha_j)} \left[\alpha_j^3 K_+(\alpha_j) \left(e^{-i\alpha_j(x-L)} \xi_j + e^{i\alpha_j x} \eta_j \right) \right] \tag{8.3}$$

Where:

N_m :   number of modes (= imaginary residual coordinates)

Successful plots can only be made for $T_p = 1.5s; 2s; 4s$ since the smaller periods give inaccurate results in this model. This can be checked in Appendix VI.8.
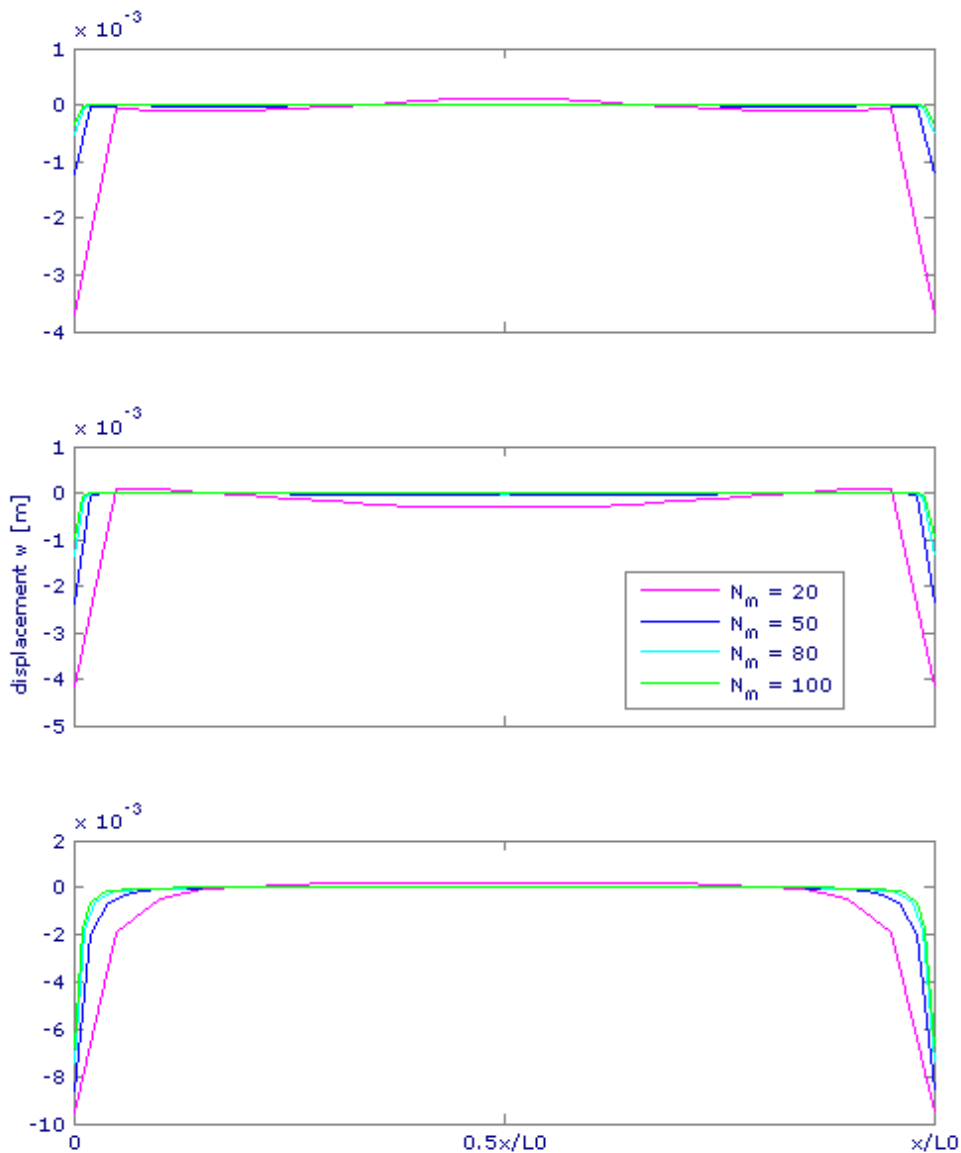
Figure 8.2   **vibration amplitudes in case of equally distributed load for T_p = 1.5 s, 2 s and 4 s**

8.1.1 Distributed stiffness and damping

Focussing on the graphs once again, long waves rule the body domain and converge to almost flat wave(peak)s when N_m increases. This can be explained as follows: the larger N_m is taken, the more decaying modes are generated and the more the amplitude will be suppressed. When N_m goes to infinity, monotonous waves and discontinuous edges will be exhibited, like we expect to observe in nature. In the opposite direction, when N_m is taken small enough, (wave)mode shapes become transparent by the formation of troughs and crests. It proves that for these large oscillation periods the displacements are mainly due to the action of the load. Therefore, under long wave conditions (load induced oscillation) when N_m is sufficiently large, we are allowed to derive a time-independent averaged value for displacement $w(x)$ as follows:

$$\overline{w}(x) \approx w\left(\frac{L}{2}\right) = \sum_{j=1}^{N_m} \frac{\tanh(\alpha_j H)}{K'_2(\alpha_j)} \left[\alpha_j^3 K_+(\alpha_j) e^{i\alpha_j L/2} (\xi_j + \eta_j) \right] \tag{8.4}$$

where the rigid body is supposed to maintain an everlasting contact with the fluid. From the midpoint value of $w(x)$ distributed stiffness and damping parameters will be derived and used as input for the multibody system. Subsequently, we introduce Kappa as $K(\omega) = Bq_0 / (\overline{w}(x))$ and per definition k_d and c_d read:

$$\begin{aligned} k_d(\omega) &= \mathrm{Re}\left[K(\omega)\right] \\ c_d(\omega) &= \mathrm{Im}\left[K(\omega)\right]/i\omega \end{aligned} \tag{8.5}$$

where Re and Im concerns the real and imaginary part of Kappa, respectively.

Figure 8.3 gives a table with calculated damping and stiffness parameters for the periods $T_p = 1.5s, 2s, 4s$. Negative stiffness is supposed to be unexpected, since it can be interpreted as negative floatation. However, its magnitude is not as high as what has been calculated. When appealing for midpoint values for approximated averaged values, we accept the deviation error by measuring at the wave crests. For $T_p = 1.5s, 4s$ there exist positive deviation and for $T_p = 2s$, negative deviation, overrating respectively positive and negative stiffness values. The same happens for negative damping, but negative damping has to be expected here as well. Negative damping indicates energy absorbance to possibly perform resonant amplification. Consequently, the higher the load oscillates, the larger the probability for resonance and the lower the load oscillates, the more and longer the fluid will be pushed aside and the more the body will be submitted to a damped motion.
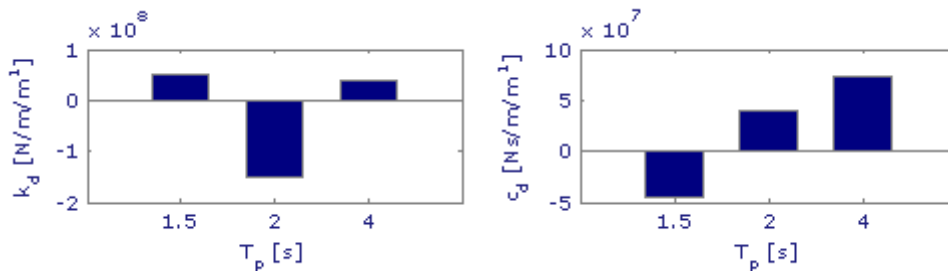

Figure 8.3 **bar graph with distributed stiffness and damping parameters for N_m=80**

TUDelft

8.1.2 Added mass

Added mass or added fluid mass will be derived and used to pre-assess the natural frequency of the multibody system in order to measure the stiffness and damping parameters from the previous subsection as good as possible. The adjective 'added' refers to the 'extra' mass that influences the vibrating motion of a floating (or immersed) object, according to Bessel [6]. For the schematization, we may assume that the fluid simply will be pushed aside due to vibrations. This is, obviously, a rough approximation since we assume that the amount of fluid that will be pushed aside equals the amount displaced fluid. The fluid limitation does not change and therefore it does not fully agree with reality. However, when load oscillations are high enough, the amplitude of the movement is significantly smaller than geometric measures, this is approximately true. When calculating added mass, the influence of the (free surface) waves may be ignored if frequencies are high. Also, it may be assumed that the flow (beneath the body element) has no influence on the added mass. Consequently, the fluid flows across the entire area are in-phase and therefore proportional to the velocity of the body. The relationship between the vibrating velocity and the potential at the interface body / fluid is the measure of the added mass:

$$\alpha_{am}(\omega) = \varphi(x,0) \Big/ \frac{\partial w}{\partial t}(x,0) = 1 \Big/ \big(\alpha_j \tanh(\alpha_j H)\big) \qquad (8.6)$$

Where:

$\varphi(x,0):$ fluid velocity potential at the interface body / fluid

$\dfrac{\partial w}{\partial t}(x,0):$ vibrating velocity at the interface

The variable α_{am} represents an estimation of the influence depth of the body that appeared to be constant over the x domain and to depend only on the frequency. It is sufficient now to multiply α_{am} with the fluid density and the body length in order to obtain the added mass (per metre width):

$$m_f(\omega) = \rho L \alpha_{am}(\omega) \qquad (8.7)$$

Where:

$\rho:$ dimensionless fluid density

$L:$ dimensionless body length

Outcomes for m_f have been enclosed in the graph of figure 8.4. It is obvious that relation between m_f and T_p is linear, since linearized approximations are involved.
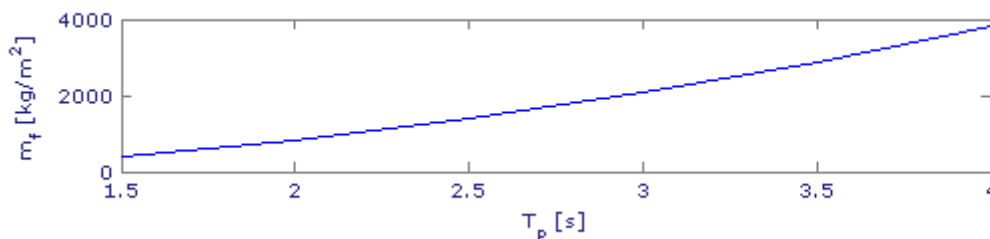

Figure 8.4   graph with frequency dependent m_f representing added mass for $N_m=80$

8.1.3 Added stiffness and damping

Since waves and currents are out of the scope of this thesis, added stiffness and damping are out of the scope as well.

8.1.4 Short wave approximation; resonant amplification + singular matrix validation

The short wave approximation can be applied within specific bounds. The upper bound is defined by the rate between body- and wave length. If the body length is significantly smaller than the wavelength, then body kinematics is primarily controlled by a long wave, which curve can be outlined by approximately the first mode only.

In the accessory algorithm we find that in matrix c_{jm} the column corresponding to α_0 is significantly larger than all other columns. By setting all other elements to zero, basically, all decaying modes close to the edges are neglected. As a result, expression 8.1 for the body deflection in case of a periodic equally distributed load remains unchanged, however, the complex amplitudes in the system 8.2 can explicitly be denoted now:

$$\xi_m = c_{m0}\eta_0 + f_m^1$$
$$\eta_m = c_{m0}\xi_0 + f_m^2$$

$$c_{m0} = \frac{\alpha_0^2 e^{i\alpha_0 L} K_+(\alpha_0)}{\alpha_m^2 K'_-(\alpha_0)(\alpha_0 + \alpha_m)}, c_{00} = \frac{e^{i\alpha_0 L} K_+(\alpha_0)}{2\alpha_0 K'_-(\alpha_0)} \tag{8.8}$$

$$\xi_0 = \frac{f_0^1 + cf_0^2}{1 - c_{00}^2} = \eta_0 = \frac{f_0^2 + cf_0^1}{1 - c_{00}^2} = \frac{(1 + c_{00})f_0}{1 - c_{00}^2}, f_0 = f_0^{1,2} = \frac{1}{\alpha_0^3 K_\pm(0)}$$

$$f_m^{1,2} = f_m = \frac{1}{\alpha_m^3 K_\pm(0)}$$

Where:

0 :   number corresponding to real residue

the complete derivation can be seen in Appendix IV.6.

8.1.4.1 Resonant amplification

From expression 8.6 we may expect an increase in the amplitude height due to the external load, but it is, as discussed before, not for one-hundred percent certain if resonant amplification will occur. Therefore, the objective is to evaluate the conditions under which resonant vibrations will be exhibited. This can be done by examining the nature of waves, i.e. incoming, reflecting or transmitting waves. Expressions for these waves are derived in the form of complex amplitudes being subtracted from formulas in Appendix IV.6. These complex amplitudes are denoted as R for reflection and T for transmission and are associated with waves at infinite distance from both edges of the body element. All decaying waves have vanished at infinity and under 'short wave conditions' these waves may be neglected at the edges too. The reflected wave at the left edge of the body element compensates the incoming wave. Beneath the body reflected and transmitted waves propagate because of the physical edges, as shown in figure 8.5.
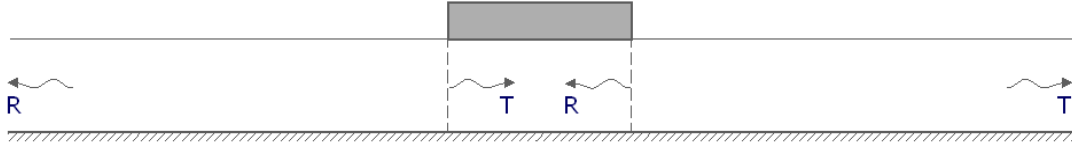
TUDelft

Figure 8.5   waves in the x-domain

The main part of the body deflection is a superposition of two waves of the same length: transmitted into the fluid beneath the body and reflected from the other edge. If these waves are in phase, then the deflection amplitude is doubled. Zero reflection correspond to total transmission. Both expressions for complex amplitude R and T are evaluated in Appendix IV.6 and yields:

$$R = \frac{i}{K_+(\gamma)K'_1(\gamma)}\left[\sum_{j=1}^{\infty}\frac{\alpha_j^2 e^{i\alpha_j L}K_+^2(\alpha_j)}{K'(\alpha_j)(\alpha_j-\gamma)}\xi_j - \frac{1}{\gamma K_-(0)}\right] \tag{8.9}$$

$$T = \frac{-ie^{-i\gamma L}}{K_+(\gamma)K'_1(\gamma)}\left[\sum_{j=1}^{\infty}\frac{\alpha_j^2 e^{i\alpha_j L}K_+^2(\alpha_j)}{K'(\alpha_j)(\alpha_j-\gamma)}\eta_j - \frac{1}{\gamma K_+(0)}\right] \tag{8.10}$$

Where for computation purpose the symbol ∞ will be replaced by N_m and the complex amplitudes ξ and η attributes to equation 8.1. With allowance for normalisation, we transform reflection and transmission amplitudes into ditto coefficients by obtaining normalized values for R and T :

$$R_{norm} = |R|/(|R|+|T|)$$
$$T_{norm} = |T|/(|R|+|T|) \tag{8.11}$$

Where:
$|R|$:   absolute value of R
$|T|$:   absolute value of T

For normalized reflection and transmitted wave coefficients the following equality follows from equation 8.9:

$$R_{norm} + T_{norm} = 1 \tag{8.12}$$

Resonant amplification corresponds to zero reflection and therefore it is sufficient to evaluate $|R| = 0$ in order to satisfy this section's objective. Under 'short wave conditions' and to retain only the solitairy oscillating wave in the expression for $|R|$ it is allowed to rewrite expression 8.9 as follows:

$$R = \frac{\dfrac{i}{K_+(\gamma)K'_1(\gamma)}\left[\dfrac{\alpha_0^2 e^{i\alpha_0 L}K_+^2(\alpha_0)}{K'(\alpha_0)(\alpha_0-\gamma)}\xi_0 - \dfrac{1}{\gamma K_-(0)}\right] = }{\dfrac{i}{K_+(\gamma)K'_1(\gamma)K_\pm(0)}\left[\dfrac{2c_{00}(1+c_{00})}{(\alpha_0-\gamma)(1+c_{00}^2)} - \dfrac{1}{\gamma}\right]} \tag{8.13}$$

where R is evaluated in residue α_0 as an expression of c_{00}. Both real and imaginary part in the bracketed term of this expression must be zero for $|R| = 0$ what leaves c_{00} to be equal to:

$$\frac{\alpha_0 - \gamma}{\alpha_0 + \gamma} \tag{8.14}$$

Since α_0 and γ are real values, we may say that $Im\left[c_{00}\right] = 0$. Substituting $Im\left[c_{00}\right] = 0$ in expression 8.8 for c_{00} result in the next equality:

$$Arg\left[K_+^2\left(\alpha_0\right)\right] + \alpha_0 L = \pi k \quad k = 1, 2, .. \tag{8.15}$$

what must be true for resonant amplification. As can be viewed in figure 8.6, none of the predefined periods satisfy equality 8.15, concluding that we do not deal with resonant amplification. Nevertheless, (strong) amplification can be expected where the imaginary value for c is closest to zero. For example, we refer to $T_p = 1.5s$, where large amplitudes are expected because of negative damping. As early as the stage of derivation at equations 8.9 and 8.10, to be precise, it could already be seen that the possibility for resonant amplification is always zero. By comparing both equations with each other, zero reflection can only be achieved when simultaneously zero transmission will be achieved, so in a case when no waves are propagating. The bracketed terms are under all circumstances identical since the complex amplitudes are equal for this symmetric case to return a fifty-fifty wave coefficient distribution.

Concluding this subsection, resonant amplitudes will never be experienced when the load is vibrating in firmly large periods and the fluid depth is kept at its minimum level. This is in good agreement with comparable investigations [4,5].
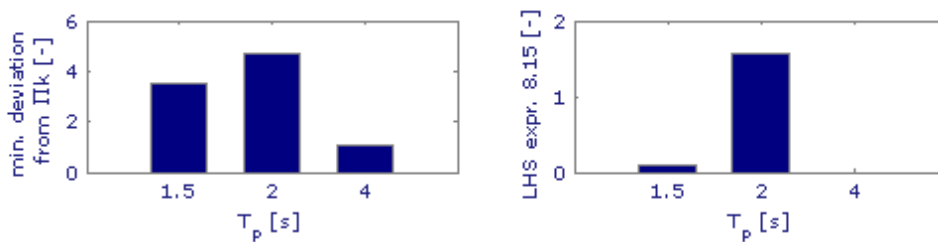

Figure 8.6   **application of equality 8.15 to predefined periods**

8.1.4.2 Singular matrix validation

The second objective of this subsection is to 'discuss' a proper boundary value for an approximated computation that must replace the 'exact' computation for the complex amplitudes ξ and η when singularities are involved. See for the theorem Appendix IV.5. Because of singularities there exist not only one unique solution what might lead to unreliable outcomes, especially when values are close to zero. To avoid this, the smallest entries must be set to zero, while the largest ones remain untouched in the matrix. Until

TUDelft

this point, for all performed computations only the first singularity is significantly large (Thus, the others must be set to zero). Therefore, the approximated computation is a so called rank-one-computation. For the lack of a proper numerical boundary value (floating point tolerance would be insufficient) we establish an intuitive way to evaluate the second singularity: short wave approximation. Within the bounds, the shortwave approximation can give sufficient good results because it simply evade singular matrix computation. In the graph of figure 8.7, we demonstrate a boundary condition for which the rank-two-computation ($t = 2$) will probably be more reliable with respect to a rank–one-computation. For the determination the trial-and-error-method has been applied, from which some unsuccessful attempts are gathered in Appendix IV.8. Note that the transition is marked by the (modal) shape of the curves rather than the level of coincidence. We must bear in mind that the conditions to use the short wave approximation are not optimal in this case since L is not much bigger than one. The lower bound of the second entry is equal to around 0.12 when $N_m = 80$ and attributes to a period of $T_p = 1.5s$ in combination with a fluid depth of $H_0 = 1.6m$.
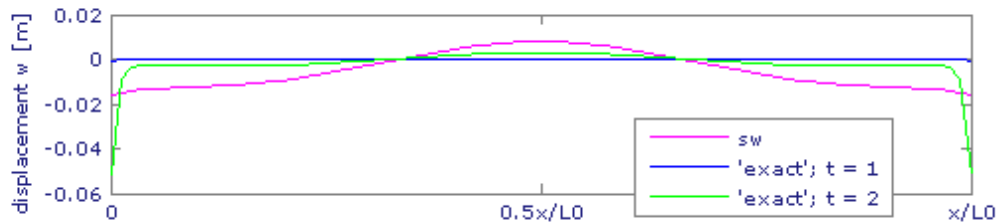
Figure 8.7   **intuitive determination of boundary condition for second singularity**

8.1.5 Steady state vibrations for variable fluid depth

As previously assumed, we also carried out a second series of calculations with variable quantities for the fluid depth H_0 because we are also interested in an upper bound for fluid depth. Unfortunately, this easiest kind of approach to the problem turned out not to be successful. We see that the deeper fluid becomes, the more crests and troughs start to grow to contribute to inaccurate modelling. However, this wave growth can be compensated by inserting more decaying waves, at least when load induced oscillation periods are performed, i.e. higher periods. Figure 8.8 gives an example of applying a larger depth first and let N_m grow afterward to demonstrate that calculations for $H_0 = 1.6m$ can be performed with comparable accuracy with respect to $H_0 = 1.1m$. Further steps in fluid depth increase will eventually correspond all to flat curves by a growing amount of waves. Therefore, the bound is not mathematical but purely physical and follows from the linear wave theory, that characterizes the fluid by its 'depth/wavelength'-relationship. Specifically, we mean that the field of applicability of the wave diffraction method is bounded at the point where rotating particles inside our short waves do not feel the bottom anymore. Roughly estimating, the maximum fluid depth will be approximately $H_0 = 1.6m$ using the rule of thumb for deep water and surface gravity waves. For depths larger than $1.6m$, $H_0 = 1.6m$ can be implemented as upper bound.
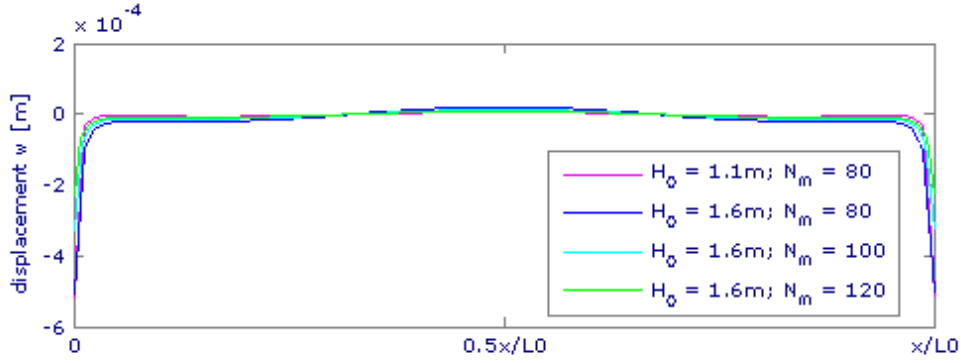
*T̃U*Delft

Figure 8.8 example of vibration amplitudes for $T_p = 1.5s$ with variable wave heights

8.2 Steady state vibrations for rotational motion

In the multibody system, besides the vertical motion also rotational motion will be performed by the acting load. Rotational motion can be simulated by simply reshaping the time periodic load into a prismatic form. The static situation is depicted in figure 8.9.

Vibrating amplitudes will be evaluated in a manner analogously to the ones attributed to the vertical motion. This is possible because body and fluid properties do not change shape in the new situation.
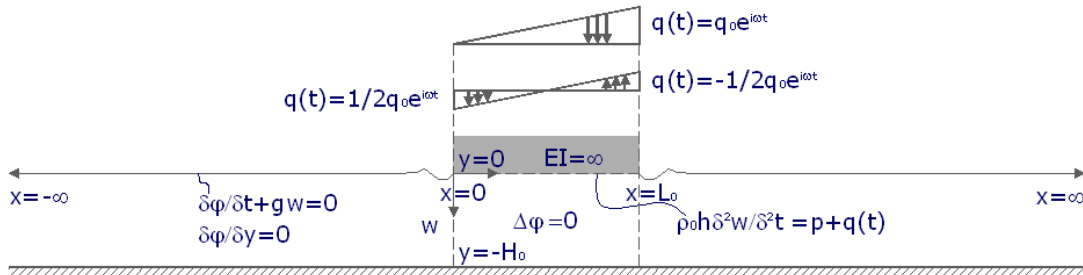
Figure 8.9 flow diagram with applied boundaries in case of the steady state vibrations for rotational motion

The expression for the body deflection is identical too, however, the derivation of the damping and stiffness parameters requires an expression for the angle of rotation in the formula. By taking the derivative to x, expression 8.1 transforms into:

$$\theta(x) = -\frac{\partial w(x)}{\partial x} = \sum_{j=1}^{\infty} \frac{\tanh(\alpha_j H)}{K'_2(\alpha_j)} \left[\alpha_j^4 K_+(\alpha_j) \left(-ie^{-i\alpha_j(x-L)} \xi_j + ie^{i\alpha_j x} \eta_j \right) \right] \tag{8.16}$$

With the system:

$$\begin{bmatrix} 1 & -c_{jm} \\ -c_{jm} & 1 \end{bmatrix} \begin{bmatrix} \xi_j \\ \eta_j \end{bmatrix} = \begin{bmatrix} f_j^1 \\ f_j^2 \end{bmatrix}$$

$$c_{jm} = \frac{\alpha_m^2 e^{i\alpha_m L} K_+(\alpha_m)}{\alpha_j^2 K'_-(\alpha_m)(\alpha_m + \alpha_j)} \tag{8.17a}$$

TUDelft

$$f_j^1 = \frac{1}{\alpha_j^3 K_+(0)}\left(\frac{i}{\alpha_j L}+1\right), f_j^2 = -\frac{i}{\alpha_j^4 L K_-(0)} \qquad \{triangular\}$$

(8.17b)

$$f_j^1 = \frac{1}{\alpha_j^3 K_+(0)}\left(\frac{i}{\alpha_j L}+\frac{1}{2}\right), f_j^2 = -\frac{1}{\alpha_j^3 K_-(0)}\left(\frac{i}{\alpha_j L}+\frac{1}{2}\right) \quad \{trapezoidal\}$$

In Appendix IV, the corresponding algorithm has been reconstructed from the original one with different values for f_j. All relevant formulas are summarized in Appendix IV.6.

For $T_p = 1.5s; 2s; 4s$ and $N_m = 20, 50, 80, 100$ in total six graphs are obtained in which vibration angles and amplitudes are plotted on the relative length scale. These graphs are shown in the figures 8.10 and 8.11.
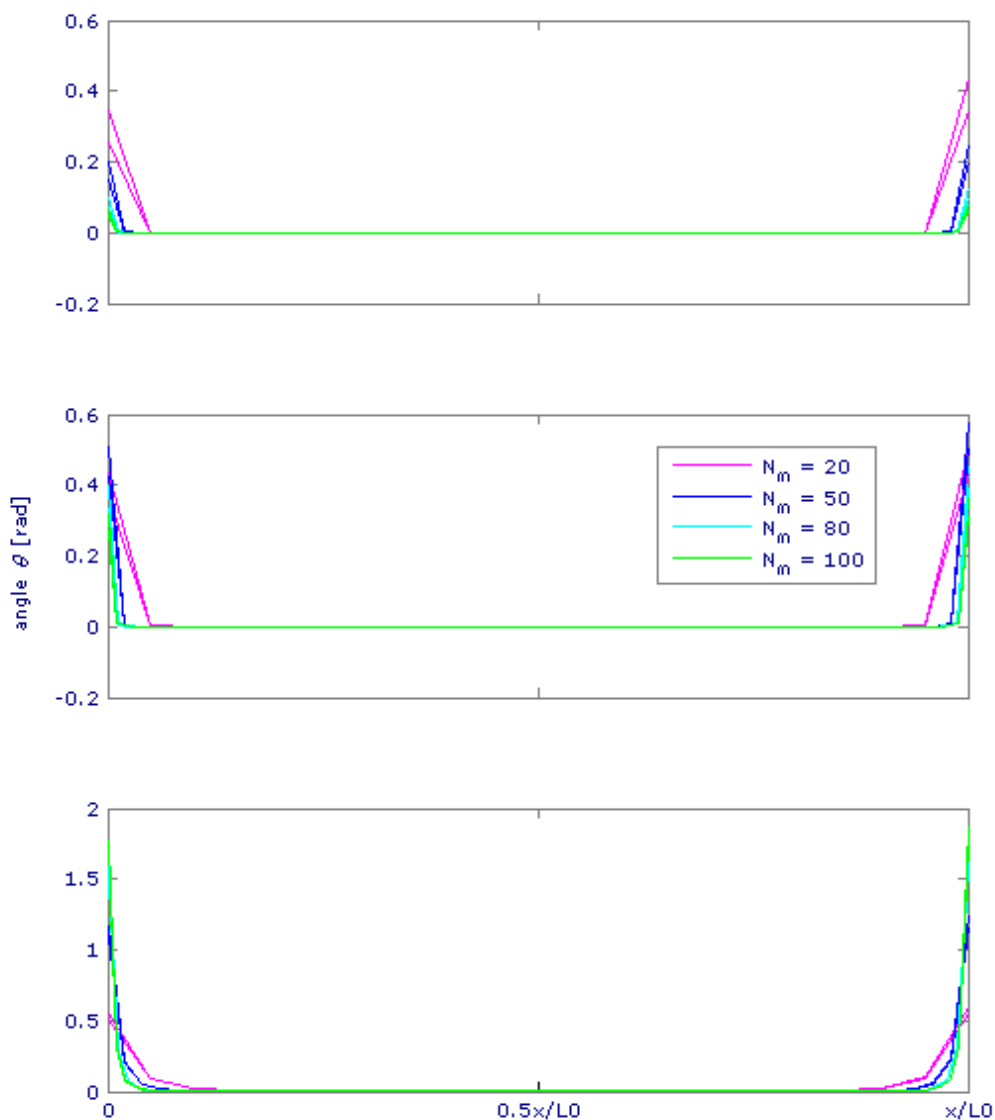
Figure 8.10   **vibration angles in case of prismatic shaped loads for T_p = 1.5 , 2 and 4 s**
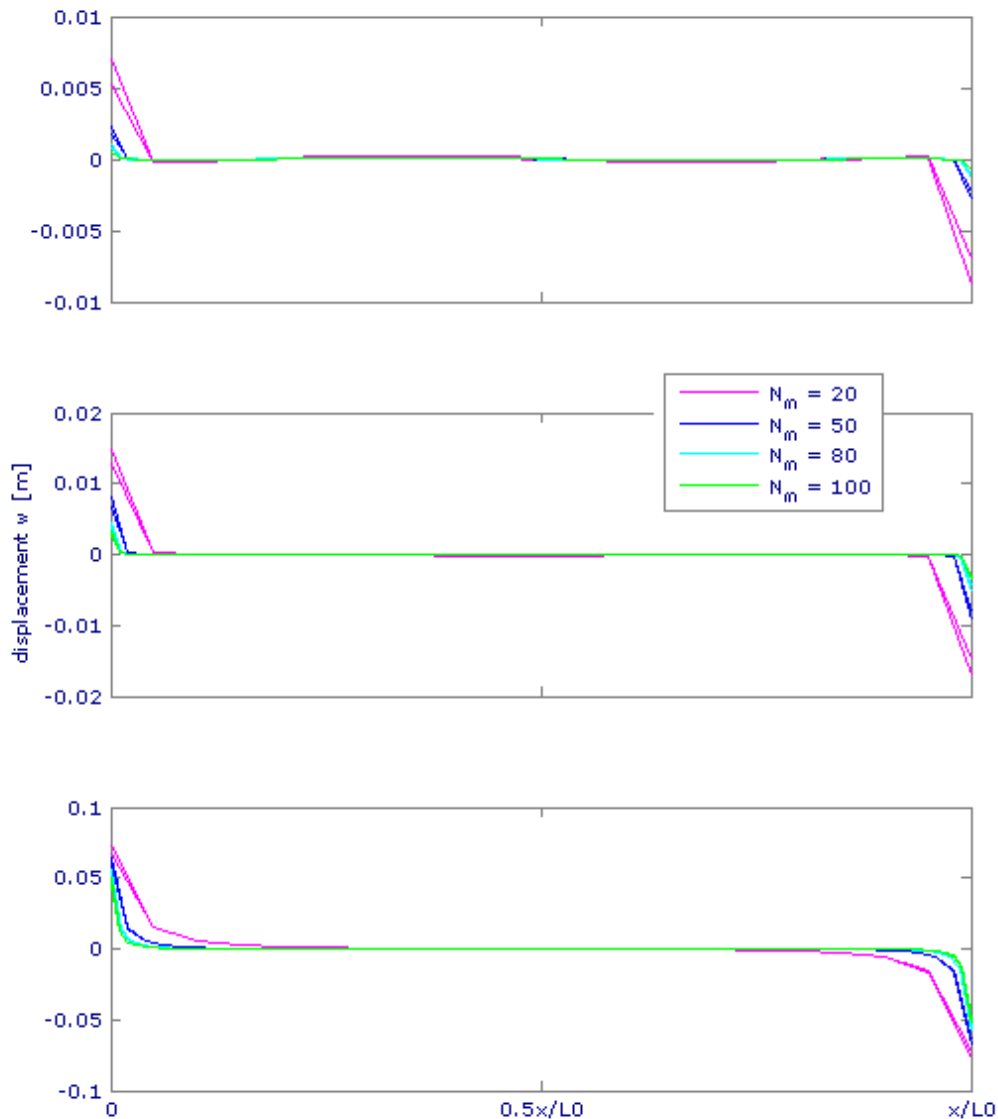
TUDelft

Figure 8.11   vibration amplitudes in case of prismatic shaped loads for T_p = 1.5 , 2 and 4 s

The graphs show the convergent tendency of the curves when N_m increases, just like in section 8.1. Unlike these graphs, mode shapes become badly visible, but it seems to be a scaling problem. In figure 8.11, in which mode shapes are quite well visible, anti-symmetrical shapes do sharply emerge for $N_m = 20$ induced by corresponding triangular and trapezoidal shaped loads. Concentrating on the edges, lines do no longer coincide and triangular load induced deflections turns out to be somewhat larger than the trapezoidal load induced deflections at the right edge. At the left edge, the opposite can be observed: triangular load induced deflections are slightly smaller. By elaborating the system in expression 8.17, the exact rate in complex amplitudes will be derived to establish our observations:

TUDelft

$$\xi_{j,c} = \xi_{j,i} + \frac{c_{jm}+1}{2\alpha_j^3 K_\pm(0)}$$

$$\eta_{j,c} = \eta_{j,i} + \frac{c_{jm}+1}{2\alpha_j^3 K_\pm(0)}$$

(8.18)

In expression 8.18, the subscripts c and i refer to respectively the triangular and trapezoidal shaped loads, to be subjected to respectively closed and intermediate body rotations. Note that when a positive displacement is directed downward, ξ_j, the (complex) amplitude of the rightward propagating wave will be enhanced by the additional term since both terms are positive whereas η_j, the amplitude of the leftward propagating wave, will be suppressed since η_j is negative. A load concentration at the right for the triangular load obviously result in amplitude enhancement at the right. However, if N_m increases, additional terms die out rapidly and balance the amplitudes as long as the loads have equal magnitudes, thus:

$$\int_0^{L_0} q(x,t)\,dx = const.$$

(8.19)

Equal magnitudes means equal displacements independent of the load's (shape) distribution[1]. Therefore, we may define one average value for $\theta(x)$ for both cases which yields:

$$\bar{\theta}(x) \approx \theta\left(\frac{L}{2}\right) = \sum_{j=1}^{N_m} \frac{\tanh(\alpha_j H)}{K'_2(\alpha_j)} \left[\alpha_j^4 K_+(\alpha_j)\left(ie^{i\alpha_j L/2}\left(-\xi_j + \eta_j\right)\right)\right]$$

(8.20)

in which N_m is taken sufficiently large and for which the average value will be approached by the midpoint value, excluding discontinuous edges in calculation. In the definition for k_d and c_d in expression 8.5 we define Kappa as:

$$K(\omega) = BM_0 \Big/ \left(\bar{\theta}(x)L_0\right)$$

(8.21)

where $M_{0,c} = 1/3\, q_0 L_0^2$ and $M_{0,i} = 1/12\, q_0 L_0^2$ Figure 8.12 gives damping and stiffness parameters for the periods $T_p = 1.5s, 2s, 4s$ for both types of loads. Analysing the parameters, a rate of four is everywhere to discover. This can directly be derived from the moment rate in expression 8.21 since we calculated equal averaged rotation angles. As early as section 5, the ratio of four has deliberately been derived here since we calculated buoyancy forces as a function of the same rotation angle.

As for the vertical case, negative stiffness for $T_p = 2s$ emerges too in figure 8.13, but when it comes to damping the tables are turned. Now, the probability for resonance is bigger when motions are slower. This implies that it makes indeed a big difference how propagating waves are being generated, by vertical perturbation of the fluid surface or by seesawing the surface, for an optimal energy transfer. Anyhow, resonance or no resonance, vibration amplitudes are, on the average, significantly bigger here; up to more than 30 times larger near the edges for $T_p = 2s$.

---

[1] Linear surface gravity waves from a different 'source' transform to identical waves because of their dispersion relation.
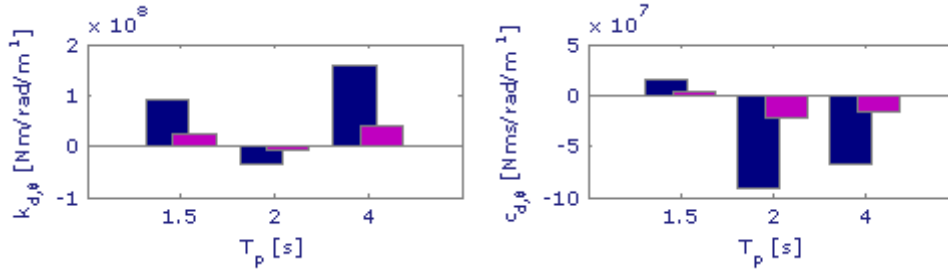
TUDelft

Figure 8.12   histogram with distributed stiffness and damping parameters for rotation

8.2.1 Resonant amplification

Resonant amplification or resonance occurs when energy from the vibrating load will be transferred to the fluid to locally increase the (average) fluid level. The objective is to evaluate new conditions for which resonance will occur, in the same way as has been done in section 8.1.3.1. In section 8.1.3.1, we described how maximum body deflections can be created by the interaction of propagating reflected and transmitted waves. It is necessary for the waves to be in phase right beneath the body to grow to a maximum level. To appeal for maximum rotation, however, waves of the same length must obviously get into phase too but both ends of the body must be in a phase shift of half the wave length (λ_p) to get to extreme pitching motions. This explains why lower oscillations are most likely to cause for resonance in the pitched motion, because the corresponding period reads:

$$T_p \approx \frac{\lambda_p}{\sqrt{gH_0}} = 2.13s \tag{8.22}$$

when $H_0 = 1.1m$ and $\lambda_p = 2L_0 = 7m$. In the same time, there must be zero reflection at minus infinity for maximum transmission near the body as well. Transmitted and reflected waves are expressed as complex amplitudes R and T Both expressions are evaluated in Appendix IV.7 and yields:

$$R = \frac{i}{K_+(\gamma)K'_1(\gamma)}\left[\sum_{j=1}^{\infty}\frac{\alpha_j^2 e^{i\alpha_j L}K_+^2(\alpha_j)}{K'(\alpha_j)(\alpha_j - \gamma)}\xi_j - \frac{i}{\gamma^2 L K_-(0)}\right] \quad \{triangular\}$$

$$R = \frac{i}{K_+(\gamma)K'_1(\gamma)}\left[\sum_{j=1}^{\infty}\frac{\alpha_j^2 e^{i\alpha_j L}K_+^2(\alpha_j)}{K'(\alpha_j)(\alpha_j - \gamma)}\xi_j + \frac{1}{2\gamma K_-(0)} - \frac{i}{\gamma^2 L K_-(0)}\right] \quad \{trapezoidal\} \tag{8.23}$$

$$T = \frac{-ie^{-i\gamma L}}{K_+(\gamma)K'_1(\gamma)}\left[\sum_{j=1}^{\infty}\frac{\alpha_j^2 e^{i\alpha_j L}K_+^2(\alpha_j)}{K'(\alpha_j)(\alpha_j - \gamma)}\eta_j + \frac{i}{\gamma^2 L K_+(0)}\right] \quad \{triangular\}$$

$$T = \frac{-ie^{-i\gamma L}}{K_+(\gamma)K'_1(\gamma)}\left[\sum_{j=1}^{\infty}\frac{\alpha_j^2 e^{i\alpha_j L}K_+^2(\alpha_j)}{K'(\alpha_j)(\alpha_j - \gamma)}\eta_j + \frac{1}{2\gamma K_+(0)} + \frac{i}{\gamma^2 L K_+(0)}\right] \quad \{trapezoidal\} \tag{8.24}$$

Where for the computation the symbol ∞ will be replaced by N_m and the complex amplitudes ξ and η attributes to equation 8.11. After normalization, we evaluate $|R| = 0$ twice from a simplified version of expression 8.17:

TUDelft

$$R = \frac{i}{K_+(\gamma)K'_1(\gamma)LK_\pm(0)}\left[\frac{2c_{00}(i+\alpha_0 L - c_{00})}{\alpha_0(\alpha_0 - \gamma)(1-c_{00}^2)} - \frac{i}{\gamma^2}\right] \qquad \{triangular\}$$

$$R = \frac{i}{K_+(\gamma)K'_1(\gamma)K_\pm(0)}\left[\frac{2c_{00}(1-c_{00})(1/2\,\alpha_0 L + i)}{\alpha_0(\alpha_0 - \gamma)L(1-c_{00}^2)} + \frac{1}{2\gamma} - \frac{i}{\gamma^2 L}\right] \{trapezoidal\}$$

(8.25)

in which all decaying waves have been omitted and in which c_{00} has been adapted. Both real and imaginary part in the bracketed term of this expression must be zero for $|R| = 0$. Substitution of $|R| = 0$ into expressions 5.25 gives:

$$\left(\alpha_0 L - \text{Re}[c_{00}]\right)\text{Re}[c_{00}] + \left(\text{Im}[c_{00}] - 1\right)\text{Im}[c_{00}] = 0 \qquad \{triangular\}$$

$$-\left(\alpha_0 + \gamma\right)\alpha_0 L\left(\text{Re}^2[c_{00}] - \text{Im}^2[c_{00}]\right) + 2\alpha_0\gamma L\,\text{Re}[c_{00}] -$$
$$4\gamma\,\text{Im}[c_{00}] + 8\gamma\,\text{Re}[c_{00}]\text{Im}[c_{00}] + (\alpha_0 - \gamma)\,\alpha_0 L = 0 \qquad \{trapezoidal\}$$

(8.26)

which must be true for resonant amplification. In case of four predefined periods no resonance will occur, according to figure 8.13. In line with subsection 8.1.3.1, strong amplification can be expected where $|R| \approx 0$. For $T_p = 4s$ largest amplitudes are obtained and expected because of negative damping in combination with positive stiffness. Positive stiffness must be addressed to the previous sentence since negative damping is even stronger at $T_p = 2s$ but in combination with negative stiffness, apparently, amplification will be suppressed.

For the same reason, $T_p = 2.13s$ does not satisfy our predefined expectations as well. Applying equations 8.9 and 8.10 to the problem, a fifty-fifty wave coefficient distribution will be calculated in every situation, to fall back again into the conclusion of section 8.1.3.1. Unfortunately, the lack of information from comparable investigations makes it impossible to validate the outcome.
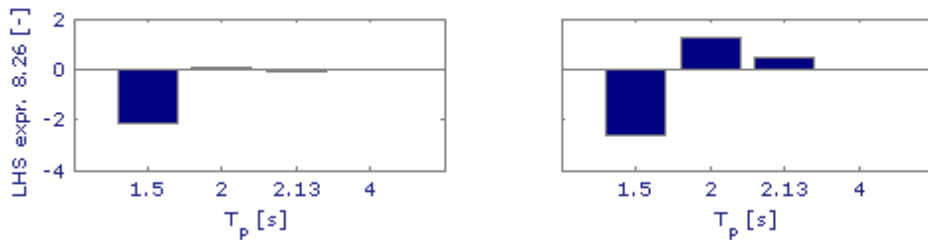

Figure 8.13   application of equation 8.26 to predefined oscillation periods left and right images distinguish situation with triangular and trapezoidal resp.

TUDelft

9 Implementing traffic to an optimized rigid multibody system

In previous sections especially the qualitative aspects of traffic and wave diffraction has been considered. In this section, quantitative aspects, dimensions and hydraulic parameter values, will be determined for implementation into the rigid multibody system.

9.1 Acceptable serviceability and safety level

According to TNO Bouw en Ondergrond and TNO Voertuigentechniek, driving a vehicle with 80 km/h across a floating thoroughfare will be experienced as 'comfortable' when vertical accelerations and rotation angles of the deck do not exceed ten percent of the gravitational acceleration and five degrees, respectively. However, what this comfort level will be when this vehicle reaches 100 km/h or 120 km/h is unknown and, therefore, must be determined. Determining the vertical acceleration levels, we introduce the following assumption: the comfort level will be fully correlated with the total amount of energy of the vehicle. In other words: when a certain energy level has been exceeded, the passage felt no longer pleasant. This energy level is supposed to be constant. The total amount of energy equals the kinetic energy and the potential or 'stored' energy. Ignoring rotational energy from the wheels, gearbox losses, etc, kinetic energy of the vehicle is a function of vehicle mass and (squared) velocity. Potential energy is stored in mass, gravitational acceleration and position of the vehicle. Since mass, gravitation and position are constants and acceleration level is known for 80 km/h, the ratio between vehicle velocity squared and vertical acceleration is constant too when the total energy level is constant. The acceleration levels can therefore be derived as follows:

$$a_{max,c} = \frac{(80/3.6)^2}{(c/3.6)^2} a_{max,80}$$

(9.1)

Where:

$a_{max,c}$:   vertical acceleration level of the vehicle corresponding with velocity c

The vertical acceleration level of the vehicle corresponding to 80 km/h is denoted as $a_{max,c}$. Strictly speaking, this value is not exactly ten percent of g, since vehicle suspension and tires always reduce the vehicle acceleration relatively to the deck. Regarding the model, we are allowed to neglect this influence, causing a reduction of 45 and 65 percent for 100 and 120km/h, respectively, with respect to the 80km/h level. In figure 9.1, different levels are resembled in a graph.

As it comes to the level of rotation angles, appealing to the Dutch code NOA 2007, the limitation demand for five degrees can be excluded by the recommendation of 1.8 degrees for 80 km/h. According to the code, 1.35 degrees is recommended for 100 and 120 km/h. Figure 9.1 shows the percentages of the gradients versus different vehicle velocities, in a manner analogous to the code.
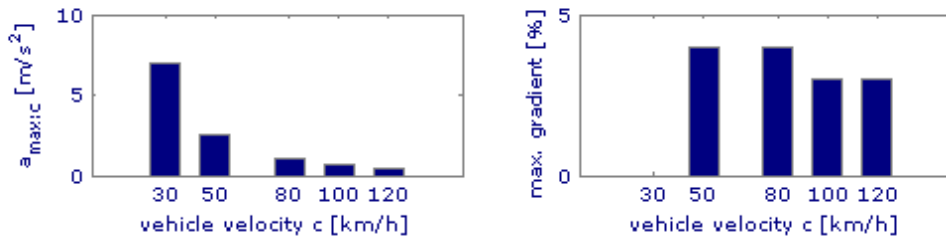
TUDelft

Figure 9.1   bar graphs with maximum vertical acceleration levels and gradient percentages for different vehicle velocities

9.2   Implementing wave diffraction

This subject has indirectly been announced in subsection 5.3: optimization of the rigid multibody system by implementing wave diffraction. In this subsection, we predefine hydrodynamic parameters and try out if the multibody system behaves differently with respect to a buoyancy-based-system.

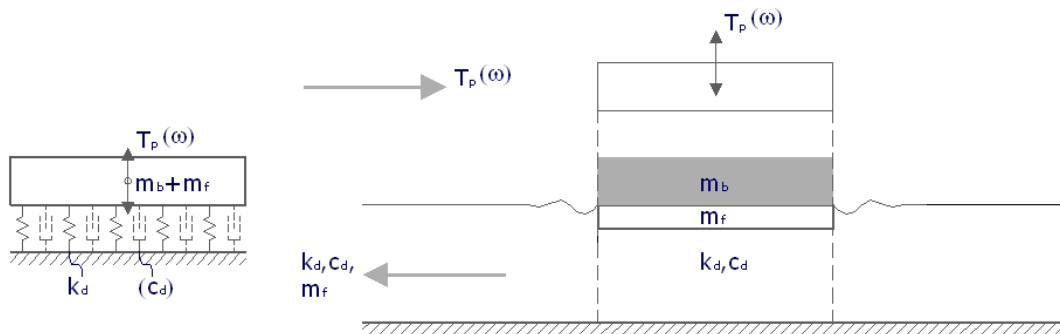### 9.2.1 Hydrodynamic parameters

Figure 9.2   relationship between wave diffraction and mass-spring model

The natural frequency of the multibody system will be applied as input argument for the external frequency in the wave diffraction model in order to derive appropriate hydrodynamic parameters. However, this approach leads to implicit computational steps to be taken. The natural frequency depend on added mass and stiffness and, in turn, added mass and stiffness are output arguments of the wave diffraction model. To illustrate the calculation procedure, the (parameter) relationship between the wave diffraction model and a simple mass-spring model with inclusion of added mass and buoyancy stiffness is schematically depicted in figure 9.2. Since frequency and stiffness parameters are collective in- and output variables for both models, we will plot two graphs (one for the wave diffraction model and one for the mass-spring model) in one figure with frequency and stiffness on both axes. The natural frequency with corresponding stiffness parameter can be found where both lines intersect.

Stiffness from the wave diffraction model is calculated with Matlab, whereas buoyancy stiffness can be obtained by the formula:

$$k_d = \omega_0^2 \left(\rho_0 A + B m_f \right) \tag{9.2}$$

which is a result of a variable transformation of expression 6.18 with inclusion of added mass. In expression 9.2, $\omega_0 = 2\pi/T_p$ and $\rho_0 = 102.5\,kg/m^3$, $A = 8.64 m^2$ and $B = 5.4 m$. All remaining variables are conform section 8.1. A 'trial and error' – calculation then shows that the intersection point has the following coordinates: $\{2.778s; 0.053\,MN/m/m^1\}$

The calculation of the intersection point can be made much quicker if buoyancy stiffness is determined by static buoyancy. Expression 9.2 changes into:

$$k_d = \omega_0^2 \left(\rho_0 A + B m_f \right) = \rho g B \tag{9.3}$$

A wave diffraction model, with frequency as input and added mass and damping as output arguments, would be sufficient enough to obtain the unknown coordinate, as schematically indicated in the figure below. From expression 9.2, an alternative expression (with respect to expression 8.6) for added mass,

$$m_f = \rho g/\omega_0^2 - \rho_0 h = m_t - m_b \tag{9.4}$$

with $h = A/B = 1.6 m$ can be derived. This expression provides insight in how the mass is composed; the first term represents the total mass (m_t) and the second term the mass of a pontoon (body element) (m_b) per square meter horizontal plane.

Completion of $T_p = 2.778s$ result in $m_{f,w} = 1753.9\,kg/m^2$ what implies an invariant influence depth of $\alpha_{am} = 1.75 m$. This is a new requirement in the preliminary design of the floating thoroughfare. For $T_p = 2.778s$, Matlab generates for the corresponding damping parameter $c_{d,w} = 66.84\,MNs/m/m^1$.
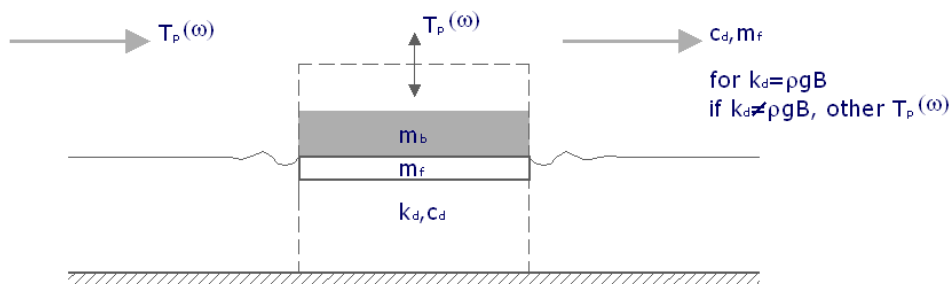

Figure 9.3 **alternative calculation scheme**

For rotational motions, new natural frequencies must be derived with corresponding hydrodynamic parameters. Therefore, we may reassume the stiffness parameters independent of the frequency and equal to the static buoyancy value. However, the algorithm for the added mass is not valid anymore, m_f is no longer constant over the body length. See figure 9.4.
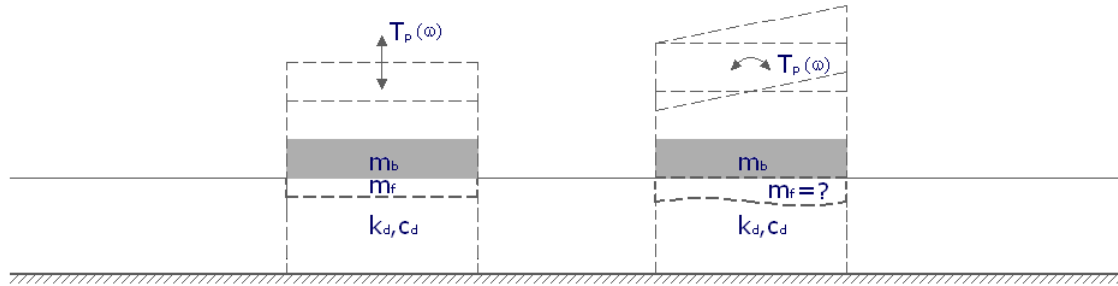
TUDelft

Figure 9.4   **added mass cannot be taken constant over the x domain in case of rotation.**

Nevertheless, a solution to this problem is still straightforward; since we are interested in an acceptable average value in stead of a fully analytic description, we choose to introduce an equivalent value for m_f. This can be done by the 'trial and error' method; once the natural frequency is known from the wave diffraction model, the equivalent value for the added mass, $m_{f,\theta}$, can be estimated from the buoyancy model.

Accordingly, with $k_{d,\theta} = 0.216/0.054 \, MNm/rad/m^1$ the period reads $T_p = 2.018s$. For $T_p = 2.018s$ we obtain $m_{f,\theta} = 797.5 \, kg/m^2$ for closed and $m_{f,\theta} = 672.9 \, kg/m^2$ for intermediate positioned bodies. The corresponding damping parameters are $c_{d,\theta} = -67.12/-16.78 \, MNms/rad/m^1$.

Successively, figure 9.5 shows graphically the coordinates: $\{2.778s; 0.053 \, MN/m/m^1\}$ and figure 9.6 will affirm the coordinates: $\{2.018s; 0.216 \, MNm/m/m^1\}$ for both the vertical and rotational case.
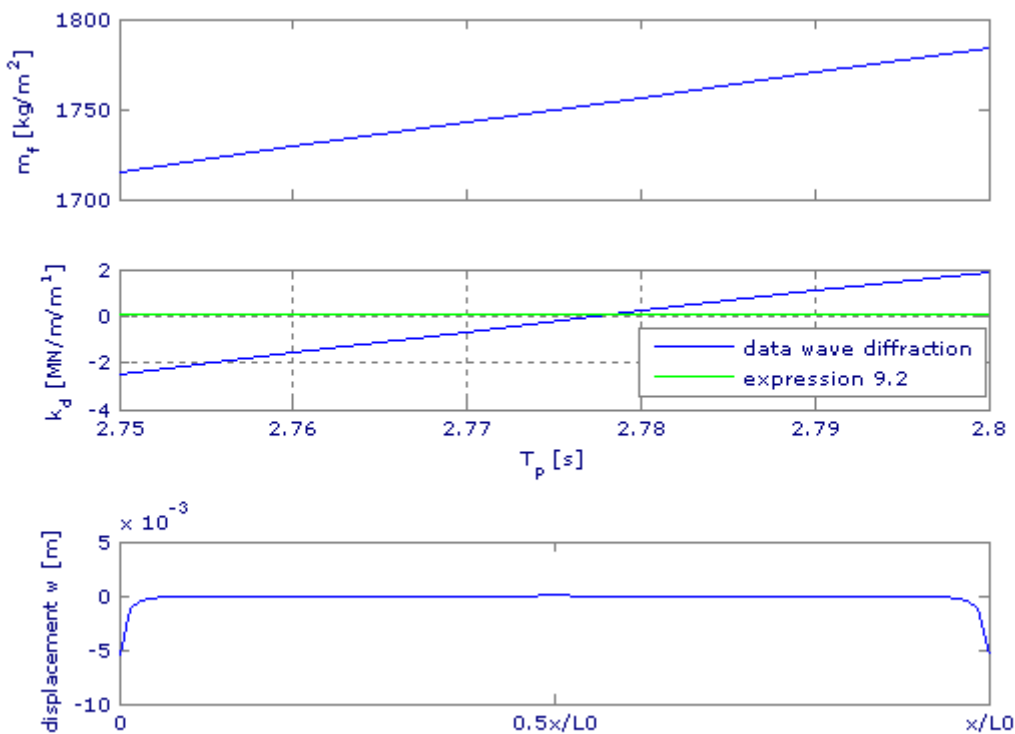

Figure 9.5   **from the top downward: added mass versus period, determination period and stiffness parameter and body displacement corresponding to a period of 2.778s**
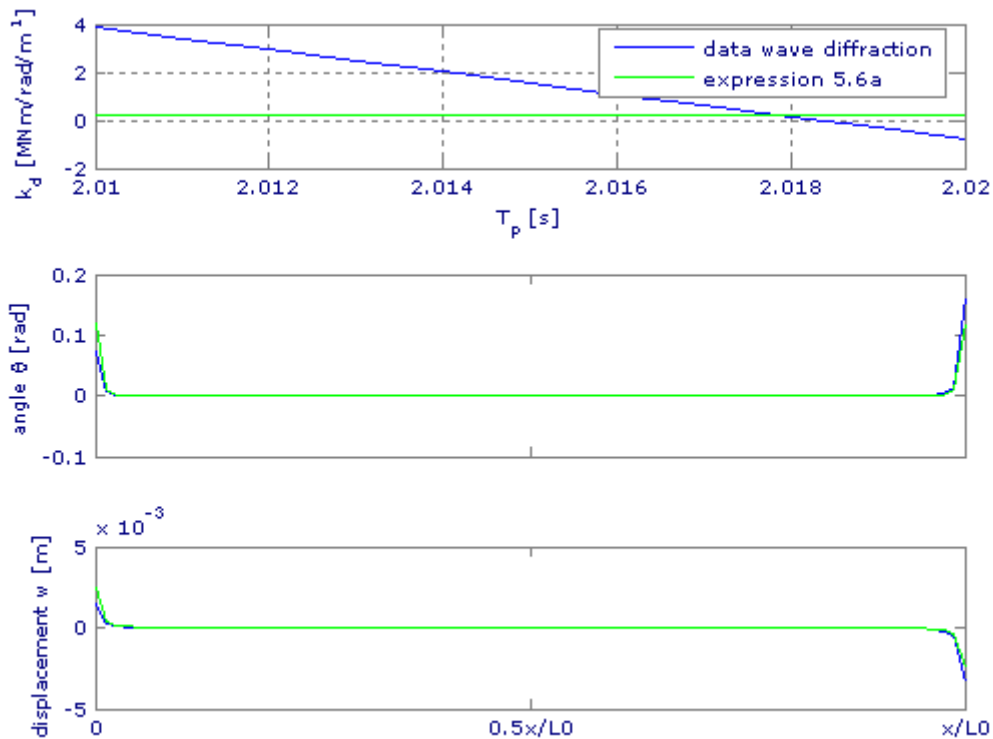
Figure 9.6 **from the top downward: determination period and stiffness parameter (closed body), body angle/displacement corresponding to a period of 2,018s .**

9.2.2 Wave diffraction versus buoyancy

The (hydro)dynamic behaviour of the floating thoroughfare is supposed to be realistically simulated when parameters, obtained by the wave diffraction approximation, will be implemented in the multibody system. Against our better judgement, we used to implement parameters obtained via a static equilibrium consideration (static buoyancy) because of ease and simplicity. Suppose that two systems, a wave diffraction-based-system and a buoyancy-based-system, behave quite similar, then buoyancy will be preferred in stead of wave diffraction. Therefore, in this subsection, we will concentrate on (dis)similarities in the responses of both systems, for example, when systems move in their eigen motion. For convenience, we reconsider the uncoupled or superimposed system from subsection 6.2.2, in which a series of five bodies will be submitted to an initial displacement of 0.1m. Figure 9.7 displays a schematization belonging to systems that are distinguished by hydrodynamic parameters: buoyancy (k_d), buoyancy + added mass (k_d, m_f) and wave diffraction approximation (k_d, m_f, c_d).
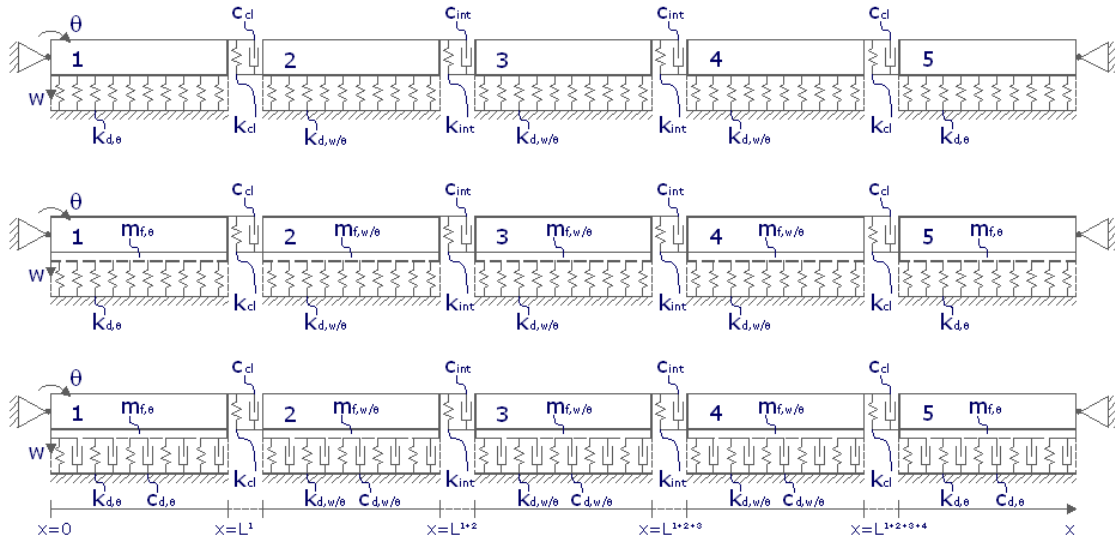
TUDelft

Figure 9.7 **from the top downward: buoyancy approximation, buoyancy + added mass and wave diffraction approximation**

The natural frequencies in case of simple buoyancy can be read out of subsection 6.2.2. The values are:

$$\omega_{0,1} = 0.720 + 14.004i$$
$$\omega_{0,3} = 0.422 + 11.969i$$
$$\omega_{0,5} = 6.802 * 10^{-4} + 7.430i$$

Taking into account the added mass of $m_{f,w} = 1753.9\,kg/m^2$ ($m_{f,\theta} = 797.5/672.9\,kg/m^2$), a new equilibrium will be found for frequencies:

$$\omega_{0,1} = 0.129 + 5.939i$$
$$\omega_{0,3} = 0.043 + 4.075i$$
$$\omega_{0,5} = 0.028 + 2.706i$$

In case of wave diffraction, with $c_{d,w} = 66.84\,MNs/m/m^1$ ($c_{d,\theta} = -67.12/-16.78\,MNms/rad/m^1$), the natural frequencies become:

$$\omega_{0,1} = 6419.1 + 0i$$
$$\omega_{0,3} = -3008.7 + 0i$$
$$\omega_{0,5} = -0.007 + 0i$$

Preceding any graphical judgement, numerical judgement already tells us that something does not strike the right note here! By reconstructing the (fictitious) composed system's displacement out of equation

$$w^n(t) = A_n e^{\left(-\text{Re}\left[\omega_0^n\right]t\right)} \cos\left(\text{Im}\left[\omega_0^n\right]t\right) \quad for \ \{n|1 \le n \le 2N - 4\} \tag{9.5}$$

with: $A_n = 0.1/n\,m$ and $N = 5$, it becomes clear why; in the plot for wave diffraction, unrealistic unstable behaviour serves our true suspicion in a graphical way. Causality in this case is quite clear; wrong damping output is the consequence of wrong frequencies,

since (negative) damping attributes to instability. An explanation is however less clear, but it is doing some good if we think in terms of conditions and concessions. From the wave diffraction approximation, parameters are generated under steady state conditions. If they were generated under non-steady conditions, for example in eigen motions, values would have been different. A plausible explanation according to section 8; calculating w halfway the body when dealing with a (slightly) curved interfaces overestimates the amount of energy (read: damping) through the edges. Since calculation at $x = 0$ and $x = L$ is out of the question for the same reason, we are forced to do concessions to come to an appropriate answer; 'least inaccurate' calculation is expected to coincide with calculation just outside the body, where 'interface errors' literally fade away. At the free surface, displacement w seems much larger and therefore new damping values are even much smaller than before ($c_{d,w}$ is more than thousand times smaller and $c_{d,\theta}$ more than hundred thousand times smaller than before.) To be quite positive about the new magnitudes, we examine the following commentary:

- vertical damping is close to critical which is in good agreement with reality. The critical damping value reads: $c_{d,w,cr} = 2\omega_0 m = 46845\, Ns/m/m$[1] which is 70 percent (in stead of 0.07 percent) of vertical damping capacity! Now, over damping becomes reliable. The minor importance of rotational damping however is in assessable but no less reliable for the same reason.

- negative (real parts in the) natural or eigen frequencies do not exist in a system in which $c_{cl/int}$ is brought down to zero. With $k_{cl/int} = 6*10^4\, N/m$, the series of test frequencies becomes:

$$\omega_{0,1} = 0.024 + 5.889i$$
$$\omega_{0,3} = 0.101 + 3.665i$$
$$\omega_{0,5} = 5.352 + 0i$$

what adds value to the credibility of the new found magnitudes once again. Critical is the first mode because it contains the lowest positive real integer of all natural frequencies.

Output, numerical or graphical, from wave diffraction is expected to be quite similar to output from buoyancy and added mass. At first sight, it seems paradoxical – answering the objective question with this comment – but it is not: aiming at recalculated frequencies for wave diffraction[1]:

$$\omega_{0,1} = 0.150 + 5.885i$$
$$\omega_{0,3} = 0.120 + 3.657i$$
$$\omega_{0,5} = 5.357 + 0i$$

it states that both systems have - by approximation- identical fundamental modes. In figure 9.8, responses with comparable amplitudes over the time interval underline that there is similarity to some extent. On the other hand, differences 'diverge' from the second to the third mode – to an over damped versus a typically

---

[1] Besides c_d , T_p (and through it m_f) must be revaluated, however, the effect is negligible according to the steepness in the graphs of figures 9.5 and 9.6 and therefore this is omitted.

TUDelft

under-damped mode – to emphasize that actually dissimilarities will dominate the total system (including rotation). This limits the replacement of a wave diffraction approximation to a certain extent.
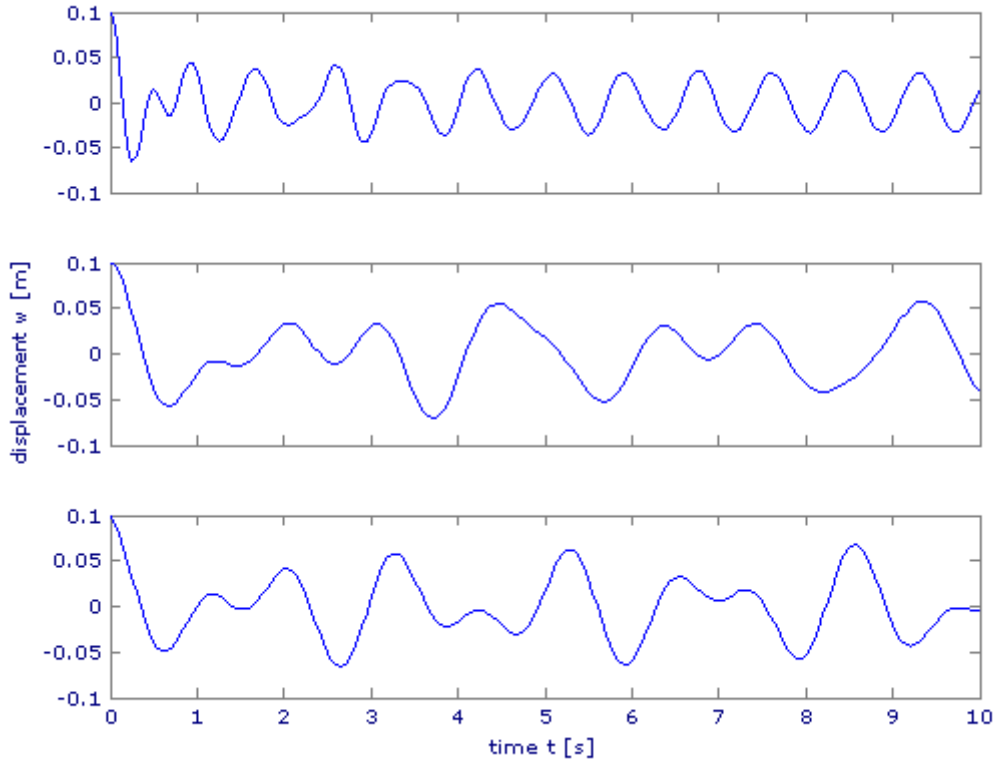

Figure 9.8   **response of superimposed system to an initial displacement of 0.1m in case of buoyancy, buoyancy with added mass and wave diffraction, respectively.**

9.3   Model verification

In this subsection, we implement a vehicle with constant speed as two external concentrated moving loads to the optimized multibody system for model verification purposes. In this sentence, the word 'optimized' refers to the inclusion of the wave diffraction approximation. Model verification as objective requires a proper translation of field conditions to match the computational model (multibody system) with the prototype as good as possible. To this end, we verify the model, in which the joint stiffness and damping parameters work as 'tuning tools'.

9.3.1 Field conditions

Field conditions will be specified by (new) vehicle characteristics, measurement locations and track dimensions.

Firstly, vehicle characteristics are not equal to design characteristics proposed in section 7: TNO Voertuigentechniek performed the series of tests with a BMW, type 520i and accordingly we account for a mass reduction (1990 – 1535 = 455kg) and wheel base stretching (2.88 – 2.76 = 0.12m). Secondly, measurements are categorized by vehicle and

TUDelft

track measurements and by design velocities. For 30, 50, 80 and >80 km/h, six or seven tests were employed and, at the same time, vehicle and track kinematics have been measured. In TNO-report "Testresultaten prototype Drijvende Weg" (Test results prototype Floating Thoroughfare) 2003 all data of the prototype has been documented. Measuring track kinematics, a couple of sensors have been lined up along both edges. Lining up against driving direction, at one, nine and fifteen meter distance from zero (i.e. at $x = 40.75m$ or 1.5m ahead from the centre of the twelfth pontoon) six devices were installed that return the data signal. Thirdly, the track length was 70 meters.

When the test vehicle had a speed of 30 km/h the measured vertical displacements are practically the best displacements for verification. From the series of six with 30 km/h, the third is most valuable, see figure 9.19.

During the test measurement, the test driver was surely most successful in driving a steady 30 km/h on the interval for which the vehicle passes the structure (between 18.2 and 26.6 seconds approximately). Besides this, he did not lurch too much either (velocities perpendicular to the driving direction are close to zero). The corresponding displacements can distinctively be seen in figure 9.10.
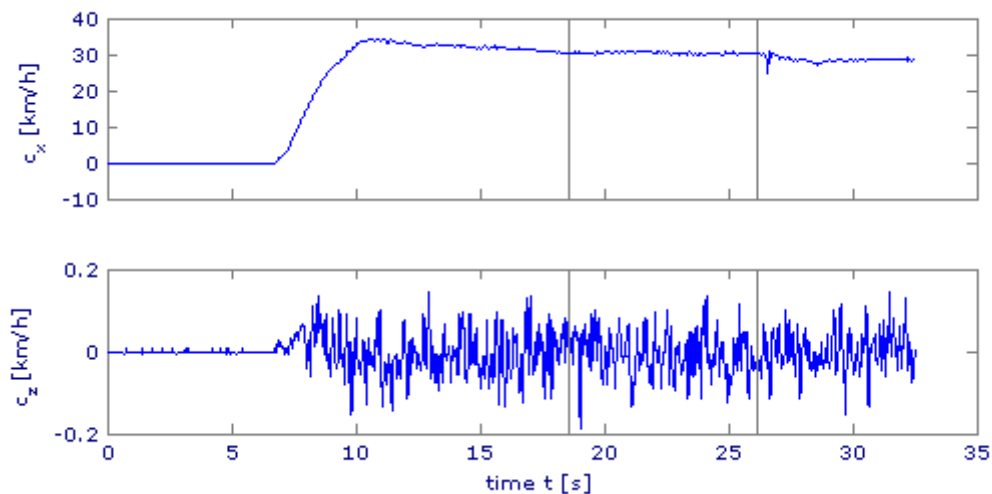

Figure 9.9   **test vehicle velocity against time (filename: KQ0WG30, nrs: 03)**
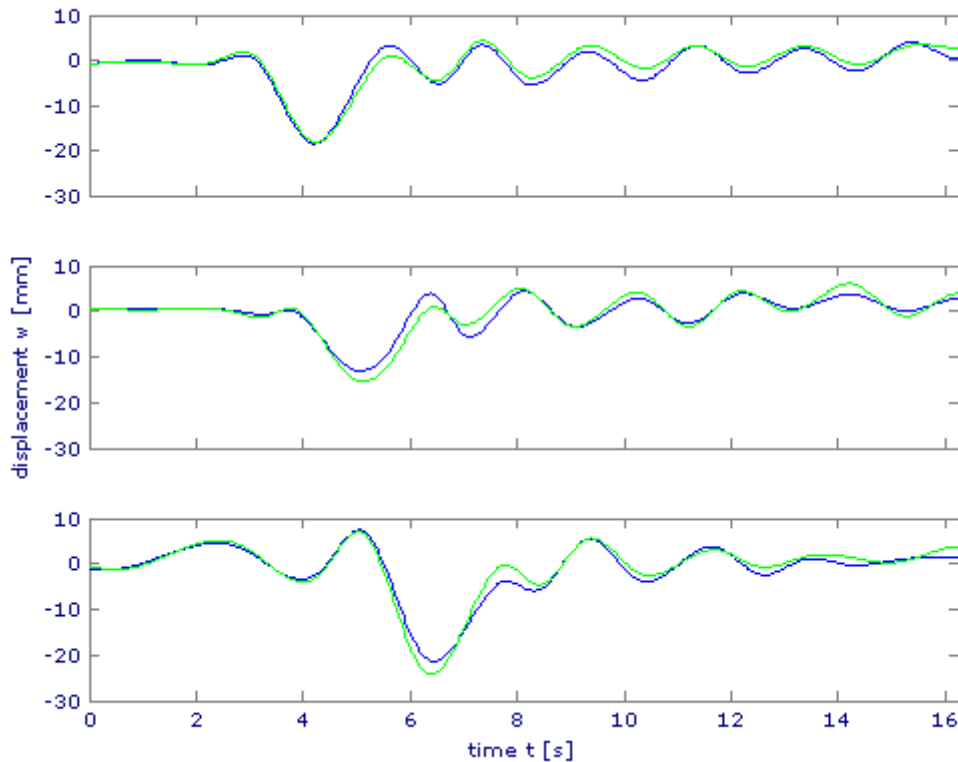
TUDelft

Figure 9.10   recorded displacements at waypoints 15, 9 and 1

Before the major impact, at 4.15, 4.87 and 6.25 seconds, the measured pontoon has already been brought into movement, as if the pontoon 'feels' the vehicle earlier. When the major impact occurs, the vehicle has yet been passed away for a second or more. This can be confirmed by calculating the average time from the distance over the structure divided by the average velocity. At the moment of crossing, time runs for 3.21, 3.93 and 4.89 seconds at waypoint 15, 9 and 1 respectively. According to the graph, at this time the corresponding pontoon reaches the top just before the big impact. (this proves that masses are inert) After contact, oscillation continues while the motion slowly fade away. The unexpected variations between the track edges (North and South sides) can not be explained by driving performances as was noticed before. It is more likely for wind waves (max. period of 1 second) which were artificially generated during the tests to put in an appearance. This can more or less be confirmed by the existence of initial displacements, which applies only due to an external factor like wind waves. Nevertheless, 'clean' tests are not available so we must deal with these 'imperfections'.

9.3.2 Varying the joint damping

By implementing field conditions together with the hydrodynamic parameters from section 9.2.1 in the multibody system, the tests can be simulated as well. Figure 9.11 shows the schematization of the system.
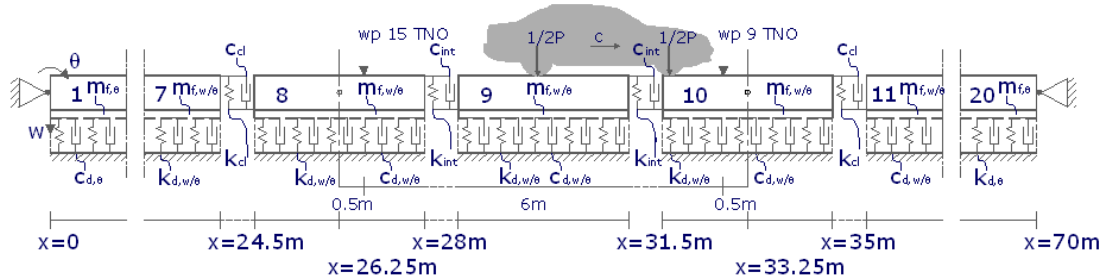

Figure 9.11   schematization of multibody system for verification.

In the compilation of all structural and hydrodynamic parameters of figure 9.13, joint stiffness ($k_{cl/int}$) and damping ($c_{cl/int}$) are undetermined. Therefore, these two sets of parameters are exclusive variables in computation. In stead of throwing ourselves upon a time consuming parameter study now, we prefer trying to save computational time by analysing the joint dynamic behaviour first. Analysing here yields the determination of points of application and vectors related to all dynamic forces that exist through (material) stiffness and friction. Once the analysis has been done, magnitudes of these forces and their kinematical displacements will be estimated (for example from figure 9.10) in order to assess values for $k_{cl/int}$ and $c_{cl/int}$ with:

$$k_{cl/int} = F_k / \hat{w}_{max}$$
$$c_{cl/int} \approx 4F_c / \left(\pi \hat{w}_{max} \omega \right)$$

(9.6)

In equation 9.6, F_k and F_c are reaction forces developed through stiffness and damping and $\hat{w}_{max}$ denotes the maximum kinematical deflection. The damping approximation is based on a periodical damping by coulomb or dry friction [2].

In figure 9.12, the most important elements in the joints, the row locks, are schematically drawn in fixated (left) and non-fixated (right) position. To illustrate how a closed row lock looks like, a photograph has been included here too.
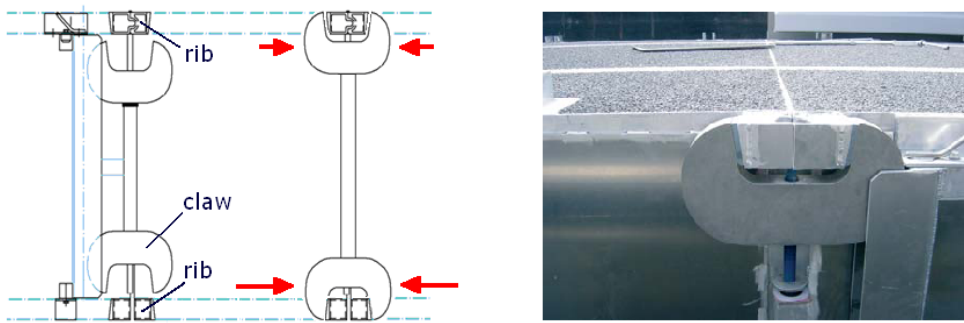
TUDelft

Figure 9.12   autoCAD drawing of cross-section and a close up of a row lock

The mechanism of the joint is based on 'fixed' rotation near the deck of the structure exhibiting the desired smooth transition from body to body under motion. In the design, a convex-shaped rib at the end of a body fits perfectly to the concave-shaped rib at the end of its adjacent body. A row lock keeps both ribs into position. Imagine that when a vehicle passes, a friction force will be initiated along the convex-concave plane if the ribs move relatively from each other. Only if the row lock is fixated (locked), the upper claw of the lock respond with a force (small red arrows in figure 9.12) that initiates this friction force. Due to (coulomb) friction, the structural motion is a damped motion. In the lowest claw of the lock, also a reaction force (large red arrows in figure 9.12) will be developed which could even become bigger than its upper neighbour (big external moments), but there will be no damping. Due to these forces, the structural deflections are minimized. Hence, it can be concluded that all row locks react 'stiff' whereas the concave-convex-shaped ribs provides for damping.

Taking the next step toward a solution, force magnitudes will be derived by applying the dynamic equilibrium consideration around a joint. Therefore, the mechanical schematization must satisfy the prototype schematization as good as possible. However, this requirement is unsatisfied as long as vertical dashpots and ditto springs perform the joint mechanical conditions for the model (see figure 9.11). Replacing them, for example, by rotational (coulomb) dampers and horizontal (linear) springs is a major step in the right direction, but since equations of motion change radically then (Appendix II and III), we accept the consequences of continuing in order to save ourselves from more discomfort.

Unfortunately, in this stage, concessions to the model means concessions to validation. This means that only frequencies and eigen motions, when amplitudes are small, can be validated. A positive consequence is that it becomes easier to obtain 'equivalent' structural parameters now; it follows that $k_{cl/int} = 0\,N/m$ because vertical springs deliver no contribution to horizontal (material) stiffness. Only $c_{cl/int}$ turns out to be unknown making the implementation of a parameter study much more straightforward. A 'best fit' can be agreed for $c_{cl/int} = 1 - 2 * 10^3\,Ns/m$.
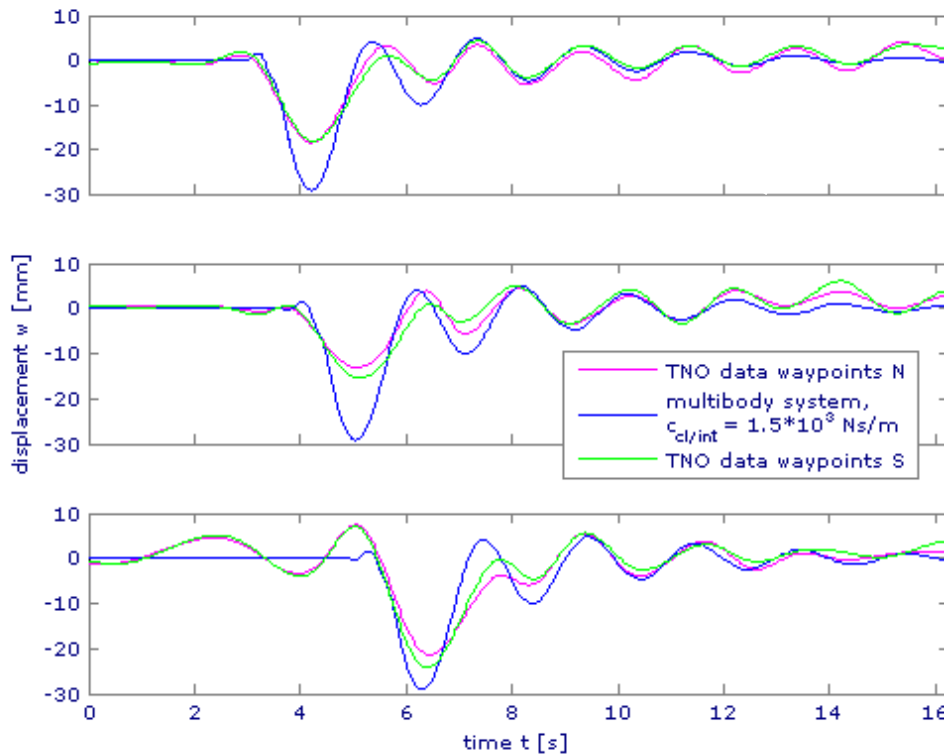
TUDelft

Figure 9.13   recorded and simulated displacements at waypoints 15, 9 and 1

The displacements from the multibody system should be equal to the mean of the measured displacements, at the North- and Southside, theoretically speaking. For the greater part this is certainly not true, according to figure 9.13, but when body motion is no longer exerted by the vehicle (in approximately the second half of the graphs) this is nearly true. Although the data is not free of noise, it is quite certain that concessions are causing the largest deviation in displacement output. The following arguments must be carried out:

- There is initial movement growing in time. Or in other words: the closer to waypoint 1, the more the initial displacement is intensified. This is the result of a 'stiffer' connection that passes through (vehicle) energy much faster. Another explanation could be found in the generation of propagating waves. By suppressing the fluid surface beneath on body repeatedly, waves are generated that propagate toward other bodies. In the model, this phenomenon is neglected since wave diffraction from the bodies is calculated individually. These waves, however, could become critical only if the wave velocity comes close to the vehicle velocity. For an average depth of five meters, the wave velocity in formula form reads:

$$c_{wave} = \sqrt{\frac{g}{k} \tanh(H_0 k)} \qquad\qquad (9.7)$$

in which the wave number $k = 2\pi/L_0$. After implicit calculation, the answer to equation 9.7 is $c_{wave} \approx 4.3\, m/s$ which is about two times slower with respect to the vehicle velocity(!) It is unlikely for propagating waves to significantly participate in the initial displacement.

- Significantly large displacements in the prototype are opposed by the joint mechanism. In the multibody system, these will not be opposed.
- There exist an out-of-the-phase difference that is annulated in the graph for verification purposes. Measurements must be corrected by 1 and 3.5 meters for waypoint 1 and 9 respectively. If we increase $k_{cl/int}$, the phase difference decreases. However, $k_{cl/int}$ is not capable for verification. Damping parameters $c_{cl/int}$ and c_d and frequency related parameters T_p (m_f) are capable and they more or less succeeded the test.
- An interface condition for the joint is: no internal displacements are allowed. Inside the joints, internal displacements will always occur but by increasing $c_{cl/int}$ and/or $k_{cl/int}$, they can be minimized. Using the equalities of 9.8, this can be checked for the validated model:

$$3.5\theta^1 = w^2 - 1.75\theta^2$$
$$w^i + 1.75\theta^i = w^{i+1} - 1.75\theta^{i+1} \quad for\ \{i\,|\,2 \leq i \leq 18\} \tag{9.8}$$
$$w^{19} + 1.75\theta^{19} = -3.5\theta^{20}$$

Figure 9.14 proves that – irrespective of whether it is safe to drive across such structure or not - there is a mismatch with the prototype.

As a final remark, it must be noticed that external waves will be kept outside the scope of this thesis. Because their size, it is expected for them to be of minor importance for the structural movement.
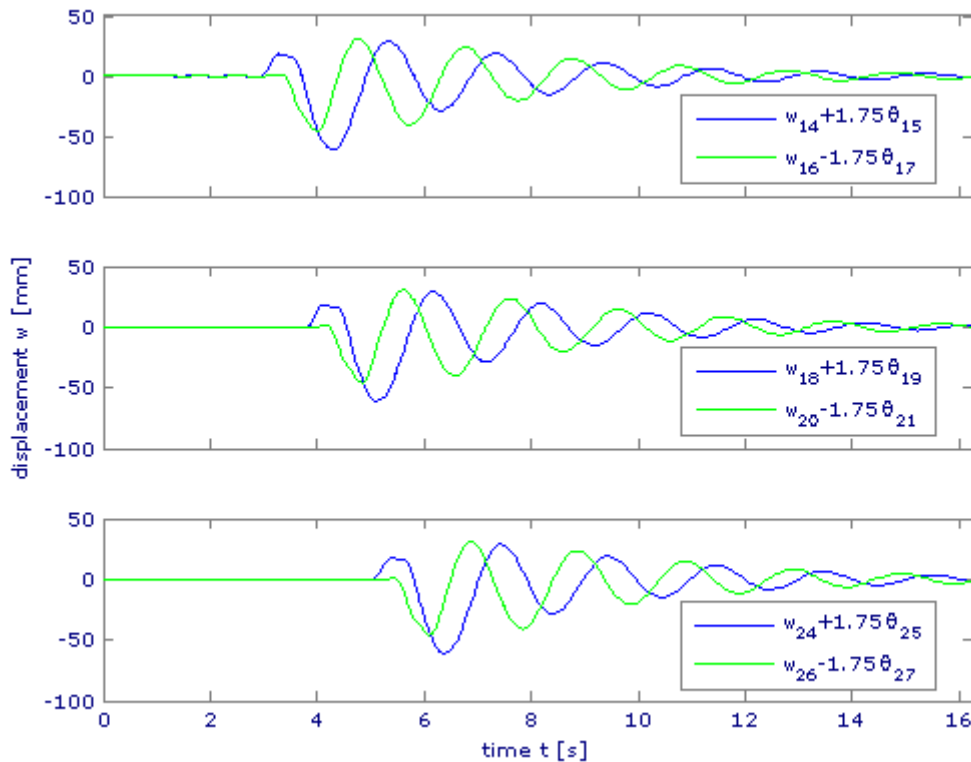

Figure 9.14   mutual displacement between coupled bodies due to internal displacements in joints; at x = 49. 52.5 and 56 m respectively,

TUDelft

9.4   Parameter study

Due to the difference between joint mechanisms in the multibody system and the prototype, model verification could not be fully implemented. Nevertheless, performing simulations with the optimized rigid multibody system makes sense as long as the system's hydrodynamic behaviour is 'credible' and internal displacements can be manipulated by structural parameters.

For this reason, a parameterstudy will be conducted on the multibody system. The parameters are the number of bodies, the length of the bodies and 'tuning tools' for the joints, respectively N, L^i, $c_{cl/int}$ and $k_{cl/int}$. To avoid complex or statistical traffic simulations, as discussed in section 4, we propose two scenarios as criterion for the road:

1.   Entering the structure by a solitary vehicle that exerts the most extreme deflection.
2.   Allowing a series of equally distant vehicles with identical velocities to create instability to the structure.

Based on these scenarios, simulations are repeated with different designvelocities, beginning at 80 and ending at 120 km/h.

9.4.1 Reference model verification

Preceding the parameter study, we must realize the importance of a verified reference model. After verification, parameter quantities are much easier to be found. Because questionable representations of structural movements underlie the parameter quantities of the present reference model:

$N = 20$, $L^i = 3.5m$, $c_{cl/int} = 1.5*10^3\,Ns/m$ and $k_{cl/int} = 0\,N/m$,

this verification need to be completed. A completion can be arranged via requirements denoted in subsection 9.1 but there is no guarantee that it works. In order to meet these requirements, displacements are less important, but angles and acceleration all the more. In formula form, we must satisfy:

$$a_c \leq a_{max,c}$$
$$\theta \leq \theta_{max}$$

(9.9)

in which a_c and θ are the vertical deck acceleration and the deck gradient, respectively. $a_{max,c}$ and θ_{max} represent the upper bounds for both measures, that depend on the (design)velocity. a_c and θ will be calculated with Matlab trough $[\texttt{t, y}]$, output of the ODE23-solver. The corresponding code can be found in Appendix V3. In the Matlab output, θ appears at uneven entries in the displacement vector **y** but for a_c an extra transformation is required to the matrix equation of motion:

$$\mathbf{M\ddot{y}} + \mathbf{C\dot{y}} + \mathbf{Ky} = \mathbf{F}(t)$$

(9.10)

Dividing the LHS and RHS of the equation by **M** (or multiplying by **M⁻¹**) and making $\mathbf{\ddot{y}}$ free in the LHS, we obtain from equation 9.10:

TUDelft

$$\ddot{\mathbf{y}} = \mathbf{M^{-1}}\left(-\mathbf{C}\dot{\mathbf{y}} - \mathbf{K}\mathbf{y} + \mathbf{F}(t)\right) \tag{9.11}$$

in which the matrices $\mathbf{M}$, $\mathbf{C}$ and $\mathbf{K}$ are known and the vectors $\dot{\mathbf{y}}$ and $\mathbf{y}$ and $\mathbf{F}(t)$ are previously determined per time step. Hence, a_c appears on even entries in the acceleration vector $\ddot{\mathbf{y}}$ and applies to the centre of gravity of each body. Inside the force vector $\mathbf{F}(t)$, vehicle characteristics must be replaced by design vehicle characteristics.

Far away from waypoint 15, 9 and 1, in $x = 3.5m$, unstable behaviour for 30 km/h is generated as can be seen in figure 9.15. Furthermore, the reference model turns out to be impractical too; with $k_{cl/int} = 0\,N/m$ and letting $c_{cl/int}$ further increase, accelerations and displacements will continue in time. This is obviously a complete nonsense. From a practical point of view, $k_{cl/int}$ will be upgraded to a minimum of $4*10^3\,N/m$ in order to get rid of instability throughout the system. Graphical results pertaining to $1*10^5\,N/m$ are shown in figure 9.16 for a clear confirmation.

With a new reference,

$N = 20$, $L^i = 3.5m$, $c_{cl/int} = 1.5*10^3\,Ns/m$ and $k_{cl/int} = 4*10^3\,N/m$,

the demand for safe and comfort accelerations $a_c \leq a_{max,c}$ is effectively satisfied.
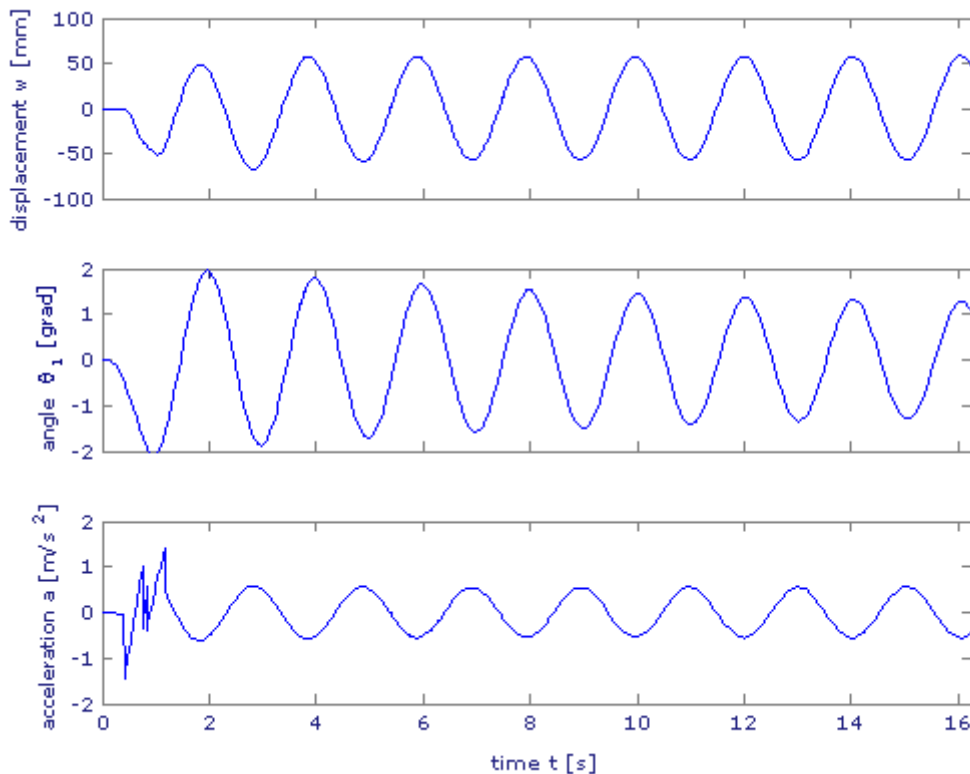
Figure 9.15   **simulation with x = 3.5 m and c = 30 km/h**

TUDelft
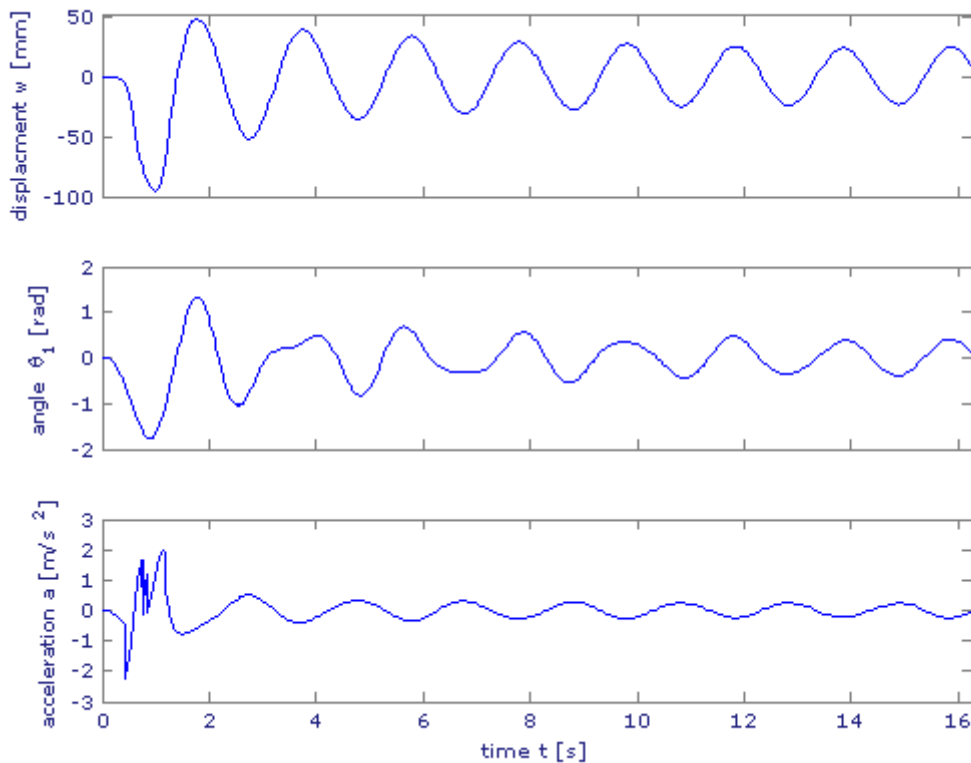
Figure 9.16   **simulation with** $k_{cl/int} = 1*10^5\ N/m$ **, x = 3.5 m and c = 30 km/h**

9.4.2 Entering structure with single vehicle

Simulations with 80, 100 and 120 km/h will complete simulations with 30 km/h. Outcomes associated with 30 km/h will be used as reference for simulations with 80 km/h and until 120km/h, the procedure will be repeated. Complying for economical and technical feasible solutions, the following strategy holds: After a miscalculation, we start evaluating $c_{cl/int}$ (or $k_{cl/int}$) and only when attempts are no longer successful, we move on to $L^{2,19}$. The remaining lengths together, denoted as $\{L^i\ \ for\,\{i\,|\,i=1,20 \cap 3 \le i \le 18\}\}$ will be evaluated when $L^{2,19}$ gives no satisfying results anymore. As a matter of fact, manipulation by distributed parameters over the joints and $L^{1,20}$ as 'tuning tools' are determined to be unsuccessful, as can be seen in Appendix VI. For each simulation, just one parameter differs from the reference model.

There is a 8.4 seconds-lasting-contact between vehicle and structure, when driving 80 km/h. On this interval, from figure 9.17 it can be seen that conditions have been stabilized at the entrance of the structure.
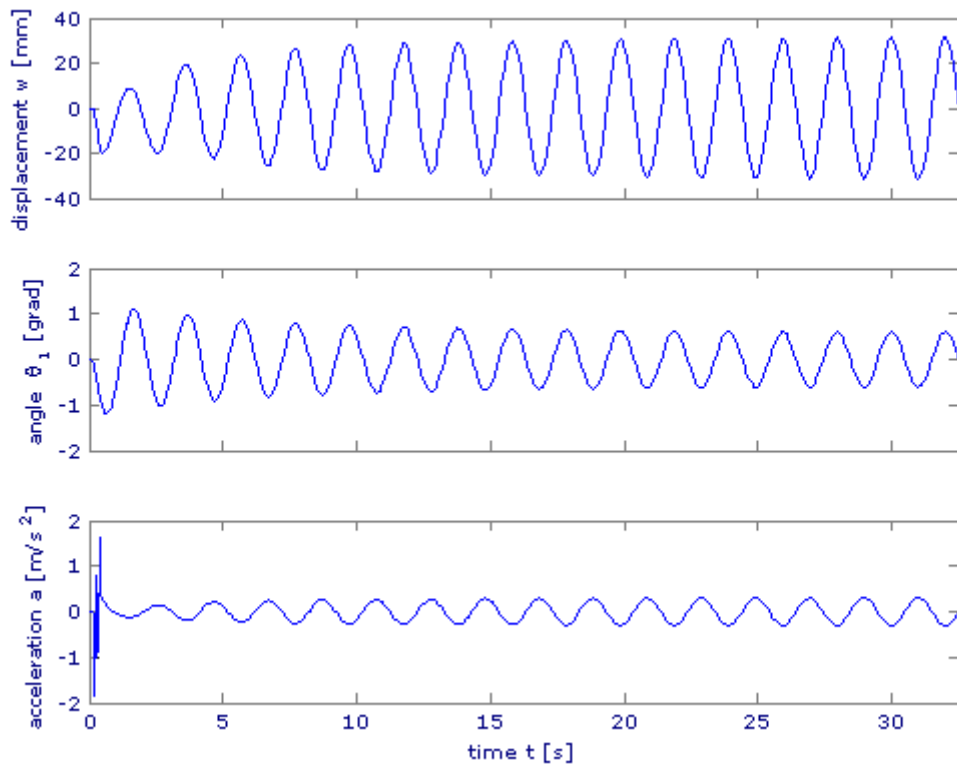
Figure 9.17   **simulation with x = 3.5 m and c = 80 km/h**

In figure 9.18, 4 graphs have been plotted with $c_{cl/int}$ and $k_{cl/int}$ versus quality measures a_c and θ. It can be noticed that acceleration a_c gradually increases when $k_{cl/int}$ increases and that there is no significant decrease until $c_{cl/int}$ increases. Angle θ, on the other hand, gradually decreases everywhere in the graphs and furthermore it comes nowhere close to the upper bound of 1.8 degrees. It seems sufficient to upgrade $c_{cl/int}$ to $1*10^5\,Ns/m$ in order to meet the requirements and to get rid of unrealistic stabilized conditions as well.
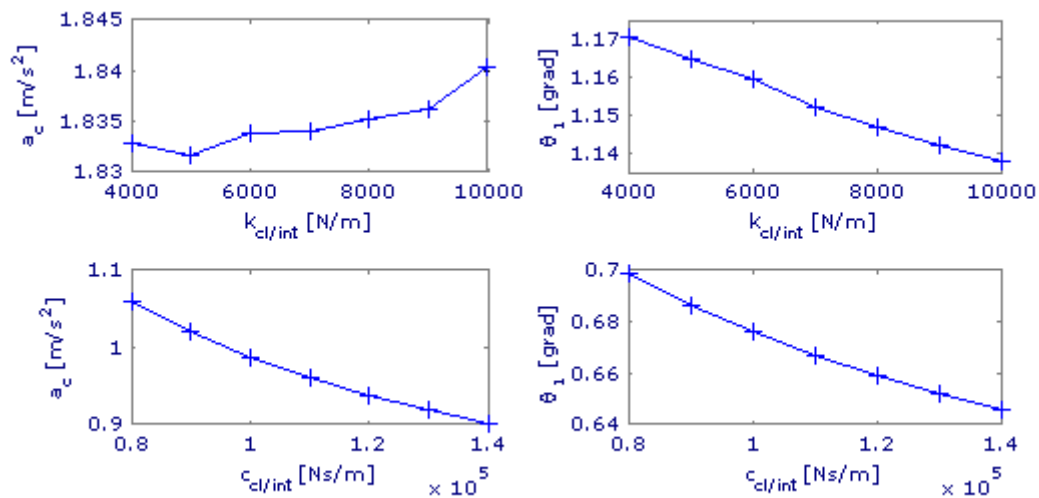
Figure 9.18   **simulation with 7 different values for $k_{cl/int}$ and $c_{cl/int}$ when c = 80 km/h**

The simulative output belonging to 100 km/h resembles the 80 km/h output quite well, but since requirements are tightening up, new simulations must follow. Focussing on accelerations in figure 9.18, through $k_{cl/int}$, we are able to tune the structural stability and no longer the vertical accelerations. Through $c_{cl/int}$, we are able to tune accelerations although there is no much room for tuning. Accelerations increase only when $c_{cl/int}$ exceeds $4*10^5 \, Ns/m$ and therefore a significant drop must come through $L^{2,19}$.

It is important to realize that pontoon stretching involves extensive computation due to correlation between body length and added mass and body length and fluid damping.

For a couple of L^i quantities, m_f and c_d are determined and resembled in figure 9.19. The second row in figure 9.20 underlines the success of this measure; when $L^{2,19} = 5m$, $a_c \leq 0.65 \, m/s^2$. Further optimization ensures that $a_c \leq 0.65 \, m/s^2$ can be achieved by a combination of $c_{cl/int} = 4*10^5 \, Ns/m$ and $L^{2,19} = 4m$ and a new reference embodies the parameters:

$N = 20$, $\quad L^i = 3.5m \quad \{i \mid i = 1,20 \cap 3 \leq i \leq 18\}$, $\quad L^{2,19} = 4m \quad c_{cl/int} = 4*10^5 \, Ns/m \quad$ and $k_{cl/int} = 4*10^3 \, N/m$.
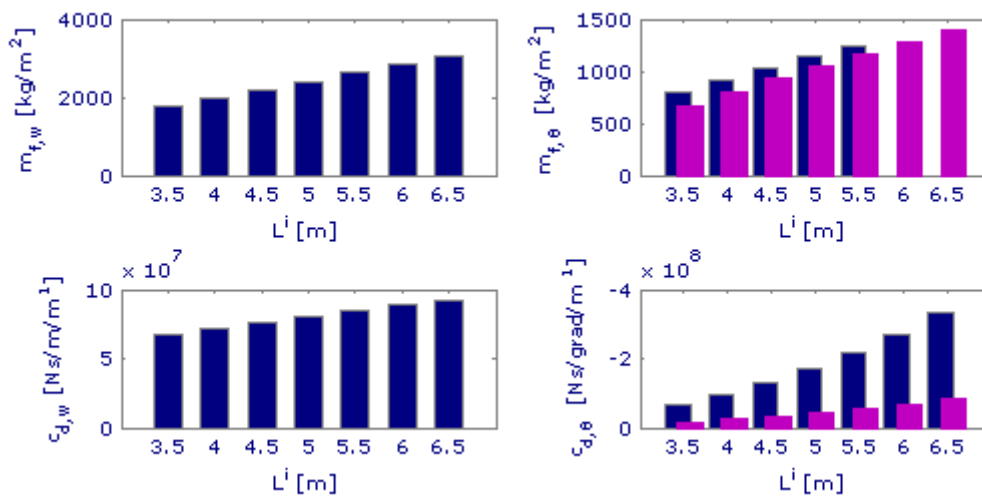
Figure 9.19   **added mass and distributed damping relative to the body length L^i. In the right bar graph, blue and magenta represent the closed and intermediate body values, resp.**
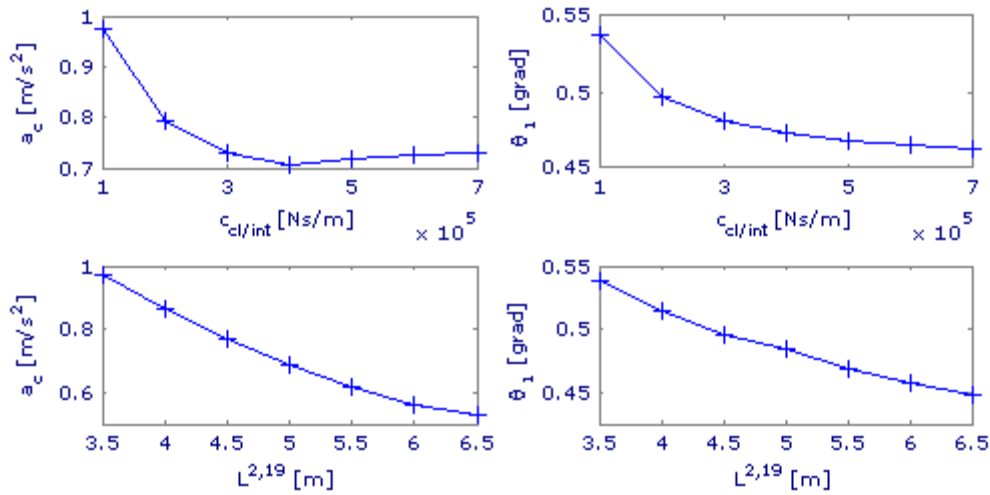
Figure 9.20   simulation with 7 different values for $c_{cl/int}$ and $L^{2,19}$ when c = 100 km/h

Even with 120 km/h on the clock, surpricingly similar results are obtained compared to 100 km/h. Once again, new simulations must be employed because of new requirements.

Since $a_c < 0.45\,m/s^2$, there is no room to manoeuvre for both $k_{cl/int}$ and $c_{cl/int}$ and therefore we fully count on L^i. Tuning L^i is most efficient when accelerations in the system do not vary too much from each other, what can be maintained by respecting the following relationship between $L^{2,19}$ and L^i :

$$L^i = L^{2,19} - 1m \quad \{i \mid i = 1,20 \cap 3 \leq i \leq 18\} \tag{9.10}$$

Figure 9.21 proves that $a_c \leq a_{c,max}$ is true as long as $L^{2,19} > 5.5m$ $\left(L^i > 4.5m\right)$ making an average body 1.5 times longer. The dashed line proves that accelerations halfway the structure stay close to the critical extremes due to the body stretch. Figures 9.22 and 9.23 separately display the critical responses for:

$N = 20$, $L^i = 4.5m$ $\{i \mid i = 1,20 \cap 3 \leq i \leq 18\}$, $L^{2,19} = 5.5m$ $c_{cl/int} = 4*10^5\,Ns/m$ and $k_{cl/int} = 4*10^3\,N/m$.

in case of 120 km/h and 30-100 km/h, respectively.
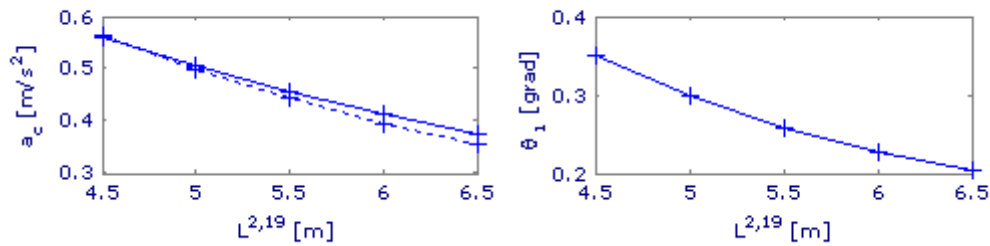
Figure 9.21   simulation with 5 different values for $L^{2,19}$ when c = 120 km/h
            ($L^i = L^{2,19} - 1m$ $\{i \mid i = 1,N \cap 3 \leq i \leq N-2\}$
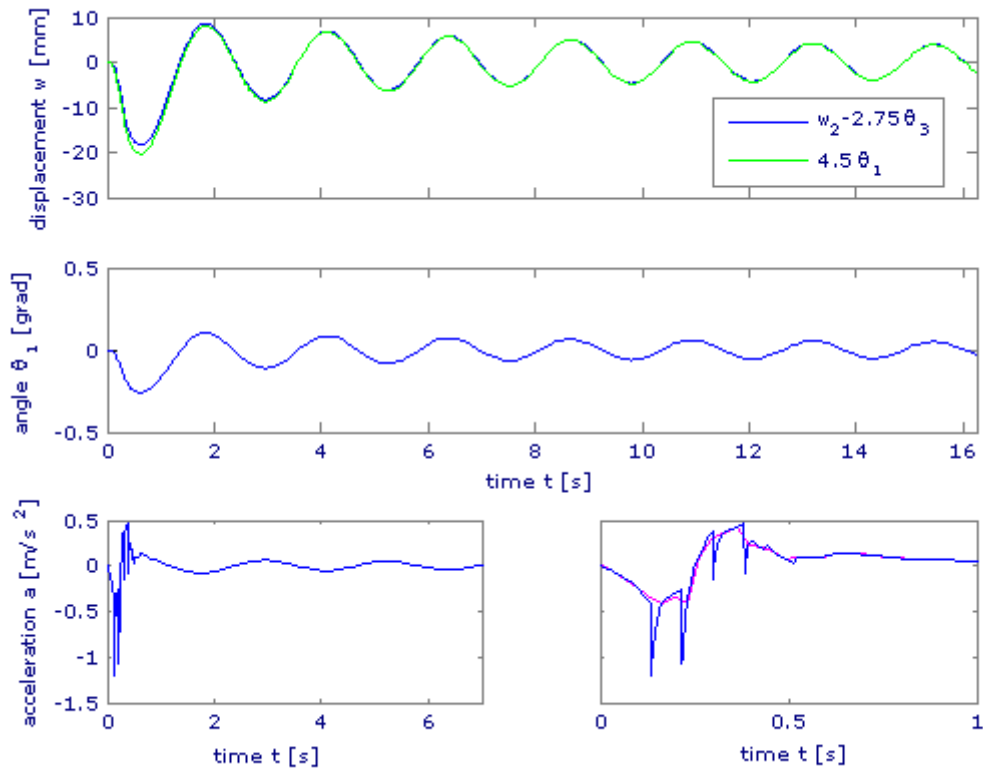
Figure 9.22   **simulation with x = 4.5 m and c = 120 km/h**
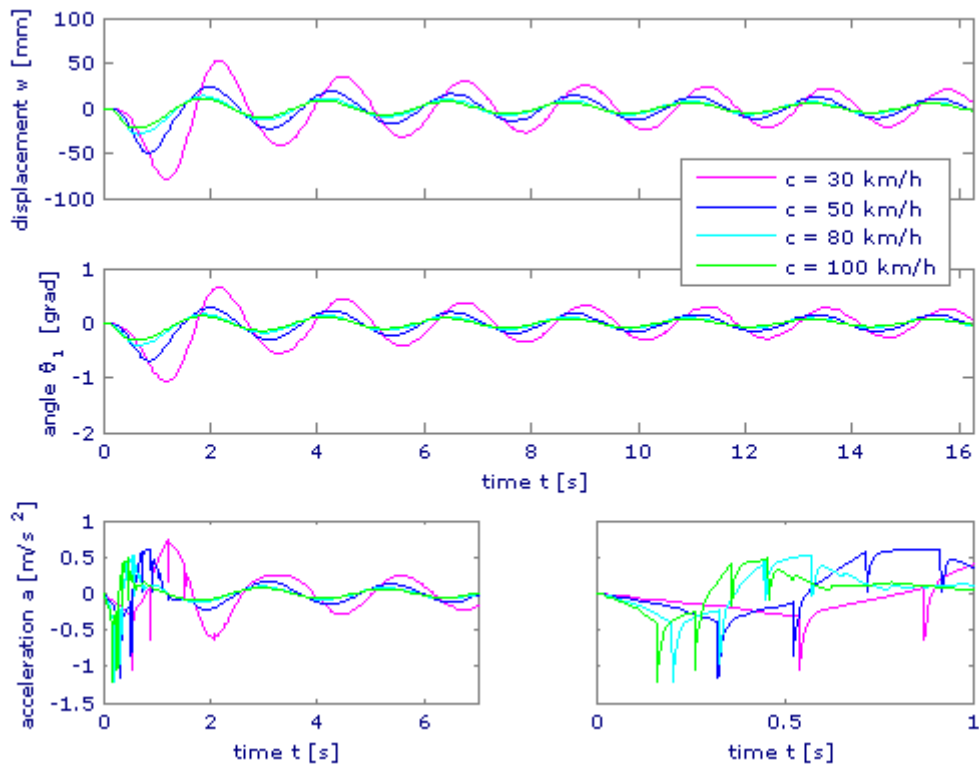
Figure 9.23   **simulations with x = 4.5 m and c = 30, 50 80 and 100 km/h**

Two final observations should be made in response of the figures 9.22 and 9.23 :

1. new parameter quantities minimizes the system's maximal mutual displacement to just 3 to 4 mm for 120 km/h! The discontinuities in the system's horizontal alignment do not hinder a solitary vehicle, but still can be annoying for following vehicles.

2. in the oscillatory course of accelerations, sharp peaks loom up as discordant notes. Per plot, 4 of them are noticeable; the fist one occurs when front wheels releases the first and enters the second pontoon and the second one follows from the back wheels. Two secondary peaks represent the responses that belong to releasing the second and entering the third pontoon. The higher the velocity becomes, the narrower the peaks are and consequently for large values of c their influence may be neglected. In case of low velocities, however, the peaks are wide enough to make themselves felt, but they do not exceed the bounds anymore.

9.4.3 Resonance by multiple vehicle

Resonance, characterized from nuisance to seriously hazardous, can be developed when frequencies through an external load (excitation frequencies) come close to (one of the) eigen frequencies governed by the multibody system. It develops through magnitude as well as cyclic appearance of an external load, becoming in-phase with the (harmonic) movement of the structure itself. A cyclic appearance can be simulated by taking a(n) (infinite) series of equally distant vehicles with identical speeds to exert to the multibody system. The vehicle's mutual distance (md) and velocity c are then key parameters in computation because these determine the critical frequency. Apart from this, the length of the structure is important to create enough space for many vehicles to govern the 'undesired' instability. Critical frequencies are complex eigen frequencies with a negative real part. One eigen frequency out of 38 (76 including complex conjugates) fulfils this condition:

$$\omega_{0,19} = -0.010 + 2.799i$$

What implies that when vehicles passes every $2\pi/2.799 = 2.24s$, there is a chance to generate resonant behaviour. Hence, per (design) velocity, all critical values for md can be defined and figure 9.24 shows the results thereof:

TUDelft

Velocity c [km/h]	Critical mutual distance md [m]
30	18.7
50	31.2
80	49.9
100	62.3
120	74.8

Figure 9.24 **table with values for critical mutual distance**

Using Matlab codes in Appendix V.3, plots as made in fig 9.25 – 9.28 for different places and velocities evidently show the presence of resonance in this situation. Via cyclic appearance, apparently, these vehicles are able to exhibit forces that are big enough to transfer the energy for resonance too.
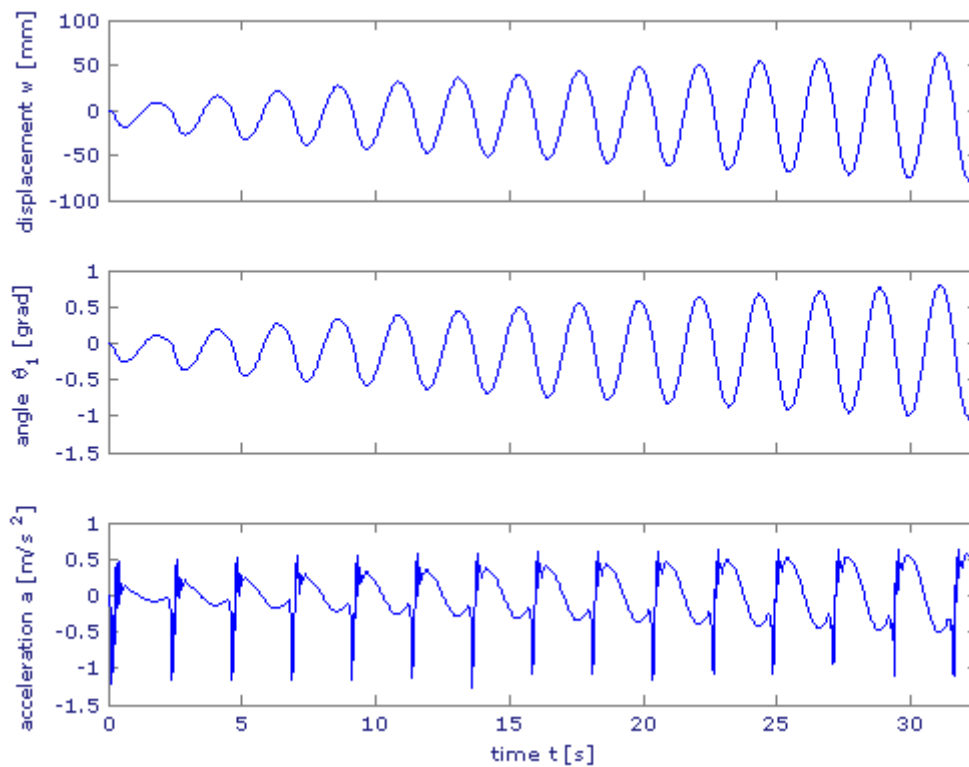
Figure 9.25 **simulation with , x = 4.5 m, md = 74.8 m and c = 120 km/h**
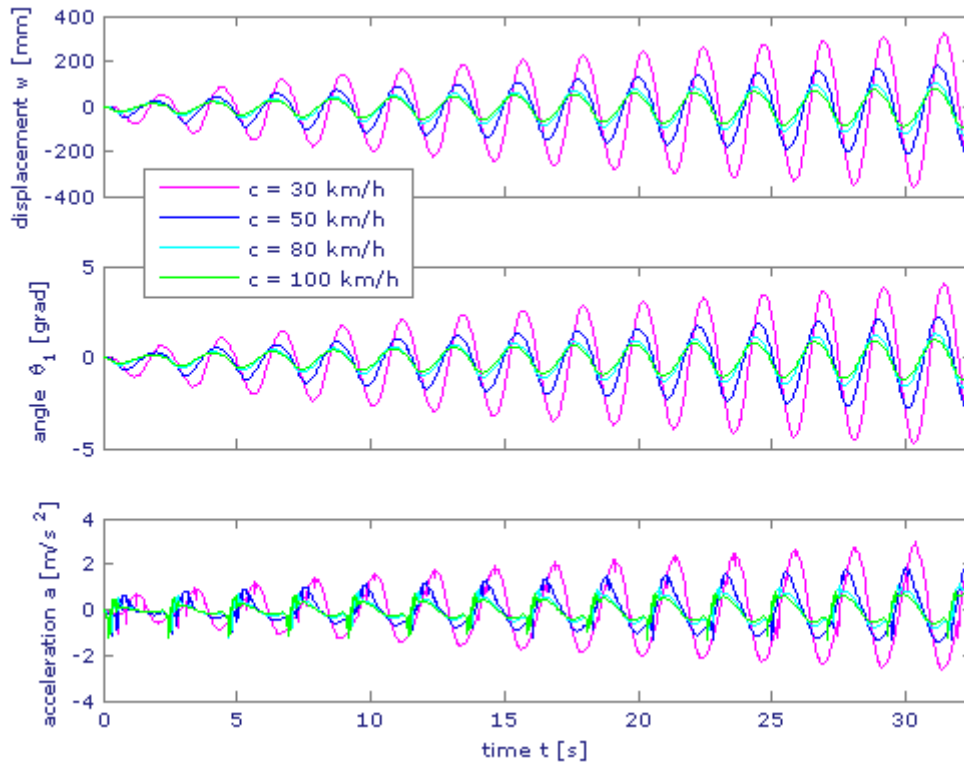
Figure 9.26 simulation with , x = 4.5 m , md = 18.7, 31.2, 49.9, 62.3 m and c = 30, 50, 80 and 100 km/h
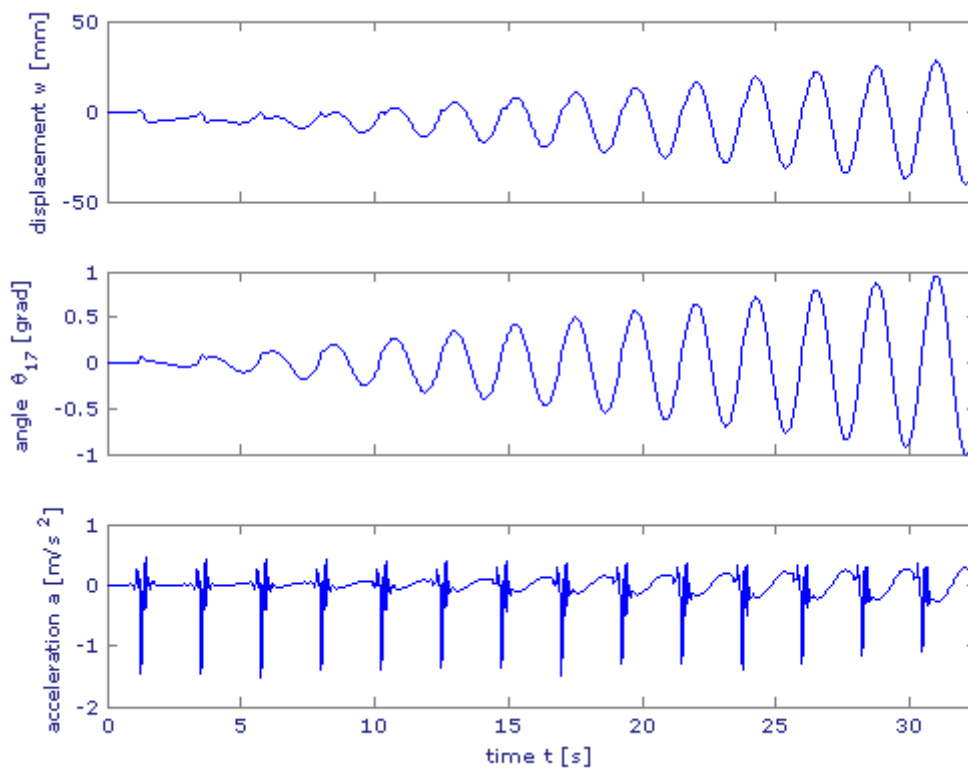
Figure 9.27 simulation with , x = 41.5 m, md = 74.8 m and c = 120 km/h
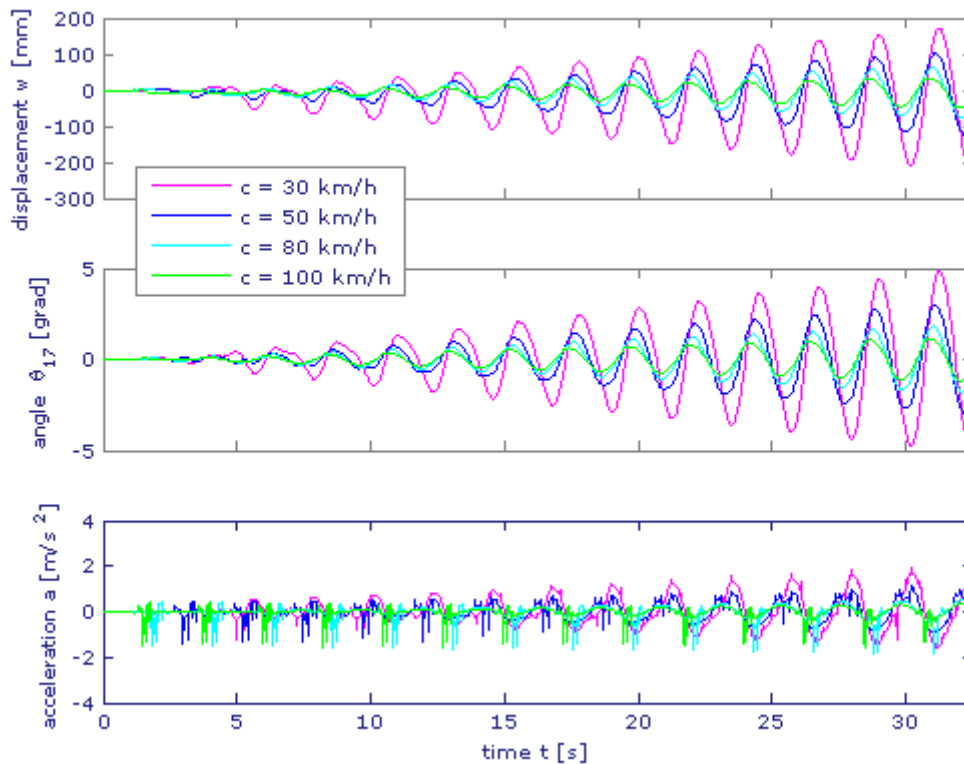
Figure 9.28   **simulation with , x = 41.5 m , md = 18.7, 31.2, 49.9, 62.3 m and c = 30, 50, 80 and 100 km/h**

After simulating virtual resonance under predetermined conditions, the question arises if resonance will occur in real time situations under the same conditions.

In section 2, we noted that hazardous oscillations can occur in floating bridges when these structures are induced by various types of repetitive occurring dynamic loads. Until the time that this particular question can be answered, we can only refer to comparative research or other experience.

Nevertheless, if resonance takes place under all circumstances, what could we do for safety? From a technical point of view, 'shifting' the system's eigenfrequency outside the bounds of the excitation frequency can be attempted first. Bounds can be found in distances which are theoretically unrealizable for passenger cars or which are unpractical for humans to survey. A second attempt is perhaps trying to diminish (acceleration-) amplitudes, what could be enough for safety too. To find out – if and to what extent – the eigenfrequency anticipates to (one of the) 'tuning tools' we make use of a so-called Frequency-domain response analysis. We will treat this analysis in section 10 and therefore we come back to all of this later.

Besides technical measures, informative measures may also be undertaken. One could think for example of warning systems but these are quite expensive and therefore not as indispensable as they look like at first sight.

TUDelft

9.5 Configuration of joint

Joints are physically the most important elements in the thoroughfares design. If a thoroughfare is safe for traffic depend – especially for $c < 80\,km/h$ - on how the joints are performing. Designers from XX-architecten managed to design a functional and esthetical sound version of them, but with this typically temporary character. This was laid down in rules and elaborated in design principles.

In the design process for permanent joints, principles must be abandoned and others must be developed. For permanent purposes, basic principles as simplicity, ability to a fast (de)coupling and reliability are very valuable for joints; their number becomes in numerous when a road is many times longer than the prototype.

As constructor, we limit ourselves to provide the technical data for the (preliminary) design. the data contains all the maximum forces that occur in the joints due to relocation, the same forces we discussed in subsection 9.3.2. The magnitude of these forces can be determined by regrouping equation 5.7 and 5.13 around joint j and omitting all hydrodynamic parameters:

$$\mathbf{F}_k^j = \sum_{j=i} \mathbf{K}_{(k_d=0,c_d=0)}^i \mathbf{y}^{ij}, \quad \mathbf{y}^{ij} = \begin{bmatrix} w^i & \theta^i & w^{i+1} & \theta^{i+1} \end{bmatrix}^j$$

$$\mathbf{F}_c^j = \sum_{j=i} \mathbf{C}_{(k_d=0,c_d=0)}^i \dot{\mathbf{y}}^{ij}, \quad \dot{\mathbf{y}}^{ij} = \begin{bmatrix} \dot{w}^i & \dot{\theta}^i & \dot{w}^{i+1} & \dot{\theta}^{i+1} \end{bmatrix}^j$$

(9.12)

$\mathbf{F}_k^j$ and $\mathbf{F}_c^j$ are force vectors composed from reaction forces in the damper and (material) stiffness of joint j due to translation and rotation of adjacent bodies. The forces are time-dependent variables and only the maximum values are important. Therefore vector expression 9.12 must be reduced to a scalar expression:

$$F_{k,max}^j = \left\{ \mathbf{F}_k^j \right\}_{max}$$

$$F_{c,max}^j = \left\{ \mathbf{F}_c^j \right\}_{max}$$

(9.13)

For controlling safety and comfort, besides the forces, also the maximum internal displacement per joint will be determined. This can be done by a consideration of mutual body displacements, as illustrated in subsection 9.3.2. Analogously, we write:

$$\Delta w^j = \begin{cases} 4.5\theta^1 - w^2 + 2.75\theta^2 & for \left\{ j = 1 \right\} \\ w^i + 2.75\theta^i - w^{i+1} + 2.75\theta^{i+1} & for \left\{ \begin{matrix} i,j \mid 2 \leq i \leq 18, \\ 2 \leq j \leq 17 \end{matrix} \right\} \\ w^{19} + 2.75\theta^{19} + 4.5\theta^{20} & for \left\{ j = 18 \right\} \end{cases}$$

(9.14)

And for the same reason the maximum internal displacement per joint reads:

$$\Delta w_{max}^j = \left\{ \Delta w^j \right\}_{max}$$

(9.15)

TUDelft
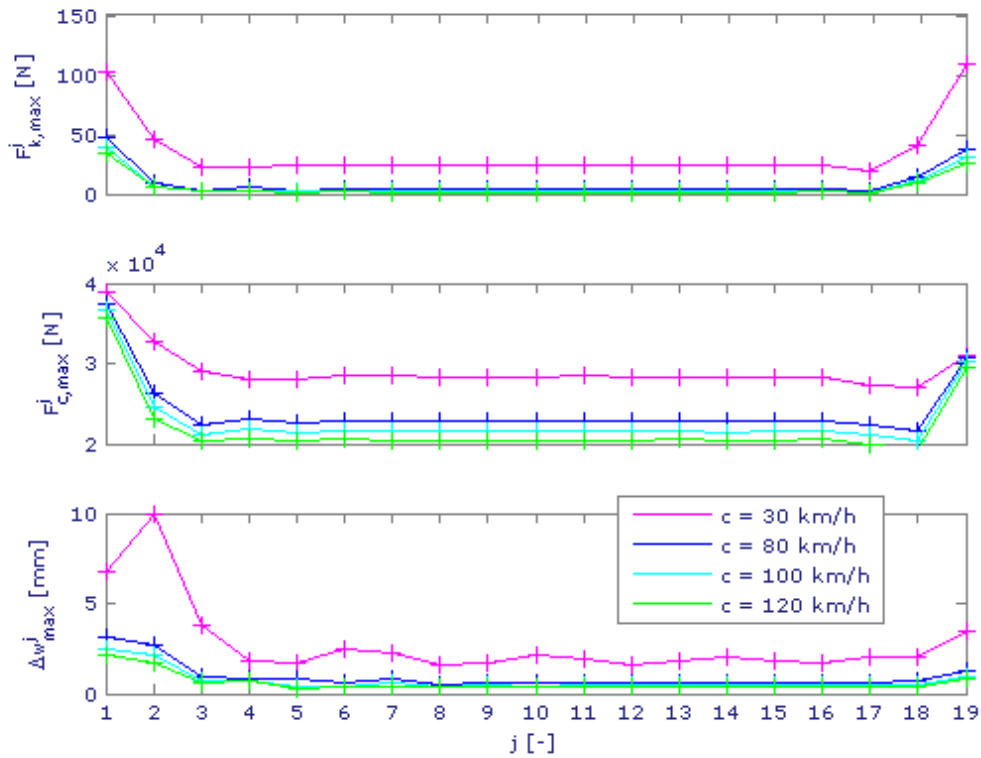
Figure 9.29   **maximum joint forces and internal displacments**

Figure 9.29 evaluates the maximum forces acting on all joints as result of vehicle movement. What immediately catches the eye is a force concentration near the entrance of the structure in contrast to a monotonous course in the field. This confirms that the right decision is made about one of the two critical scenarios proposed for the parameter study: the impact at the entrance.

Large forces implies large internal displacements. The corresponding maximum internal displacements in all joints are just 2 mm on average, but with 8mm of deviation in case of 30 km/h. This is typically for the second joint since the second pontoon is longer than its neighbours and thus governing a stronger pitching motion than its neighbours as well.

10 Frequency-domain response analysis

With the frequency-domain response analysis, the amplitude of the steady state output of a system as a function of the input frequency can be determined. The objective is to examine the critical input frequency, elaborated in section 9, and measures that are effective (tuning tools) in affecting the quantity and (acceleration) amplitudes attributed to this frequency.

10.1 Multiple vehicle: approximated accelerations of the deck

As stated in section 6, the complex modal analysis must be applied for the calculation.

The equations of motion gives:

$$\mathbf{M}\ddot{\mathbf{y}} + \mathbf{C}\dot{\mathbf{y}} + \mathbf{K}\mathbf{y} = \mathbf{F}(t) \tag{10.1}$$

Where $\mathbf{M}$, $\mathbf{C}$ and $\mathbf{K}$ are $2N-2$-by-$2N-2$ matrices and $\mathbf{y}$ and $\mathbf{F}$ are 1–by-$2N-2$ vectors. $\mathbf{F}(t)$ is approximated by the harmonic function:

$$\mathbf{F}(t) \approx \hat{\mathbf{F}}\cos(\omega t) \tag{10.2}$$

with $\hat{\mathbf{F}}$ as amplitude what describes the repetitive character when a sequence of equally distant vehicles are involved. Proceeding with equality signs only, the harmonic force can also be written as the real part of a complex function, with complex amplitude:

$$\hat{\mathbf{F}}\cos(\omega t) = |\mathbf{F}(\omega)|\cos(\omega t) = \mathrm{Re}\left[\mathbf{F}(\omega)e^{i\omega t}\right] \tag{10.3}$$

The particular solution to equation 10.1 equals:

$$\mathbf{y}(t) = |\mathbf{y}(\omega)|\cos(\omega t + \theta(\omega)) \tag{10.4}$$

Or in the form of the real part of a complex function with complex amplitude:

$$\mathbf{y}(t) = \mathrm{Re}\left[\mathbf{y}(\omega)e^{i\omega t}\right] \tag{10.5}$$

We will simplify the nomenclature by omitting the symbol Re and - at the end of the operation.- the imaginary part is disregarded. Substituting equation 10.3 and 10.5 into 10.1 yields:

$$-\omega^2\mathbf{M}\mathbf{y}(\omega) + i\omega\mathbf{C}\mathbf{y}(\omega) + \mathbf{K}\mathbf{y}(\omega) = \mathbf{F}(t) \tag{10.6}$$

which is the force displacement relationship expressed in complex amplitudes. With the dynamic-stiffness coefficient $\mathbf{S}_{yF}(\omega)$, equation 10.6 changes into:

$$\mathbf{F}(t) = \left(-\omega^2\mathbf{M} + i\omega\mathbf{C} + \mathbf{K}\right)\mathbf{y}(\omega) = \mathbf{S}_{yF}(\omega)\mathbf{y}(\omega) \tag{10.7}$$

TUDelft

With the dynamic –flexibility coefficient or transfer function $\mathbf{H}_{yF}(\omega) = \mathbf{S}_{yF}(\omega)^{-1}$, the maximum real amplitude follows from:

$$\mathbf{y}(\omega) = \mathbf{H}_{yF}(\omega)\mathbf{F}(\omega) \tag{10.8}$$

Because a synchronic force is applied (see equation 10.2), the phase angles are zero and consequently equation 10.8 can be written as:

$$\left|\mathbf{y}(\omega)\right| = \left|\mathbf{H}_{yF}(\omega)\right|\left|\mathbf{F}(\omega)\right| \tag{10.9}$$

Now, the transfer function for the synchronic force $\mathbf{F}(t) = \hat{\mathbf{F}}\cos(\omega t)$ is acting on all degrees of freedom and not fixed in one point, so:

$$\mathbf{H}_{yF}(\omega) = \sum_{i=1}^{2N-2}\mathbf{H}_{y_iF_i}(\omega) \tag{10.10}$$

expecting the central body in the system to give the striking results. Actually, we are interested in the acceleration of the structure, more than the displacement. Therefore the amplitude of the acceleration can be derived by the amplitude of the displacement by taking the derivative to t twice:

$$\ddot{\mathbf{y}}(t) = \frac{d}{dt}\mathbf{y}(\omega)e^{i\omega t} = -\omega^2\mathbf{y}(\omega)e^{i\omega t} \tag{10.11}$$

Now the amplitudes of the accelerations becomes:

$$\left|\ddot{\mathbf{y}}(\omega)\right| = \omega^2\left|\mathbf{u}(\omega)\right| = \omega^2\left|\mathbf{H}_{yF}(\omega)\right|\left|\mathbf{F}(\omega)\right| = \left|\mathbf{H}_{\ddot{y}F}(\omega)\right|\left|\mathbf{F}(\omega)\right| \tag{10.12}$$

Conform equation 10.9, the transfer function for the acceleration is:

$$\left|\mathbf{H}_{\ddot{y}F}(\omega)\right| = \sum_{i=1}^{2N-2}\mathbf{H}_{\ddot{y}_iF_i}(\omega) \tag{10.13}$$

The transfer function is determined with the Matlab code of Appendix V.5 and distinguished graphically by phases in the parameter study (figure 10.1) – in which the effect of $c_{cl/int}$ and $k_{cl/int}$ is noticeable - , by the number of bodies (figure 10.2) and various body lengths (figure 10.3) to serve the objective of this section.

TUDelft
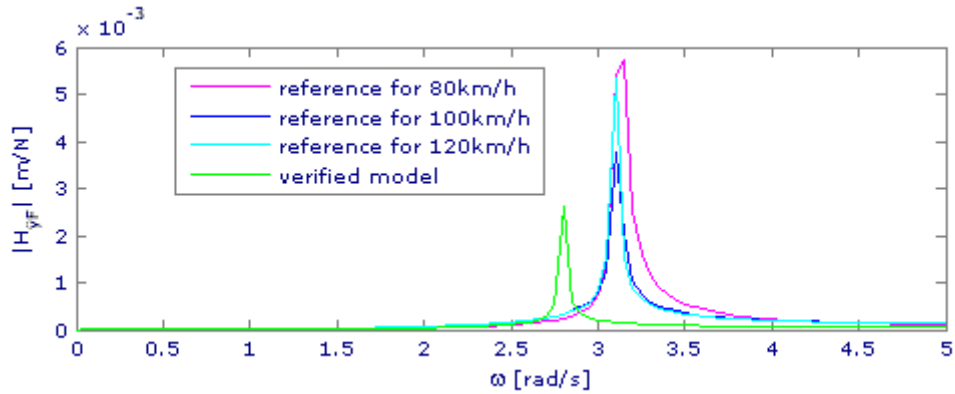
Figure 10.1   **transfer function applied to different phases in the parameter study**
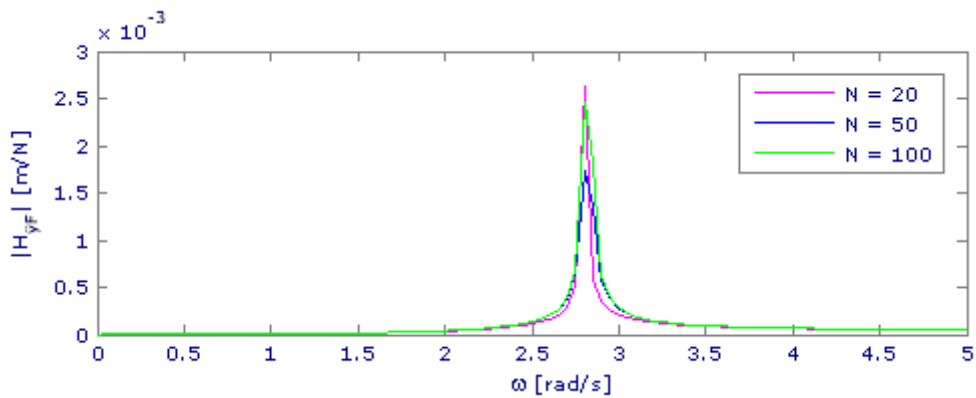
Figure 10.2   **transfer function of the multibody system (verified model) of the acceleration of the deck by a synchronic load on all bodies.**
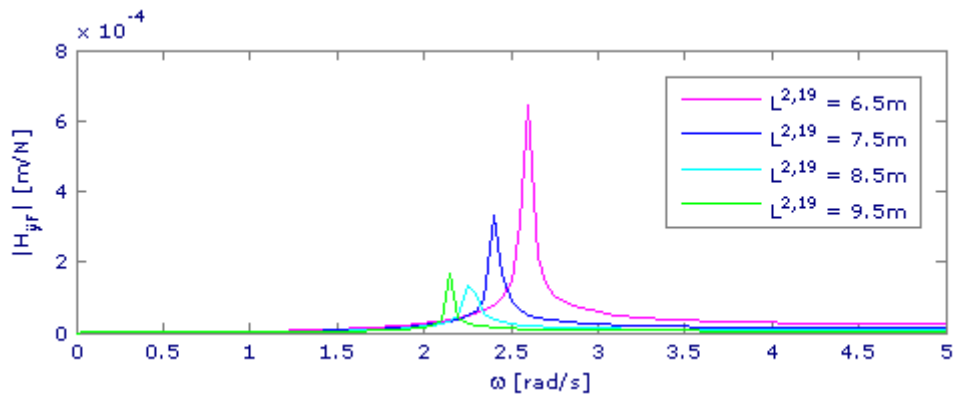
Figure 10.3   **transfer function of the multibody system applied to a different body length**
$$\left\{ L^i = L^{2,19} - 1m \quad for \left\{ i \mid i = 1,20 \cap 3 \le i \le 18 \right\} \right\}$$

Figure 10.1 validates the critical input frequency value of $2.8\,rad/s$ as the only critical frequency in the system. The transfer function behaves very consistent to the 'tuning tools' concerning the frequency, accept for $L^{2,19}$, which is responsible for the step from $3.2\,rad/s$ to $2.8\,rad/s$. However, the effect is so small that the problem is shifted rather than solved, returning to the 'safety problem' in subsection 9.4.3. A small arithmetic sample to illustrate this:

TUDelft

$L^{2,19} = 5.5m \rightarrow 9.5m$ yield $\omega = 2.8\,rad/s \rightarrow 2.16\,rad/s$ according to figure 10.3. The vehicles critical distance md shifts from 49.9 meter to 64.6 meter for 80 km/h, what approximates the initial value for 100km/h, see figure 9.24.

Concluding this attempt, it is quite unlikely with these tools to realize system improvement as such that the critical input frequency 'shifts' to outside the bound of 'technical feasibility' and 'human capability', as was noted in subsection 9.4.3. 'Shifting' is therefore out of the question.

In contrast to the consistent behaviour concerning the frequency, the transfer function behaves quite inconsistent to the 'tuning tools' concerning the maximum (acceleration) amplitude and $L^{2,19}$, once again, is giving the best results. Suppressing the (acceleration) amplitude to gain more time for drivers to adjust their speed can be the most valuable solution for the time being. In the verified model, however, there is theoretically no margin in the vertical acceleration for 120 km/h, see figures 9.22 and 9.25. Still, $L^{2,19} = 5.5m \rightarrow 6.5m$ already ensures a $\left(1 - 7*10^{-4}/2.8*10^{-3}\right)*100\% = 75\%$ amplitude reduction, according to figure 10.3. This implies that a maximum of $1.8\,m/s^2$ devaluates to $0.45\,m/s^2$, what gives more time to anticipate than the simulation time in the figures.

TUDelft

11 Conclusion and recommendations

11.1 Conclusions

- Displacements in the vertical plane dominate the deformation in the multibody system. The choice for a *rigid* multibody system is therefore justified. It is important to realize that calculated displacements are maximum displacements since traffic is schematized as (a series of) moving concentrated loads

- The natural mode is governed by the fluid whereas the higher modes exist because of the joint mechanism with vertical dampers and springs.

- The computational model is only semi feasible for validation since its virtual joint mechanisms exhibit a different behaviour with respect to the prototype mechanisms. Validation is justified if and only if fluid properties are considered. The wave diffraction approximation, describing the fluid motion, responds quite realistically, even when approximation is taken to extremes with intuitively obtained damping parameters.

- The free vibrations in the system are mainly damped by the hydrodynamic properties of the system. By tuning structural properties, the system can be made less sensible for unstable behaviour and internal joint displacements can be limited.

- The forced vibrations and vibrating accelerations in the system are effectively controlled by structural properties as joint properties and the body length. If the structure is built out of 4.5 metre long elements, while each connection between the elements can handle a maximum force in the order of 40 kN, it is even safe and comfortable to drive 120 km/h.

- Resonance can occur through the hydrodynamic properties of the system. Allowing a series of equally distant vehicles to the system all forces together will provide enough energy to generate resonance. The critical mutual distance between vehicles is executable in reality, but there is no danger, since there is enough time for a driver to respond to a hazardous situation.

- The spectral analysis and the simulations in the time domain will give almost the same results.

11.2 Recommendations

- The prototype joint mechanism should replace the joint mechanism in the multibody system to improve model verification.

- Improvement and further elaboration of the wave diffraction approximation which takes into account the fluid viscosity. In reality, there will be mud as much as water on the site what is better in attenuating the structural movement. Mud will stick to the structure to some extent.

- The structure has a relatively small density with 102.5 kg/m3. A larger density (mass) leads to smaller vibrations and accelerations, but also to higher transportation costs. This problem can be avoided by the intake of fluid in the structure, what gives a bigger mass only in its final position. Not only the pontoon

TUDelft

mass can be reduced, it has the benefit of an extra damping property since parametric damping can occur.

- Tests should be extended to include heavier vehicles like trucks.
- It should be examined if a horizontal and lateral motion will be of consequence.

TUDelft

References

[1] Shabana, A. A. (2005) 'Dynamics of multibody systems' third edition.

[2] Spijkers, J. M. J, Vrouwenvelder, A.C.W.M, Klaver, E.C. (2005) lecture notes ct4140: 'Structural Dynamics', Delft University of technology.

[3] Duffy, D. G. (2004) 'Transform methods for solving partial differential equations', second edition.

[4] Tkacheva, L. A. (2005) 'Action of a Periodic Load on an Elastic Floating Plate', publication

[5] Tkacheva, L. A. (2003) 'Plane Problem of Surface Wave Diffraction on a Floating Elastic Plate', published in Fluid Dynamics

[6] Kolkman, P.A. and Jongeling T.H.G. (1996) 'Dynamic Behaviour of Hydraulic Structures', part A 'structures in flowing fluid', Dutch Ministry of Transport.

I Description and characteristics of the prototype

The prototype was tested in Hedel and consisted of floating aluminium units (pontoons) with joints at both ends to facilitate connection to neighbouring units. Each of the floating units has dimensions of 3.5m x 5.4m x 1.6m (length x width x height) and has a weight of 3100 kg. Extra units can easily been inserted. Special attention was paid to the joints, which were executed as row locks with a fixate-facility to keep the locks into position.

Figure I.1   **photograph of prototype in Hedel**

The fixate-facility gives extra stiffness to the joints in order to exhibit smooth transitions under different circumstances. Between end-unit and land a special 'land-flap' (aanlandingsklep) was placed; at the unit-side connected as a fixed hinge and the landward-side as a sliding hinge. As a result of this, no 'unwanted forces' can enter the structure. Measurements to the prototype were executed under normal conditions (traffic and current perpendicular to the structure of 1 m/s) and under special conditions where the structure is also exposed to (spectral) waves and wind pressure. These measurements required extra equipment as mooring piles and external floats. Mooring piles must provide its horizontal fixation. External floats provided more stability and protected the deck from spilling water during a wave attack.

The total length of the structure, including the 'land-flaps', was 70 metres. The total width was 8.6 metres and near the land-flaps 10.45 metres.

Only passenger cars (weight: 2 tons, max. velocity: 80 km/h), an incidental vehicle from the emergency service (weight 8-10 tons, max. velocity: 30 km/h) and pedestrians were allowed to make use of the passage.

Deflections, stresses and its dynamic behaviour were recorded by TNO Bouw en Ondergrond, while TNO Voertuigtechniek collected data from the vehicles to determine the comfort level. Regarding the comfort level, a maximum vertical acceleration of the deck of

TUDelft

1/10 of the gravitational acceleration and a maximum angle of rotation of 5 degrees were predefined. With regard to the maximum angle of rotation the designers maintained the Dutch standard for designing 'conservative' non-highway structures (RONA) for traffic with maximum velocity of 80 km/h. The prototype met all demands of safety and serviceability.

Figure I.2   photograph of prototype with test vehicle

II Derivation of body stiffness and – damping matrices

The aim is to find a relation between force and displacement or velocity of each body that can be expressed in respectively a body stiffness or - damping matrix. Since we consider infinitesimally small displacements, the system becomes linear and the so called displacement method [2] can be applied. In this case, the displacement method offers a quick and stable alternative for determination of elementary matrices with respect to the method based on Lagrange's equation of Appendix III.

The derivation process starts with drawing the system in two different positions per body in which in turn one degree of freedom is assumed positive while the others were hold fixed. This implies that they are zero. The external forces can be derived and after balancing them we immediately write the Newton-Euler equation for each body:

$$m\ddot{w}^i - \sum_i F_w^i = 0$$
$$J\ddot{\theta}^i - \sum_i F_\theta^i = 0$$

(II.1)

The body matrices for both stiffness and damping can be composed from:

$$\mathbf{F^i} = \mathbf{K^i y} \rightarrow \begin{bmatrix} F_w \\ F_\theta \end{bmatrix}^i = \begin{bmatrix} k_{1,1} & k_{1,2} & k_{1,3} & k_{1,4} & k_{1,5} & k_{1,6} \\ k_{2,1} & k_{2,2} & k_{2,3} & k_{2,4} & k_{2,5} & k_{2,6} \end{bmatrix}^i \begin{bmatrix} w^{i-1} \\ \theta^{i-1} \\ w^i \\ \theta^i \\ w^{i+1} \\ \theta^{i+1} \end{bmatrix}$$

(II.2)

$$\mathbf{F^i} = \mathbf{C^i \dot{y}} \rightarrow \begin{bmatrix} F_w \\ F_\theta \end{bmatrix}^i = \begin{bmatrix} c_{1,1} & c_{1,2} & c_{1,3} & c_{1,4} & c_{1,5} & c_{1,6} \\ c_{2,1} & c_{2,2} & c_{2,3} & c_{2,4} & c_{2,5} & c_{2,6} \end{bmatrix}^i \begin{bmatrix} \dot{w}^{i-1} \\ \dot{\theta}^{i-1} \\ \dot{w}^i \\ \dot{\theta}^i \\ \dot{w}^{i+1} \\ \dot{\theta}^{i+1} \end{bmatrix}$$

(II.3)

Equation II.2 and II.3 show that the degree of freedom of body i only affects the degree(s) of freedom of the body that is directly attached to it, body $i-1$ and $i+1$. Figure II.1-8 visualizes the displacement method as explained above for all (generalized) bodies.
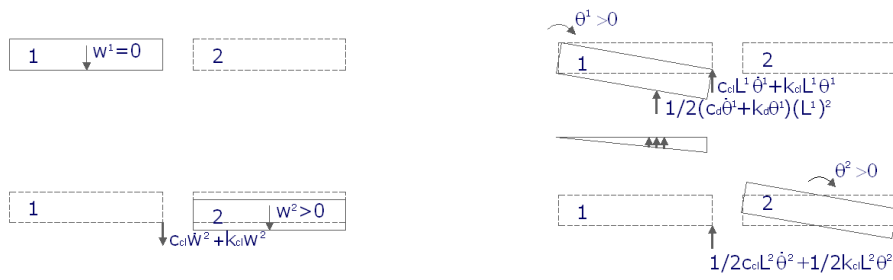
Figure II.1   **kinetic force of body 2 and kinematical forces affecting the vertical (l) and angular (r) degree of freedom of body 1**
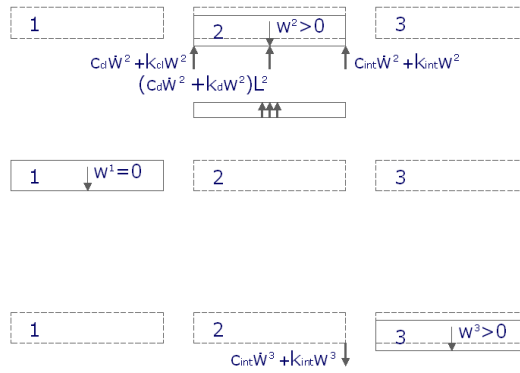
Figure II.2   **kinetic force of body 3 and kinematical forces affecting the vertical degree of freedom of body 2**
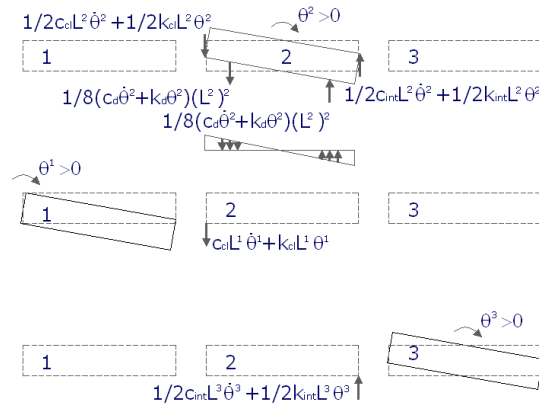
Figure II.3   **kinetic force of body 1 and 3 and kinematic forces affecting the angular degree of freedom of body 2**
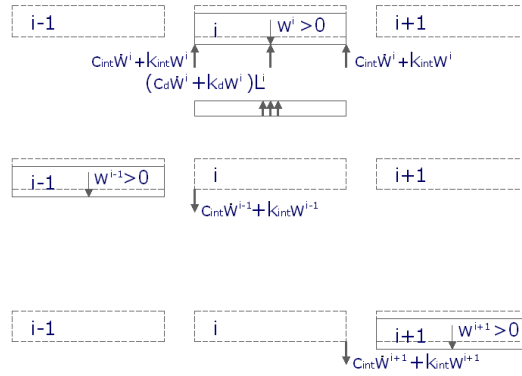
Figure II.4   **kinetic force of body i-1 and i+1 and kinematical forces affecting the vertical degree of freedom of body i**
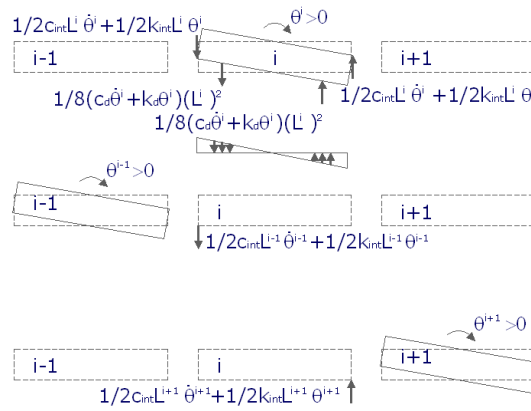
Figure II.5   **kinetic force of body i-1 and i+1 and kinematical forces affecting the angular degree of freedom of body i**
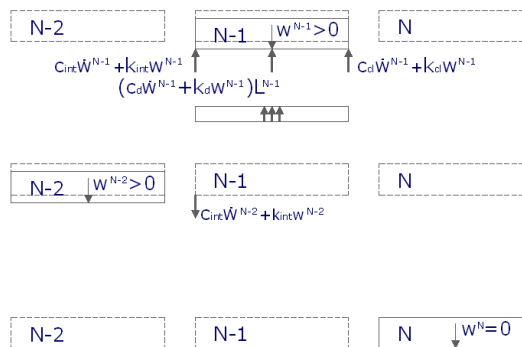
Figure II.6   **kinetic force of body N-2 and N and kinematical forces affecting the vertical degree of freedom of body N-1**

TUDelft

$1/2c_{int}L^{N-1}\dot{\theta}^{N-1}+1/2k_{int}L^{N-1}\theta^{N-1}$ $\theta^{N-1}>0$

| N-2 | N-1 | N |

$1/8(c_d\dot{\theta}^{N-1}+k_d\theta^{N-1})(L^{N-1})^2$ $1/2c_{cl}L^{N-1}\dot{\theta}^{N-1}+1/2k_{cl}L^{N-1}\theta^{N-1}$
$1/8(c_d\dot{\theta}^{N-1}+k_d\theta^{N-1})(L^{N-1})^2$

$\theta^{N-2}>0$

| N-2 | N-1 | N |

$1/2c_{int}L^{N-2}\dot{\theta}^{N-2}+1/2k_{int}L^{N-2}\theta^{N-2}$

$\theta^{N}>0$

| N-2 | N-1 | N |

$c_dL^{N}\dot{\theta}^{N}+k_dL^{N}\theta^{N}$
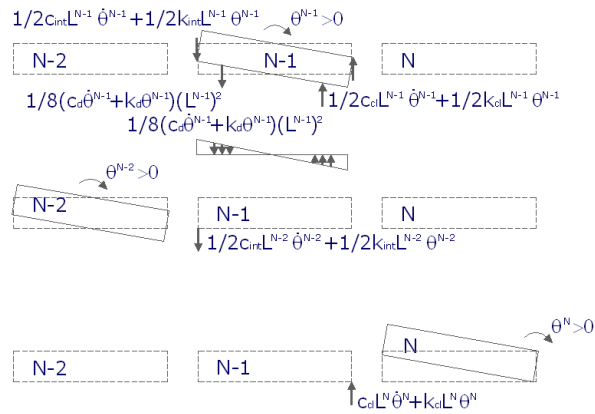
Figure II.7   kinetic force of body N-2 and N and kinematical forces affecting the angular degree of freedom of body N-1

| N-1 | $w^{N-1}>0$ | N |

$c_dW^{N-1}+k_{cl}W^{N-1}$

$\theta^{N-1}>0$

| N-1 | N |

$1/2c_{cl}L^{N-1}\dot{\theta}^{N-1}+1/2k_{cl}L^{N-1}\theta^{N-1}$

| N-1 | N | $w^{N}=0$ |

$\theta^{N}>0$

| N-1 | N |

$c_dL^{N}\dot{\theta}^{N}+k_dL^{N}\theta^{N}$ $1/2(c_d\dot{\theta}^{N}+k_d\theta^{N})(L^{N})^2$
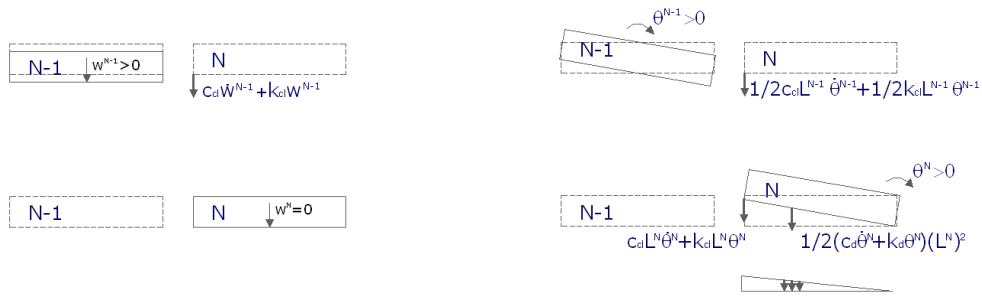
Figure II.8   kinetic force of body N-1 and kinematical forces affecting the vertical (I) and angular degree of freedom of body N

TUDelft

III Validation equation of motion; derivation via Lagrange's equation

Since the direct application of Newton's second law becomes difficult when large scale bodies are considered, the introduction of D'Alembert's principle and the Lagrange's equation to derive the dynamic equations of motions is almost indispensable. In contrast to Newton's second law, the application of Lagrange's equation requires scalar quantities such as the kinetic energy, potential energy and virtual work. However, if all motions may be considered as infinitesimally small and all springs in the system as linear, what is to some extent well accepted, also the direct application of Newton's second law requires scalar quantities as independent external forces, as shown in section 2 and II.

The aim of this section is to derive the dynamic equations of motion via a vector analysis containing the Lagrange's equation as an consistent tool for verification purposes.

III.1 Rigid body Mechanics, Kinematics and Dynamics

The configuration of a body in the two dimensional system need four independent coordinates, i.e. two coordinates for translation and two coordinates for the orientation of the body. These coordinates are called generalized coordinates. In the coordinate system, $X_1 X_2$ is denoted as the axes of the inertial frame fixed in time and $X_1^i X_2^i$ as the axes of the global frame of reference fixed in the origin of body i. (we explicitly use the vector notation $X_1 X_2$ instead of the Cartesian coordinates xy) Now, by introducing vectors (including properties) between the frames and the body i mechanics, kinematics and dynamics of a rigid body can be described.

III.1.1 Mechanics / Kinematics
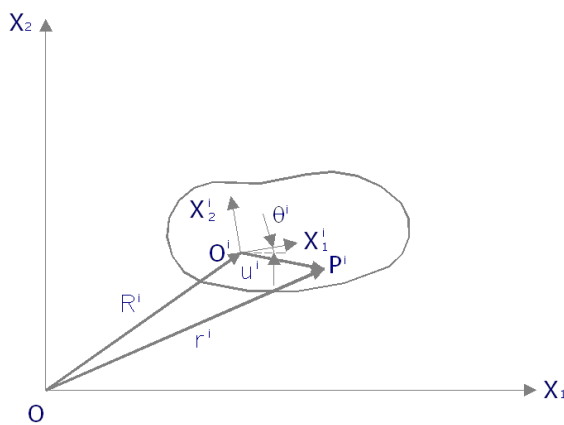
Figure III.1   body coordinate system

The global position of an arbitrary point p^i on the body i can be defined (figure III.1) as:

$$\mathbf{r}^i = \mathbf{R}^i + \mathbf{u}^i \qquad\qquad\qquad\qquad (III.1)$$

Where:

$\mathbf{r}^i$:   global position of point p^i

TUDelft

$\mathbf{R}^i$:   position vector of the origin o^i of the body reference

$\mathbf{u}^i$:   position vector of point p^i in the body coordinate system

Unlike deformable bodies, the distance between o^i and p^i remains constant during the body motion i.e. $\mathbf{u}^i$ is constant in time. Now sticking to the inertial reference this vector, however, need to be transformed to the inertial frame. This can be obtained by developing a transformation matrix $\mathbf{A}^i$: Firstly, θ^i is introduced as the angle that describes the body orientation and secondly unit vectors need to be sketched in both frames. The relation between the unit vectors in both frames now determines the matrix, as shown in equality III.2:

$$\left. \begin{array}{l} i_1 = \cos\theta^i i_1^i - \sin\theta^i i_2^i \\ i_2 = \sin\theta^i i_1^i + \cos\theta^i i_2^i \end{array} \right\} \mathbf{A}_i = \begin{bmatrix} \cos\theta^i & -\sin\theta^i \\ \sin\theta^i & \cos\theta^i \end{bmatrix} \tag{III.2}$$

For infinitesimal rotations variant matrix $\mathbf{A}^i$ can be derived as follows:

$$\left. \begin{array}{l} \sin\theta^i \approx \theta^i \\ \cos\theta^i \approx 1 \end{array} \right\} \mathbf{A}_i = \begin{bmatrix} \cos\theta^i & -\sin\theta^i \\ \sin\theta^i & \cos\theta^i \end{bmatrix} \approx \begin{bmatrix} 1 & -\theta^i \\ \theta^i & 1 \end{bmatrix} \tag{III.3}$$

Equation III.1 after transformation becomes:

$$\mathbf{r}^i = \mathbf{R}^i + \mathbf{A}^i \overline{u}^i \tag{III.4}$$

Where:

$\mathbf{A}^i$:   rotation matrix for body i

$\overline{u}^i$:   position vector of point p^i in the body coordinate system

Position vector $\mathbf{R}^i$ and angle scalar θ^i describes respectively the body translation and orientation. These coordinates, also called generalized coordinates, can be used to describe the body configuration i.e. the position, velocity and acceleration in an arbitrary point on the body i. $\mathbf{q}_r^i$ represents the vector of the generalized coordinates. i.e.:

$$\mathbf{q}_r^i = \begin{bmatrix} R_1^i & R_2^i & \theta^i \end{bmatrix}^T \tag{III.5}$$

Where:

R_1^i :   position of the origin o^i of the body reference in X_1 direction

R_2^i :   position of the origin o^i of the body reference in X_2 direction

θ^i :   angle that describes the orientation of the body (or angle between X_1 and X_1^i)

The position vector as described above has been determined already as vector $\mathbf{r}^i$. See equation III.4. In order to obtain the velocity vector a simply differentiation of equation III.4 with respect to time will hold. This yields:

$$\mathbf{v}^i = \dot{\mathbf{r}}^i = \dot{\mathbf{R}}^i + \dot{\mathbf{A}}^i \overline{u}^i \tag{III.6}$$

Where:

$\mathbf{v}^i$:   velocity vector of point p^i

$\dot{\mathbf{R}}^i$:   velocity vector of the origin o^i of the body reference

$\dot{\mathbf{A}}^i$:   rotation matrix for body i differentiated with respect to time

TUDelft

The definition of ω^i, the angular velocity vector of body i, reads;

$$\omega^i = \dot{\theta}^i \mathbf{i}_3^i \tag{III.7}$$

Where:

$\dot{\theta}^i$:   angular velocity of body i with respect to o^i

$\mathbf{i}_3^i$:   unit vector that passes through point p^i and is perpendicular to $\mathbf{i}_1^i$ and $\mathbf{i}_2^i$

By differentiating equation III.6 with respect to time , an expression for the acceleration vector can be obtained in terms of the coordinates $\mathbf{q}_r^i$ and their derivatives after introducing the equality $\dot{\mathbf{A}}^i \bar{u}^i = \mathbf{A}^i \left(\bar{\omega}^i \times \bar{u}^i \right) = \omega^i \times \mathbf{u}^i$ to rewrite equation III.6, as follows:

$$\mathbf{a}^i = \dot{\mathbf{v}}^i = \ddot{\mathbf{R}}^i + \dot{\omega}^i \times \mathbf{u}^i + \omega^i \times \dot{\mathbf{u}}^i \tag{III.8}$$

Where:

$\mathbf{a}^i$:   acceleration vector of point p^i

$\ddot{\mathbf{R}}^i$:   acceleration vector of the origin o^i of the body reference

$\dot{\omega}^i$:   angular acceleration of the body i

$\dot{\mathbf{u}}^i$:   velocity vector of point p^i

If the angular acceleration vector α^i of body i will be denoted as:

$$\alpha^i = \ddot{\theta}^i \mathbf{i}_3^i \tag{III.9}$$

Where:

$\ddot{\theta}^i$:   angular acceleration of body i with respect to o^i

and we use the equality $\dot{\mathbf{A}}^i \bar{u}^i = \mathbf{A}^i \left(\bar{\omega}^i \times \bar{u}^i \right) = \omega^i \times \mathbf{u}^i$ again, the acceleration vector of point p^i can be written in the familiar vector form as:

$$\mathbf{a}^i = \ddot{\mathbf{R}}^i + \alpha^i \times \mathbf{u}^i + \omega^i \times \left(\omega^i \times \mathbf{u}^i \right) \tag{III.10}$$

Where:

$\alpha^i \times \mathbf{u}^i$:   tangential component of the acceleration of point p^i with respect to o^i

$\omega^i \times \left(\omega^i \times \mathbf{u}^i \right)$: normal component of the acceleration of point p^i with respect to o^i

III.1.2 Dynamics

The dynamic equations which will be derived by a vector analysis and by the displacement method are called Newton-Euler equations. The part that describes the translation of the body is called the Newton equations and the part that describes the orientation of the body is called the Euler equations. In this case of only vertical translation and orientation in a two dimensional space, the Newton Euler equation reduces to two scalar equations that can be written for body i as:

$$\begin{aligned} m^i a_2^i &= F^i \\ J^i \ddot{\theta}^i &= M^i \end{aligned} \tag{III.11}$$

Where:

m^i :   total mass of the rigid body i

a_2^i :   scalar that defines the vertical acceleration of the centre of mass of body i

F^i :   scalar representing vertical forces acting on the body centre of mass
J^i :   mass moment of inertia defined with respect to the centre of mass
$\ddot{\theta}^i$:   angular acceleration of the rigid body i with respect to the centre of mass
M^i :   moment acting on the body

As will be shown in the next paragraphs, the choice for the body reference to be the centre of mass of the body leads to significant simplifications in the form of the dynamic equations. Newton-Euler equations have no inertia coupling between the translational and rotational coordinates of the rigid body.

III.2 Virtual work and generalized forces

An essential step in the Lagrange formulation of the dynamic equations of the multibody systems is the evaluation of the generalized forces associated with the system generalized coordinates. In this section, the generalized forces (consisting of external forces, constraint forces and/or inertial forces) are introduced by application of virtual work, starting with a brief summary of virtual work.

III.2.1 Virtual work

Virtual work of a force is defined to be the dot product of the force with the virtual change in the position vector of the point of application of the force, in this case: arbitrary point p^i on the body i . Coming back to the regular notation, the formula for virtual work of body i yields:

$$\delta W^i = \mathbf{F}^{iT} \delta \mathbf{r}_p^i \qquad\qquad\qquad \text{(III.12)}$$

Where:

δW^i :   scalar for virtual work of body i
$\mathbf{F}^{iT}$:   (transposed) vector for external, constraint and/or inertial forces
$\delta \mathbf{r}_p^i$:   virtual change in the position vector of point p^i

A transformation of the position vector to generalized coordinates can be obtained by application of the Taylor's expansion:

$$\delta \mathbf{r}_p^i = \sum_{j=1}^{N} \frac{\partial \mathbf{r}_p^i}{\partial q_j} \delta q_j \qquad\qquad\qquad \text{(III.13)}$$

Where:

$\dfrac{\partial \mathbf{r}_p^i}{\partial q_j}$:   derivative of the position vector with respect to its generalized coordinate

δq_j :   virtual change in the position vector of point p^i expressed in generalized coordinates

III.2.2 Generalized forces

Generalized forces denotes all forces in a point that 'causes' the change in position of that specific point associated with its generalized coordinates. Making a next step toward the formulation of the dynamic equations, the principle of virtual work can, for this moment of analysing, be used to derive an expression for the generalized forces.

Considering dynamic equilibrium the resultant of the forces acting on a rigid body is equal to the rate of change of momentum of this body. i.e.:

$$\mathbf{F}^i = \dot{\mathbf{P}}^i \quad or \quad \mathbf{F}^i - \dot{\mathbf{P}}^i = 0 \tag{III.14}$$

Where:
$\mathbf{F}^i$:   sum of forces acting on the body i
$\dot{\mathbf{P}}^i$:   rate of change in momentum of the body
according to Newton's second law. The dynamic equilibrium implies that the virtual work of all bodies together is zero, so from equation III.12 and III.14 we obtain:

$$\sum_{i=1}^{N}\left(\mathbf{F}^i - \dot{\mathbf{P}}^i\right)\delta r^i = 0 \quad or \quad \sum_{i=1}^{N}\left(\mathbf{F}_e^i + \mathbf{F}_c^i - \dot{\mathbf{P}}^i\right)\delta r^i = 0 \tag{III.15}$$

Where:
N :   notation for the total number of the bodies
$\mathbf{F}_e^i$:   vector containing the sum of the external forces
$\mathbf{F}_c^i$:   vector containing sum of the constraint forces
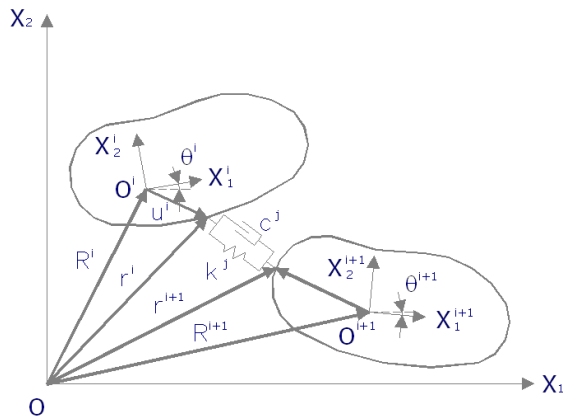
Figure III.2   spring-damper element as generalized force
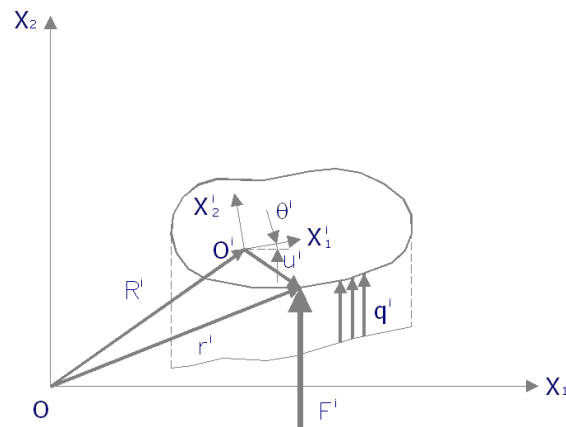
Figure III.3   buoyancy as generalized force
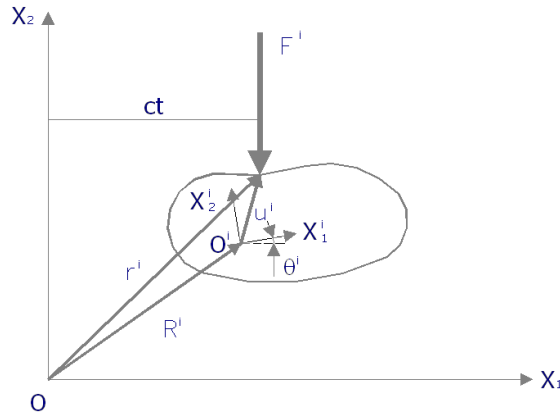
Figure III.4   traffic as generalized force

By writing down the second term in equation III.14 with a dichotomy in the vector force, we emphasize that there is a structural difference between external forces and constraint forces. External forces, composed of traffic forces and buoyancy forces, are independent forces with respect to all remaining bodies in the multibody system and constraint forces (joint forces) are not independent. A second reason implies the difference in assigning point P for the determination of virtual work. Initially, N equations representing the external forces and $2N-2$ constraint equations will be obtained. But extended computation, however, will eliminate $2N-2$ constraint equations to N constraint equations, but this will be treated in the next section.

After substitution of equation III.15 into III.13 we obtain the so called D'Alembert's principle:

$$\sum_{i=1}^{N}\left(\mathbf{F}_e^i + \mathbf{F}_c^i - \dot{\mathbf{P}}^i\right)\sum_{j=1}^{N}\frac{\partial \mathbf{r}_p^i}{\partial q_j}\delta q_j = 0 \qquad\qquad\text{(III.16)}$$

by defining $\bar{Q}_j$ to be all generalized forces affecting body j, the result yields:

$$\sum_{j=1}^{N}Q_j\delta q_j = \bar{\mathbf{Q}}^T\delta\mathbf{q} = 0 \qquad\qquad\text{(III.17)}$$

Where:
$\bar{\mathbf{Q}}^T$:   (transposed) vector of generalized forces of the total multibody system. If the components of the vector of generalized coordinates is independent, $\bar{\mathbf{Q}}^T = 0$

III.3 Kinetic energy and Lagrangian dynamics

In this section, D'Alembert's principle associated with the principle of kinetic energy will pass the review.

III.3.1 Kinetic energy

Kinetic energy is per definition energy in a motion produced by forces. The kinetic energy formulation in the Lagrange's equation can directly be derived form the balance of momentum, based on Newton's second law:

$$m^i \dot{\mathbf{r}}^i = F^i dt \tag{III.18}$$

Where:

dt :   time step covering the balanced space or area

Introducing a graph with $F^i dt$ on the vertical and $\dot{\mathbf{r}}^i$ on the horizontal axis the function will show a straight line for m^i starting in the origin. Define T^i as the area beneath the function and the expression for kinetic energy reads:

$$T^i = \frac{1}{2} F^i dt \dot{\mathbf{r}}^i = \frac{1}{2} m^i \dot{\mathbf{r}}^{iT} \dot{\mathbf{r}}^i \tag{III.19}$$

III.3.2 Lagrangian dynamics

We define $\mathbf{r}^i$ to depend on a set of system generalized coordinates <u>and time</u>! Following the procedure from the preceding section of virtual work and generalized forces, we continue with rewriting the component of the generalized force associated with the generalized force for just one body:

$$Q_j = \sum_{i=1}^{N} \mathbf{F}^{iT} \frac{\partial \mathbf{r}^i}{\partial q_j} \tag{III.20}$$

The virtual work of the inertia force in equation III.12 can be rewritten for all inertia forces as:

$$\delta W^i = \sum_{i=1}^{N} m_i \ddot{\mathbf{r}}^i \partial \mathbf{r}^i \tag{III.21}$$

Deductive computation, using expressions for kinetic energy (III.19), for D'Alemberts principle (III.20) and virtual work (III.21) including differentiation properties for $\ddot{\mathbf{r}}^i$ in equation III.21, lead to the next expression for equation III.16, i.e. the D'Alembert's – Lagrange equation [1]:

$$\sum_{j} \left[\frac{d}{dt} \left(\frac{\partial T}{\partial \dot{q}_j} \right) - \frac{\partial T}{\partial q_j} - Q_j \right] \delta q_j = 0 \tag{III.22}$$

If the generalized coordinates q_j are linearly independent, equation III.22 reduces to the Lagrange equation, which is given by:

$$\frac{d}{dt} \left(\frac{\partial T}{\partial \dot{q}_j} \right) - \frac{\partial T}{\partial q_j} - Q_j = 0 \tag{III.23}$$

TUDelft

III.4 Derivation of the equations of motion using Lagrange's equation
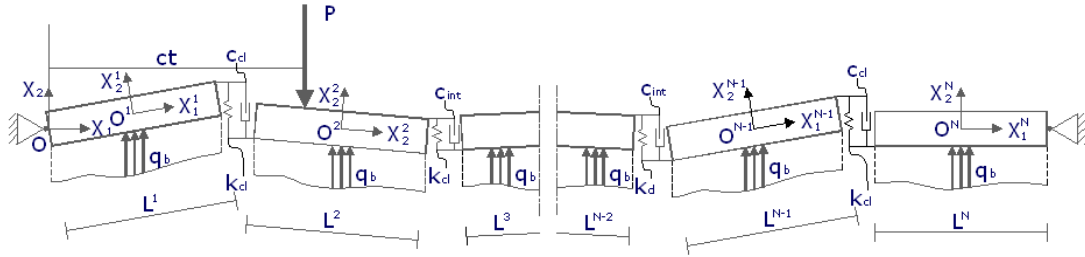
Figure III.5   rigid multibody system for Lagrange formulation

Thus far, the focus lies primarily on the theory of physical principles like mechanics, kinematics, virtual work, kinetic energy, etc. This section will be attributed to the system characteristic elements in the Lagrange equation, like the mass matrix of the rigid bodies and the implementation of the generalized forces. Figure III.5 shows the complete rigid multibody system for the Lagrange formulation.

III.4.1 Mass matrix of rigid bodies

Due to the difference in body rotation a different approach is required in the vector analysis concerning the mass matrices of rigid bodies. However, if the origins of the body references are attached to the mass centre of each body, simplified calculations can be performed; For both cases, closing and intermediate bodies, elimination of the inertia coupling becomes valid between the translation and the rotation of the body reference.

The derivation of the mass matrices begins with rewriting the velocity vector of p^i (equation III.6) as follows:

$$\dot{\mathbf{r}}^i = \dot{\mathbf{R}}^i - \mathbf{A}^i \tilde{\bar{u}}^i \bar{\mathbf{G}}^i \dot{\theta}^i \qquad (III.24)$$

Where:

$\tilde{\bar{u}}^i$:   skew matrix in which the integers denotes position of point p^i in the body coordinate system.

$\bar{\mathbf{G}}^i$:   matrix in which the integers denote the directional (unit) vectors.

In addition, the latter term in equation III.6 was transformed as follows: in the equality $\dot{\mathbf{A}}^i \bar{u}^i = \mathbf{A}^i \left(\bar{\omega}^i \times \bar{u}^i \right) = \omega^i \times \mathbf{u}^i$ from equation III.8 the cross product was replaced by a product of a skew matrix and a vector: $\dot{\mathbf{A}}^i \bar{u}^i = \mathbf{A}^i \left(\bar{\omega}^i \times \bar{u}^i \right) = \mathbf{A}^i \tilde{\bar{\omega}}^i \bar{u}^i = -\mathbf{A}^i \tilde{\bar{u}}^i \bar{\omega}^i$ where, per definition

$\tilde{\bar{u}}^i = \begin{bmatrix} 0 & 0 & \bar{u}_2^i \\ 0 & 0 & -\bar{u}_1^i \\ -\bar{u}_2^i & \bar{u}_1^i & 0 \end{bmatrix}$, $\bar{\omega}^i = \omega^i = \dot{\theta}^i i_3^i = \bar{\mathbf{G}}^i \dot{\theta}^i$ and $\bar{\mathbf{G}}^i = \begin{bmatrix} 0 & 0 & 0 \\ 0 & 0 & 0 \\ 0 & 0 & 1 \end{bmatrix}$. Thereby showing that the mass only rotates along the third axis.

In partitioned form the velocity vector can be written for two different types of bodies as follows:

$$\dot{\mathbf{r}}^i = \begin{cases} \begin{bmatrix} \mathbf{0_3} & -\dot{\mathbf{A}}^i \tilde{\bar{u}}^i \bar{\mathbf{G}}^i \end{bmatrix} \begin{bmatrix} \dot{\mathbf{R}}^i \\ \dot{\theta}^i \end{bmatrix} & for \left\{ i \mid i = 1, N \right\} \\[2em] \begin{bmatrix} \mathbf{I_3} & -\dot{\mathbf{A}}^i \tilde{\bar{u}}^i \bar{\mathbf{G}}^i \end{bmatrix} \begin{bmatrix} \dot{\mathbf{R}}^i \\ \dot{\theta}^i \end{bmatrix} & for \left\{ i \mid 2 \leq i \leq N - 1 \right\} \end{cases} \qquad (III.25)$$

Where:

$\mathbf{0_3}$:   3 x 3 null matrix, $\dot{\mathbf{R}}^i$ is zero because this length does not change in time

$\mathbf{I_3}$:   3 x 3 identity matrix

This expression can be substituted into equation III.19 in order to obtain an expression of kinetic energy as a product of the mass matrix and generalized velocity vectors:

$$T^i = \frac{1}{2}\dot{\mathbf{q}}_r^{iT}\mathbf{M}^i\dot{\mathbf{q}}_r^i \qquad (III.26)$$

Where $\mathbf{q}_r^i = \begin{bmatrix} \mathbf{R}^{iT} & \theta^{iT} \end{bmatrix}^T$ and

$$\mathbf{M}^i = \begin{cases} \int_{V^i} \rho^i \begin{bmatrix} \mathbf{0} & \mathbf{0} \\ symm & \bar{\mathbf{G}}^{iT}\tilde{\bar{u}}^{iT}\tilde{\bar{u}}^i\bar{\mathbf{G}}^i \end{bmatrix} dV^i & for\ \{i\,|\,i = 1, N\} \\[4mm] \int_{V^i} \rho^i \begin{bmatrix} \mathbf{I} & -\bar{\mathbf{G}}^i\tilde{\bar{u}}^i\mathbf{A}^i \\ symm & \bar{\mathbf{G}}^{iT}\tilde{\bar{u}}^{iT}\tilde{\bar{u}}^i\bar{\mathbf{G}}^i \end{bmatrix} dV^i & for\ \{i\,|\,2 \le i \le N-1\} \end{cases} \qquad (III.27)$$

are subtracted from this expression, taking into account the rules of integration. One can verify that $\mathbf{M}^i$ can be written as:

$$\mathbf{M}^i = \begin{bmatrix} m_{RR}^i & m_{R\theta}^i \\ symm & m_{\theta\theta}^i \end{bmatrix} \qquad (III.28)$$

Where:

$$m_{RR}^i = \begin{cases} \int_{V^i} \rho^i \mathbf{0} dV^i = 0 & for\ \{i\,|\,i = 1, N\} \\[3mm] \int_{V^i} \rho^i \mathbf{I} dV^i & for\ \{i\,|\,2 \le i \le N-1\} \end{cases} \qquad (III.29)$$

$$m_{R\theta}^i = \begin{cases} -\int_{V^i} \rho^i \mathbf{0} dV^i = 0 & for\ \{i\,|\,i = 1, N\} \\[3mm] -\int_{V^i} \rho^i \mathbf{A}^i \tilde{\bar{u}}^i \bar{\mathbf{G}}^i dV^i & for\ \{i\,|\,2 \le i \le N-1\} \end{cases} \qquad (III.30)$$

$$m_{\theta\theta}^i = \int_{V^i} \rho^i \bar{\mathbf{G}}^{iT}\tilde{\bar{u}}^{iT}\tilde{\bar{u}}^i\bar{\mathbf{G}}^i dV^i \qquad (III.31)$$

For $\{i\,|\,2 \le i \le N-1\}$, m_{RR}^i turns out to be a 3 x 3 mass matrix with integer m^i on the main diagonal. m^i denotes the total mass of the body i. the matrix $m_{R\theta}^i$ which represents the inertia coupling between the translation and rotation of the body reference is zero for all cases because $\tilde{\bar{u}}^i$ represents a skew matrix (no integers on the main diagonal) that implies the null matrix when it comes to integration with respect to the mass. It is possible to rewrite the integral in the equation for $m_{\theta\theta}^i$, which yields:

$$m_{\theta\theta}^i = \int_{V^i} \rho^i \bar{\mathbf{G}}^{iT}\tilde{\bar{u}}^{iT}\tilde{\bar{u}}^i\bar{\mathbf{G}}^i dV^i = \bar{\mathbf{G}}^{iT} \int_{V^i} \rho^i \tilde{\bar{u}}^{iT}\tilde{\bar{u}}^i dV^i \bar{\mathbf{G}}^i = \bar{\mathbf{G}}^{iT}\mathbf{I}_{\theta\theta}^i\bar{\mathbf{G}}^i \qquad (III.32)$$

Where:

$$\mathbf{I}_{\theta\theta}^i = \begin{bmatrix} i_{11} & i_{12} & i_{13} \\ & i_{22} & i_{23} \\ symm & & i_{33} \end{bmatrix} \qquad (III.33)$$

Where:

$\mathbf{I}_{\theta\theta}^i$:   inertia tensor

TUDelft

$i_{i=j}$: mass moments of inertia

$i_{i \neq j}$: products of inertia

During elaboration, we can encounter the following steps:

$$i_{11} = \int_{V^i} \rho^i \left[\left(\bar{u}_2^i \right)^2 \ \left(\bar{u}_3^i \right)^2 \right] dV^i$$

$$i_{11} = \int_{-h/2}^{h/2} \rho^i \left[(h)^2 \ (0)^2 \right] dh = \frac{1}{12} \rho^i h^3$$

$$i_{22} = \int_{V^i} \rho^i \left[\left(\bar{u}_1^i \right)^2 \ \left(\bar{u}_3^i \right)^2 \right] dV^i$$

$$i_{22} = \begin{cases} \int_0^L \rho^i \left[\left(L^i \right)^2 \ (0)^2 \right] dh = \frac{1}{3} \rho^i \left(L^i \right)^3 & for \{ i \mid i = 1, N \} \\ \int_{-L/2}^{L/2} \rho^i \left[\left(L^i \right)^2 \ (0)^2 \right] dh = \frac{1}{12} \rho^i \left(L^i \right)^3 & for \{ i \mid 2 \le i \le N - 1 \} \end{cases}$$

$$i_{33} = \int_{V^i} \rho^i \left[\left(\bar{u}_1^i \right)^2 \ \left(\bar{u}_2^i \right)^2 \right] dV^i$$

$$i_{22} = \begin{cases} \int_0^L \int_{-h/2}^{h/2} \rho^i \left[\left(L^i \right)^2 \ (h)^2 \right] dh dL^i = \frac{1}{12} \rho^i h L^i \left(4 \left(L^i \right)^2 + (h)^2 \right) & for \{ i \mid i = 1, N \} \\ \int_{-L/2}^{L/2} \int_{-h/2}^{h/2} \rho^i \left[\left(L^i \right)^2 \ (h)^2 \right] dh dL^i = \frac{1}{12} \rho^i h L^i \left(\left(L^i \right)^2 + (h)^2 \right) & for \{ i \mid 2 \le i \le N - 1 \} \end{cases}$$

$$i_{12} = \int_{V^i} \rho^i \bar{u}_1^i \bar{u}_2^i dV^i$$

$$i_{12} = \begin{cases} -\int_0^L \int_{-h/2}^{h/2} \rho^i h L^i dh dL^i = -\frac{1}{8} \rho^i h^2 \left(L^i \right)^2 & for \{ i \mid i = 1, N \} \\ -\int_{-L/2}^{L/2} \int_{-h/2}^{h/2} \rho^i L^i h dh dL^i = -\frac{1}{16} \rho^i h^2 \left(L^i \right)^2 & for \{ i \mid 2 \le i \le N - 1 \} \end{cases}$$

$$i_{13} = -\int_{V^i} \rho^i \bar{u}_1^i \bar{u}_3^i dV^i = 0$$

$$i_{23} = -\int_{V^i} \rho^i \bar{u}_2^i \bar{u}_3^i dV^i = 0$$

Substitution of above characters in the inertia tensor yields:

$$\mathbf{I}_{\theta\theta}^i = \begin{cases} \begin{bmatrix} \frac{1}{12} \rho^i h^3 & -\frac{1}{8} \rho^i h^2 \left(L^i \right)^2 & 0 \\ & \frac{1}{3} \rho^i \left(L^i \right)^2 & 0 \\ symm & & \frac{1}{12} \rho^i h L^i \left(4 \left(L^i \right)^2 + (h)^2 \right) \end{bmatrix} & for \{ i \mid i = 1, N \} \\ \begin{bmatrix} \frac{1}{12} \rho^i h^3 & -\frac{1}{16} \rho^i h^2 \left(L^i \right)^2 & 0 \\ & \frac{1}{3} \rho^i \left(L^i \right)^2 & 0 \\ symm & & \frac{1}{12} \rho^i h L^i \left(\left(L^i \right)^2 + (h)^2 \right) \end{bmatrix} & for \{ i \mid 2 \le i \le N - 1 \} \end{cases} \qquad \text{(III.34)}$$

Substitution into equation (III.32) yields:

$$\mathbf{m}_{\theta\theta}^{i} = \begin{cases} \begin{bmatrix} 0 & 0 & 0 \\ & 0 & 0 \\ symm & & \dfrac{1}{12}\rho^{i}hL^{i}\left(4\left(L^{i}\right)^{2}+\left(h\right)^{2}\right) \end{bmatrix} & for\left\{i\mid i=1,N\right\} \\[2em] \begin{bmatrix} 0 & 0 & 0 \\ & 0 & 0 \\ symm & & \dfrac{1}{12}\rho^{i}hL^{i}\left(\left(L^{i}\right)^{2}+\left(h\right)^{2}\right) \end{bmatrix} & for\left\{i\mid 2\le i\le N-1\right\} \end{cases} \tag{III.35}$$

Defining the mass matrix **M** of the total multibody system to be the sum of N independent $\mathbf{M}^{i}$ matrices, we denote:

$$\mathbf{M} = \begin{bmatrix} J^{1} & 0 & & & & & & & \\ 0 & m^{2} & 0 & & & zeros & & & \\ & 0 & J^{2} & 0 & & & & & \\ & \vdots & & \ddots & \vdots & & & & \\ & & & 0 & m^{i} & 0 & & & \\ & & & & 0 & J^{i} & 0 & & \\ & & & & & \vdots & \ddots & \vdots & \\ & zeros & & & & 0 & m^{N-1} & 0 & \\ & & & & & & 0 & J^{N-1} & 0 \\ & & & & & & & 0 & J^{N} \end{bmatrix} \tag{III.36}$$

Where:

J^{i} : mass moment of inertia corresponding with scalar or integer from equation III.35 for body i .

m^{i} : mass of the body corresponding with the scalar or integer from equation III.29 representing the vertical motion

III.4.2 Generalized forces

Generalized forces are distinguished by their nature; Constraints versus non-constraints. Within the non-constraints we separate foundation related forces and traffic induced forces.

III.4.2.1 Constraint or joint forces

Figure III.6   **illustrative example: derivation of the first joint force expressed in vectors**

Joint forces will be characterized by spring-damper elements that interconnect the body elements. Realizing that a spring-damper element acts in a direction opposite to the direction of extension we may write virtual work due to joint forces affecting body i as:

$$\delta W^i = -\mathbf{F}^{ijT}\left(\delta\mathbf{r}_p^i - \delta\mathbf{r}_p^{i+1}\right) \tag{III.37}$$

Where:

δW^i : virtual work due to joint, constraint force j acting on body i.

$\mathbf{F}^{ijT}$: (transposed) vector of joint force j acting on body i.

$\left(\delta\mathbf{r}_p^i - \delta\mathbf{r}_p^{i+1}\right)$: virtual change in the position vector representing joint j. (located between body i and its successive joint at the right hand side)

Because damping and stiffness specifications of the joints (rowlocks) have not been measured in the pilot, no judgement is made about its performance. It is however the ease to (pre)suppose viscous damping and linear stiffness because of working with simple linear spring- damper elements and associated time-independent stiffness - and damping scalars or vectors, consequently. Rewriting $\mathbf{F}^{ijT}$ as a product of the global position and global velocity vectors and substituting this into equations III.37, the expression for virtual work transforms into:

$$\delta W^i = \left\{\mathbf{k}^{JT}\left(\mathbf{r}_p^i - \mathbf{r}_p^{i+1}\right) + \mathbf{c}^{JT}\left(\dot{\mathbf{r}}_p^i - \dot{\mathbf{r}}_p^{i+1}\right)\right\}\left(\delta\mathbf{r}_p^i - \delta\mathbf{r}_p^{i+1}\right) \tag{III.38}$$

Where:

$\mathbf{k}^{JT}$: (transposed) stiffness vector representing the stiffness of joint j.

$\mathbf{c}^{JT}$: (transposed) damping vector representing the damping of joint j.

In partitioned form equation III.38 can be written as:

$$\delta W^i = \begin{cases} \left[\bar{\mathbf{k}}^{JT} \quad \bar{\mathbf{k}}^{JT}\mathbf{A}^i\bar{u}^i\left(\theta^{-1}\right)^i\right]\begin{bmatrix}\mathbf{R}^i\\\theta^i\end{bmatrix} - \left[\bar{\mathbf{k}}^{JT} \quad -\bar{\mathbf{k}}_j^T\mathbf{A}^{i+1}\bar{u}^{i+1}\left(\theta^{-1}\right)^{i+1}\right]\begin{bmatrix}\mathbf{R}^{i+1}\\\theta^{i+1}\end{bmatrix} + \\ \left[\bar{\mathbf{c}}^{JT} \quad -\bar{\mathbf{c}}^{JT}\mathbf{A}^i\tilde{\bar{u}}^i\bar{\mathbf{G}}^i\right]\begin{bmatrix}\dot{\mathbf{R}}^i\\\dot{\theta}^i\end{bmatrix} - \left[\bar{\mathbf{c}}^{JT} \quad -\bar{\mathbf{c}}^{JT}\mathbf{A}^{i+1}\tilde{\bar{u}}^{i+1}\bar{\mathbf{G}}^{i+1}\right]\begin{bmatrix}\dot{\mathbf{R}}^{i+1}\\\dot{\theta}^{i+1}\end{bmatrix} \\ \left\{-\left[\mathbf{I_2} \quad \mathbf{A}_\theta^{\ i}\bar{\mathbf{u}}^i\right]\begin{bmatrix}\delta\mathbf{R}^i\\\delta\theta^i\end{bmatrix} + \left[\mathbf{I_2} \quad \mathbf{A}_\theta^{\ i+1}\bar{\mathbf{u}}^{i+1}\right]\begin{bmatrix}\delta\mathbf{R}^{i+1}\\\delta\theta^{i+1}\end{bmatrix}\right\} \end{cases} \tag{III.39}$$

Where:

$\bar{\mathbf{k}}^{JT}$: stiffness vector in the body coordinate system.

$\bar{\mathbf{c}}^{JT}$: damping vector in the body coordinate system.

Writing virtual work in partitioned form makes subtraction of the expressions for the generalized forces easier, because:

$$\delta W^i = \begin{bmatrix}\mathbf{Q}_R^{iT} & \mathbf{Q}_\theta^{iT}\end{bmatrix}\begin{bmatrix}\delta\mathbf{R}^i\\\delta\theta^i\end{bmatrix} \tag{III.40}$$

Where:

$\mathbf{Q}_R^{iT}$: (transposed) vector of generalized forces associated with the generalized coordinate $\mathbf{R}^i$.

$\mathbf{Q}_\theta^{iT}$: (transposed) vector of generalized forces associated with the generalized coordinate θ^i.

In the model, the number of modified stiffness – and damping vectors (parameters) is limited to two; a distinction is made between intermediate joints and closing joints. We reject the number of modified joints to the number of inertial different body elements. To account for the differences between intermediate body elements / joints and closed body elements / joints we elaborate the vectors of generalized forces as follows:

$$
\mathbf{Q}_R^{jT} = \begin{cases}
\begin{aligned}
&-\left[\bar{\mathbf{c}}^{JT} \ -\bar{\mathbf{c}}^{JT}\mathbf{A}^i\tilde{\bar{U}}^i\bar{\mathbf{G}}^i\right]\begin{bmatrix}\dot{\mathbf{R}}^i\\\dot{\theta}^i\end{bmatrix} - \left[\bar{\mathbf{k}}^{JT} \ \bar{\mathbf{k}}^{JT}\mathbf{A}^i\bar{U}^i\left(\theta^{-1}\right)^i\right]\begin{bmatrix}\mathbf{R}^i\\\theta^i\end{bmatrix} + \\
&\left[\bar{\mathbf{c}}^{JT} \ -\bar{\mathbf{c}}^{JT}\mathbf{A}^{i+1}\tilde{\bar{U}}^{i+1}\bar{\mathbf{G}}^{i+1}\right]\begin{bmatrix}\dot{\mathbf{R}}^{i+1}\\\dot{\theta}^{i+1}\end{bmatrix} + \left[\bar{\mathbf{k}}^{JT} \ -\bar{\mathbf{k}}^{JT}\mathbf{A}^{i+1}\bar{U}^{i+1}\left(\theta^{-1}\right)^{i+1}\right]\begin{bmatrix}\mathbf{R}^{i+1}\\\theta^{i+1}\end{bmatrix}
\end{aligned} & for \begin{Bmatrix} i,j\,|\,i,j= \\ 1\cap i=N, \\ j=N-1 \end{Bmatrix} \\[4em]
\begin{aligned}
&-\left[\bar{\mathbf{c}}^{j\text{-}1T} \ -\bar{\mathbf{c}}^{j\text{-}1T}\mathbf{A}^i\tilde{\bar{U}}^i\bar{\mathbf{G}}^i\right]\begin{bmatrix}\dot{\mathbf{R}}^i\\\dot{\theta}^i\end{bmatrix} - \left[\bar{\mathbf{k}}^{j\text{-}1T} \ \bar{\mathbf{k}}^{j\text{-}1T}\mathbf{A}^i\bar{U}^i\left(\theta^{-1}\right)^i\right]\begin{bmatrix}\mathbf{R}^i\\\theta^i\end{bmatrix} - \\
&\left[\bar{\mathbf{c}}^{JT} \ -\bar{\mathbf{c}}^{JT}\mathbf{A}^i\tilde{\bar{U}}^i\bar{\mathbf{G}}^i\right]\begin{bmatrix}\dot{\mathbf{R}}^i\\\dot{\theta}^i\end{bmatrix} - \left[\bar{\mathbf{k}}^{JT} \ \bar{\mathbf{k}}^{JT}\mathbf{A}^i\bar{U}^i\left(\theta^{-1}\right)^i\right]\begin{bmatrix}\mathbf{R}^i\\\theta^i\end{bmatrix} + \\
&\left[\bar{\mathbf{c}}^{j\text{-}1T} \ -\bar{\mathbf{c}}^{j\text{-}1T}\mathbf{A}^{i-1}\tilde{\bar{U}}^{i-1}\bar{\mathbf{G}}^{i-1}\right]\begin{bmatrix}\dot{\mathbf{R}}^{i-1}\\\dot{\theta}^{i-1}\end{bmatrix} + \left[\bar{\mathbf{k}}^{j\text{-}1T} \ \bar{\mathbf{k}}^{j\text{-}1T}\mathbf{A}^{i-1}\bar{U}^{i-1}\left(\theta^{-1}\right)^{i-1}\right]\begin{bmatrix}\mathbf{R}^{i-1}\\\theta^{i-1}\end{bmatrix} + \\
&\left[\bar{\mathbf{c}}^{JT} \ \bar{\mathbf{c}}^{JT}\mathbf{A}^{i+1}\tilde{\bar{U}}^{i+1}\bar{\mathbf{G}}^{i+1}\right]\begin{bmatrix}\dot{\mathbf{R}}^{i+1}\\\dot{\theta}^{i+1}\end{bmatrix} + \left[\bar{\mathbf{k}}^{JT} \ -\bar{\mathbf{k}}^{JT}\mathbf{A}^{i+1}\bar{U}^{i+1}\left(\theta^{-1}\right)^{i+1}\right]\begin{bmatrix}\mathbf{R}^{i+1}\\\theta^{i+1}\end{bmatrix}
\end{aligned} & for \begin{Bmatrix} i,j\,|\,2\le i, \\ j\le N-1 \end{Bmatrix}
\end{cases}
$$

$$
\mathbf{Q}_\theta^{jT} = \begin{cases}
\begin{aligned}
&-\left[\bar{\mathbf{c}}^{JT}\mathbf{A}_\theta^i\bar{\mathbf{u}}^i \ -\bar{\mathbf{c}}^{JT}\mathbf{A}^i\tilde{\bar{U}}^i\bar{\mathbf{G}}^i\mathbf{A}_\theta^i\bar{\mathbf{u}}^i\right]\begin{bmatrix}\dot{\mathbf{R}}^i\\\dot{\theta}^i\end{bmatrix} - \\
&\left[\bar{\mathbf{k}}^{JT}\mathbf{A}_\theta^i\bar{\mathbf{u}}^i \ \bar{\mathbf{k}}^{JT}\mathbf{A}^i\bar{U}^i\left(\theta^{-1}\right)^i\mathbf{A}_\theta^i\bar{\mathbf{u}}^i\right]\begin{bmatrix}\mathbf{R}^i\\\theta^i\end{bmatrix} + \\
&\left[\bar{\mathbf{c}}^{JT}\mathbf{A}_\theta^i\bar{\mathbf{u}}^i \ -\bar{\mathbf{c}}^{JT}\mathbf{A}^{i+1}\tilde{\bar{U}}^{i+1}\bar{\mathbf{G}}^{i+1}\mathbf{A}_\theta^i\bar{\mathbf{u}}^i\right]\begin{bmatrix}\dot{\mathbf{R}}^{i+1}\\\dot{\theta}^{i+1}\end{bmatrix} + \\
&\left[\bar{\mathbf{k}}^{JT}\mathbf{A}_\theta^i\bar{\mathbf{u}}^i \ -\bar{\mathbf{k}}^{JT}\mathbf{A}^{i+1}\bar{U}^{i+1}\left(\theta^{-1}\right)^{i+1}\mathbf{A}_\theta^i\bar{\mathbf{u}}^i\right]\begin{bmatrix}\mathbf{R}^{i+1}\\\theta^{i+1}\end{bmatrix}
\end{aligned} & for \begin{Bmatrix} i,j\,|\,i,j= \\ 1\cap i=N, \\ j=N-1 \end{Bmatrix} \\[6em]
\begin{aligned}
&-\left[\bar{\mathbf{c}}^{j\text{-}1T}\mathbf{A}_\theta^i\bar{\mathbf{u}}^i \ -\bar{\mathbf{c}}^{j\text{-}1T}\mathbf{A}^i\tilde{\bar{U}}^i\bar{\mathbf{G}}^i\mathbf{A}_\theta^i\bar{\mathbf{u}}^i\right]\begin{bmatrix}\dot{\mathbf{R}}^i\\\dot{\theta}^i\end{bmatrix} - \\
&\left[\bar{\mathbf{k}}^{j\text{-}1T}\mathbf{A}_\theta^i\bar{\mathbf{u}}^i \ \bar{\mathbf{k}}^{j\text{-}1T}\mathbf{A}^i\bar{U}^i\left(\theta^{-1}\right)^i\mathbf{A}_\theta^i\bar{\mathbf{u}}^i\right]\begin{bmatrix}\mathbf{R}^i\\\theta^i\end{bmatrix} - \\
&\left[\bar{\mathbf{c}}^{JT}\mathbf{A}_\theta^i\bar{\mathbf{u}}^i \ -\bar{\mathbf{c}}^{JT}\mathbf{A}^i\tilde{\bar{U}}^i\bar{\mathbf{G}}^i\mathbf{A}_\theta^i\bar{\mathbf{u}}^i\right]\begin{bmatrix}\dot{\mathbf{R}}^i\\\dot{\theta}^i\end{bmatrix} - \\
&\left[\bar{\mathbf{k}}^{JT}\mathbf{A}_\theta^i\bar{\mathbf{u}}^i \ \bar{\mathbf{k}}^{JT}\mathbf{A}^i\bar{U}^i\left(\theta^{-1}\right)^i\mathbf{A}_\theta^i\bar{\mathbf{u}}^i\right]\begin{bmatrix}\mathbf{R}^i\\\theta^i\end{bmatrix} + \\
&\left[\bar{\mathbf{c}}^{j\text{-}1T}\mathbf{A}_\theta^i\bar{\mathbf{u}}^i \ -\bar{\mathbf{c}}^{j\text{-}1T}\mathbf{A}^{i-1}\tilde{\bar{U}}^{i-1}\bar{\mathbf{G}}^{i-1}\mathbf{A}_\theta^i\bar{\mathbf{u}}^i\right]\begin{bmatrix}\dot{\mathbf{R}}^{i-1}\\\dot{\theta}^{i-1}\end{bmatrix} + \\
&\left[\bar{\mathbf{k}}^{j\text{-}1T}\mathbf{A}_\theta^i\bar{\mathbf{u}}^i \ \bar{\mathbf{k}}^{j\text{-}1T}\mathbf{A}^{i-1}\bar{U}^{i-1}\left(\theta^{-1}\right)^{i-1}\mathbf{A}_\theta^i\bar{\mathbf{u}}^i\right]\begin{bmatrix}\mathbf{R}^{i-1}\\\theta^{i-1}\end{bmatrix} + \\
&+\left[\bar{\mathbf{c}}^{JT}\mathbf{A}_\theta^i\bar{\mathbf{u}}^i \ \bar{\mathbf{c}}^{JT}\mathbf{A}^{i+1}\tilde{\bar{U}}^{i+1}\bar{\mathbf{G}}^{i+1}\mathbf{A}_\theta^i\bar{\mathbf{u}}^i\right]\begin{bmatrix}\dot{\mathbf{R}}^{i+1}\\\dot{\theta}^{i+1}\end{bmatrix} + \\
&\left[\bar{\mathbf{k}}^{JT}\mathbf{A}_\theta^i\bar{\mathbf{u}}^i \ -\bar{\mathbf{k}}^{JT}\mathbf{A}^{i+1}\bar{U}^{i+1}\left(\theta^{-1}\right)^{i+1}\mathbf{A}_\theta^i\bar{\mathbf{u}}^i\right]\begin{bmatrix}\mathbf{R}^{i+1}\\\theta^{i+1}\end{bmatrix}
\end{aligned} & for \begin{Bmatrix} i,j\,|\,2\le i, \\ j\le N-1 \end{Bmatrix}
\end{cases}
$$

(III.41/42)

The last step in derivation encloses the transformation of partitioned vectors and matrices into scalars to obtain simple scalar equations.

TUDelft

Joint forces are acting in vertical direction in the global frame and difference is required for intermediate and closing constraints, so:

$$\overline{\mathbf{k}}^{jT} = \begin{cases} \begin{bmatrix} 0 & k_{cl} \end{bmatrix}^T & for\{j \mid j = 1, N-1\} \\ \begin{bmatrix} 0 & k_{int} \end{bmatrix}^T & for\{j \mid 2 \le j \le N-2\} \end{cases} \tag{III.43}$$

$$\overline{\mathbf{c}}^{jT} = \begin{cases} \begin{bmatrix} 0 & c_{cl} \end{bmatrix}^T & for\{j \mid j = 1, N-1\} \\ \begin{bmatrix} 0 & c_{int} \end{bmatrix}^T & for\{j \mid 2 \le j \le N-2\} \end{cases} \tag{III.44}$$

Assuming an infinitesimally small size of the joint, the expressions for the generalized forces become purely functions of its generalized coordinates. If we apply:

$$\lim_{h \to 0} \delta W^i \tag{III.45}$$

consequently, we find for the position vector of point P^i, denoted in equation III.4:

$$\overline{\mathbf{u}}^i = \begin{cases} \lim_{h \to 0} \begin{bmatrix} L^i/2 & h/2 \end{bmatrix}^T = \begin{bmatrix} L^i/2 & 0 \end{bmatrix}^T \\ \lim_{h \to 0} \begin{bmatrix} -L^{i+1}/2 & -h/2 \end{bmatrix}^T = \begin{bmatrix} -L^{i+1}/2 & 0 \end{bmatrix}^T \end{cases} for\{i \mid 1 \le i \le N-1\} \tag{III.46}$$

to be scalars that are constant in time for rigid bodies.

Thus far, we derived expressions for virtual work for each element, affected by constraint forces from spring-dashpot elements. Taking into account all constraint forces, we must apply two more forces acting at the fixed positions of the system. The reason why we expelled introducing these constraint forces lies in the different approach of defining them. We will implement in the equations for virtual work two constraint equations:

$$\mathbf{R}^{i-1} + \mathbf{A}^{i-1}\overline{\mathbf{u}}^{i-1} - \mathbf{R}^i - \mathbf{A}^i\overline{\mathbf{u}}^i = 0 \quad for\{i = 1\}$$
$$\mathbf{R}^i + \mathbf{A}^i\overline{\mathbf{u}}^i - \mathbf{R}^{i+1} - \mathbf{A}^{i+1}\overline{\mathbf{u}}^{i+1} = 0 \quad for\{i = N\} \tag{III.47}$$

in which we elaborate the so called ground constraints $\left(R_2^0 = 0, \theta^0 = 0, R_2^{N+1} = 0, \theta^{N+1} = 0\right)$ and fill in the vector from equation III.46 to obtain the next equality:

$$R_2^i = L^i/2\,\theta^i \quad for\{i \mid i = 1, N\} \tag{III.48}$$

Substitution of this equality into both expressions for the generalized joint forces, keeping in mind the limit of equation III.45, yields the scalar notation of the generalized joint forces for each element:

$$
\mathbf{Q}_R^{i\,T} =
\begin{cases}
\left.\begin{array}{l}
-\bar{c}_{cl}L^i\dot{\theta}^i - \bar{k}_{cl}L^i\theta^i + \bar{c}_{cl}\dot{R}_2^{i+1} - \\
\bar{c}_{cl}\,L^{i+1}/2\,\dot{\theta}^{i+1} + \bar{k}_{cl}R_2^{i+1} - \bar{k}_{cl}\,L^{i+1}/2\,\theta^{i+1}
\end{array}\right\} & \text{for } \{i=1\} \\[2em]
\left.\begin{array}{l}
-\bar{c}_{cl}\dot{R}_2^i + \bar{c}_{cl}\,L^i/2\,\dot{\theta}^i - \bar{k}_{cl}R_2^i + \bar{k}_{cl}\,L^i/2\,\theta^i - \\
\bar{c}_{int}\dot{R}_2^i - \bar{c}_{int}\,L^i/2\,\dot{\theta}^i - \bar{k}_{int}R_2^i - \bar{k}_{int}\,L^i/2\,\theta^i + \\
\bar{c}_{cl}\dot{R}_2^{i-1} + \bar{c}_{cl}L^{i-1}\dot{\theta}^{i-1} + \bar{k}_{cl}R_2^{i-1} + \bar{k}_{cl}L^{i-1}\theta^{i-1} + \\
\bar{c}_{int}\dot{R}_2^{i+1} - \bar{c}_{int}\,L^{i+1}/2\,\dot{\theta}^{i+1} + \bar{k}_{int}R_2^{i+1} - \bar{k}_{int}\,L^{i+1}/2\,\theta^{i+1}
\end{array}\right\} & \text{for } \{i=2\} \\[3em]
\left.\begin{array}{l}
-\bar{c}_{int}\dot{R}_2^i - \bar{c}_{int}\,L^i/2\,\dot{\theta}^i - \bar{k}_{int}R_2^i - \bar{k}_{int}\,L^i/2\,\theta^i - \\
\bar{c}_{int}\dot{R}_2^i + \bar{c}_{int}\,L^i/2\,\dot{\theta}^i - \bar{k}_{int}R_2^i + \bar{k}_{int}\,L^i/2\,\theta^i + \\
\bar{c}_{int}\dot{R}_2^{i-1} + \bar{c}_{int}\,L^{i-1}/2\,\dot{\theta}^{i-1} + \bar{k}_{int}R_2^{i-1} + \bar{k}_{int}\,L^{i-1}/2\,\theta^{i-1} + \\
\bar{c}_{int}\dot{R}_2^{i+1} - \bar{c}_{int}\,L^{i+1}/2\,\dot{\theta}^{i+1} + \bar{k}_{int}R_2^{i+1} - \bar{k}_{int}\,L^{i+1}/2\,\theta^{i+1}
\end{array}\right\} & \text{for } \{i\,|\,3 \le i \le N-2\} \\[3em]
\left.\begin{array}{l}
-\bar{c}_{int}\dot{R}_2^i - \bar{c}_{int}\,L^i/2\,\dot{\theta}^i - \bar{k}_{int}R_2^i - \bar{k}_{int}\,L^i/2\,\theta^i - \\
\bar{c}_{cl}\dot{R}_2^i + \bar{c}_{cl}\,L^i/2\,\dot{\theta}^i - \bar{k}_{cl}R_2^i + \bar{k}_{cl}\,L^i/2\,\theta^i + \\
\bar{c}_{int}\dot{R}_2^{i-1} + \bar{c}_{int}\,L^{i-1}/2\,\dot{\theta}^{i-1} + \bar{k}_{int}R_2^{i-1} + \bar{k}_{int}\,L^{i-1}/2\,\theta^{i-1} + \\
\bar{c}_{cl}\dot{R}_2^{i+1} - \bar{c}_{cl}L^{i+1}\dot{\theta}^{i+1} + \bar{k}_{cl}R_2^{i+1} - \bar{k}_{cl}L^{i+1}\theta^{i+1}
\end{array}\right\} & \text{for } \{i=N-1\} \\[3em]
\left.\begin{array}{l}
\bar{c}_{cl}L^i\dot{\theta}^i + \bar{k}_{cl}L^i\theta^i + \bar{c}_{cl}\dot{R}_2^{i-1} + \\
\bar{c}_{cl}L^{i-1}\dot{\theta}^{i-1} + \bar{k}_{cl}R_2^{i-1} + \bar{k}_{cl}L^{i-1}\theta^{i-1}
\end{array}\right\} & \text{for } \{i=N\}
\end{cases}
$$

(III.49)

$$
\mathbf{Q}_\theta^{i\,T} =
\begin{cases}
\left.\begin{array}{l}
-\bar{c}_{cl}\left(L^i\right)^2\dot{\theta}^i - \bar{k}_{cl}\left(L^i\right)^2\theta^i + \bar{c}_{cl}L^i\dot{R}_2^{i+1} - \\
\bar{c}_{cl}L^i\,L^{i+1}/2\,\dot{\theta}^{i+1} + \bar{k}_{cl}L^iR_2^{i+1} - \bar{k}_{cl}\,L^iL^{i+1}/2\,\theta^{i+1}
\end{array}\right\} & \text{for } \{i=1\} \\[2em]
\left.\begin{array}{l}
\bar{c}_{cl}\,L^i/2\,\dot{R}_2^i - \bar{c}_{cl}\left(L^i/2\right)^2\dot{\theta}^i + \bar{k}_{cl}\,L^i/2\,R_2^i - \\
\bar{k}_{cl}\left(L^i/2\right)^2\theta^i - \bar{c}_{int}\,L^i/2\,\dot{R}_2^i - \bar{c}_{int}\left(L^i/2\right)^2\dot{\theta}^i - \\
\bar{k}_{int}\,L^i/2\,R_2^i - \bar{k}_{int}\left(L^i/2\right)^2\theta^i - \bar{c}_{cl}\,L^i/2\,\dot{R}_2^{i-1} - \\
\bar{c}_{cl}L^{i-1}\,L^i/2\,\dot{\theta}^{i-1} - \bar{k}_{cl}\,L^i/2\,R_2^{i-1} - \bar{k}_{cl}L^{i-1}\,L^i/2\,\theta^{i-1} + \\
\bar{c}_{int}\,L^i/2\,\dot{R}_2^{i+1} - \bar{c}_{int}\,L^i/2\,L^{i+1}/2\,\dot{\theta}^{i+1} + \bar{k}_{int}\,L^i/2\,R_2^{i+1} - \\
\bar{k}_{int}\,L^i/2\,L^{i+1}/2\,\theta^{i+1}
\end{array}\right\} & \text{for } \{i=2\} \\[4em]
\left.\begin{array}{l}
-\bar{c}_{int}\,L^i/2\,\dot{R}_2^i - \bar{c}_{int}\left(L^i/2\right)^2\dot{\theta}^i - \bar{k}_{int}\,L^i/2\,R_2^i - \\
\bar{k}_{int}\left(L^i/2\right)^2\theta^i + \bar{c}_{int}\,L^i/2\,\dot{R}_2^i - \bar{c}_{int}\left(L^i/2\right)^2\dot{\theta}^i + \\
\bar{k}_{int}\,L^i/2\,R_2^i - \bar{k}_{int}\left(L^i/2\right)^2\theta^i - \bar{c}_{int}\,L^i/2\,\dot{R}_2^{i-1} - \\
\bar{c}_{int}L^{i-1}/2\,L^i/2\,\dot{\theta}^{i-1} - \bar{k}_{int}\,L^i/2\,R_2^{i-1} - \bar{k}_{int}L^{i-1}/2\,L^i/2\,\theta^{i-1} + \\
\bar{c}_{int}\,L^i/2\,\dot{R}_2^{i+1} - \bar{c}_{int}\,L^i/2\,L^{i+1}/2\,\dot{\theta}^{i+1} + \bar{k}_{int}\,L^i/2\,R_2^{i+1} - \\
\bar{k}_{int}\,L^i/2\,L^{i+1}/2\,\theta^{i+1}
\end{array}\right\} & \text{for } \{i\,|\,3 \le i \le N-2\} \\[4em]
\left.\begin{array}{l}
-\bar{c}_{int}\,L^i/2\,\dot{R}_2^i - \bar{c}_{int}\left(L^i/2\right)^2\dot{\theta}^i - \bar{k}_{int}\,L^i/2\,R_2^i - \\
\bar{k}_{int}\left(L^i/2\right)^2\theta^i + \bar{c}_{cl}\,L^i/2\,\dot{R}_2^i - \bar{c}_{cl}\left(L^i/2\right)^2\dot{\theta}^i + \\
\bar{k}_{cl}\,L^i/2\,R_2^i - \bar{k}_{cl}\left(L^i/2\right)^2\theta^i - \bar{c}_{int}\,L^i/2\,\dot{R}_2^{i-1} - \\
\bar{c}_{int}L^{i-1}/2\,L^i/2\,\dot{\theta}^{i-1} - \bar{k}_{int}\,L^i/2\,R_2^{i-1} - \bar{k}_{int}L^{i-1}/2\,L^i/2\,\theta^{i-1} + \\
\bar{c}_{cl}\,L^i/2\,\dot{R}_2^{i+1} - \bar{c}_{cl}\,L^i/2\,L^{i+1}\dot{\theta}^{i+1} + \bar{k}_{cl}\,L^i/2\,R_2^{i+1} - \\
\bar{k}_{cl}\,L^i/2\,L^{i+1}\theta^{i+1}
\end{array}\right\} & \text{for } \{i=N-1\} \\[4em]
\left.\begin{array}{l}
-\bar{c}_{cl}\left(L^i\right)^2\dot{\theta}^i - \bar{k}_{cl}\left(L^i\right)^2\theta^i - \bar{c}_{cl}L^i\dot{R}_2^{i-1} - \\
\bar{c}_{cl}L^{i-1}/2\,L^i\dot{\theta}^{i-1} - \bar{k}_{cl}L^iR_2^{i-1} - \bar{k}_{cl}L^{i-1}/2\,L^i\theta^{i-1}
\end{array}\right\} & \text{for } \{i=N\}
\end{cases}
$$

(III.50)

TUDelft

III.4.2.2 Buoyancy forces

Figure III.7   illustrative example: derivation of the buoyancy force expressed in vectors and affecting the second body element

The buoyancy force is a rectangular or trapezoidal shaped reactive force that will be reactivated against the bottom of a rigid body when it is pushed downward trough the fluid surface for the heave or pitch motion respectively. The relationship between force and displacement is linear once more and the fluid can be characterized by a field of springs (Winkler foundation). Lumping each distributed buoyancy force in its point of application, see figure III.7, makes it prompt sensible for a vector analysis.

With the application of buoyancy forces to the problem we must realize that we agree restrictiveness in the multibody system once again. For example: the force on body i is considered independent from all other forces in the multibody system. In reality, this will never happen although we may almost speak of zero correlation if infinitely small displacements are performed and when mutual distance between body elements is big enough. Another example contains allowance of negative (downward) values for buoyancy.

Truly, there must be some static buoyancy to prevent losing contact with the fluid (figure). Moreover, drag forces along the sides of the bodies oppose the downward motion to make buoyancy forces to much optimistic when drag is neglected. After all, nothing has even been said about energy losses that emerge when fluid is pushed aside...
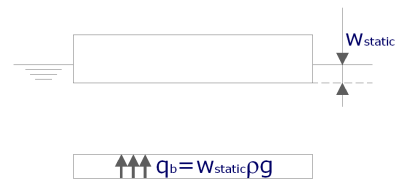
Figure III.8   static buoyancy

In a manner analogously to virtual work of the joint force we write virtual work due to buoyancy forces affecting body i as:

$$\delta W^i = -\mathbf{F}^{iT}\delta\mathbf{r}_p^i \qquad\qquad\qquad (III.51)$$

Where:

δW^i :   virtual work due to a buoyancy force acting on body i.

$\mathbf{F}^{iT}$:   (transposed) vector of the buoyancy force acting on body i.

$\delta\mathbf{r}_p^i$:   virtual change in the position vector located in the centre of gravity of the acting force.

Rewriting $\mathbf{F}^{ijT}$ as a product of the global position and global velocity vectors and substituting this into equations III.51, the expression for virtual work transforms into:

$$\delta W^i = \begin{cases} -\int\limits_0^L \left(\mathbf{k}_d^{iT}\mathbf{r}_p^i + \mathbf{c}_d^{iT}\dot{\mathbf{r}}_p^i \right)\delta\mathbf{r}_p^i du_1^i & for\ \{i\,|\,i=1,N\} \\[2mm] -\int\limits_{-L/2}^{L/2} \left(\mathbf{k}_d^{iT}\mathbf{r}_p^i + \mathbf{c}_d^{iT}\dot{\mathbf{r}}_p^i \right)\delta\mathbf{r}_p^i du_1^i & for\ \{i\,|\,2 \le i \le N-1\} \end{cases} \tag{III.52}$$

Where:

$\mathbf{k}_d^{iT}$:   (transposed) stiffness vector representing the distributed stiffness of the foundation governing body i.

$\mathbf{c}_d^{iT}$:   (transposed) damping vector representing the distributed viscous damping governing body i.

In partitioned form equation III.52 can be written as:

$$\delta W^i = \begin{cases} -\int\limits_0^L \left\{ \begin{bmatrix} \mathbf{k}_d^{iT} & \mathbf{k}_d^{iT}\mathbf{A}^i u_p^i \theta^{-1i} \end{bmatrix} \begin{bmatrix} \mathbf{R}^i \\ \theta^i \end{bmatrix} + \begin{bmatrix} \mathbf{c}_d^{iT} & -\mathbf{c}_d^{iT}\mathbf{A}^i \tilde{\bar{u}}^i \bar{\mathbf{G}}^i \end{bmatrix} \begin{bmatrix} \dot{\mathbf{R}}^i \\ \dot{\theta}^i \end{bmatrix} \right\} \\ \qquad\qquad \begin{bmatrix} \mathbf{I}_2 & \mathbf{A}_\theta{}^i u_p^i \end{bmatrix} du_1^i \begin{bmatrix} \delta\mathbf{R}^i \\ \delta\theta^i \end{bmatrix} & for\ \{i\,|\,i=1,N\} \\[6mm] -\int\limits_{-L/2}^{L/2} \left\{ \begin{bmatrix} \mathbf{k}_d^{iT} & \mathbf{k}_d^{iT}\mathbf{A}^i u_p^i \theta^{-1i} \end{bmatrix} \begin{bmatrix} \mathbf{R}^i \\ \theta^i \end{bmatrix} + \begin{bmatrix} \mathbf{c}_d^{iT} & -\mathbf{c}_d^{iT}\mathbf{A}^i \tilde{\bar{u}}^i \bar{\mathbf{G}}^i \end{bmatrix} \begin{bmatrix} \dot{\mathbf{R}}^i \\ \dot{\theta}^i \end{bmatrix} \right\} \\ \qquad\qquad \begin{bmatrix} \mathbf{I}_2 & \mathbf{A}_\theta{}^i u_p^i \end{bmatrix} du_1^i \begin{bmatrix} \delta\mathbf{R}^i \\ \delta\theta^i \end{bmatrix} & for\ \{i\,|\,2 \le i \le N-1\} \end{cases} \tag{III.53}$$

Henceforth, we write down immediately the expression the generalized forces:

$$\mathbf{Q}_R^{i\,T} = \begin{cases} -\int\limits_0^L \left(k_d^i R_2^i + c_d^i \dot{R}_2^i \right) du_1^i = -\left(k_d^i R_2^i + c_d^i \dot{R}_2^i \right) L^i & for\ \{i\,|\,i=1,N\} \\[2mm] = -1/2\left(k_d^i \theta^i + c_d^i \dot{\theta}^i \right)\left(L^i \right)^2 \\[2mm] -\int\limits_{-L/2}^{L/2} \left(k_d^i R_2^i + c_d^i \dot{R}_2^i \right) du_1^i = idem & for\ \{i\,|\,2 \le i \le N-1\} \end{cases} \tag{III.54}$$

$$\mathbf{Q}_\theta^{i\,T} = \begin{cases} -\int\limits_0^L \left\{ k_d^i \begin{bmatrix} \theta & 1 \end{bmatrix}^T \begin{bmatrix} u_1^i \\ u_2^i \end{bmatrix} + c_d^i \begin{bmatrix} \dot{\theta} & 1 \end{bmatrix}^T \begin{bmatrix} u_1^i \\ u_2^i \end{bmatrix} \right\} \begin{bmatrix} 1 & -\theta \end{bmatrix}^T \begin{bmatrix} u_1^i \\ u_2^i \end{bmatrix} d\bar{u}_1^i & for\ \{i\,|\,i=1,N\} \\[2mm] = -\dfrac{1}{3}\left(k_d^i \theta^i + c_d^i \dot{\theta}^i \right)\left(L^i \right)^3 \\[2mm] -\int\limits_{-L/2}^{L/2} \left\{ k_d^i \begin{bmatrix} \theta & 1 \end{bmatrix}^T \begin{bmatrix} u_1^i \\ u_2^i \end{bmatrix} + c_d^i \begin{bmatrix} \dot{\theta} & 1 \end{bmatrix}^T \begin{bmatrix} u_1^i \\ u_2^i \end{bmatrix} \right\} \begin{bmatrix} 1 & -\theta \end{bmatrix}^T \begin{bmatrix} u_1^i \\ u_2^i \end{bmatrix} d\bar{u}_1^i & for\ \{i\,|\,2 \le i \le N-1\} \\[2mm] = -\dfrac{1}{12}\left(k_d^i \theta^i + c_d^i \dot{\theta}^i \right)\left(L^i \right)^3 \end{cases} \tag{III.55}$$

and hold back deductive calculations. In III.54 and III.55 we reduce the vectors into scalars, because:

$$\mathbf{R}^i = \begin{bmatrix} 0 & R_2^i \end{bmatrix}^T$$

$$\mathbf{c}_d^{iT} = \begin{bmatrix} 0 & c_d^i \end{bmatrix}^T \tag{III.56}$$

$$\mathbf{k}_d^{iT} = \begin{bmatrix} 0 & k_d^i \end{bmatrix}^T$$

In which $k_d^i = \rho g B^i$ and $c_d^i = 0$ when purely buoyancy is considered and we took account for the next cross product by transformation to $\mathbf{Q}_\theta^i$:

$$\mathbf{Q}_\theta^{iT} = \mathbf{F}^{iT}\mathbf{A}_\theta^i \bar{u}_p^i = \pm \left| \bar{u}_p^i \times \left(\mathbf{A}^{iT}\mathbf{F}^i\right) \right| = \begin{bmatrix} i_1^i & i_2^i & i_3^i \\ \bar{u}_{p,1}^i & \bar{u}_{p,2}^i & 0 \\ \theta\mathbf{F}^i & \mathbf{F}^i & 0 \end{bmatrix} = \mathbf{F}^i \bar{u}_{p,1}^i i_3^i - \theta\mathbf{F}^i \bar{u}_{p,2}^i i_3^i \qquad \text{(III.57)}$$
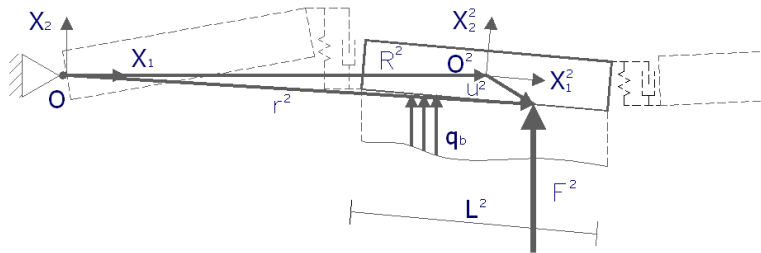
III.4.2.3 Traffic induced forces
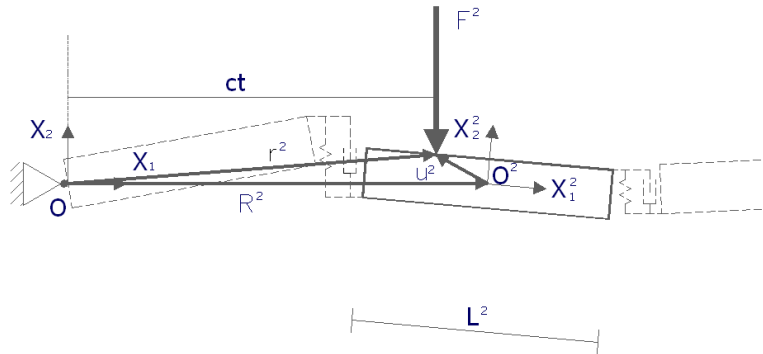
Figure III.9   **illustrative example: derivation of the traffic force expressed in vectors and affecting the second body element**

A traffic induced force can be modelled by a concentrated load P which propagates on the domain:

$$\left\{ x \mid 0 \le x \le \sum_1^N L_n \right\} \qquad \text{(III.58)}$$

with a constant velocity c. We suppose the concentrated load P resembles more or less the actual, more distributed vehicle induced force in particular this stage of research (vector analysis). In the modelling stage, for example, we reconstruct single and multiple vehicle induced loads from this concentrated load, in proportion of the topic of interest. A single vehicle can be reconstructed as two concentrated loads near the front and rear axis. In the algebra we apply superposition principle for two loads with a constant spatial offset or time delay. Creating multiple vehicles is then just an extension of the principle with more loads and ditto offsets. Shear forces, friction forces, energy dissipation via vehicle suspension, etc. are beyond the scope of the rigid multibody system analysis.

We may recall for the third time the expression for virtual work, denoted in equation III.12:

$$\delta W^i = \mathbf{F}^{iT} \delta \mathbf{r}_p^i \qquad \text{(III.59)}$$

Where:
δW^i :   virtual work due to a traffic induced force acting on body i.
$\mathbf{F}^{iT}$:   (transposed) vector of the induced force acting on body i.

Unlike for joint forces and buoyancy forces, $\mathbf{F}^{iT}$ is an independent integer with respect to its generalized coordinates, so we can directly rewrite equation III.59 in the partitioned form:

$$\delta W^i = \mathbf{F}^{iT}\delta\mathbf{r}^i_p = \mathbf{F}^{iT}\begin{bmatrix}\mathbf{I} & \mathbf{A}^i_\theta u^i_p\end{bmatrix}\begin{bmatrix}\delta\mathbf{R}^i \\ \delta\theta^i\end{bmatrix} = \begin{bmatrix}\mathbf{F}^{iT} & \mathbf{F}^{iT}\mathbf{A}^i_\theta u^i_p\end{bmatrix}\begin{bmatrix}\delta\mathbf{R}^i \\ \delta\theta^i\end{bmatrix} \qquad \text{(III.60)}$$

It is sufficient now to come up with the expressions obtained for both generalized forces:

$$\mathbf{Q}^{iT}_R = \mathbf{F}^{iT} = \begin{bmatrix}0 & P^i_2\end{bmatrix}^T \qquad \text{(III.61)}$$

$$Q^i_\theta = \mathbf{F}^{iT}\mathbf{A}^i_\theta u^i_p = \pm\left|\bar{u}^i_p \times \left(\mathbf{A}^{iT}\mathbf{F}^i\right)\right| = \begin{vmatrix} i^i_1 & i^i_2 & i^i_3 \\ \bar{u}^i_{p,1} & \bar{u}^i_{p,2} & 0 \\ 0 & P^i_2 & 0 \end{vmatrix} = P^i_2\bar{u}^i_{p,1}i^i_3 \qquad \text{(III.62)}$$

in which we introduce a time dependent function if we replace the global position vector for $\mathbf{F}^{iT}$ by the following vector:

$$\mathbf{r}^i = \begin{bmatrix}ct & 0\end{bmatrix}^T \qquad \text{(III.63)}$$

Where:

c :   integer for the constant velocity of the traffic induced force.

t :   time associated with the position of the traffic induced force.

Substitution of equation III.63 into III.4 result in a scalar notation for $\bar{u}^i_{p,1}$:

$$\bar{u}^i_{p,1} = ct - R^i_1 \qquad \text{(III.64)}$$

Substituting expression III.64 into III.62 gives a time dependent expression for the generalized force associated with the generalized coordinate θ^i :

$$Q^i_\theta(t) = P^i_2\left(ct - R^i_1\right) \qquad \text{(III.65)}$$

III.4.3 Newton-Euler matrix equation

In this end section, the development of the previous sections can be used to construct the Newton-Euler matrix equation for a rigid body in our multibody system.

To this end, we will use many of the obtained identities, in particular the relationship between the angular velocity and the time derivative of the orientational (i.e. Euler's) coordinates. For convenience, however, and to avoid drowning in writing extended derivations we restrict ourselves to prescriptions only.

If the joint reaction forces are treated as externally applied forces, Lagrange equation of motion can be written for all bodies as:

$$\frac{d}{dt}\left(\frac{\partial T^i}{\partial\dot{\mathbf{q}}^i_r}\right) - \frac{\partial T^i}{\partial\mathbf{q}^i_r} = \bar{\mathbf{Q}}^{iT} \qquad \text{(III.66)}$$

In which the bracketed term denotes the quadratic velocity vector. In the right hand side of equation III.66 the generalized and actual forces are composed as one vector. Henceforth, we elaborate all terms in equation III.66 separately, beginning with the left

hand side. Substituting matrix III.27 into equation III.25 produces a manageable equation for virtual work:

$$T^i = \frac{1}{2}\dot{\mathbf{R}}^{iT}\mathbf{m}_{RR}^i\dot{\mathbf{R}}^i + \frac{1}{2}\dot{\theta}^{iT}\mathbf{m}_{\theta\theta}^i\dot{\theta}^i \tag{III.67}$$

After substitution of equation III.67 into equation III.60, differentiation with respect to the generalized coordinates, velocities and time taking into account the chain rule of differentiation and equalities as $\bar{\omega}^i = \bar{\mathbf{G}}^i\dot{\theta}^i$ and $\dot{\bar{\mathbf{G}}}^i\dot{\theta}^i = 0$ and furthermore dividing the vector $\bar{\mathbf{Q}}^{iT}$ into its generalized integers, we end up with the following (uncoupled) matrix expression for equation III.66:

$$\mathbf{m}_{RR}^i\ddot{\mathbf{R}}^i = \bar{\mathbf{Q}}_R^{i\,T}$$
$$\mathbf{m}_{\theta\theta}^i\ddot{\theta}^i = \bar{\mathbf{Q}}_\theta^i - 2\dot{\bar{\mathbf{G}}}^{iT}\bar{\mathbf{I}}_{\theta\theta}^i\bar{\omega}^i \tag{III.68}$$

Concluding with a remark, it stated that $\dot{\bar{\mathbf{G}}}^i = 0$, so the second term in the right side of the Euler equation disappears. Assembling expressions III.29 and III.35 for mass matrices and external force vectors in equations III.49, III.50, III.54, III.55, III.61 and III.62 to substitute into equation III.68 result in the applied matrix equation in general coordinates:

$$
\begin{aligned}
&\begin{bmatrix} 0 & 0 \\ 0 & J^i \end{bmatrix}\begin{bmatrix} \ddot{R}_2^i \\ \ddot{\theta}^i \end{bmatrix} = \begin{bmatrix} 0 & -\bar{c}_{cl}L^i - \frac{1}{2}c_d^i\left(L^i\right)^2 \\ 0 & -\bar{c}_{cl}\left(L^i\right)^2 - \frac{1}{3}c_d^i\left(L^i\right)^3 \end{bmatrix}\begin{bmatrix} \dot{R}_2^i \\ \dot{\theta}^i \end{bmatrix} + \begin{bmatrix} 0 & -\bar{k}_{cl}L^i - \frac{1}{2}k_d^i\left(L^i\right)^2 \\ 0 & -\bar{k}_{cl}\left(L^i\right)^2 - \frac{1}{3}k_d^i\left(L^i\right)^3 \end{bmatrix}\begin{bmatrix} R_2^i \\ \theta^i \end{bmatrix} + \\[2ex]
&\begin{bmatrix} \bar{c}_{cl} & -\bar{c}_{cl}\,L^{i+1}/2 \\ \bar{c}_{cl}L^i & -\bar{c}_{cl}L^i\,L^{i+1}/2 \end{bmatrix}\begin{bmatrix} \dot{R}_2^{i+1} \\ \dot{\theta}^{i+1} \end{bmatrix} + \begin{bmatrix} \bar{k}_{cl} & -\bar{k}_{cl}\,L^{i+1}/2 \\ \bar{k}_{cl}L^i & -\bar{k}_{cl}L^iL^{i+1}/2 \end{bmatrix}\begin{bmatrix} R_2^{i+1} \\ \theta^{i+1} \end{bmatrix} + \\[2ex]
&\begin{cases} \begin{bmatrix} P_2^i & P_2^i\left(ct - R_1^i\right) \end{bmatrix}^T & for\ \left\{t\,|\,R_1^i/c < t \le \left(R_1^i + L^i\right)/c\right\} \\ \begin{bmatrix} 0 & 0 \end{bmatrix}^T & elsewhere \end{cases}
\end{aligned}
\quad\Bigg\}\ for\ \{i = 1\}
$$

$$
\begin{aligned}
&\begin{bmatrix} m^i & 0 \\ 0 & J^i \end{bmatrix}\begin{bmatrix} \ddot{R}_2^i \\ \ddot{\theta}^i \end{bmatrix} = \begin{bmatrix} -\left(\bar{c}_{cl} + \bar{c}_{int}\right) - c_d^iL^i & -\left(\bar{c}_{int} - \bar{c}_{cl}\right)L^i/2 \\ -\left(\bar{c}_{int} - \bar{c}_{cl}\right)L^i/2 & -\left(\bar{c}_{cl} + \bar{c}_{int}\right)\left(L^i/2\right)^2 - \frac{1}{12}c_d^i\left(L^i\right)^3 \end{bmatrix}\begin{bmatrix} \dot{R}_2^i \\ \dot{\theta}^i \end{bmatrix} + \\[2ex]
&\begin{bmatrix} -\bar{k}_{cl} - \bar{k}_{int} - k_d^iL^i & -\left(\bar{k}_{int} - \bar{k}_{cl}\right)L^i/2 \\ -\left(\bar{k}_{int} - \bar{k}_{cl}\right)L^i/2 & -\left(\bar{k}_{cl} + \bar{k}_{int}\right)\left(L^i/2\right)^2 - \frac{1}{12}k_d^i\left(L^i\right)^3 \end{bmatrix}\begin{bmatrix} R_2^i \\ \theta^i \end{bmatrix} + \\[2ex]
&\begin{bmatrix} \bar{c}_{cl} & \bar{c}_{cl}L^{i-1} \\ -\bar{c}_{cl}\,L^i/2 & -\bar{c}_{cl}L^{i-1}\,L^i/2 \end{bmatrix}\begin{bmatrix} \dot{R}_2^{i-1} \\ \dot{\theta}^{i-1} \end{bmatrix} + \begin{bmatrix} \bar{k}_{cl} & \bar{k}_{cl}L^{i-1} \\ -\bar{k}_{cl}\,L^i/2 & -\bar{k}_{cl}L^{i-1}\,L^i/2 \end{bmatrix}\begin{bmatrix} R_2^{i-1} \\ \theta^{i-1} \end{bmatrix} + \\[2ex]
&\begin{bmatrix} \bar{c}_{int} & -\bar{c}_{int}\,L^{i+1}/2 \\ \bar{c}_{int}\,L^i/2 & -\bar{c}_{int}\,L^i/2\,L^{i+1}/2 \end{bmatrix}\begin{bmatrix} \dot{R}_2^{i+1} \\ \dot{\theta}^{i+1} \end{bmatrix} + \begin{bmatrix} \bar{k}_{int} & -\bar{k}_{int}\,L^{i+1}/2 \\ \bar{k}_{int}\,L^i/2 & -\bar{k}_{int}\,L^i/2\,L^{i+1}/2 \end{bmatrix}\begin{bmatrix} R_2^{i+1} \\ \theta^{i+1} \end{bmatrix} + \\[2ex]
&\begin{cases} \begin{bmatrix} P_2^i & P_2^i\left(ct - R_1^i\right) \end{bmatrix}^T & for\ \left\{t\,|\,\left(R_1^i - L^i/2\right)/c < t \le \left(R_1^i + L^i/2\right)/c\right\} \\ \begin{bmatrix} 0 & 0 \end{bmatrix}^T & elsewhere \end{cases}
\end{aligned}
\quad\Bigg\}\ for\ \{i = 2\}
$$

$$\tag{III.69a}$$

$$
\begin{bmatrix} m^i & 0 \\ 0 & J^i \end{bmatrix}\begin{bmatrix} \ddot{R}_2^i \\ \ddot{\theta}^i \end{bmatrix} = \begin{bmatrix} -2\bar{c}_{int}-c_d^i L^i & 0 \\ 0 & -2\bar{c}_{int}\left(L^i/2\right)^2-\dfrac{1}{12}c_d^i\left(L^i\right)^3 \end{bmatrix}\begin{bmatrix} \dot{R}_2^i \\ \dot{\theta}^i \end{bmatrix}+
$$

$$
\begin{bmatrix} -2\bar{k}_{int}-k_d^i L^i & 0 \\ 0 & -2\bar{k}_{int}\left(L^i/2\right)^2-\dfrac{1}{12}k_d^i\left(L^i\right)^3 \end{bmatrix}\begin{bmatrix} R_2^i \\ \theta^i \end{bmatrix}+
$$

$$
\begin{bmatrix} \bar{c}_{int} & \bar{c}_{int}\,L^{i-1}/2 \\ -\bar{c}_{int}\,L^i/2 & -\bar{c}_{int}\,L^{i-1}/2\,L^i/2 \end{bmatrix}\begin{bmatrix} \dot{R}_2^{i-1} \\ \dot{\theta}^{i-1} \end{bmatrix}+\begin{bmatrix} \bar{k}_{int} & \bar{k}_{int}\,L^{i-1}/2 \\ -\bar{k}_{int}\,L^i/2 & -\bar{k}_{int}\,L^{i-1}/2\,L^i/2 \end{bmatrix}\begin{bmatrix} R_2^{i-1} \\ \theta^{i-1} \end{bmatrix}+
$$

$$
\begin{bmatrix} \bar{c}_{int} & -\bar{c}_{int}\,L^{i+1}/2 \\ \bar{c}_{int}\,L^i/2 & -\bar{c}_{int}\,L^i/2\,L^{i+1}/2 \end{bmatrix}\begin{bmatrix} \dot{R}_2^{i+1} \\ \dot{\theta}^{i+1} \end{bmatrix}+\begin{bmatrix} \bar{k}_{int} & -\bar{k}_{int}\,L^{i+1}/2 \\ \bar{k}_{int}\,L^i/2 & -\bar{k}_{int}\,L^i/2\,L^{i+1}/2 \end{bmatrix}\begin{bmatrix} R_2^{i+1} \\ \theta^{i+1} \end{bmatrix}+
$$

$$
\begin{cases} \begin{bmatrix} P_2^i & P_2^i\left(ct-R_1^i\right) \end{bmatrix}^T & for\ \left\{t\,\middle|\,\left(R_1^i-L^i/2\right)\middle/c < t \le \left(R_1^i+L^i/2\right)\middle/c\right\} \\ \begin{bmatrix} 0 & 0 \end{bmatrix}^T & elsewhere \end{cases}
$$

for $\{i\,|\,3 \le i \le N-2\}$

$$
\begin{bmatrix} m^i & 0 \\ 0 & J^i \end{bmatrix}\begin{bmatrix} \ddot{R}_2^i \\ \ddot{\theta}^i \end{bmatrix} = \begin{bmatrix} -\left(\bar{c}_{int}+\bar{c}_{cl}\right)-c_d^i L^i & -\left(\bar{c}_{int}-\bar{c}_{cl}\right)L^i/2 \\ -\left(\bar{c}_{int}-\bar{c}_{cl}\right)L^i/2 & -\left(\bar{c}_{int}+\bar{c}_{cl}\right)\left(L^i/2\right)^2-\dfrac{1}{12}c_d^i\left(L^i\right)^3 \end{bmatrix}\begin{bmatrix} \dot{R}_2^i \\ \dot{\theta}^i \end{bmatrix}+
$$

$$
\begin{bmatrix} -\left(\bar{k}_{int}+\bar{k}_{cl}\right)-k_d^i L^i & -\left(\bar{k}_{int}-\bar{k}_{cl}\right)L^i/2 \\ -\left(\bar{k}_{int}-\bar{k}_{cl}\right)L^i/2 & -\left(\bar{k}_{int}+\bar{k}_{cl}\right)\left(L^i/2\right)^2-\dfrac{1}{12}k_d^i\left(L^i\right)^3 \end{bmatrix}\begin{bmatrix} R_2^i \\ \theta^i \end{bmatrix}+
$$

$$
\begin{bmatrix} \bar{c}_{int} & \bar{c}_{int}\,L^{i-1}/2 \\ -\bar{c}_{int}\,L^i/2 & -\bar{c}_{int}\,L^{i-1}/2\,L^i/2 \end{bmatrix}\begin{bmatrix} \dot{R}_2^{i-1} \\ \dot{\theta}^{i-1} \end{bmatrix}+\begin{bmatrix} \bar{k}_{int} & \bar{k}_{int}\,L^{i-1}/2 \\ -\bar{k}_{int}\,L^i/2 & -\bar{k}_{int}\,L^{i-1}/2\,L^i/2 \end{bmatrix}\begin{bmatrix} R_2^{i-1} \\ \theta^{i-1} \end{bmatrix}+
$$

$$
\begin{bmatrix} \bar{c}_{cl} & -\bar{c}_{cl}L^{i+1} \\ \bar{c}_{cl}\,L^i/2 & -\bar{c}_{cl}\,L^i/2\,L^{i+1} \end{bmatrix}\begin{bmatrix} \dot{R}_2^{i+1} \\ \dot{\theta}^{i+1} \end{bmatrix}+\begin{bmatrix} \bar{k}_{cl} & -\bar{k}_{cl}L^{i+1} \\ \bar{k}_{cl}\,L^i/2 & -\bar{k}_{cl}\,L^i/2\,L^{i+1} \end{bmatrix}\begin{bmatrix} R_2^{i+1} \\ \theta^{i+1} \end{bmatrix}+
$$

$$
\begin{cases} \begin{bmatrix} P_2^i & P_2^i\left(ct-R_1^i\right) \end{bmatrix}^T & for\ \left\{t\,\middle|\,\left(R_1^i-L^i/2\right)\middle/c < t \le \left(R_1^i+L^i/2\right)\middle/c\right\} \\ \begin{bmatrix} 0 & 0 \end{bmatrix}^T & elsewhere \end{cases}
$$

for $\{i = N-1\}$

$$
\begin{bmatrix} 0 & 0 \\ 0 & J^i \end{bmatrix}\begin{bmatrix} \ddot{R}_2^i \\ \ddot{\theta}^i \end{bmatrix} = \begin{bmatrix} 0 & \bar{c}_{cl}L^i-\dfrac{1}{2}c_d^i\left(L^i\right)^2 \\ 0 & -\bar{c}_{cl}\left(L^i\right)^2-\dfrac{1}{3}c_d^i\left(L^i\right)^3 \end{bmatrix}\begin{bmatrix} \dot{R}_2^i \\ \dot{\theta}^i \end{bmatrix}+\begin{bmatrix} 0 & \bar{k}_{cl}L^i-\dfrac{1}{2}k_d^i\left(L^i\right)^2 \\ 0 & -\bar{k}_{cl}\left(L^i\right)^2-\dfrac{1}{3}k_d^i\left(L^i\right)^3 \end{bmatrix}\begin{bmatrix} R_2^i \\ \theta^i \end{bmatrix}+
$$

$$
\begin{bmatrix} \bar{c}_{cl} & \bar{c}_{cl}L^{i-1} \\ -\bar{c}_{cl}L^i & -\bar{c}_{cl}\,L^{i-1}/2\,L^i \end{bmatrix}\begin{bmatrix} \dot{R}_2^{i-1} \\ \dot{\theta}^{i-1} \end{bmatrix}+\begin{bmatrix} \bar{k}_{cl} & \bar{k}_{cl}L^{i-1} \\ -\bar{k}_{cl}L^i R_2^{i-1} & -\bar{k}_{cl}\,L^{i-1}/2\,L^i \end{bmatrix}\begin{bmatrix} R_2^{i-1} \\ \theta^{i-1} \end{bmatrix}+
$$

$$
\begin{cases} \begin{bmatrix} P_2^i & P_2^i\left(ct-R_1^i\right) \end{bmatrix}^T & for\ \left\{t\,\middle|\,\left(R_1^i-L^i\right)\middle/c < t \le R_1^i\middle/c\right\} \\ \begin{bmatrix} 0 & 0 \end{bmatrix}^T & elsewhere \end{cases}
$$

for $\{i = N\}$

(III.69b)

TUDelft

IV Wave diffraction

The effect of the frequency and the nature of the acting load on the vibration amplitudes of the fluid in the neighbourhood of a rigid floating strip is investigated numerically. The word 'strip' may be replaced by 'body' or 'pontoon'.

IV.1 Assumptions and problem formulation

The static situation is illustrated in figure IV.1 and shows a floating strip which doesn't perturb the water surface.
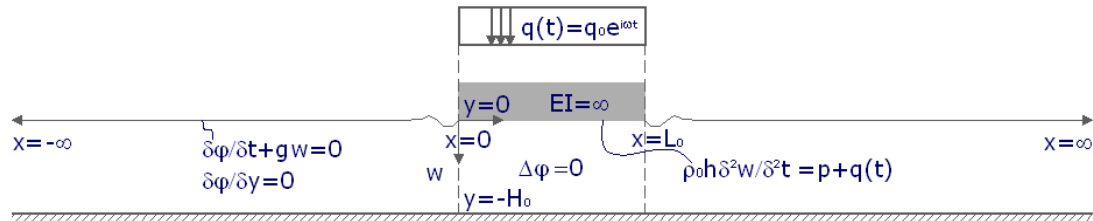
Figure IV.1   **flow diagram with applied boundaries in case of the steady state vibrations for vertical motion**

EI :   flexural rigidity
h :   strip thickness
L_0 :   strip length
H_0 :   depth

By using plausible assumptions for the fluid and the strip useful continuity equations and boundary conditions will be obtained. So, by making the fluid ideal and incompressible and keeping the flow irrotational the fluid velocity potential φ must satisfy the Laplace equation:

$$\Delta \varphi = 0 \quad for \left\{ y \mid -H_0 < y < 0 \right\} \tag{IV.1}$$

The bottom can be characterized as impervious, so the boundary at the bottom for the fluid velocity potential:

$$\frac{\partial \varphi}{\partial y} = 0 \quad for \left\{ y \mid y = -H_0 \right\} \tag{IV.2}$$

For the upper boundary the following continuity expression is valid for the whole domain:

$$\frac{\partial \varphi}{\partial y} = \frac{\partial w}{\partial t} \quad for \left\{ y \mid y = 0 \right\} \tag{IV.3}$$

For the free surface Bernoulli's equation can be transformed into:

$$\frac{\partial \varphi}{\partial t} + gw = 0 \quad for \left\{ x, y \mid x \in (-\infty, 0) \cup (L_0, \infty), y = 0 \right\} \tag{IV.4}$$

Where:
g :   gravitational acceleration
w :   vertical displacement of the upper surface of the fluid

TUDelft

A time-periodic pressure with the form $q(x)e^{i\omega t}$ acts on the strip. In this section a equally distributed load will be considered:

$$q(t) = q_0 e^{i\omega t} \tag{IV.5}$$

Where:

q_0 :   magnitude of the distributed load;

Unlike 1D plate equations, in the continuity equation of the strip only inertia forces, pressure and external forces are balanced. Bending forces, however, will not occur in the rigid strip because of infinite rigidity. As a matter of fact, obtaining explicit analytic solutions for wave diffraction would not have been possible if a 1D plate equation with infinite rigidity was implemented. Therefore the next equation holds for the strip:

$$\rho_0 h \frac{\partial^2 w}{\partial t^2} = p + q(t) \quad for \{x, y \mid 0 < x < L_0, y = 0\} \tag{IV.6}$$

Where:

p :   hydrodynamic pressure; $p = -\rho\left(\partial\varphi/\partial t + gw\right)$ according to Bernoulli

ρ :   fluid density

ρ_0 :   strip or unit density

ω :   radian frequency

The equation shows no dependency in x, but that does not mean that the water surface (w) on the this interval stays flat all the time. As a consequence of this, the rigid strip can never stay in contact with the surface all the time while in the model it does. For that reason equation IV.6 may be applied as long as w doesn't vary too much within the boundaries of x.

IV.2 Steady state formulation

For the steady state condition the velocity potential can be represented in the form:

$$\varphi = \phi\left(x, y\right)e^{i\omega t} \tag{IV.7}$$

In what follows, the dimensionless variables $\varphi = \varphi\omega\rho/q_0, w = w\rho g/q_0, p = q_0 p,$
$x = x/l, y = y/l, t = \omega t, L = L_0/l, H = H_0/l$ will be inserted and two new variables will be introduced; the characteristic length $l = g/\omega^2$ and the dimensionless draft $d = \rho_0 h/\rho l$. After substitution of expressions IV.1 into IV.7 the Laplace equation reads:

$$\frac{\partial^2 \phi}{\partial x^2} + \frac{\partial^2 \phi}{\partial y^2} = 0 \quad for \{y \mid -H < y < 0\} \tag{IV.8}$$

In this way, the boundary condition at the bottom turns into:

$$\frac{\partial \phi}{\partial y} = 0 \quad for \{y \mid y = -H\} \tag{IV.9}$$

For the free surface, substitution of expression IV.7 into equation IV.4, taking the derivative to t once and taking into account continuity expression of IV.3 are successively the steps to be taken to a steady state formulation:

TUDelft

$$\frac{\partial \phi}{\partial y} - \phi = 0 \quad for\left\{x,y \mid x \in (-\infty,0) \cup (L,\infty), y = 0\right\} \tag{IV.10}$$

Analogous to the last substitution, the continuity equation can be obtained:

$$(1-d)\frac{\partial \phi}{\partial y} - \phi = i \quad for\left\{x,y \mid 0 < x < L, y = 0\right\} \tag{IV.11}$$

Where only the draft of the strip seems to affect the nature of the surface wave compared to its free relative. Furthermore, if $d = 1$ the inertia effect has been eliminated, what seems not realistic. If $d = 0$, the free surface is influenced by the external force only, what is also unrealistic.

IV.3 Frequency domain analysis

The analysis of the hydro elastic behaviour of the fluid in the neighbourhood of the rigid strip will be performed within the frame work of the linear theory. To this end, the system of partial differential equations, IV.8 until IV.11, will be transformed into the frequency domain with the help of the Fourier transformation technique. Defining Fourier Transforms implies that the radiation condition must be checked. Because there is no source of energy at infinity, all inward propagating waves are aphysical which means that they must be disregarded. The Fourier Transform formula reads:

$$\Phi(\alpha,y) = \int_{-\infty}^{\infty} \phi(x,y) e^{i\alpha x} dx \tag{IV.12}$$

Where Φ denotes the transformed velocity potential and α the spectral frequency. Transformation of the Laplacian of expression IV.8 result in $\partial^2 \Phi(\alpha,y)/\partial y^2 - \alpha^2 \Phi = 0$. All Φ must satisfy this equation from which the general expression gives:

$$\Phi(\alpha,y) = C_1(\alpha)\cosh(\alpha y) + C_2(\alpha)\sinh(\alpha y) \tag{IV.13}$$

Returning to the boundary condition at the bottom IV.9, the general expression becomes, after transformation and substitution of expression IV.9 into IV.13:

$$\Phi(\alpha,y) = C_1(\alpha)\left(\cosh(\alpha(y+H))/\cosh(\alpha H)\right) \tag{IV.14}$$

For the free surface condition IV.10 and the continuity condition IV.11, however, the transformation is less straightforward; it is very difficult to find a general transform that applies over the entire spatial domain for both equations. The Wiener-Hopf technique [3], as a matter of fact, is a popular method to avoid this problem by defining Fourier Transforms over the specified regions and then uses function-theoretic analysis to piece them together for the solution. To this background, both equations IV.10 and IV.11 will be constructed as follows:

$$\Phi_-(\alpha,y) = \int_{-\infty}^{0} \phi(x,y)e^{i\alpha x}dx$$

$$\Phi_1(\alpha,y) = \int_{0}^{L} \phi(x,y)e^{i\alpha x}dx$$

$$\Phi_+(\alpha,y) = \int_{L}^{\infty} \phi(x,y)e^{i\alpha(x-L)}dx \qquad \text{(IV.15)}$$

$$\Phi(\alpha,y) = \Phi_-(\alpha,y) + \Phi_1(\alpha,y) + \Phi_+(\alpha,y)e^{i\alpha L}$$

Where the subscript refers to the specified region. Integrals of equation IV.15 where the function ϕ is replaced by the free surface condition of IV.10 will be denoted by D :

$$D(\alpha) = D_-(\alpha) + D_1(\alpha) + D_+(\alpha)e^{i\alpha L} \qquad \text{(IV.16)}$$

and analogous expressions in which the continuity condition of IV.11 is taken as the integrand will be denoted by F :

$$F(\alpha) = F_-(\alpha) + F_1(\alpha) + F_+(\alpha)e^{i\alpha L} \qquad \text{(IV.17)}$$

After transformation of expression IV.10 and substitution of this result into IV.13 the general expression of D will be:

$$D(\alpha) = C_1(\alpha)\big(\alpha \tanh(\alpha H) - 1\big) \qquad \text{(IV.18)}$$

Where the last term is better known as the dispersion relation of free surface waves, $K_1 \equiv \alpha \tanh(\alpha H) - 1 = 0$. Following the same steps as for D, F has the form:

$$F(\alpha) = C_1(\alpha)\big((1-d)\alpha \tanh(\alpha H) - 1\big) \qquad \text{(IV.19)}$$

With $K_2 \equiv (1-d)\alpha \tanh(\alpha H) - 1 = 0$ as dispersion relation. The dispersion relation is the ratio between energy and momentum of the wave. Finally, all integrands can be expressed in one equation. A little algebra shows that this equation yields:

$$F_-(\alpha) + (1/\alpha)\big(e^{i\alpha L} - 1\big) + F_+(\alpha)e^{i\alpha L} = D_1(\alpha)K(\alpha) \qquad \text{(IV.20)}$$

Where $D_-(\alpha) = D_+(\alpha) = 0$ comes from the boundary conditions, $F_1(\alpha) = (1/\alpha)\big(e^{i\alpha L} - 1\big)$ and $K(\alpha) = K_2(\alpha)/K_1(\alpha)$ are obtained via elimination of $C_1(\alpha)$.

So far, finding an expression for IV.20 was quite a regular task, but elaborating this expression shall be far from regular. Elaborating the integrands of equation IV.20 means applying Cauchy's residue theorem [3] because its variables are complex. According to Cauchy's residue theorem the function's analyticity domain and its singularities has to be known. Besides this, the Wiener-Hopf technique requires a factorization of the function, i.e. a decomposition over the two domains analogous to Φ_- and Φ_+. Consequently, only K has singularities so that it may be represented in the factorized form as follows:

$$K(\alpha) = K_+(\alpha)K_-(\alpha) \qquad \text{(IV.21)}$$

Where K has two singularities (poles) on the real axis at the points $\pm\alpha_0$ and an infinite number of imaginary poles at $\pm\alpha_n = \pm in\pi/H$ $for\{n \mid n = 1,2,...\}$ as $n \to \infty$. If a situation

occurs with K in the dominator of a function or integrand, then of course, the poles come from the nominator of K; i.e. two poles on the real axis at the points $\pm\gamma$ and an infinite number of imaginary poles at $\pm\gamma_n = \pm in\pi/H$ $for\ \{n\,|\,n=1,2,...\}$ as $n\rightarrow\infty$ and $d<1$.

The poles are calculated in Matlab with `fzero` and `fsolve` statements for real and imaginairy poles respectively as can be seen in Appendix V.4.

The analyticity domains are shown in figure IV.2
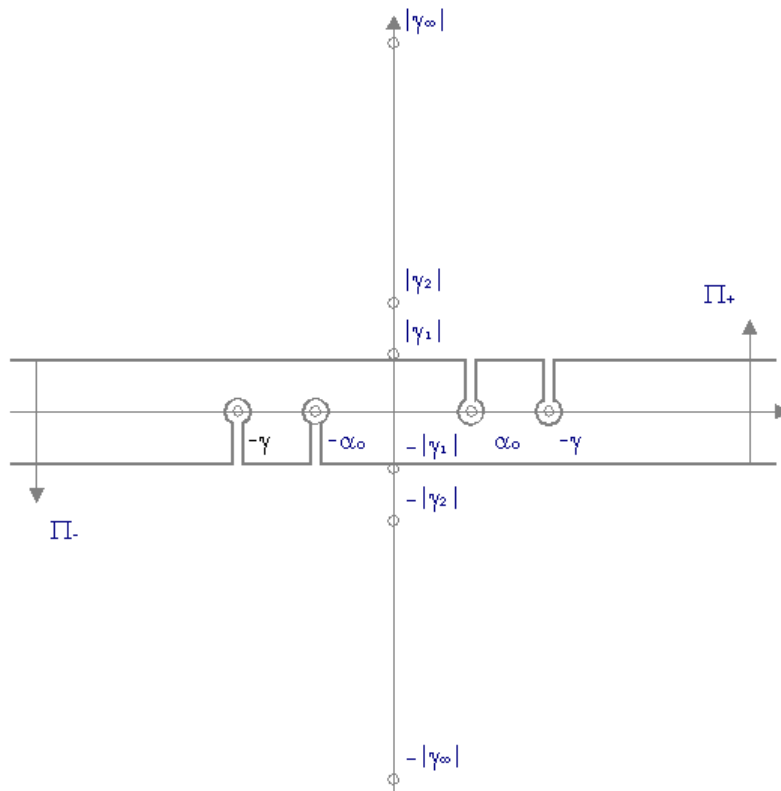
Figure IV.2   Analyticity domains

Where:

Π^+:   half plane where $\mathrm{Im}(\alpha)>-|\gamma_1|$ with cuts around $-\alpha_0$ and $-\gamma$
Π^-:   half plane where $\mathrm{Im}(\alpha)<|\gamma_1|$ with cuts around α_0 and γ

Choosing Π^+ and Π^- as such leads to the most simplified mathematical expressions for the problem. With known analyticity domains explicit expressions can be accomplished for both integrands $K_+(\alpha)$ and $K_-(\alpha)$ In doing so, the Infinite Product Theorem [3] will be introduced as a useful tool. It says that $K(\alpha)$ as an entire function, i.e. analytic on the entire domain, with simple zeros can be written as an infinite product in its poles as follows:

$$K(\alpha) = K(0)\exp\left[\alpha K'(0)/K(0)\right]\prod_{n=1}^{\infty}\left(1-\frac{\alpha}{\alpha_n}\right)e^{\frac{\alpha}{\alpha_n}} \qquad (IV.22)$$

Where:

$K(0)$:   is 1 because $K(\alpha)$ has no single root in the origin
$\exp\left[\alpha K'(0)/K(0)\right]$: uniquely determined analytic function which means that the term

before the product will have no roots in the complex plane. The term

is equal to 1 since $K'(0) = 0$. Unlike [3], we use the $\dfrac{\alpha^2 - \alpha_0{}^2}{\alpha^2 - \gamma^2}$ -term in order to be able to subtract all real roots (zeros and poles) in the complex plane

Equation (IV.22) reduces to:

$$K(\alpha) = \frac{\alpha^2 - \alpha_0{}^2}{\alpha^2 - \gamma^2} \prod_{n=1}^{\infty}\left(1 - \frac{\alpha}{\alpha_n}\right)e^{\frac{\alpha}{\alpha_n}} \tag{IV.23}$$

Where $K(\alpha)$ has been divided by two real zeros and multiplied with its two real poles. A useful expression for $K_+(\alpha)$ and $K_-(\alpha)$ follows after substitution of IV.23 into IV.21:

$$K_\pm(\alpha) = \frac{\alpha \pm \alpha_0}{\alpha \pm \gamma} \prod_{n=1}^{\infty}\left(1 - \frac{\alpha}{\alpha_n}\right)e^{\frac{\alpha}{\alpha_n}} \tag{IV.24}$$

Coming back to the integrand equation of IV.20, two integrands are unknown; F and D so two equations are needed to solve them. Therefore we multiply equation IV.20 by $e^{-i\alpha L}/K_-(\alpha)$ and after arranging functions by their analytic domains, we denote:

$$\frac{F_+(\alpha)}{K_+(\alpha)} + \frac{1}{\alpha K_+(\alpha)} - \frac{1}{\alpha K_+(0)} + U_+(\alpha) + M_+(\alpha) =$$

$$D_1(\alpha)K_-(\alpha)e^{-i\alpha L} - \frac{1}{\alpha K_-(0)} - U_-(\alpha) - M_-(\alpha) \tag{IV.25}$$

$$U_+(\alpha) + U_-(\alpha) = \frac{F_-(\alpha)e^{-i\alpha L}}{K_+(\alpha)} \qquad U_\pm(\alpha) = \pm\frac{1}{2\pi i}\int_{-\infty\mp i\sigma}^{\infty\mp i\sigma}\frac{e^{-i\varsigma L}F_-(\varsigma)d\varsigma}{K_+(\varsigma)(\varsigma - \alpha)}$$

$$M_+(\alpha) + M_-(\alpha) = -\frac{e^{-i\alpha L}}{\alpha K_+(\alpha)} \qquad M_\pm(\alpha) = \mp\frac{1}{2\pi i}\int_{-\infty\mp i\sigma}^{\infty\mp i\sigma}\frac{e^{-i\varsigma L}d\varsigma}{\varsigma K_+(\varsigma)(\varsigma - \alpha)}$$

Where on left- and right-hand sides of the equation we have functions which are analytic in the domains Π^+ and Π^- respectively. Due to Cauchy's Residue Theorem explicit expressions for the integrands $U_\pm(\alpha)$ and $M_\pm(\alpha)$ can be obtained as well as an additional third term in the equation. After dividing by $K_-(\alpha)$, the second equation becomes:

$$\frac{F_-(\alpha)}{K_-(\alpha)} - \frac{1}{\alpha K_-(\alpha)} + \frac{1}{\alpha K_-(0)} + V_-(\alpha) + N_-(\alpha) =$$

$$D_1(\alpha)K_+(\alpha) + \frac{1}{\alpha K_+(0)} - V_+(\alpha) - N_+(\alpha) \tag{IV.26}$$

$$V_+(\alpha) + V_-(\alpha) = \frac{F_+(\alpha)e^{i\alpha L}}{K_-(\alpha)} \qquad V_\pm(\alpha) = \pm\frac{1}{2\pi i}\int_{-\infty\mp i\sigma}^{\infty\mp i\sigma}\frac{e^{i\varsigma L}F_+(\varsigma)d\varsigma}{K_-(\varsigma)(\varsigma - \alpha)}$$

$$N_+(\alpha) + N_-(\alpha) = \frac{e^{i\alpha L}}{\alpha K_-(\alpha)} \qquad N_\pm(\alpha) = \pm\frac{1}{2\pi}\int_{-\infty\mp i\sigma}^{\infty\mp i\sigma}\frac{e^{i\varsigma L}d\varsigma}{\varsigma K_-(\varsigma)(\varsigma - \alpha)}$$

For the analytic continuation, we may define a function $f(\alpha)$ which is analytic over the entire complex plane. Liouville's theorem [3] states that as $|\alpha| \to \infty$ and $f(\alpha) = O\left(|\alpha|^k\right)$, then $f(\alpha)$ is a polynomial of degree $\leq k$. For the behaviour of the functions $F_\pm(\alpha)$ and $D_1(\alpha)$ as $|\alpha| \to \infty$, we refer to earlier investigations [4,5]. It was determined there that the

order of both functions $F_{\pm}(\alpha)$ and $D_1(\alpha)$ is never higher than $O\left(|\alpha|^{\lambda+3}\right)$ and $O\left(|\alpha|^{\lambda+1}\right)$, $\lambda < 1$ respectively, due to conditions of local boundedness of energy. At infinity, the function $K_{\pm}(\alpha)$ is of the order $O\left(|\alpha|^0\right)$ because $\prod\limits_{n=1}^{\infty}\left(1-\dfrac{\alpha}{\alpha_n}\right)e^{\frac{\alpha}{\alpha_n}} \to 1$ as $|\alpha| \to \infty$. As a result $f(\alpha)$ cannot grow faster than $\left(|\alpha|^{-1}\right)$ and the polynomial is zero if k is negative. Thus, from IV.25:

$$\frac{F_+(\alpha)}{K_+(\alpha)} + \frac{1}{\alpha K_+(\alpha)} - \frac{1}{\alpha K_+(0)} + U_+(\alpha) + M_+(\alpha) = 0 \tag{IV.27}$$

And analogously, from equation IV.26:

$$\frac{F_-(\alpha)}{K_-(\alpha)} - \frac{1}{\alpha K_-(\alpha)} + \frac{1}{\alpha K_-(0)} + V_-(\alpha) + N_-(\alpha) = 0 \tag{IV.28}$$

Or going over to expressions with Cauchy's integrals besides introducing a new function $\Psi_+(\alpha) = F_+(\alpha) + 1/\alpha$:

$$\frac{\Psi_+(\alpha)}{K_+(\alpha)} + \frac{1}{2\pi i}\int_{-\infty-i\sigma}^{\infty-i\sigma}\frac{e^{-i\varsigma L}\Psi_-(\varsigma)d\varsigma}{K_+(\varsigma)(\varsigma-\alpha)} = \frac{1}{\alpha K_+(0)} \tag{IV.29}$$

and with $\Psi_-(\alpha) = F_-(\alpha) - 1/\alpha$ for IV.28:

$$\frac{\psi_-(\alpha)}{K_-(\alpha)} - \frac{1}{2\pi i}\int_{-\infty+i\sigma}^{\infty+i\sigma}\frac{e^{i\varsigma L}\Psi_+(\varsigma)d\varsigma}{K_-(\varsigma)(\varsigma-\alpha)} = -\frac{1}{\alpha K_-(0)} \tag{IV.30}$$

$K_+(\alpha)$ has zeros at $-\alpha_j$ for $\{j \mid j = 1,2,...\}$ and in the origin and has poles at $-\gamma$ and $-\gamma_j$ for $\{j \mid j = 1,2,...\}$. The integrand has poles at $\varsigma = 0, \alpha$ and $\varsigma = -\alpha_j$ for $\{j \mid j = 1,2,...\}$

IV.4 Solution of the system; determination of w, k, c and m$_f$

We will evaluate the equations IV.29 and IV.30 by the theory of residues for the solution of the system. Therefore equation IV.29 transforms into:

$$\frac{\Psi_+(\alpha_j)}{\alpha_j^2 K_+(\alpha_j)} - \sum_{m=1}^{\infty}\frac{e^{i\alpha_m L}\Psi_-(-\alpha_m)}{\alpha_j^2 K'_+(-\alpha_m)(\alpha_m+\alpha_j)} = \frac{1}{\alpha_j^3 K_+(0)} \tag{IV.31}$$

after we divide left- and right-hand sides by α_j^2. For equation IV.30 this yields:

$$\frac{\Psi_-(\alpha_j)}{\alpha_j^2 K_-(\alpha_j)} - \sum_{m=1}^{\infty}\frac{e^{i\alpha_m L}\Psi_+(\alpha_m)}{\alpha_j^2 K'_-(\alpha_m)(\alpha_m-\alpha_j)} = -\frac{1}{\alpha_j^3 K_-(0)} \tag{IV.32}$$

We introduce new unknowns

$$\xi_j = \frac{\Psi_+(\alpha_j)}{\alpha_j^2 K_+(\alpha_j)}, \quad \eta_j = \frac{\Psi_-(-\alpha_j)}{\alpha_j^2 K_-(-\alpha_j)} \tag{IV.33}$$

For these unknowns, together with substitution of $\Psi_-\left(-\alpha_m\right) = \eta_m \alpha_m^2 K_-\left(-\alpha_m\right)$, $\Psi_+\left(\alpha_m\right) = \xi_m \alpha_m^2 K_+\left(\alpha_m\right)$, $\displaystyle\sum_{m=1}^{\infty} \eta_m = \eta_j$, $\displaystyle\sum_{m=1}^{\infty} \xi_m = \xi_j$ and per definition $K_-\left(-\alpha\right) = K_+\left(\alpha\right)$ and $\alpha_j = -\alpha_j$, we obtain the system:

$$\xi_j - \frac{\alpha_m^2 e^{i\alpha_m L} K_+\left(\alpha_m\right)}{\alpha_j^2 K'_-\left(\alpha_m\right)\left(\alpha_m + \alpha_j\right)} \eta_j = \frac{1}{\alpha_j^3 K_+\left(0\right)}$$

$$\eta_j - \frac{\alpha_m^2 e^{i\alpha_m L} K_+\left(\alpha_m\right)}{\alpha_j^2 K'_-\left(\alpha_m\right)\left(\alpha_m + \alpha_j\right)} \xi_j = \frac{1}{\alpha_j^3 K_-\left(0\right)}$$

(IV.34)

or in matrix form:

$$\begin{bmatrix} 1 & -c_{jm} \\ -c_{jm} & 1 \end{bmatrix} \begin{bmatrix} \xi_j \\ \eta_j \end{bmatrix} = \begin{bmatrix} f_j^1 \\ f_j^2 \end{bmatrix}$$

(IV.35)

Where:

$$c_{jm} = \frac{\alpha_m^2 e^{i\alpha_m L} K_+\left(\alpha_m\right)}{\alpha_j^2 K'_-\left(\alpha_m\right)\left(\alpha_m + \alpha_j\right)}$$

$$f_j^1 = \frac{1}{\alpha_j^3 K_+\left(0\right)} = f_j^2 = \frac{1}{\alpha_j^3 K_-\left(0\right)}$$

Via the left-hand side of equation IV.25 or IV.26 the formula for body deflection $w\left(x\right)$ can be derived. Choosing arbitrarily the first equation gives:

$$D_1\left(\alpha\right) K_-\left(\alpha\right) e^{-i\alpha L} - U_-\left(\alpha\right) - M_-\left(\alpha\right) - \frac{1}{\alpha K_+\left(0\right)} = 0$$

(IV.36)

After reconstruction, for $D_1\left(\alpha\right)$ we find:

$$D_1\left(\alpha\right) = \frac{e^{-i\alpha L}}{K_-\left(\alpha\right)} \left[-\frac{1}{2\pi i} \int_{-\infty+i\sigma}^{\infty+i\sigma} \frac{e^{-i\varsigma L} \Psi_-\left(\varsigma\right) d\varsigma}{K_+\left(\varsigma\right)\left(\varsigma - \alpha\right)} + \frac{1}{\alpha K_+\left(0\right)} \right]$$

(IV.37)

Using equation IV.14 and IV.18 ($D_1\left(\alpha\right) = D\left(\alpha\right)$) and the inverse Fourier transformation, we obtain:

$$\phi\left(x,y\right) = \frac{1}{2\pi} \int_{-\infty}^{\infty} \frac{e^{-i\alpha\left(x-L\right)} \cosh\left(\alpha\left(y+H\right)\right)}{\cosh\left(\alpha H\right) K_-\left(\alpha\right) K_1\left(\alpha\right)} \left[-\frac{1}{2\pi i} \int_{-\infty+i\sigma}^{\infty+i\sigma} \frac{e^{-i\varsigma L} \Psi_-\left(\varsigma\right) d\varsigma}{K_+\left(\varsigma\right)\left(\varsigma - \alpha\right)} + \frac{1}{\alpha K_+\left(0\right)} \right] d\alpha$$

(IV.38)

After differentiation with respect to y in $y = 0$, we write:

$$\frac{\partial \phi}{\partial y}\left(x,0\right) = \frac{1}{2\pi} \int_{-\infty}^{\infty} \frac{e^{-i\alpha\left(x-L\right)} \alpha \tanh\left(\alpha H\right)}{K_-\left(\alpha\right) K_1\left(\alpha\right)} \left[-\frac{1}{2\pi i} \int_{-\infty+i\sigma}^{\infty+i\sigma} \frac{e^{-i\varsigma L} \Psi_-\left(\varsigma\right) d\varsigma}{K_+\left(\varsigma\right)\left(\varsigma - \alpha\right)} + \frac{1}{\alpha K_+\left(0\right)} \right] d\alpha$$

(IV.39)

In the outer integral the integration path must be chosen that it lies completely within the intersection of the domains Π^+ and Π^- We choose the same paths as we did for K; on the real axis with cuts around $-\alpha_0$ and $-\gamma$ from below and around the points α_0 and γ

from above (figure IV.2). In the inner integral the integration path lies within the domain Π^-. With analytic continuation, we define this integral over the entire domain using the theory of residues:

$$\frac{1}{2\pi i}\int_{-\infty+i\sigma}^{\infty+i\sigma}\frac{e^{-i\varsigma L}\Psi_-(\varsigma)d\varsigma}{K_+(\varsigma)(\varsigma-\alpha)}=-\frac{e^{-i\alpha L}\Psi_-(\alpha)}{K_+(\alpha)}+\sum_{j=1}^{\infty}\frac{e^{i\alpha_j L}\Psi_-(-\alpha_j)}{K'_+(-\alpha_j)(\alpha_j+\alpha)}$$

(IV.40)

From IV.39 it follows that:

$$\frac{\partial\phi}{\partial y}(x,0)=\begin{aligned}&-i\sum_{j=1}^{\infty}\frac{e^{-i\alpha_j(x-L)}\alpha_j\tanh(\alpha_j H)K_+(\alpha_j)}{K'_2(\alpha_j)}\\&\left[\sum_{m=1}^{\infty}\frac{e^{i\alpha_m L}\Psi_-(\alpha_m)}{K'_+(-\alpha_m)(\alpha_m+\alpha_j)}+\frac{1}{\alpha_j K_+(0)}\right]-\\&i\sum_{j=1}^{\infty}\frac{e^{i\alpha_j x}\alpha_j\tanh(\alpha_j H)\Psi_-(-\alpha_j)}{K'_2(\alpha_j)}\end{aligned}$$

(IV.41)

The body deflection can be determined from $w(x)=i\dfrac{\partial\phi}{\partial y}(x,0)$. After substitution of IV.31 and $\Psi_-(-\alpha_j)=\eta_j\alpha_j^2 K_+(\alpha_j)$ into equation IV.41 we find for w :

$$w(x)=\sum_{j=1}^{\infty}\frac{\tanh(\alpha_j H)}{K'_2(\alpha_j)}\left[\alpha_j^3 K_+(\alpha_j)\left(e^{-i\alpha_j(x-L)}\xi_j+e^{i\alpha_j x}\eta_j\right)\right]$$

(IV.42)

The values of ξ_j and η_j comprehend the complex amplitudes of waves travelling from the right edges of the plate to the right and from the left edge to the left respectively. The deflection amplitude at the interface of strip and fluid appears to be variable, as a consequence of omitting the material properties (see section IV.1). With allowance for generalization, we may define the average value

$$\overline{w}(x)=\frac{1}{L}\int_0^L w(x)dx=\frac{i}{L}\sum_{j=1}^{\infty}\frac{\tanh(\alpha_j H)}{K'_2(\alpha_j)}\left[\alpha_j^2 K_+(\alpha_j)\left(1-e^{i\alpha_j L}\right)(\xi_j+\eta_j)\right]$$

(IV.43)

For the realization of distributed stiffness and damping parameters we introduce Kappa as $K(\omega)=q_0\big/\big(\overline{w}(x)L_0\big)$ when $w(x)$ is expressed in metric dimensions (Section IV.1). Per definition we note for the parameters

$$\begin{aligned}k_d(\omega)&=\mathrm{Re}\big[K(\omega)\big]\\c_d(\omega)&=\mathrm{Im}\big[K(\omega)\big]/i\omega\end{aligned}$$

(IV.44)

Where Re and Im concerns the real and imaginary part of Kappa, respectively.
From equation IV.38, exactly the same steps can be taken to express also $\phi(x,0)$ in residual coordinates. The term will be used to determine the following variable:

$$\alpha_{am}(x)=\varphi(x,0)\bigg/\frac{\partial w}{\partial t}(x,0)=\phi(x,0)\bigg/\frac{\partial\phi}{\partial y}(x,0)$$

(IV.45)

that will be accepted as a measure for added mass as a consequence of the vertical motion. The variable α_{am} represents an estimation of the influence depth of the body on the x domain. When the frequency is high, this estimation is most secure. Elaboration of equation IV.45 lead to the simple formula:

$$\alpha_{am} = 1 / \left(\alpha_j \tanh \left(\alpha_j H \right) \right) \qquad \text{(IV.46)}$$

revealing that this variable is constant over the x domain. It is sufficient now to multiply α_{am} with the fluid density and the body length in order to obtain the added mass (per metre width):

$$m_f \left(\omega \right) = \rho L_0 \alpha_{am} \left(\omega \right) \qquad \text{(IV.47)}$$

Where $\alpha_{am} \left(\omega \right)$ is expressed in metric dimensions.

IV.5 Additional to VI.4: Computational algorithm for complex amplitudes

The matrix in equation IV.35 is (almost) singular what means that we cannot directly apply the (general) matrix operation $\mathbf{Ax} = \mathbf{b} \rightarrow \mathbf{x} = \left(\mathbf{A} \right)^{-1} \mathbf{b}$ to the problem. In fact, there are infinitely many solutions for $\mathbf{x}$ instead of one unique because of the existence of singularities[1]. In the field of linear algebra, there is a special tool available to deal with singularities: Singular Value Decomposition[2] (SVD). SVD is an important factorization with applications for signal processing or statistics which can be used for constructing an approximated (complex) matrix for $\mathbf{A}$, for example. For $\mathbf{A}$ there exist in the field $\Re$ a factorization of the form:

$$\mathbf{A} = \mathbf{USV}^{*} \qquad \text{(IV.45)}$$

Where:

$\mathbf{U}$:   unitary matrix over $\Re$

$\mathbf{S}$:   diagonal matrix with non-negative numbers on the diagonal

$\mathbf{V}^{*}$:   conjugate transpose of $\mathbf{V}$. $\mathbf{V}^{*}$ is a unitary matrix over $\Re$

The columns of $\mathbf{V}$ form a set of orthonormal 'input' or 'analysing' basis vector directions of $\mathbf{A}$. (these are the eigenvalues of $\mathbf{A}^{*}\mathbf{A}$) The columns of $\mathbf{U}$ form a set of orthonormal 'output' basis vector directions for $\mathbf{A}$. (these are the eigenvalues of $\mathbf{AA}^{*}$) The diagonal values in matrix $\mathbf{S}$ are the singular values, which can be thought of as scalar 'gain controls' by which each corresponding input is multiplied to give a corresponding output. (these are the square roots of the eigenvalues of $\mathbf{AA}^{*}$ and $\mathbf{A}^{*}\mathbf{A}$ that correspond with the same columns in $\mathbf{U}$ and $\mathbf{V}$. We aim at minimizing diagonal matrix $\mathbf{S}$ into $\tilde{\mathbf{S}}$ with specific rank r so that $\mathbf{A}$ transforms into $\tilde{\mathbf{A}}$ as:

$$\tilde{\mathbf{A}} = \mathbf{U}\tilde{\mathbf{S}}\mathbf{V}^{*} \qquad \text{(IV.46)}$$

---

[1] singularities are poles in calculus and complex analysis, but in the field of linear algebra, they are only definable.
[2] see Matlab manual or wikipedia website.

TUDelft

where $\tilde{\boldsymbol{S}}$ contains only the r largest singular values (the other singular values are replaced by zero). Generally, the criterion for r can only be estimated by signal processing or statistics, however, under favourable conditions it is allowed to simply reduce the number of r. In our case, all entries in $\boldsymbol{S}$ are infinitesimally small, except for the first one. In other words: $\boldsymbol{S}$ is almost a rank one matrix, thus $r = 1$. The reduced version of the SVD is called the truncated SVD and denotes:

$$\tilde{\boldsymbol{A}} = \boldsymbol{U}_t \tilde{\boldsymbol{S}}_t \boldsymbol{V}_t^* \tag{IV.47}$$

Only the t column vectors of $\boldsymbol{U}$ and t row vectors of $\boldsymbol{V}^*$ corresponding to the t largest singular values $\boldsymbol{S}$ are calculated, with $t = 1$. It is obvious now that the truncated SVD is no longer an exact decomposition of the original matrix $\boldsymbol{A}$, but as discussed here, is in a very useful sense the closest approximation to $\boldsymbol{A}$ that can be achieved. In addition to section IV.4, the algorithm for matrix IV.35 slightly changes:

$$\boldsymbol{A}\boldsymbol{x} = \boldsymbol{b} \rightarrow \boldsymbol{U}\boldsymbol{S}\boldsymbol{V}^*\boldsymbol{x} = \boldsymbol{b} \rightarrow \boldsymbol{U}_t \tilde{\boldsymbol{S}}_t \boldsymbol{V}_t^*\boldsymbol{x} \approx \boldsymbol{b} \rightarrow \boldsymbol{x} \approx \left(\boldsymbol{V}_t^*\right)^{-1}\left(\left(\tilde{\boldsymbol{S}}_t\right)^{-1}\left(\left(\boldsymbol{U}_t\right)^{-1}\boldsymbol{b}\right)\right) \tag{IV.48}$$

Matlab codes concerning the application of the SVD are listed in Appendix V.4.

IV.6 Short wave approximation. Resonance amplification

We will consider an uniform approximation to get around the difficulty of singular matrix computation. If the plate length is significantly smaller then the wavelength, then $L \gg 1$. In the matrix the column corresponding to α_0 is significantly larger than all other columns. We may therefore consider a short wave approximation by setting the other elements to zero. This means that the potential (IV.38) close to the strip will be carried out only by one real mode while the other modes will be neglected since they damp out much faster. The system in equation IV.35 can clearly be inverted. As a result, we obtain the following explicit representations: c_{jm} reduces to:

$$c_{00} = \frac{e^{i\alpha_0 L}K_+\left(\alpha_0\right)}{2\alpha_0 K'_-\left(\alpha_0\right)} \tag{IV.49}$$

From the system in IV.34 we derive:

$$\begin{aligned} \xi_m &= c_{m0}\eta_0 + f_m^1 \\ \eta_m &= c_{m0}\xi_0 + f_m^2 \end{aligned} \tag{IV.50}$$

Where:

$$c_{m0} = \frac{\alpha_0^2 e^{i\alpha_0 L}K_+\left(\alpha_0\right)}{\alpha_m^2 K'_-\left(\alpha_0\right)\left(\alpha_0 + \alpha_m\right)}$$

$$\xi_0 = \frac{f_0^1 + cf_0^2}{1 - c_{00}^2} = \eta_0 = \frac{f_0^2 + cf_0^1}{1 - c_{00}^2} = \frac{(1 + c_{00})f_0}{1 - c_{00}^2}, f_0 = f_0^{1,2} = \frac{1}{\alpha_0^3 K_\pm(0)}$$

$$f_m^{1,2} = f_m = \frac{1}{\alpha_m^3 K_\pm(0)}$$

and elaboration of IV.50 gives:

$$\xi_m = \eta_m = \frac{\alpha_0\left(1 - c_{00}^2\right) + \alpha_m\left(1 + 2c_{00}\right)}{\alpha_m^3 K_\pm(0)\left(\alpha_0 + \alpha_m\right)\left(1 - c_{00}^2\right)}$$

(IV.51)

which replaces the exact complex amplitudes in equation IV.42:

$$w_{sw}(x) = \sum_{j=1}^{N_m} \frac{\tanh\left(\alpha_j H\right)}{K'_2\left(\alpha_j\right)}\left[\frac{\left(\alpha_0\left(1 - c_{00}^2\right) + \alpha_m\left(1 + 2c_{00}\right)\right)K_+\left(\alpha_j\right)}{\left(\alpha_0 + \alpha_m\right)K_\pm(0)\left(1 - c_{00}^2\right)}\left(e^{-i\alpha_j(x-L)} + e^{i\alpha_j x}\right)\right]$$

(IV.52)

when N_m represent the number of modes taken into account. From the function IV.50 and IV.52 we expect an increase in the deflection amplitude under the action of the external load. As a result of this, we may expect resonant amplitudes to occur and therefore we need to evaluate the conditions under which these amplitudes will be exhibited. This can be done by consideration of the nature of the (surface) waves, i.e. by incoming, reflecting or transmitting waves. At the left edge of the strip, the diffracted potential is a reflected wave of the form:

$$\phi(x,0) = Re^{-i\gamma x}$$

(IV.53)

and at the right edge the potential is represented by a transmitted wave of the form:

$$\phi(x,0) = Te^{i\gamma x}$$

(IV.54)

The reflected wave at the left edge of the strip compensates the incoming wave and also beneath the strip reflected and transmitted waves propagate because of the physical edges, as shown in figure IV.3.
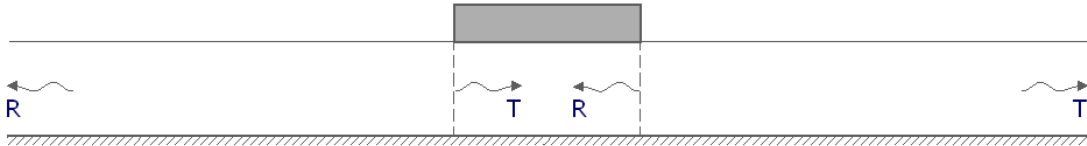
Figure IV.3   waves (potentials) in the x-domain

The main part of the plate deflection is a superposition of two waves of the same length: transmitted into the fluid beneath the strip and reflected from the other edge. If these wave are in phase, then the deflection amplitude is doubled. Zero reflection correspond to total transmission correspond to maximum deflections beneath the strip. The complex amplitude R can be determined by evaluating the residue at the point $\alpha = \gamma$ in expression IV.38 as follows:

$$R = \begin{array}{c} \dfrac{ie^{i\gamma L}}{K_-(\gamma)K'_1(\gamma)}\left[-\dfrac{1}{2\pi i}\int\limits_{-\infty+i\sigma}^{\infty+i\sigma}\dfrac{e^{-i\varsigma L}\Psi_-(\varsigma)d\varsigma}{K_+(\varsigma)(\varsigma-\gamma)}+\dfrac{1}{\gamma K_+(0)}\right]= \\[3mm] \dfrac{i}{K_+(\gamma)K'_1(\gamma)}\left[\dfrac{1}{2\pi i}\int\limits_{-\infty-i\sigma}^{\infty-i\sigma}\dfrac{e^{i\varsigma L}\Psi_+(\varsigma)d\varsigma}{K_-(\varsigma)(\varsigma-\gamma)}-\dfrac{1}{\gamma K_-(0)}\right]= \\[3mm] \dfrac{i}{K_+(\gamma)K'_1(\gamma)}\left[\sum\limits_{j=1}^{\infty}\dfrac{e^{i\alpha_j L}\Psi_+(\alpha_j)}{K'_-(\alpha_j)(\alpha_j-\gamma)}-\dfrac{1}{\gamma K_-(0)}\right]= \\[3mm] \dfrac{i}{K_+(\gamma)K'_1(\gamma)}\left[\sum\limits_{j=1}^{\infty}\dfrac{\alpha_j^2 e^{i\alpha_j L}K_+^2(\alpha_j)}{K'(\alpha_j)(\alpha_j-\gamma)}\xi_j-\dfrac{1}{\gamma K_-(0)}\right] \end{array} \qquad \text{(IV.55)}$$

Evaluating the residue at the point $\alpha=-\gamma$, the complex transmission amplitude T reads:

$$T = \begin{array}{c} \dfrac{-ie^{-i\gamma L}}{K_-(-\gamma)K'_1(-\gamma)}\left[\dfrac{1}{2\pi i}\int\limits_{-\infty+i\sigma}^{\infty+i\sigma}\dfrac{e^{-i\varsigma L}\Psi_-(\varsigma)d\varsigma}{K_+(\varsigma)(\varsigma+\gamma)}+\dfrac{1}{\gamma K_+(0)}\right]= \\[3mm] \dfrac{-ie^{-i\gamma L}}{K_+(\gamma)K'_1(\gamma)}\left[-\sum\limits_{j=1}^{\infty}\dfrac{e^{i\alpha_j L}\Psi_-(-\alpha_j)}{K'_+(-\alpha_j)(-\alpha_j+\gamma)}+\dfrac{1}{\gamma K_+(0)}\right]= \\[3mm] \dfrac{-ie^{-i\gamma L}}{K_+(\gamma)K'_1(\gamma)}\left[\sum\limits_{j=1}^{\infty}\dfrac{\alpha_j^2 e^{i\alpha_j L}K_+^2(\alpha_j)}{K'(\alpha_j)(\alpha_j-\gamma)}\eta_j-\dfrac{1}{\gamma K_+(0)}\right] \end{array} \qquad \text{(IV.56)}$$

where for the computation the symbol ∞ will be replaced by N_m and the complex amplitudes ξ and η attributes to equation IV.52. With allowance for normalisation, we transform reflection and transmission amplitudes into ditto coefficients by obtaining normalized values for R and T:

$$R_{norm}=|R|/(|R|+|T|)$$
$$T_{norm}=|T|/(|R|+|T|) \qquad \text{(IV.57)}$$

Where:

$|R|$:   absolute value of R

$|T|$:   absolute value of T

For normalized reflection and transmitted wave coefficients the following equality follows from equation IV.57:

$$R_{norm}+T_{norm}=1 \qquad \text{(IV.58)}$$

Resonant amplification corresponds to zero reflection and therefore it is sufficient to evaluate $|R|=0$ in order to satisfy this section's objectives. Under 'short wave conditions' and to retain only the one oscillation wave in the expression for $|R|$ we are able to rewrite expression VI.5 as follows:

$$R = \begin{array}{c} \dfrac{i}{K_+(\gamma)K'_1(\gamma)}\left[\dfrac{\alpha_0^2 e^{i\alpha_0 L}K_+^2(\alpha_0)}{K'(\alpha_0)(\alpha_0-\gamma)}\xi_0-\dfrac{1}{\gamma K_-(0)}\right]= \\[3mm] \dfrac{i}{K_+(\gamma)K'_1(\gamma)K_\pm(0)}\left[\dfrac{2c_{00}(1+c_{00})}{(\alpha_0-\gamma)(1+c_{00}^2)}-\dfrac{1}{\gamma}\right] \end{array} \qquad \text{(IV.59)}$$

where R is evaluated in residue α_0 as an expression of c_{00}. Both real and imaginary part in the bracketed term of this expression must be zero for $|R| = 0$ what leaves c_{00} to be equal to:

$$\frac{\alpha_0 - \gamma}{\alpha_0 + \gamma} \tag{IV.60}$$
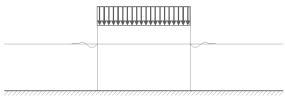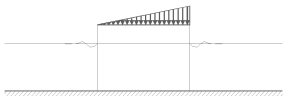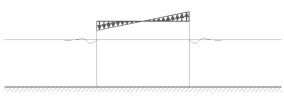
Since α_0 and γ are real values, we may say that $\text{Im}\big[c_{00}\big] = 0$. Substituting $\text{Im}\big[c_{00}\big] = 0$ in expression IV.49 for c_{00} result in the next equality:

$$Arg\big[K_+^2(\alpha_0)\big] + \alpha_0 L = \pi k \quad k = 1, 2, .. \tag{IV.61}$$

what must be true for resonant amplification. Note that this expression is nothing more than a useful tool and not the exact solution to the problem.

IV.7 Wave diffraction with different acting loads

In the multibody system, besides the vertical motion also rotational motion will be performed by the acting load. Rotational motion can be simulated by simply reshaping the time periodic load into a prismatic form. Consequently, vibrating amplitudes can be evaluated in a manner analogously to the ones attributed to the vertical motion. We summarize relevant outcomes in table IV.1:

Eq.			
IV.5	$q(t) = q_0 e^{i\omega t}$	$q(x,t) = q_0 (x/L_0) e^{i\omega t}$	$q(x,t) = q_0 (x/L_0 - 1/2) e^{i\omega t}$
IV.11	$(1-d)\dfrac{\partial \phi}{\partial y} - \phi = i$	$(1-d)\dfrac{\partial \phi}{\partial y} - \phi = \dfrac{ix}{L_0}$	$(1-d)\dfrac{\partial \phi}{\partial y} - \phi = i\left(\dfrac{x}{L_0} - \dfrac{1}{2}\right)$
IV.20	$F_1(\alpha) = (1/\alpha)(e^{i\alpha L} - 1)$	$F_1(\alpha) = (1/\alpha)$ $\big((i/\alpha L + 1)e^{i\alpha L} - i/\alpha L\big)$	$F_1(\alpha) = (1/\alpha)$ $\big((i/\alpha L + 1/2)e^{i\alpha L} - i/\alpha L + 1/2\big)$

TUDelft

Eq.			
IV.25	$\dfrac{F_+(\alpha)}{K_+(\alpha)} + \dfrac{1}{\alpha K_+(\alpha)} - \dfrac{1}{\alpha K_+(0)} +$ $U_+(\alpha) + M_+(\alpha) = D_1(\alpha)K_-(\alpha)e^{-i\alpha L}$ $-\dfrac{1}{\alpha K_-(0)} - U_-(\alpha) - M_-(\alpha)$ $U_+(\alpha)+U_-(\alpha) = \dfrac{F_-(\alpha)e^{-i\alpha L}}{K_+(\alpha)}$ $U_\pm(\alpha) = \pm\dfrac{1}{2\pi i}\displaystyle\int_{-\infty\mp i\sigma}^{\infty\mp i\sigma}\dfrac{e^{-i\varsigma L}F_-(\varsigma)d\varsigma}{K_+(\varsigma)(\varsigma-\alpha)}$ $M_+(\alpha)+M_-(\alpha) = -\dfrac{e^{-i\alpha L}}{\alpha K_+(\alpha)}$ $M_\pm(\alpha) = \mp\dfrac{1}{2\pi i}\displaystyle\int_{-\infty\mp i\sigma}^{\infty\mp i\sigma}\dfrac{e^{-i\varsigma L}d\varsigma}{\varsigma K_+(\varsigma)(\varsigma-\alpha)}$	$\dfrac{F_+(\alpha)}{K_+(\alpha)} + \dfrac{1}{\alpha K_+(\alpha)} + \dfrac{i}{\alpha^2 L K_+(\alpha)} -$ $\dfrac{1}{\alpha K_+(0)} - \dfrac{i}{\alpha^2 L K_+(0)} + U_+(\alpha) +$ $J_+(\alpha) = D_1(\alpha)K_-(\alpha)e^{-i\alpha L}$ $-\dfrac{1}{\alpha K_-(0)} - \dfrac{i}{\alpha^2 L K_-(0)} - U_-(\alpha) -$ $J_-(\alpha)$ $U_+(\alpha)+U_-(\alpha) = \dfrac{F_-(\alpha)e^{-i\alpha L}}{K_+(\alpha)}$ $U_\pm(\alpha) = \pm\dfrac{1}{2\pi i}\displaystyle\int_{-\infty\mp i\sigma}^{\infty\mp i\sigma}\dfrac{e^{-i\varsigma L}F_-(\varsigma)d\varsigma}{K_+(\varsigma)(\varsigma-\alpha)}$ $J_+(\alpha)+J_-(\alpha) = -\dfrac{ie^{-i\alpha L}}{\alpha^2 L K_+(\alpha)}$ $J_\pm(\alpha) = \mp\dfrac{1}{2\pi L}\displaystyle\int_{-\infty\mp i\sigma}^{\infty\mp i\sigma}\dfrac{e^{-i\varsigma L}d\varsigma}{\varsigma K_+(\varsigma)(\varsigma-\alpha)}$	$\dfrac{F_+(\alpha)}{K_+(\alpha)} + \dfrac{1}{2\alpha K_+(\alpha)} + \dfrac{i}{\alpha^2 L K_+(\alpha)} -$ $\dfrac{1}{2\alpha K_+(0)} - \dfrac{i}{\alpha^2 L K_+(0)} + U_+(\alpha) +$ $M_+(\alpha) + J_+(\alpha) = D_1(\alpha)K_-(\alpha)e^{-i\alpha L}$ $-\dfrac{1}{2\alpha K_-(0)} - \dfrac{i}{\alpha^2 L K_-(0)} - U_-(\alpha) -$ $M_-(\alpha) - J_-(\alpha)$ $U_+(\alpha)+U_-(\alpha) = \dfrac{F_-(\alpha)e^{-i\alpha L}}{K_+(\alpha)}$ $U_\pm(\alpha) = \pm\dfrac{1}{2\pi i}\displaystyle\int_{-\infty\mp i\sigma}^{\infty\mp i\sigma}\dfrac{e^{-i\varsigma L}F_-(\varsigma)d\varsigma}{K_+(\varsigma)(\varsigma-\alpha)}$ $M_+(\alpha)+M_-(\alpha) = -\dfrac{e^{-i\alpha L}}{2\alpha K_+(\alpha)}$ $M_\pm(\alpha) = \mp\dfrac{1}{4\pi i}\displaystyle\int_{-\infty\mp i\sigma}^{\infty\mp i\sigma}\dfrac{e^{-i\varsigma L}d\varsigma}{\varsigma^2 K_+(\varsigma)(\varsigma-\alpha)}$ $J_+(\alpha)+J_-(\alpha) = -\dfrac{ie^{-i\alpha L}}{\alpha^2 L K_+(\alpha)}$ $J_\pm(\alpha) = \mp\dfrac{1}{2\pi L}\displaystyle\int_{-\infty\mp i\sigma}^{\infty\mp i\sigma}\dfrac{e^{-i\varsigma L}d\varsigma}{\varsigma K_+(\varsigma)(\varsigma-\alpha)}$
IV.26	$\dfrac{F_-(\alpha)}{K_-(\alpha)} - \dfrac{1}{\alpha K_-(\alpha)} + \dfrac{1}{\alpha K_-(0)} +$ $V_-(\alpha) + N_-(\alpha) = D_1(\alpha)K_+(\alpha) +$ $\dfrac{1}{\alpha K_+(0)} - V_+(\alpha) - N_+(\alpha)$ $V_+(\alpha)+V_-(\alpha) = \dfrac{F_+(\alpha)e^{i\alpha L}}{K_-(\alpha)}$ $V_\pm(\alpha) = \pm\dfrac{1}{2\pi i}\displaystyle\int_{-\infty\mp i\sigma}^{\infty\mp i\sigma}\dfrac{e^{i\varsigma L}F_+(\varsigma)d\varsigma}{K_-(\varsigma)(\varsigma-\alpha)}$ $N_+(\alpha)+N_-(\alpha) = \dfrac{e^{i\alpha L}}{\alpha K_-(\alpha)}$ $N_\pm(\alpha) = \pm\dfrac{1}{2\pi}\displaystyle\int_{-\infty\mp i\sigma}^{\infty\mp i\sigma}\dfrac{e^{i\varsigma L}d\varsigma}{\varsigma K_-(\varsigma)(\varsigma-\alpha)}$	$\dfrac{F_-(\alpha)}{K_-(\alpha)} - \dfrac{i}{\alpha^2 L K_-(\alpha)} + \dfrac{i}{\alpha^2 L K_-(0)} +$ $V_-(\alpha) + N_-(\alpha) + O_-(\alpha) =$ $D_1(\alpha)K_+(\alpha) + \dfrac{i}{\alpha^2 L K_+(0)} -$ $V_+(\alpha) - N_+(\alpha) - O_+(\alpha)$ $V_+(\alpha)+V_-(\alpha) = \dfrac{F_+(\alpha)e^{i\alpha L}}{K_-(\alpha)}$ $V_\pm(\alpha) = \pm\dfrac{1}{2\pi i}\displaystyle\int_{-\infty\mp i\sigma}^{\infty\mp i\sigma}\dfrac{e^{i\varsigma L}F_+(\varsigma)d\varsigma}{K_-(\varsigma)(\varsigma-\alpha)}$ $N_+(\alpha)+N_-(\alpha) = \dfrac{e^{i\alpha L}}{\alpha K_-(\alpha)}$ $N_\pm(\alpha) = \pm\dfrac{1}{2\pi}\displaystyle\int_{-\infty\mp i\sigma}^{\infty\mp i\sigma}\dfrac{e^{i\varsigma L}d\varsigma}{\varsigma K_-(\varsigma)(\varsigma-\alpha)}$ $O_+(\alpha)+O_-(\alpha) = \dfrac{ie^{i\alpha L}}{\alpha^2 L K_-(\alpha)}$ $O_\pm(\alpha) = \pm\dfrac{1}{2\pi L}\displaystyle\int_{-\infty\mp i\sigma}^{\infty\mp i\sigma}\dfrac{e^{i\varsigma L}d\varsigma}{\varsigma^2 K_-(\varsigma)(\varsigma-\alpha)}$	$\dfrac{F_-(\alpha)}{K_-(\alpha)} + \dfrac{1}{2\alpha K_-(\alpha)} - \dfrac{i}{\alpha^2 L K_-(\alpha)} -$ $\dfrac{1}{2\alpha K_-(0)} + \dfrac{i}{\alpha^2 L K_-(0)} + V_-(\alpha)$ $N_-(\alpha) + O_-(\alpha) = D_1(\alpha)K_+(\alpha) -$ $\dfrac{1}{2\alpha K_+(0)} + \dfrac{i}{\alpha^2 L K_+(0)} - V_+(\alpha)$ $-N_+(\alpha) - O_+(\alpha)$ $V_+(\alpha)+V_-(\alpha) = \dfrac{F_+(\alpha)e^{i\alpha L}}{K_-(\alpha)}$ $V_\pm(\alpha) = \pm\dfrac{1}{2\pi i}\displaystyle\int_{-\infty\mp i\sigma}^{\infty\mp i\sigma}\dfrac{e^{i\varsigma L}F_+(\varsigma)d\varsigma}{K_-(\varsigma)(\varsigma-\alpha)}$ $N_+(\alpha)+N_-(\alpha) = \dfrac{e^{i\alpha L}}{2\alpha K_-(\alpha)}$ $N_\pm(\alpha) = \pm\dfrac{1}{4\pi}\displaystyle\int_{-\infty\mp i\sigma}^{\infty\mp i\sigma}\dfrac{e^{i\varsigma L}d\varsigma}{\varsigma K_-(\varsigma)(\varsigma-\alpha)}$ $O_+(\alpha)+O_-(\alpha) = \dfrac{ie^{i\alpha L}}{\alpha^2 L K_-(\alpha)}$ $O_\pm(\alpha) = \pm\dfrac{1}{2\pi L}\displaystyle\int_{-\infty\mp i\sigma}^{\infty\mp i\sigma}\dfrac{e^{i\varsigma L}d\varsigma}{\varsigma^2 K_-(\varsigma)(\varsigma-\alpha)}$
IV.27	$\dfrac{F_+(\alpha)}{K_+(\alpha)} + \dfrac{1}{\alpha K_+(\alpha)} - \dfrac{1}{\alpha K_+(0)} +$ $U_+(\alpha) + M_+(\alpha) = 0$	$\dfrac{F_+(\alpha)}{K_+(\alpha)} + \dfrac{1}{\alpha K_+(\alpha)} + \dfrac{i}{\alpha^2 L K_+(\alpha)} -$ $\dfrac{1}{\alpha K_+(0)} - \dfrac{i}{\alpha^2 L K_+(0)} + U_+(\alpha) +$ $J_+(\alpha) = 0$	$\dfrac{F_+(\alpha)}{K_+(\alpha)} + \dfrac{1}{2\alpha K_+(\alpha)} + \dfrac{i}{\alpha^2 L K_+(\alpha)} -$ $\dfrac{1}{2\alpha K_+(0)} - \dfrac{i}{\alpha^2 L K_+(0)} + U_+(\alpha) +$ $M_+(\alpha) + J_+(\alpha) = 0$
IV.28	$\dfrac{F_-(\alpha)}{K_-(\alpha)} - \dfrac{1}{\alpha K_-(\alpha)} + \dfrac{1}{\alpha K_-(0)} +$ $V_-(\alpha) + N_-(\alpha) = 0$	$\dfrac{F_-(\alpha)}{K_-(\alpha)} - \dfrac{i}{\alpha^2 L K_-(\alpha)} + \dfrac{i}{\alpha^2 L K_-(0)} +$ $V_-(\alpha) + N_-(\alpha) + O_-(\alpha) = 0$	$\dfrac{F_-(\alpha)}{K_-(\alpha)} + \dfrac{1}{2\alpha K_-(\alpha)} - \dfrac{i}{\alpha^2 L K_-(\alpha)} -$ $\dfrac{1}{2\alpha K_-(0)} + \dfrac{i}{\alpha^2 L K_-(0)} + V_-(\alpha)$ $N_-(\alpha) + O_-(\alpha) = 0$

Eq.

IV.29

$$\frac{\Psi_+(\alpha)}{K_+(\alpha)}+\frac{1}{2\pi i}\int_{-\infty-i\sigma}^{\infty-i\sigma}\frac{e^{-i\varsigma L}\Psi_-(\varsigma)d\varsigma}{K_+(\varsigma)(\varsigma-\alpha)}=\frac{1}{\alpha K_+(0)}$$

$$\frac{\Psi_+(\alpha)}{K_+(\alpha)}+\frac{1}{2\pi i}\int_{-\infty-i\sigma}^{\infty-i\sigma}\frac{e^{-i\varsigma L}\Psi_-(\varsigma)d\varsigma}{K_+(\varsigma)(\varsigma-\alpha)}=\frac{1}{\alpha K_+(0)}\left(\frac{i}{\alpha L}+1\right)$$

$$\Psi_+(\alpha)=F_+(\alpha)+\frac{1}{\alpha}+\frac{i}{\alpha^2 L}$$

$$\frac{\Psi_+(\alpha)}{K_+(\alpha)}+\frac{1}{2\pi i}\int_{-\infty-i\sigma}^{\infty-i\sigma}\frac{e^{-i\varsigma L}\Psi_-(\varsigma)d\varsigma}{K_+(\varsigma)(\varsigma-\alpha)}=\frac{1}{\alpha K_+(0)}\left(\frac{i}{\alpha L}+\frac{1}{2}\right)$$

$$\Psi_+(\alpha)=F_+(\alpha)+\frac{1}{2\alpha}+\frac{i}{\alpha^2 L}$$

IV.30

$$\frac{\Psi_-(\alpha)}{K_-(\alpha)}-\frac{1}{2\pi i}\int_{-\infty+i\sigma}^{\infty+i\sigma}\frac{e^{i\varsigma L}\Psi_+(\varsigma)d\varsigma}{K_-(\varsigma)(\varsigma-\alpha)}=-\frac{1}{\alpha K_-(0)}$$

$$\frac{\Psi_-(\alpha)}{K_-(\alpha)}-\frac{1}{2\pi i}\int_{-\infty+i\sigma}^{\infty+i\sigma}\frac{e^{i\varsigma L}\Psi_+(\varsigma)d\varsigma}{K_-(\varsigma)(\varsigma-\alpha)}=-\frac{i}{\alpha^2 L K_-(0)}$$

$$\Psi_-(\alpha)=F_-(\alpha)-\frac{i}{\alpha^2 L}$$

$$\frac{\Psi_-(\alpha)}{K_-(\alpha)}-\frac{1}{2\pi i}\int_{-\infty+i\sigma}^{\infty+i\sigma}\frac{e^{i\varsigma L}\Psi_+(\varsigma)d\varsigma}{K_-(\varsigma)(\varsigma-\alpha)}=-\frac{1}{\alpha K_-(0)}\left(\frac{i}{\alpha L}-\frac{1}{2}\right)$$

$$\Psi_-(\alpha)=F_-(\alpha)+\frac{1}{2\alpha}-\frac{i}{\alpha^2 L}$$

IV.31

$$\frac{\Psi_+(\alpha_j)}{\alpha_j^2 K_+(\alpha_j)}-\sum_{m=1}^{\infty}\frac{e^{i\alpha_m L}\Psi_-(-\alpha_m)}{\alpha_j^2 K'_+(-\alpha_m)(\alpha_m+\alpha_j)}=\frac{1}{\alpha_j^3 K_+(0)}$$

$$\frac{\Psi_+(\alpha_j)}{\alpha_j^2 K_+(\alpha_j)}-\sum_{m=1}^{\infty}\frac{e^{i\alpha_m L}\Psi_-(-\alpha_m)}{\alpha_j^2 K'_+(-\alpha_m)(\alpha_m+\alpha_j)}=\frac{1}{\alpha_j^3 K_+(0)}\left(\frac{i}{\alpha_j L}+1\right)$$

$$\frac{\Psi_+(\alpha_j)}{\alpha_j^2 K_+(\alpha_j)}-\sum_{m=1}^{\infty}\frac{e^{i\alpha_m L}\Psi_-(-\alpha_m)}{\alpha_j^2 K'_+(-\alpha_m)(\alpha_m+\alpha_j)}=\frac{1}{\alpha_j^3 K_+(0)}\left(\frac{i}{\alpha_j L}+\frac{1}{2}\right)$$

IV.32

$$\frac{\Psi_-(\alpha_j)}{\alpha_j^2 K_-(\alpha_j)}-\sum_{m=1}^{\infty}\frac{e^{i\alpha_m L}\Psi_+(\alpha_m)}{\alpha_j^2 K'_-(\alpha_m)(\alpha_m-\alpha_j)}=-\frac{1}{\alpha_j^3 K_-(0)}$$

$$\frac{\Psi_-(\alpha_j)}{\alpha_j^2 K_-(\alpha_j)}-\sum_{m=1}^{\infty}\frac{e^{i\alpha_m L}\Psi_+(\alpha_m)}{\alpha_j^2 K'_-(\alpha_m)(\alpha_m-\alpha_j)}=-\frac{i}{\alpha^4 L K_-(0)}$$

$$\frac{\Psi_-(\alpha_j)}{\alpha_j^2 K_-(\alpha_j)}-\sum_{m=1}^{\infty}\frac{e^{i\alpha_m L}\Psi_+(\alpha_m)}{\alpha_j^2 K'_-(\alpha_m)(\alpha_m-\alpha_j)}=\frac{1}{\alpha_j^3 K_-(0)}\left(\frac{i}{\alpha_j L}-\frac{1}{2}\right)$$

IV.34

$$\xi_j-c_{jm}\eta_j=\frac{1}{\alpha_j^3 K_+(0)}$$
$$\eta_j-c_{jm}\xi_j=\frac{1}{\alpha_j^3 K_-(0)}$$

$$\xi_j-c_{jm}\eta_j=\frac{1}{\alpha_j^3 K_+(0)}\left(\frac{i}{\alpha_j L}+1\right)$$
$$\eta_j-c_{jm}\xi_j=-\frac{i}{\alpha^4 L K_-(0)}$$

$$\xi_j-c_{jm}\eta_j=\frac{1}{\alpha_j^3 K_+(0)}\left(\frac{i}{\alpha_j L}+\frac{1}{2}\right)$$
$$\eta_j-c_{jm}\xi_j=-\frac{1}{\alpha_j^3 K_-(0)}\left(\frac{i}{\alpha_j L}+\frac{1}{2}\right)$$

IV.35-
IV.43

Expressions for $w(x)$ remain unchanged, but c and k are determined by

$$\theta(x)=-\frac{\partial w(x)}{\partial x}=\sum_{j=1}^{\infty}\frac{\tanh(\alpha_j H)}{K'_2(\alpha_j)}\left[\alpha_j^4 K_+(\alpha_j)\left(-ie^{-i\alpha_j(x-L)}\xi_j+ie^{i\alpha_j x}\eta_j\right)\right],$$

$$\bar{\theta}(x)\approx\theta\left(\frac{L}{2}\right)=\sum_{j=1}^{\infty}\frac{\tanh(\alpha_j H)}{K'_2(\alpha_j)}\left[\alpha_j^4 K_+(\alpha_j)\left(ie^{i\alpha_j L/2}\left(-\xi_j+\eta_j\right)\right)\right],\ K(\omega)=M_0/\bar{\theta}(x),\ M_0=1/3\,q_0 L^2$$

IV.50

$$f_0=f_0^{1,2}=\frac{1}{\alpha_0^3 K_\pm(0)},$$
$$f_m^{1,2}=f_m=\frac{1}{\alpha_m^3 K_\pm(0)}$$

$$f_0^1=\frac{1}{\alpha_0^3 K_+(0)}\left(\frac{i}{\alpha_0 L}+1\right)$$
$$f_0^2=-\frac{1}{\alpha_0^4 L K_-(0)}$$
$$f_m^1=\frac{1}{\alpha_m^3 K_+(0)}\left(\frac{i}{\alpha_m L}+1\right)$$
$$f_m^2=-\frac{1}{\alpha_m^4 L K_-(0)}$$

$$f_0^1=\frac{1}{\alpha_0^3 K_+(0)}\left(\frac{i}{\alpha_0 L}+\frac{1}{2}\right)$$
$$f_0^2=-\frac{1}{\alpha_0^3 K_-(0)}\left(\frac{i}{\alpha_0 L}+\frac{1}{2}\right)$$
$$f_m^1=\frac{1}{\alpha_m^3 K_+(0)}\left(\frac{i}{\alpha_m L}+\frac{1}{2}\right)$$
$$f_m^2=-\frac{1}{\alpha_m^3 K_-(0)}\left(\frac{i}{\alpha_m L}+\frac{1}{2}\right)$$

IV.51

$$\xi_m=\eta_m=$$
$$\frac{2i\alpha_0\left(1-c^2\right)+\alpha_m\left(1+2c\right)}{\alpha_m^3 K_\pm(0)\left(\alpha_0+\alpha_m\right)\left(1-c^2\right)}$$
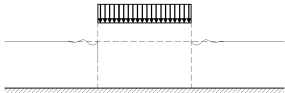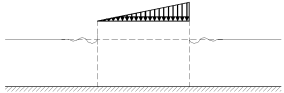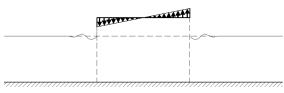
$$\xi_m=\frac{2c\left(\alpha_m\alpha_0^3 L+i\right)}{\alpha_m^6 K_\pm(0)\left(\alpha_0+\alpha_m\right)}+\frac{2c\left(\alpha_0 cL\left(1-c^2\right)+\left(ic-1\right)\right)}{\alpha_0\alpha_m^2 K_\pm(0)\left(\alpha_0+\alpha_m\right)\left(1-c^2\right)}$$

$$\eta_m=\frac{2c\left(\alpha_m c+\alpha_0\alpha_m^2 cL-\alpha_m^2\right)}{\alpha_0\alpha_m^4 L K_\pm(0)\left(\alpha_0+\alpha_m\right)\left(1-c^2\right)}+\frac{2c\left(\alpha_0 cL\left(1-c^2\right)+\left(ic-1\right)\right)}{\alpha_0\alpha_m^2 K_\pm(0)\left(\alpha_0+\alpha_m\right)\left(1-c^2\right)}$$

$$\xi_m=\frac{1/2\,\alpha_0 L+i}{\alpha_m^4 L K_\pm(0)}+\frac{2c\left(c-1\right)\left(1/2\,\alpha_0 L+i\right)}{\alpha_0\alpha_m^2 L K_\pm(0)\left(\alpha_0+\alpha_m\right)\left(1-c^2\right)}$$

$$\eta_m=\frac{-1/2\,\alpha_0 L-i}{\alpha_m^4 L K_\pm(0)}+\frac{2c\left(1-c\right)\left(1/2\,\alpha_0 L+i\right)}{\alpha_0\alpha_m^2 L K_\pm(0)\left(\alpha_0+\alpha_m\right)\left(1-c^2\right)}$$

TUDelft

Eq.

IV.55

$R = \dfrac{i}{K_+(\gamma)K'_1(\gamma)}$

$\left[\displaystyle\sum_{j=1}^{\infty}\dfrac{\alpha_j^2 e^{i\alpha_j L}K_+^2(\alpha_j)}{K'(\alpha_j)(\alpha_j-\gamma)}\xi_j - \dfrac{1}{\gamma K_-(0)}\right]$

$R = \dfrac{i}{K_+(\gamma)K'_1(\gamma)}$

$\left[\displaystyle\sum_{j=1}^{\infty}\dfrac{\alpha_j^2 e^{i\alpha_j L}K_+^2(\alpha_j)}{K'(\alpha_j)(\alpha_j-\gamma)}\xi_j - \dfrac{i}{\gamma^2 LK_-(0)}\right]$

$R = \dfrac{i}{K_+(\gamma)K'_1(\gamma)}$

$\left[\displaystyle\sum_{j=1}^{\infty}\dfrac{\alpha_j^2 e^{i\alpha_j L}K_+^2(\alpha_j)}{K'(\alpha_j)(\alpha_j-\gamma)}\xi_j + \dfrac{1}{2\gamma K_-(0)} - \dfrac{i}{\gamma^2 LK_-(0)}\right]$

IV.56

$T = \dfrac{-ie^{-i\gamma L}}{K_+(\gamma)K'_1(\gamma)}$

$\left[\displaystyle\sum_{j=1}^{\infty}\dfrac{\alpha_j^2 e^{i\alpha_j L}K_+^2(\alpha_j)}{K'(\alpha_j)(\alpha_j-\gamma)}\eta_j - \dfrac{1}{\gamma K_+(0)}\right]$

$T = \dfrac{-ie^{-i\gamma L}}{K_+(\gamma)K'_1(\gamma)}$

$\left[\displaystyle\sum_{j=1}^{\infty}\dfrac{\alpha_j^2 e^{i\alpha_j L}K_+^2(\alpha_j)}{K'(\alpha_j)(\alpha_j-\gamma)}\eta_j + \dfrac{i}{\gamma^2 LK_+(0)}\right]$

$T = \dfrac{-ie^{-i\gamma L}}{K_+(\gamma)K'_1(\gamma)}$

$\left[\displaystyle\sum_{j=1}^{\infty}\dfrac{\alpha_j^2 e^{i\alpha_j L}K_+^2(\alpha_j)}{K'(\alpha_j)(\alpha_j-\gamma)}\eta_j + \dfrac{1}{2\gamma K_+(0)} + \dfrac{i}{\gamma^2 LK_+(0)}\right]$

IV.59

$R = \dfrac{i}{K_+(\gamma)K'_1(\gamma)K_\pm(0)}$

$\left[\dfrac{2c(1+c)}{(\alpha_0-\gamma)(1+c^2)} - \dfrac{1}{\gamma}\right]$

$R = \dfrac{i}{K_+(\gamma)K'_1(\gamma)LK_\pm(0)}$

$\left[\dfrac{2c(i+\alpha_0 L-c)}{\alpha_0(\alpha_0-\gamma)(1-c^2)} - \dfrac{i}{\gamma^2}\right]$

$R = \dfrac{i}{K_+(\gamma)K'_1(\gamma)K_\pm(0)}$

$\left[\dfrac{2c(1-c)(1/2\,\alpha_0 L+i)}{\alpha_0(\alpha_0-\gamma)L(1-c^2)} + \dfrac{1}{2\gamma} - \dfrac{i}{\gamma^2 L}\right]$

not possible

IV.61

$Arg\left[K_+^2(\alpha_0)\right] + \alpha_0 L = \pi k$

$(im[c]=0)$

not possible

$\begin{pmatrix}(\alpha_0 L - \text{Re}[c])\text{Re}[c] + \\ (\text{Im}[c]-1)\text{Im}[c] = 0\end{pmatrix}$

$\begin{pmatrix}-(\alpha_0+\gamma)\alpha_0 L\left(\text{Re}^2[c]-\text{Im}^2[c]\right) + \\ 2\alpha_0\gamma L\,\text{Re}[c] - 4\gamma\,\text{Im}[c] + \\ 8\gamma\,\text{Re}[c]\text{Im}[c] + \\ (\alpha_0-\gamma)\alpha_0 L = 0\end{pmatrix}$

IV.8 Unsuccessful and invalid computation

Calculations for the following values of physical quantities: fluid depth $H_0 = 1.1m$, external force $q_0 = 1000N$, body length $L_0 = 3.5m$, body density $\rho_0 = 102.5\,kg/m^3$, fluid density $\rho = 1000\,kg/m^3$ and body height $h_0 = 1.6m$ and external period $T_p = 0.85s;1s$ bring along inaccurate results. The reason for this is that for these lower periods 'irregularities' will be generated that would not tend to smooth out by an increasing number of modes. This can be observed in the graphs that are plotted in figure IV 4. In both graphs, steep waves with large amplitudes are displayed and for the lowest period even beating takes place. However, here we accept only flat waves since we deliberately omit material properties in the plate equation, see Appendix VI.1. This can be explained as follows: without material properties, the rigid body element is modelled as a vibrating load (pressure) that perturbs the fluid surface. Consequently, waves will propagate in a zone with an increased fluctuating surface pressure. This is, obviously, a strong simplification, especially when steep waves are involved. From this it can be concluded that this method is not achieved for 'smaller' waves but for fairly long waves, i.e. for larger periods.
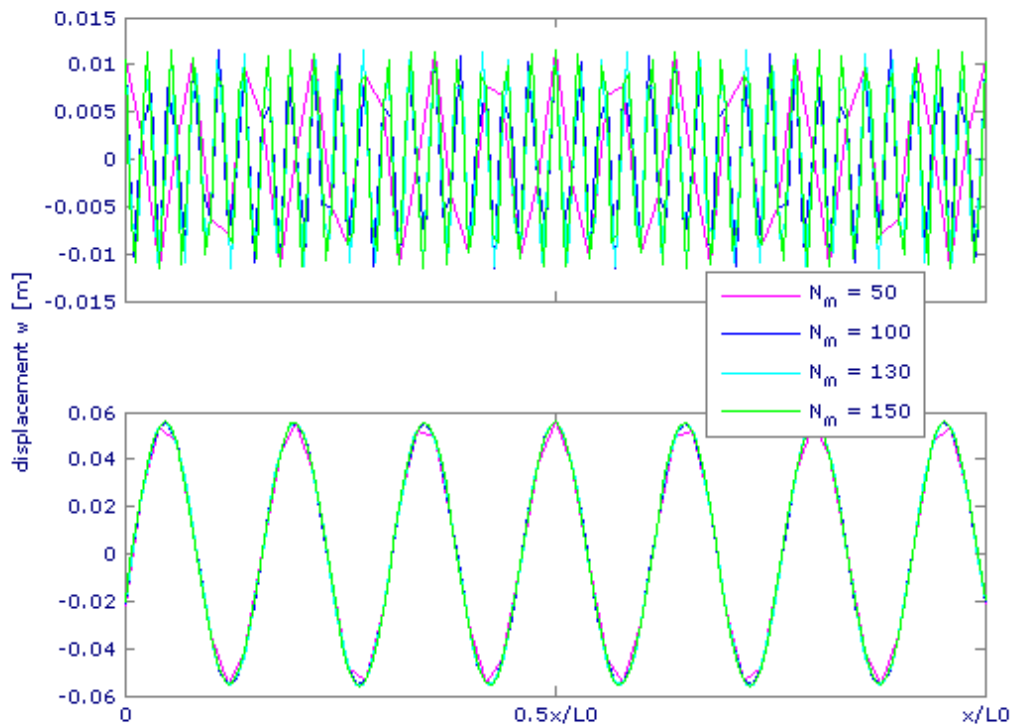
TU Delft

Figure VI.4   **vibration amplitudes for T_p = 0.85s (lower bound) and T_p = 1s**

In addition to Appendix IV.5, the lower bound for the second singularity will be determined by trial-and error and thus unsuccessful computation can practically not be avoided. By introducing the short wave approximation to the problem, we gain ourselves an intuitive tool in 'judging' between the outcomes of a rank one and a rank two computation. For a reliable and proper judgement, conditions for the short wave approximation must be as optimal as possible. This implies that T_p must be as small as possible. For $N_m = 80$, we choose H_0 to increase from $1.5m$ with steps of $0.05m$. Four corresponding plots can be viewed in figure IV.5. Note that a transition can be observed by the modal shape of the exact solution with $t = 2$ and when the short wave approximation and this solution comes close to each other. The corresponding value for the fluid depth is $H_0 = 1.6m$ and the lower bound for the second singularity reads 0.12, according to Matlab.
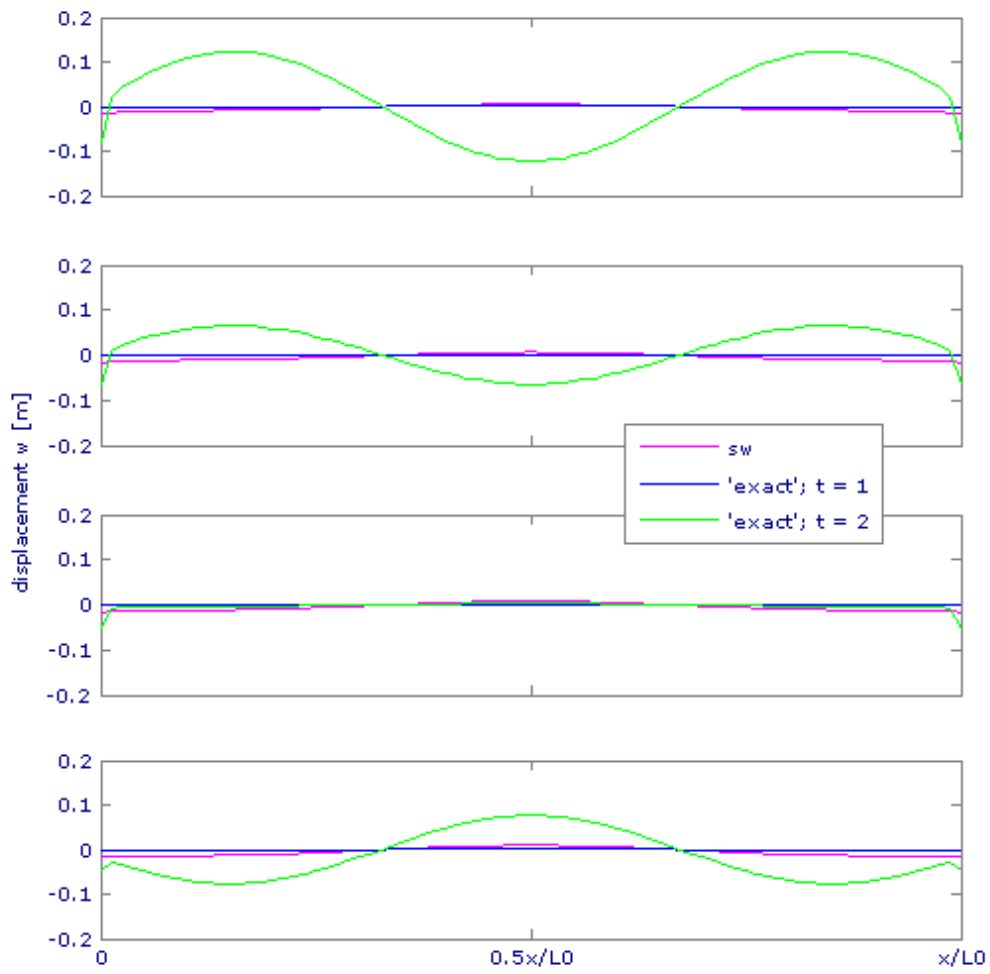
TUDelft

Figure IV.5   intuitive determination of boundary condition for second singularity

TUDelft

V Matlab codes

V.1 Input parameters

N	L1	L2	L3	B	h	c_cl	c_int	k_cl	k_int	rho_0
[nr]	[m]	[m]	[m]	[m]	[m]	[Ns/m]	[Ns/m]	[N/m]	[N/m]	[kg/m3]
20	3.5	3.5	5.4	1.6		1.5e+3	1.5e+3	1e+5	1e+5	102.5
P	c	wb	md	tend						
[N]	[m/s]	[m]	[m]	[s]						
9761	8.333	2.76	0	16.25						

Figure V.1   structural parameters.txt

H0 (>1)	q0	L0	B	Tp	rho_0	rho	h	Nm	*Nms/rad/m
[m]	[N/m2]	[m]	[m]	[s]	[kg/m3]	[kg/m3]	[m]	[-]	**Ns/m/m1
1.6	1000	3.5	5.4	1.5	102.5	1000	1.6	80	

mf1_a	mf2_v	mf2_a	mf3_v	mf3_a	cd1_a	cd2_v	cd2_a	cd3_v	cd3_a
[kg/m2]	[kg/m2]	[kg/m2]	[kg/m2]	[kg/m2]	[*]	[**]	[*]	[**]	[*]
797.5	1753.9	672.9	1753.9	672.9	-6.7e+2	6.7e+4	-1.7e+2	6.7e+4	-1.7e+2

Figure V.2   hydrodynamic parameters.txt

V.2 Mass, Damping and Stiffness matrix and eigenfrequencies

```
% input:
% importing structural parameters(.txt):
[N,L1,L2,L3,B,h,c_cl,c_int,k_cl,k_int,rho_0] =...
    textread('structural parameters.txt',...
    '%f %f %f %f %f %f %f %f %f %f %f',1,'headerlines',2);
% in which:
% N = number of bodies
% L1,2,3 = length of first, second and third body element
% B = body width
% h = body height
% c_cl = damping parameter of end joints
% c_int = damping parameter of remaining joints
% k_cl = stiffness parameter of end joints
% k_int = stiffness parameter of remaining joints
% rho_0 = body density

% importing hydrodynamic parameters(.txt):
[mf1_a,mf2_v,mf2_a,mf3_v,mf3_a,cd1_a,cd2_v,cd2_a,cd3_v,cd3_a] =...
    textread('hydrodynamic parameters.txt',...
    '%f %f %f %f %f %f %f %f %f %f',5,'headerlines',6);
% in which:
% mf2,3_v = added mass for vertical motion of second and third body element
% mf1,2,3_a = (equivalent) added mass for rotational motion of first three elements
% cd2,3_v = distributed damping for vertical motion of second and third body
element
% cd1,2,3_a = distributed damping for rotational motion of first three elements

% remaining parameters form buoyancy:
kd1_v=1000*9.81*B; kd2_v=kd1_v;kd3_v=kd2_v; %
distributed stiffness for vertical motion
kd1_a=1/3*kd1_v*L1^2;kd2_a=1/12*kd2_v*L2^2;kd3_a=1/12*kd3_v*L3^2; %
distributed stiffness for rotational motion

% symmetric multibody configuration:
Lj=L3;LN_2=Lj;LN_1=L2;LN=L1;
mfj_v=mf3_v;mfj_a=mf3_a;mfN_1_v=mf2_v;mfN_1_a=mf2_a;mfN_a=mf1_a;
kdj_v=kd3_v;kdj_a=kd3_a;kdN_1_v=kd2_v;kdN_1_a=kd2_a;kdN_a=kd1_a;
cdj_v=cd3_v;cdj_a=cd3_a;cdN_1_v=cd2_v;cdN_1_a=cd2_a;cdN_a=cd1_a;

% mass of body element per square meter:
mb=rho_0*h;

% mass matrix M:
M = zeros(2*N-2,2*N-2); %creates a 2N-2-by-2N-2 matrix, consisting of zeros
M(1,1)=1/12*((2*L1)^2+h^2)*(B*(mb+mf1_a))*L1;
M(2,2)=(B*(mb+mf2_v))*L2;
M(3,3)=1/12*(L2^2+h^2)*(B*(mb+mf2_a))*L2;
for j=4:2:2*N-6
    M(j,j)=(B*(mb+mfj_v))*Lj;
    M(j+1,j+1)=1/12*(Lj^2+h^2)*(B*(mb+mfj_a))*Lj;
end;
M(2*N-4,2*N-4)=(B*(mb+mfN_1_v))*LN_1;
M(2*N-3,2*N-3)=1/12*(LN_1^2+h^2)*(B*(mb+mfN_1_a))*LN_1;
M(2*N-2,2*N-2)=1/12*((2*LN)^2+h^2)*(B*(mb+mfN_a))*LN;
```

```matlab
save('Mass','M');

% damping matrix C:
C = zeros(2*N-2,2*N-2); %creates a 2N-2-by-2N-2 matrix, consisting of zeros (no
w1,wN)
C(1,1:3)=[c_cl*L1^2+cd1_a*L1,-c_cl*L1,0.5*c_cl*L1*L2];
C(2,1:5)=[-c_cl*L1,c_cl+c_int+cd2_v*L2,0.5*(c_int-c_cl)*L2,-c_int,...
    0.5*c_int*L3];
C(3,1:5)=[0.5*c_cl*L1*L2,0.5*(c_int-c_cl)*L2,0.25*(c_int+c_cl)*L2^2+...
    cd2_a*L2,-0.5*c_int*L2,0.25*c_int*L2*L3];
for j=4:2:2*N-6
    C(j,j-2:j+3)=[-c_int,-0.5*c_int*Lj,2*c_int+cdj_v*Lj,0,-c_int,...
        0.5*c_int*Lj];
    C(j+1,j-2:j+3)=[0.5*c_int*Lj,0.25*c_int*Lj*Lj,0,0.5*c_int*Lj^2+...
        cdj_a*Lj,-0.5*c_int*Lj,0.25*c_int*Lj^2];
end;
C(2*N-4,2*N-6:2*N-2)=[-c_int,-0.5*c_int*LN_2,c_int+c_cl+cdN_1_v*...
    LN_1,0.5*(c_cl-c_int)*LN_1,c_cl*LN];
C(2*N-3,2*N-6:2*N-2)=[0.5*c_int*LN_1,0.25*c_int*LN_2*LN_1,0.5*...
    (c_cl-c_int)*LN_1,0.25*(c_cl+c_int)*LN_1^2+cdN_1_a*LN_1,0.5*...
    c_cl*LN_1*LN];
C(2*N-2,2*N-4:2*N-2)=[c_cl*LN,0.5*c_cl*LN_1*LN,c_cl*LN^2+cdN_a*LN];
%correction pontoon length L according to L2 and LN_1 for coupling:
C(4,3)=-0.5*c_int*L2;
C(5,3)=0.25*c_int*L2*L3;
C(2*N-6,2*N-3)=0.5*c_int*LN_1;
C(2*N-5,2*N-3)=0.25*c_int*LN_2*LN_1;
save ('Damping','C');

% stiffness matrix K:
K = zeros(2*N-2,2*N-2); %creates a 2N-2-by-2N-2 matrix, consisting of zeros
K(1,1:3)=[k_cl*L1^2+kd1_a*L1,-k_cl*L1,0.5*k_cl*L1*L2];
K(2,1:5)=[-k_cl*L1,k_cl+k_int+kd2_v*L2,0.5*(k_int-k_cl)*L2,-k_int,0.5*...
    k_int*L3];
K(3,1:5)=[0.5*k_cl*L1*L2,0.5*(k_int-k_cl)*L2,0.25*(k_int+k_cl)*L2^2+...
    kd2_a*L2,-0.5*k_int*L2,0.25*k_int*L2*L3];
for j=4:2:2*N-6
    K(j,j-2:j+3)=[-k_int,-0.5*k_int*Lj,2*k_int+kdj_v*Lj,0,-k_int,0.5*...
        k_int*Lj];
    K(j+1,j-2:j+3)=[0.5*k_int*Lj,0.25*k_int*Lj*Lj,0,0.5*k_int*Lj^2+...
        kdj_a*Lj,-0.5*k_int*Lj,0.25*k_int*Lj^2];
end;
K(2*N-4,2*N-6:2*N-2)=[-k_int,-0.5*k_int*LN_2,k_int+k_cl+kdN_1_v*LN_1,0.5*...
    (k_cl-k_int)*LN_1,k_cl*LN];
K(2*N-3,2*N-6:2*N-2)=[0.5*k_int*LN_1,0.25*k_int*LN_2*LN_1,0.5*...
    (k_cl-k_int)*LN_1,0.25*(k_cl+k_int)*LN_1^2+kdN_1_a*LN_1,0.5*...
    k_cl*LN_1*LN];
K(2*N-2,2*N-4:2*N-2)=[k_cl*LN,0.5*k_cl*LN_1*LN,k_cl*LN^2+kdN_a*LN];
%correction pontoon length L according to L2 and LN_1 for coupling:
K(4,3)=-0.5*k_int*L2;
K(5,3)=0.25*k_int*L2*L3;
K(2*N-6,2*N-3)=0.5*k_int*LN_1;
K(2*N-5,2*N-3)=0.25*k_int*LN_2*LN_1;
save ('Stiffness','K');

% matrices for general damping case:
M_tilda=[zeros(2*N-2,2*N-2),M;M,C];
K_tilda=[-M,zeros(2*N-2,2*N-2);zeros(2*N-2,2*N-2),K];

% eigenfrequency:
[E,omega]=eig(K_tilda,M_tilda);

% orthogonality property check:
M_star=E'*M_tilda*E;
K_star=E'*K_tilda*E;
```

Figure V.3   matrices.m

V.3 Numerical simulation with ODE23-solver

```
% input:
% importing vehicle parameters from  structural parameters.txt:
[P,c,wb,md,tend] = textread('structural parameters.txt',...
    '%f %f %f %f %f',5,'headerlines',6);
% in which:
% P = concentrated load from vehicle
% c = vehicle velocity
% wb = wheel base
% md = mutual distance between multiple vehicles
% tend = end of simulation time

% identity and mass matrix I and M:
a=2*N-2;
I = eye(a); % eye (n) creates an n-by-n matrix with ones on the main diagonal.
load Mass % load mass from matrices.m, (run this file first)

% initial conditions:
y0=zeros(2*N-2,1);
y0(1,1)=0; %displacement second element = 0 [m]
ydot0=zeros(2*N-2,1);

% floating point tolerance in dicretization:
tol=zeros(1,4*N-4);
tol(1,1:4*N-4)=1e-6;

% output:
% time vector T and displacement vector Y based on ODE23-solver
% refers to function rigid_sv.m or rigid_mv.m, associated with single
% sehicle or multiple vehicles, respectively.
options = odeset('Mass',[I,zeros(2*N-2,2*N-2);zeros(2*N-2,2*N-2),M],...
    'NormControl','on','Stats','on');
[T,Y] = ode23s(@rigid_sv,[0 tend],[y0 ydot0],options);
```
Figure V.4   ODE23_rigid.m

```
function dy = rigid_sv(t,y)
% syntax: function dy = rigid_sv(t,y)
% space state formulation equation of motion for a single vehicle
% input:
% importing structural parameters from parameters.txt:
[N,L1,L2,L3] = textread('structural parameters.txt','%f',1,'headerlines',2);
[P,c,wb,md] = textread('structural parameters.txt','%f %f %f %f',5,'headerlines',6);
% symmetric multibody configuration:
Lj=L3;LN_2=Lj;LN_1=L2;LN=L1;

% identity, damping and stiffness matrix I,C and K:
a=2*N-2;
I = eye(a);
load Damping
load Stiffness

%time between succeeding couple of wheels passing a point:
twb = wb/c;

% exitation vector:
RHS = zeros(2*N-2,2);
for w=0:1 %0->front wheels; 1->rear wheels
    if (t>=w*twb&t<L1/c+w*twb)
        RHS(1,w+1)=P*c*(t-w*twb);
    else
        RHS(1,w+1)=0;
    end;
    if (t>=L1/c+w*twb&t<(L1+L2)/c+w*twb)
        RHS(2,w+1)=P;
        RHS(3,w+1)=P*(c*(t-w*twb)-L1-0.5*L2);
    else
        RHS(2,w+1)=0;
        RHS(3,w+1)=0;
    end;
    for j=0:2:2*N-10
        if (t>=(L1+L2+0.5*j*Lj)/c+w*twb&t<(L1+L2+(0.5*j+1)*Lj)/c+w*twb)
            RHS(4+j,w+1)=P;
```

TUDelft

```
                      RHS(5+j,w+1)=P*(c*(t-w*twb)-(L1+L2+(0.5*j+0.5)*Lj));
            else
                RHS(4+j,w+1)=0;
                RHS(5+j,w+1)=0;
            end
    end;
    if (t>=(L1+L2+(N-4)*Lj)/c+w*twb&t<(L1+L2+(N-4)*Lj+LN_1)/c+w*twb)
        RHS(2*N-4,w+1)=P;
        RHS(2*N-3,w+1)=P*(c*(t-w*twb)-(L1+L2+(N-4)*Lj+0.5*LN_1));
    else
        RHS(2*N-4,w+1)=0;
        RHS(2*N-3,w+1)=0;
    end;
    if (t>=(L1+L2+(N-4)*Lj+LN_1)+w*twb&t<(L1+L2+(N-4)*Lj+LN_1+LN)/c+w*twb)
        RHS(2*N-2,w+1)=-P*(c*(t-w*twb)-(L1+L2+(N-4)*Lj+LN_1+0.5*LN));
    else
        RHS(2*N-2,w+1)=0;
    end;
end;
RHS_vector=RHS(:,1)+RHS(:,2);
RHS_dubblevector=zeros(4*N-4,2);
RHS_dubblevector=[zeros(2*N-2,1);RHS_vector];

% output:
% dy as column vector (4*N-4 rows, 1 column)
dy = zeros(4*N-4,1);
A=[zeros(2*N-2,2*N-2),I;-K,-C];
dy=A*y+RHS_dubblevector;
```
Figure V.5   rigid_sv.m

```
function dy = rigid_mv(t,y)
% syntax: function dy = rigid_mv(t,y)
% space state formulation equation of motion for multile vehicles
% input:
% importing structural parameters from parameters.txt:
[N,L1,L2,L3] = textread('structural parameters.txt','%f',1,'headerlines',2);
[P,c,wb,md] = textread('structural parameters.txt','%f %f %f %f',5,'headerlines',6);
% symmetric multibody configuration:
Lj=L3;LN_2=Lj;LN_1=L2;LN=L1;

% identity, damping and stiffness matrix I,C and K:
a=2*N-2;
I = eye(a);
load Damping
load Stiffness

% time between succeeding couple of wheels passing a point:
twb = wb/c;
% time between succeeding passenger cars (mutual distance divided by
% velocity):
tmd = md/c;
% number of passenger cars within time interval:
nc = round(tend/tmd);

% exitation vector:
RHS = zeros(2*N-2,2*nc);
% columns with forces and moments due to frontwheel and rearwheel
% vehicle after vehicle
for w=0:1 %0->front wheels; 1->rear wheels
    for v=0:nc
        if (t>=v*tmd+w*twb&t<L1/c+v*tmd+w*twb)
            RHS(1,2*v+w+1)=P*c*(t-v*tmd-w*twb);
        else
            RHS(1,2*v+w+1)=0;
        end;
        if (t>=L1/c+v*tmd+w*twb&t<(L1+L2)/c+v*tmd+w*twb)
            RHS(2,2*v+w+1)=P;
            RHS(3,2*v+w+1)=P*(c*(t-v*tmd-w*twb)-L1-0.5*L2);
        else
            RHS(2,2*v+w+1)=0;
            RHS(3,2*v+w+1)=0;
        end;
        for j=0:2:2*N-10
            if (t>=(L1+L2+0.5*j*Lj)/c+v*tmd+w*twb&t<(L1+L2+(0.5*j+1)*...
                    Lj)/c+v*tmd+w*twb)
                RHS(4+j,2*v+w+1)=P;
```

```matlab
                    RHS(5+j,2*v+w+1)=P*(c*(t-v*tmd-w*twb)-(L1+L2+(0.5*j+0.5)*...
                        Lj));
                else
                    RHS(4+j,2*v+w+1)=0;
                    RHS(5+j,2*v+w+1)=0;
                end;
            end;
            if (t>=(L1+L2+(N-4)*Lj)/c+v*tmd+w*twb&t<(L1+L2+(N-4)*Lj+LN_1)/...
                    c+v*tmd+w*twb)
                RHS(2*N-4,2*v+w+1)=P;
                RHS(2*N-3,2*v+w+1)=P*(c*(t-v*tmd-w*twb)-(L1+L2+(N-4)*Lj+0.5*...
                    LN_1));
            else
                RHS(2*N-4,2*v+w+1)=0;
                RHS(2*N-3,2*v+w+1)=0;
            end;
            if (t>=(L1+L2+(N-4)*Lj+LN_1)+v*tmd+w*twb&t<(L1+L2+(N-4)*Lj+...
                    LN_1+LN)/c+v*tmd+w*twb)
                RHS(2*N-2,2*v+w+1)=-P*(c*(t-v*tmd-w*twb)-(L1+L2+(N-4)*Lj+...
                    LN_1+0.5*LN));
            else
                RHS(2*N-2,2*v+w+1)=0;
            end;
        end;
end;
for n=1:2*N-2
    RHS_vector(n,1)=sum(RHS(n,:));
end;
RHS_dubblevector=zeros(4*N-4,2);
RHS_dubblevector=[zeros(2*N-2,1);RHS_vector];

% output:
% dy as column vector (4*N-4 rows, 1 column)
dy = zeros(4*N-4,1); % a column vector (4*N-4 rows, 1 column)
A=[zeros(2*N-2,2*N-2),I;-K,-C];
dy=A*y+RHS_dubblevector;
```
Figure V.5   rigid_mv.m

V.4 Wave diffraction approximation

```matlab
function f = K1(x)
% syntax: function f = K1(x)
% describes dispersion relation for wave diffraction
% approximation model
% input:
[H] = textread('hydrodynamic parameters.txt',...
'%f',1,'headerlines',2);
% output:
f = x*tanh(x*H)-1
```
Figure V.6   K1.m

```matlab
function f = K2_vr(x)
% syntax: function f = K2_vr(x)
% describes dispersion relation for wave diffraction
% approximation model
% input:
[H,q0,L0,B,Tp,rho_0,rho,h] = ...
textread('hydrodynamic parameters.txt',...
'%f %f %f %f %f %f %f %f',1,'headerlines',2);
% frequency, characteristic length and draft:
omega=2*pi/Tp;
l=9.81/omega^2;
d=rho_0*h/(rho*l);
% output:
f = (1-d)*x*tanh(x*H)-1
```
Figure V.7   K2_vr.m

TUDelft

```matlab
% input:
% importing from hydrodynamic parameters(.txt):
[H,q0,L0,B,Tp,rho_0,rho,h,Nm] = ...
textread('hydrodynamic parameters.txt',...
'%f %f %f %f %f %f %f %f %f',1,'headerlines',2);
% in which:
% H = fluid depth
% qo = periodic distributed load
% L0 = body length
% Tp = period
% Nm = number of modes

% characteristic length:
omega=2*pi/Tp;
l=9.81/omega^2;
% (dimensionless) draft:
d=rho_0*h/(rho*l);
% dimensionless length of pontoon:
L=L0/l;
% computing imaginairy roots for K1:
for n=1:1:Nm
    options=optimset('Display','off');
    [a(n,1),check_K(n,1)] = fsolve(@K1,n*i*pi/H,options);
end;
% computing imaginairy roots for K2:
for n=1:1:Nm
    options=optimset('Display','off');
    [a(n,2),check_K(n,2)] = fsolve(@K2_vr,n*i*pi/H,options);
    a(n,3)=a(n,2)-a(n,1);% checking convergence as N go to infinity
end;
% computing 2 real roots for K1 (+/- gamma):
options=optimset('Display','iter');
    [gamma,check_gamma] = fzero(@K1,[0 2],options);
    %increasing H means convergence of gamma to unity, 2 is upper bound
% computing 2 real roots for K2 (+/- alpha_zero)if d<1:
options=optimset('Display','off');
    [alpha_zero,check_alpha_zero] = fsolve(@K2_vr,1/(1-d),options);
    %list for alpha (real + imaginary roots):
for n=1:1:Nm
alpha(1,1)=gamma;
alpha(n+1,1)=a(n,1);
end;
for n=1:1:Nm
alpha(1,2)=alpha_zero;
alpha(n+1,2)=a(n,2);
end;
%g has singularities as a=n*pi*i/H as n goes to infinity
for j=1:1:Nm+1
    for m=1:1:Nm+1
        for k=1:1:Nm
            % constructing loop for g_plus(-a)= prod[(1-(ak/-a))*...
            % exp(ak/-a),k:1..Nm]
            g_plus_a2(k,m)=(1+(alpha(m,2)/a(k,2)))*exp(-alpha(m,2)/a(k,2));
            g_plus_a1(k,m)=(1+(alpha(m,2)/a(k,1)))*exp(-alpha(m,2)/a(k,1));
            prod_g_plus_a2(m,1)=prod(g_plus_a2(:,m));
            prod_g_plus_a1(m,1)=prod(g_plus_a1(:,m));
            g_plus_a(m,1)=prod_g_plus_a2(m,1)/prod_g_plus_a1(m,1);
            % constructing loop for g_plus(-gamma)= prod[(1-(ak/-gamma))*...
            % exp(ak/-gamma),k:1..N]
            g_plus_g2(k,1)=(1+(gamma/a(k,2)))*exp(-gamma/a(k,2));
            g_plus_g1(k,1)=(1+(gamma/a(k,1)))*exp(-gamma/a(k,1));
            prod_g_plus_g2=prod(g_plus_g2(:,1));
            prod_g_plus_g1=prod(g_plus_g1(:,1));
            g_plus_g=prod_g_plus_g2/prod_g_plus_g1;
        end
        %K+(a):
        K_plus_a(m,1)=((alpha(m,2)+alpha_zero)/(alpha(m,2)+gamma))*...
            g_plus_a(m,1);
        %K+(gamma):
        K_plus_g =((gamma+alpha_zero)/(2*gamma))*g_plus_g;
        %K-(0)= K+(0):
        K_plus_0=alpha_zero/gamma;
        %K1(a):
        K1_a(m,1)=alpha(m,2)*tanh(alpha(m,2)*H)-1;
```

```matlab
        %K1'(gamma):
        K1_gd=tanh(gamma*H)+gamma*(1-(tanh(gamma*H))^2)*H;
        %K2'(a):
        K2_ad(m,1)=(1-d)*tanh(alpha(m,2)*H)+(1-d)*alpha(m,2)*(1-...
            (tanh(alpha(m,2)*H))^2)*H;
        %matrix for determination of eta and xi:
        C(j,m)=alpha(m,2)^2*exp(i*alpha(m,2)*L)*(K_plus_a(m,1))^2*...
            K1_a(m,1)/(alpha(j,2)^2*K2_ad(m,1)*(alpha(m,2)+alpha(j,2)));
        %+ vectors in case of vertical vibrations:
        f1(j,1)=1/(alpha(j,2)^3*K_plus_0);
        f2(j,1)=f1(j,1);
    end
end

%constructing eta(j)and xi(j) by (truncated)Singular Value-Decomposition:
b = zeros(Nm+1,1);
b = C*f1+f2;
A = zeros(Nm+1,Nm+1);
A = ones(Nm+1,Nm+1)-C^2;
[U S V] = svd(A); %singular value decomposition
s = svd(A);
tol = max(size(A))*s(1)*eps;%floating point tolerance
r = rank(A,tol);%rank computation
tol = 0.05;
r = rank(A,tol);
Sinv = zeros(Nm+1,Nm+1);
for e=1:1:r
    Sinv(e,e) = inv(s(e));
end;
xi_j = V'\(Sinv*(U\b));
eta_j = xi_j;

% output:
%constructing psi_0, psi_od, wx and wx_average from 0 to L:
x_start=0/l;
x_end=L0/l;
x_step=(x_end-x_start)/(Nm);
x=x_start:x_step:x_end;
for jj=1:1:Nm+1
    for kk=1:1:Nm+1
        psi_0_jj(jj,kk)=alpha(jj,2)^2*K_plus_a(jj,1)/K2_ad(jj,1)*...
        (exp(-i*alpha(jj,2)*(x(1,kk)-L))*xi_j(jj,1)+exp(i*alpha(jj,2)*...
        x(1,kk))*eta_j(jj,1));
        psix_0(1,kk)=-i*sum(psi_0_jj(:,kk));
        psi_0d_jj(jj,kk)=psi_0_jj(jj,kk)*alpha(jj,2)*tanh(alpha(jj,2)*H);
        psix_0d(1,kk)=-i*sum(psi_0d_jj(:,kk));
        wx(1,kk)=i*sum(psix_0d(1,kk));
    end
    w_av_jj(jj,1)=tanh(alpha(jj,2)*H)/K2_ad(jj,1)*(alpha(jj,2)^2*...
        K_plus_a(jj,1)*i*(1-exp(i*alpha(jj,2)*L))*(eta_j(jj,1)+xi_j(jj,1)));
    wx_av=sum(w_av_jj(:,1));

    % reflecting and transmitted wave coefficients |R| and |T|:
    R_jj(jj,1)=i/(K_plus_g*K1_gd)*(alpha(jj,2)^2*exp(i*alpha(jj,2)*L)*...
        (K_plus_a(jj,1))^2*K1_a(jj,1)*xi_j(jj,1)/(K2_ad(jj,1)*...
        (alpha(jj,2)-gamma)-1/(gamma*K_plus_0));
    R=sum(R_jj(:,1));
    T_jj(jj,1)=-i*exp(-i*gamma*L)/(K_plus_g*K1_gd)*(alpha(jj,2)^2*...
        exp(i*alpha(jj,2)*L)*(K_plus_a(jj,1))^2*K1_a(jj,1)*eta_j(jj,1)/...
        (K2_ad(jj,1)*(alpha(jj,2)-gamma)-1/(gamma*K_plus_0));
    T=sum(T_jj(:,1));
    T=squeeze(T);
    % normalized:
    R_norm=abs(R)/(abs(R)+abs(T));
    T_norm=abs(T)/(abs(R)+abs(T));
    % checking phase differences:
    phase_R=angle(R);
    phase_T=angle(T);
    phase_diff=abs(phase_R-phase_T);
    % checking condition |R|=0:
    check_R_zero=imag((K_plus_a(1,1))^2)/real((K_plus_a(1,1))^2)+...
        alpha_zero*L;
end
% re-enter dimensions:
psi_0=psix_0*q0/(rho*omega);
psi_0d=psix_0d*q0/(rho*omega*l);
w=wx*q0/(rho*9.81);
```

TUDelft

```
w_av=wx_av*q0/(rho*9.81*L);
w_m=mean(w);% mean value or midpoint value for w
% distributed values for stiffness and damping:
Kappa=B*q0/w_m;
kd=real(Kappa);
cd=imag(Kappa)/(i*omega);
% added mass per meter width and length:
alphax_am=psi_0./psi_0d;
alpha_am=mean(alphax_am);
mf=rho*alpha_am;
```
Figure V.8   wavediffraction.m

```
   %% 1 mode approximation (short wave approximation) %%
        %matrix for determination of eta and xi:
        C(j,m)=alpha(m,2)^2*exp(i*alpha(m,2)*L)*(K_plus_a(m,1))^2*...
            K1_a(m,1)/(alpha(j,2)^2*K2_ad(m,1)*(alpha(m,2)+alpha(j,2)));
        C_j0(j,1) = C(j,1);

        %+ vectors in case of vertical vibrations:
        f1(j,1)=1/(alpha(j,2)^3*K_plus_0);
        f2(j,1)=f1(j,1);
        f0_1=f1(1,1);
        f0_2=f2(1,1);
    end
end

%constructing eta(j)and xi(j) 1 mode approximation:
C00=(abs(alpha_zero-gamma))/gamma;
eta_j=C_j0*((f0_1+C00*f0_2)/(1-C00^2))+f2;
xi_j=C_j0*((C00*f0_1+f0_2)/(1-C00^2))+f1;
   %% end 1 mode approximation %%
```
Figure V.9   short wave approximation eta and xi in wavediffraction.m

V.5 Transfer function

```
% this file calculates the transfer function of the acceleration in every
% degree of freedom in the multibody system
% input:
[N] = textread('structural parameters.txt','%f',1,'headerlines',2);

% mass, damping and stiffness matrix I,C and K:
load Mass
load Damping
load Stiffness

% output:
% frequency steps:
omega_end=5;
stepsize=0.05;
omega=0:stepsize:omega_end;
omega_step=omega_end/stepsize+1;

% frequency response function for acceleration:
  for j=1:omega_step
      S=-omega(j)^2*M+i*omega(j)*C+K;
      H=S^-1;
      H_y=abs(H);
      H_am(:,j)=sum(H_y(:,:))*omega(j)^2;
  end
```
Figure V.6   FDA.m

VI Unsuccessful controlling of structural parameters

The strategy in the parameter study, described in section 9.5, was initially more comprehensively measured out; after a miscalculation, we evaluated k_{cl} first, since these tools are specially designed for manipulating the vertical acceleration at the entrance of the structure. Subsequently, k_{int} and $k_{cl/int}$ -in that order- were evaluated in a manner analogously to k_{cl} .

In figure VI.1 , 6 graphs have been plotted with $k_{cl/int}$, k_{cl} and k_{int} versus quality measures a_c and θ . It can be noticed that stiffness promotes accelerations while it opposes rotations, generally speaking. Stiffness as 'tuning tool' must be eliminated since accelerations should be slowed down rather than accelerated.
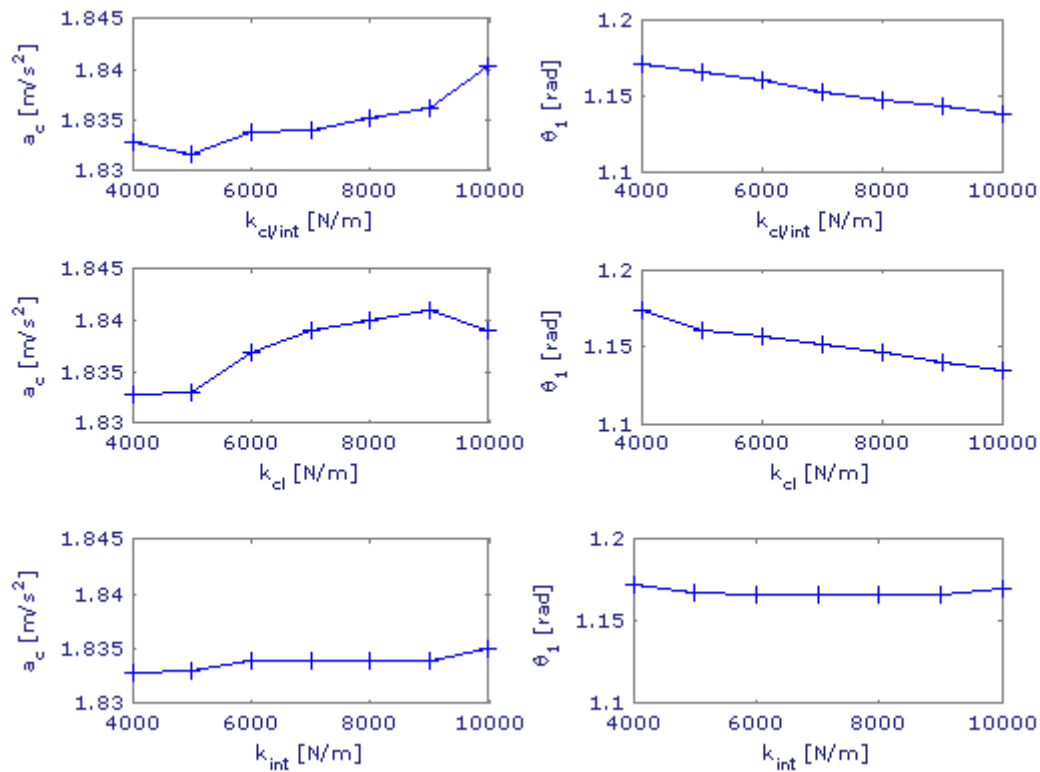

Figure VI.1   **simulation with 7 different values for** $k_{cl/int}$ **,** k_{cl} **and** k_{int} **when c = 80 km/h**

Proceeding the strategy, the same steps for c as for k will be followed.

Figure VI.2 shows 6 graphs with $c_{cl/int}$, c_{cl} and c_{int} versus the quality measures a_c and θ . It can be noticed that damping slows down accelerations now, irrespective of how it is distributed over the joints. Damping still slows down rotations, like in the stiffness response. Taking $c_{cl/int} = 1*10^5\, Ns/m$ yield $a_c = 1\, m/s^2$ what meets the requirement $a_c \le a_{max,c}$. Basically, c_{int} must be $> 1.4*10^5\, Ns/m$ and $c_{cl} \gg 1.4*10^5\, Ns/m$ in order to meet the requirement $a_c \le a_{max,c}$. Therefore, the 'damping tool' will be used to damp all joints equally. Due to close to invariant gradients, linear interpolation close to the values is justified.
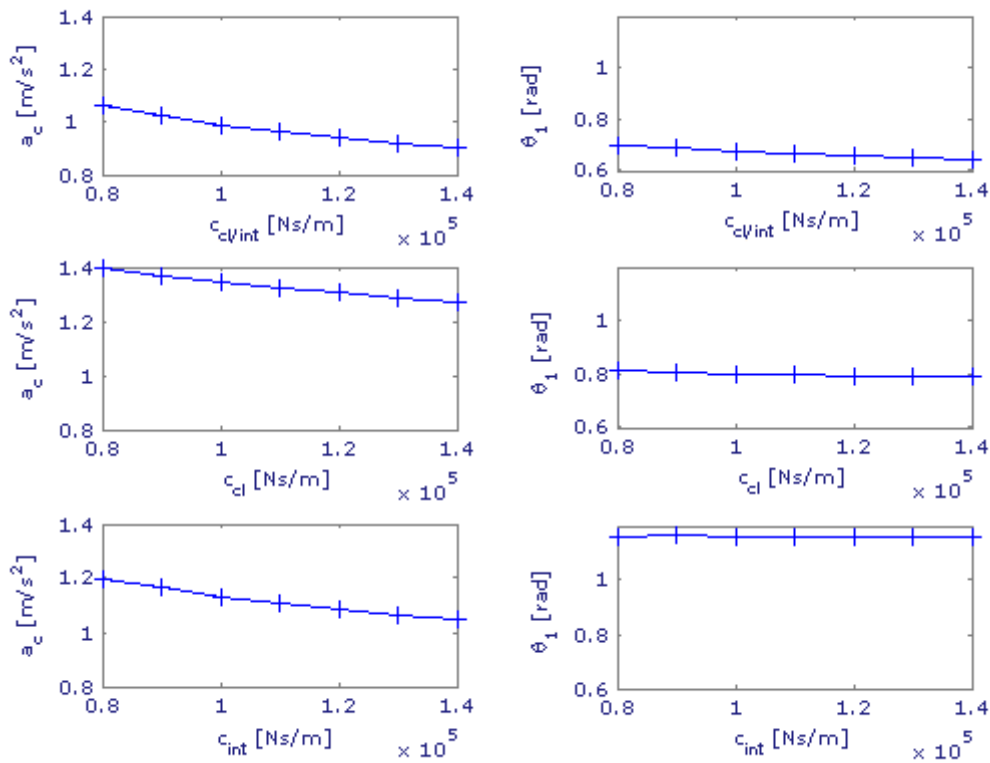
TUDelft

Figure IV.2 simulation with 7 different values for $c_{cl/int}$, c_{cl} and c_{int} when c = 80 km/h

Since the body length manipulates the body acceleration too, L^i as 'tuning tool' is implemented apart from the damping tool. However, from an economical point of view, it is important to minimize stretching of the body length due to transportability. Therefore, L^1 and L^2, and due to a symmetric configuration, L^{20} and L^{19} were appointed for evaluation, since the corresponding bodies are closest to the critical location. Simulations with 7 different values can be found in figure VI.3. Initially, L^1 can be eliminated as 'tuning tool' since L^2 is the strongest tool.
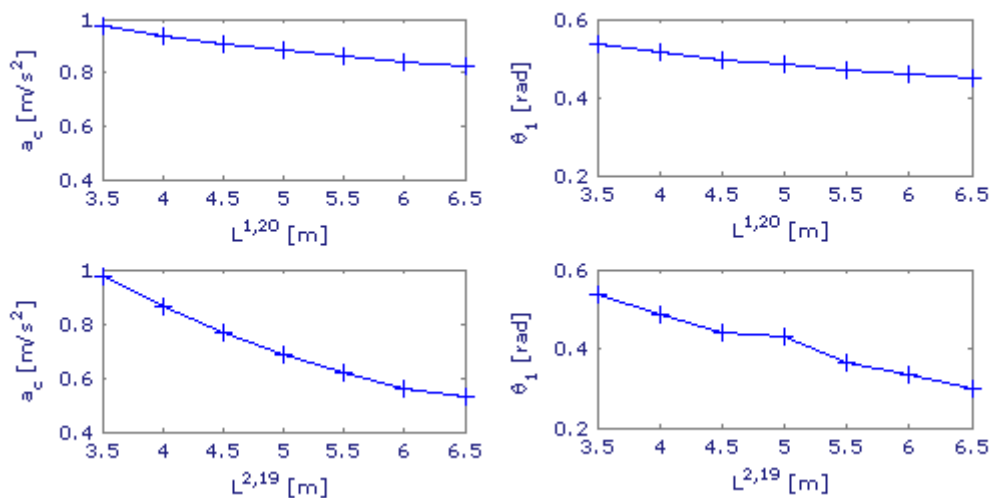

Figure 9.20 simulation with 7 different values for $L^{1,20}$ and $L^{2,19}$ when c = 100 km/h

TUDelft

TUDelft